MICROFLUIDIC AND PAPER-BASED DEVICES FOR THE ANALYSIS OF RED BLOOD CELLS: IMPROVING THE QUALITY AND ACCESSIBILITY OF DIAGNOSIS, MONITORING AND TREATMENT FOR SICKLE CELL DISEASE

A Dissertation

Presented to

the Faculty of the Department of Biomedical Engineering

University of Houston

In Partial Fulfillment

of the Requirements for the Degree

Doctor of Philosophy

in Biomedical Engineering

by

Nathaniel Z. Piety

May 2017

MICROFLUIDIC AND PAPER-BASED DEVICES FOR THE ANALYSIS OF RED BLOOD CELLS: IMPROVING THE QUALITY AND ACCESSIBILITY OF DIAGNOSIS, MONITORING AND TREATMENT FOR SICKLE CELL DISEASE

Nathaniel Z. Piety

Approved:

Chair of the Committee
Sergey S. Shevkoplyas, Ph.D.
Associate Professor
Department of Biomedical Engineering

Committee Members:

Alex George, M.D., Ph.D.
Assistant Professor
Department of Pediatrics
Baylor College of Medicine

Chandra Mohan, M.D., Ph.D.
Hugh Roy and Lillie Cranz Cullen Endowed Professor
Department of Biomedical Engineering

Sheereen Majd, Ph.D.
Assistant Professor
Department of Biomedical Engineering

Metin Akay, Ph.D.
Founding Chair
John S. Dunn Endowed Chair
Department of Biomedical Engineering

Suresh K. Khator, Associate Dean,
Cullen College of Engineering

Metin Akay, Ph.D.
Founding Chair
John S. Dunn Endowed Chair
Department of Biomedical Engineering

ACKNOWLEDGEMENTS

First and foremost I would like to express my sincere gratitude to my research advisor Dr. Sergey Shevkoplyas. Thank you for your mentorship, advice, support, criticism, humor, patience and enthusiasm over the past several years and for inspiring me to always "make what we do matter." Next, I would like to thank my mom, Jennifer Piety, for her continuous support and encouragement throughout my graduate studies and my life; without her I couldn't be the person I am today. I would also like to thank my best friend Coleman Rasof for helping me to stay sane throughout graduate school.

Next, I would like to express my gratefulness to Dr. Metin Akay for his personal support and advice throughout my graduate studies and for creating a supportive and productive environment within the department as a whole. I would also like to express my gratitude to all of the scientists and clinicians who I have had the opportunity to collaborate with throughout my studies, specifically Dr. Walter Reinhart, Dr. Alex George, Dr. Sean Gifford and Dr. Willy Flegel, as well as all departmental faculty members that I have had the opportunity to interact with and learn from. I would also like to thank the other members of my committee – Dr. Chandra Mohan and Dr. Sheereen Majd – for their insights and help constructing this dissertation.

Additionally, I would like to thank all past and current members of the Shevkoplyas Lab; firstly for tolerating me and my eccentricities and secondly for their unique contributions to our remarkably diverse, supportive, funny, inspiring and sometimes dysfunctional lab family. None of us could have done any of this alone.

Finally, I would also like to acknowledge the support I have received over the last two years from the American Heart Association via a Predoctoral Fellowship Award.

MICROFLUIDIC AND PAPER-BASED DEVICES FOR THE ANALYSIS OF RED BLOOD CELLS: IMPROVING THE QUALITY AND ACCESSIBILITY OF DIAGNOSIS, MONITORING AND TREATMENT FOR SICKLE CELL DISEASE

An Abstract

of a

Dissertation

Presented to

the Faculty of the Department of Biomedical Engineering

University of Houston

In Partial Fulfillment

of the Requirements for the Degree

Doctor of Philosophy

in Biomedical Engineering

by

Nathaniel Z. Piety

May 2017

ABSTRACT

Sickle cell disease (SCD) is a common inherited blood disorder which gives rise to life-long health problems. Technologies capable of sensitive and specific early diagnosis of SCD as well as accurate quantification of HbS exist, but are expensive, complex, slow, laborious, and also require stable electricity, specialized equipment, and well trained technicians. Additionally, tools for quantifying stored RBC quality and selecting well-preserved RBC units for transfusion to vulnerable patients (e.g., chronically transfused individuals with SCD) are currently lacking. These limitations have largely prevented implementation of universal newborn screening programs in low-income, developing regions (e.g., sub-Saharan Africa) and have made it difficult for clinicians to personalize care for individuals with SCD even in high-income, developed countries.

In this dissertation, we engineered and validated several novel microfluidic and paper-based devices which address the limitations of existing technologies and thereby increase access to quality SCD care while enabling further understanding and optimization of transfusion medicine practices. First, we created a simple, rapid and equipment-free paper-based newborn SCD screening test capable of sensitive and specific detection of sickle hemoglobin (HbS) and SCD. Next, we made a rapid, low-cost paper-based assay for quantifying HbS in blood samples based on the color intensities of bloodstain patterns in paper, which showed high correlation and agreement with 'gold-standard' quantification methods. Then, we engineered a simple microfluidic device and associated image analysis algorithm capable of high throughput, automated analysis of stored RBC morphology – a potential metric for assessing the quality of stored blood and selecting well-preserved units for vulnerable patients. Finally, we used these novel devices, in combination with commercially available technologies and previously developed microfluidic devices, to quantify the impact of two novel RBC storage and rejuvenation techniques on stored RBC quality, as well as to quantify the effect of several physiologically relevant processes – i.e., RBC morphology, osmolality, aggregation and hematocrit – on overall blood rheology.

If adopted, these novel tools for diagnosis, monitoring and treatment optimization could drastically increase the quality and accessibility of SCD care for millions of affected individuals worldwide, in both high-income, developed countries and resource-limited, developing regions.

TABLE OF CONTENTS

LIST OF FIGURES

LIST OF TABLES

NOMENCLATURE

ACS	acute chest syndrome
AMVN	artificial microvascular network
ANOVA	analysis of variance
AS-1	additive solution 1
AS-3	additive solution 3
ATP	adenosine triphosphate
CI	confidence interval
CP2D	citrate phosphate double dextrose
CPD	citrate phosphate dextrose
CV	coefficient of variation
D	discocyte
D0	fresh discocyte
D40	40,000 molecular weight dextran
D70	70,000 molecular weight dextran
DI	deformability index
E1	echinocyte 1
E2	echinocyte 2
E3	echinocyte 3
EDTA	ethylenediaminetetraacetic acid
EI	elongation index
FT	filtration time
FN	false negative
FP	false positive
G	ghost
H_2O	water
Hb	hemoglobin

HbA	adult hemoglobin
HbAA	adult normal hemoglobin profile
HbAS	adult sickle cell trait hemoglobin profile
HBB	beta-globin gene
HbF	fetal hemoglobin
HbFA	newborn normal hemoglobin profile
HbFAS	newborn sickle cell trait hemoglobin profile
HbFS	newborn sickle cell disease profile
HbS	sickle hemoglobin
HbSS	adult sickle cell disease hemoglobin profile
Hct	hematocrit
HE	hemoglobin electrophoresis
HLA	human leukocyte antigen
HPLC	high performance liquid chromatography
HSA	human serum albumin
HU	hydroxyurea
I_C	mean color intensity center spot
IEF	isoelectric focusing
I_R	mean color intensity peripheral ring
IRB	institutional review board
K_2EDTA	double potassium ethylenediaminetetraacetic acid
LOD	limit of detection
LORRCA	laser optical rotational cell analyzer
MCH	mean corpuscular hemoglobin
MCHC	mean corpuscular hemoglobin concentration
MCV	mean corpuscular volume
MI	morphology index
MMCN	multiplexed microcapillary network

MW	molecular weight
NaCl	sodium chloride
NO	nitric oxide
NSAIDs	non-steroidal anti-inflammatory drugs
O_2	oxygen
PBS	phosphate buffered saline
PDMS	polydimethylsiloxane
PVC	polyvinylchloride
PVP	polyvinylpyrrolidone
RBC	red blood cell
S	spherocyte
SA	sodium salicylate
SCA	sickle cell anemia
SCD	sickle cell disease
SCT	sickle cell trait
SD	standard deviation
SE	sphero-echinocyte
ST	stomatocyte
ST1	stomatocyte 1
ST2	stomatocyte 2
TN	true negative
TP	true positive
V_{RBC}	red blood cell velocity
WBC	white blood cell
WCC	white blood cell count

CHAPTER 1 Introduction

Sickle cell disease (SCD) is a common genetic blood disorder which results in the production of abnormal sickle hemoglobin (HbS). Unlike normal adult hemoglobin (HbA), HbS polymerizes under low oxygen conditions, causing structural and functional abnormalities in affected red blood cells (RBCs). These abnormalities cause life-long health problems, exacerbate comorbidities and ultimately result in premature death. Early detection and initiation of prophylaxis is essential for preventing early childhood mortality due to SCD, and frequent monitoring in combination with chronic treatment is required to manage SCD symptoms throughout life. Importantly, because chronic RBC transfusion therapy is one of the most prevalent forms of treatment for SCD, individuals with SCD are also at a heightened risk for adverse side effects resulting from frequent transfusion, including alloimmunization and severe iron overload. While 'gold-standard' laboratory-based technologies capable of accurately detecting and quantifying HbS (e.g., high-performance liquid chromatography – HPLC; isoelectric focusing – IEF) have existed for many years, these technologies are expensive, complicated, slow, and require stable electricity, specialized equipment, and trained technicians. These limitations have largely prevented the implementation of universal newborn screening programs in low-income, developing regions (e.g., sub-Saharan Africa) due to incompatibilities of conventional paradigms with resource-limited clinical settings, and have made it difficult for clinicians to customize care for individual patients due to a lack of real-time information during treatment.

There are therefore several urgent unmet needs to be addressed with respect to the diagnosis, monitoring and treatment of SCD. First, there is a need for a newborn screening test for SCD that is inexpensive, portable, robust and simple enough to be operated by a healthcare worker, without specialized laboratory training or equipment, in a resource-limited clinical setting. Second, there is a need for an inexpensive, rapid assay capable of quantifying HbS in near-real-time, at the bedside during RBC transfusion therapy. Third, there is a need for tools capable of quantitatively assessing the quality of stored and/or rejuvenated RBCs in order to select only well-preserved RBC units for transfusion. And lastly, there is a need for technologies capable of assessing the impact of basic, physiologically relevant processes on overall blood rheology in order to inform transfusion practices and clinical decision making.

In this dissertation we describe the development and validation of novel microfluidic and paper-based technologies for the analysis of RBCs, which address these urgent needs for improving the diagnosis, monitoring and treatment of SCD. In Chapter 2 we provide a brief overview of the most important aspects of SCD pathophysiology as well as the current SCD diagnosis, monitoring and treatment practices. Chapters 2 – 7 describe the development, validation and use of specific technologies. In Chapter 8 we conclude with a brief summary. The specific objectives of Chapters 2 – 7 are described in detail below.

Objective 1: ***Engineer and validate a paper-based test capable of screening newborns for sickle cell disease.*** The best opportunity for detecting individuals with SCD in resource-limited settings is at the time of birth, before families leave the birthing center. We have previously developed a simple, low-cost, equipment- and electricity-free paper-based test capable of diagnosing SCD in adults and children older than six months of age, based on the characteristic pattern of blood stains formed in paper. However, the previous test was not sensitive enough to detect the presence of HbS in newborn blood samples – which typically contain 6.5 ± 2.8% HbS for sickle cell trait (SCT) and 10.2 ± 3.9% HbS for SCD. We designed a test which separated the lysis and deoxygenation steps of the previous test and utilized filtration to remove cellular debris, thereby sufficiently improving the limit of detection of the test to enable screening of newborns. The test was validated for a population of newborns (n = 160) with unknown SCD status at the obstetric center of the Primero de Maio hospital in Cabinda, Angola. The test was capable of detecting the presence of HbS with 81.8% sensitivity and 83.3% specificity, and identified SCD newborns with 100.0% sensitivity and 70.7% specificity.

Objective 2: ***Engineer and validate a paper-based assay capable of quantifying sickle hemoglobin concentration in blood samples from patients with sickle cell disease.*** The primary therapy for combating the most devastating complications of SCD is RBC transfusion, however frequent transfusion comes with the risk of negative side effects such as iron overload and alloimmunization. Thus, it is of extreme importance to judiciously monitor HbS concentration and RBC transfusion volume in order to effectively prevent complications of SCD while simultaneously minimizing the risk of adverse transfusion-related side effects. One of the key measurements used to guide chronic transfusion and hydroxyurea therapies for SCD is HbS concentration. We designed a simple, low-cost paper-based assay and associated image analysis algorithm capable of quantifying HbS in blood samples based on the relative color intensities of the center spot

(containing polymerized HbS trapped by the paper substrate) and the peripheral ring (containing other soluble forms of hemoglobin) of blood stains formed in paper. The assay was validated for a cohort of SCD patients (n = 88) receiving transfusion or hydroxyurea therapies. The assay showed high correlation ($R^2 = 0.86$) and strong agreement (standard deviation of difference = 7% HbS) with conventional hemoglobin electrophoresis (HE) measurements, which is sufficient to guide clinical decision making.

Objective 3: ***Engineer and validate a microfluidic device for high-throughput analysis of stored red blood cell morphology.*** During hypothermic storage RBCs accumulate damage and undergo echinocytosis, where the cells lose volume and surface membrane via vesiculation and become increasingly spiculated and spherical, resulting in an increasingly heterogeneous population of well and poorly preserved RBCs with different morphologies. We have previously shown that RBC shape, independent of other factors, is related to the ability of RBCs to perfuse an artificial microvascular network (AMVN) and is therefore an indicator of RBC quality as well as a potential metric for selecting well-preserved units for transfusion to vulnerable patients (e.g., frequently transfused individuals with SCD). Manual visual morphology analysis of RBCs in blood smears is slow, laborious and notoriously difficult to standardize. We designed a microfluidic device and associated image analysis algorithm capable of automating stored RBC morphology analysis. The microfluidic device, which requires no external instrumentation to drive flow, orients RBCs into a single, non-overlapping layer optimized for imaging which flows past the field of view of a microscope, enabling automated acquisition of high-quality images of a large number of RBCs without searching for 'good working areas' or manually refocusing the microscope. The image analysis algorithm then isolates individual RBCs from the background, extracts RBC metrics (e.g., cross-sectional area, form factor), then sorts the RBCs into morphology categories using a binary decision tree (or alternatively multiparameter cluster analysis) based on these metrics. We used the system to quantify the morphology and cell diameter of more than one million RBCs – the largest study of stored RBC morphology to date.

Objective 4: ***Use microfluidic tools to quantitatively assess the quality of stored and/or rejuvenated red blood cells.*** It is known that the quality of stored RBCs varies due to donor-to-donor variation and differences in storage duration and conditions. Storage and/or rejuvenation strategies which maximize the fraction of well-preserved RBCs within stored units are especially important for SCD patients because they are chronically transfused and are therefore exposed to numerous RBC units from different donors and blood

centers. Several approaches to improving the quality of stored blood have been proposed, including changes to the way blood is stored as well as rejuvenation solutions designed to recover the chemical and mechanical properties of RBCs after storage. We used multiple microfluidic devices – including an AMVN inspired by the layout of mesentery microvasculature, a multiplexed microcapillary network (MMCN) which challenges RBCs with constrictions narrowing from 5 to 3 μm in width, and the morphology analysis system described in Chapter 5, as well as commercially available ektacytometers – Laser Optical Rotational Cell Analyzer (LORRCA; Mechatronics Instruments) and RheoScan-D (RheoMeditech) – to quantify the properties of stored and/or rejuvenated RBCs. We performed a split-unit (n = 9) comparison study over the course of 6 weeks of hypothermic storage and showed that storage under anaerobic conditions decreased the rate of RBC rheological property degradation; additionally we showed that the microfluidic devices were more sensitive to changes in RBC properties than the commercially available ektacytometers. Additionally, we used the AMVN to show that stored RBCs washed in a 1% human serum albumin (HSA) solution recovered their ability to perfuse the AMVN at higher rates.

<u>Objective 5:</u> Use microfluidic tools to elucidate how physiologically relevant processes impact their rheological properties of red blood cells. The AMVN microfluidic device described in Chapter 6 is a versatile tool which enables controlled, reproducible investigation of rheology in a biologically-relevant model inspired by the microcirculation. The AMVN challenges RBCs with cell-cell interactions, cell deformation through constrictions of various dimensions, and a range of shear stresses. First, we used the AMVN to show that changes in RBC shape (induced via treatment with different concentration of sodium salicylate), independent of any other factors, altered the ability of RBCs to perfuse the AMVN. Next, we used the AMVN to show that, despite significant changes in RBC morphology and deformability in response to changes in suspension osmolality from 179 – 423 mOsm/kg H_2O, AMVN perfusion rate varied less than 10% from its highest value at isosmotic conditions. We also used the AMVN to show that, while the presence or absence of RBC aggregation (induced via suspension in aggregating and non-aggregating mediums of equal viscosity) did not alter AMVN perfusion rate, the presence of RBC aggregation increased capillary hematocrit, suggesting that aggregation may increase the overall oxygen transport capacity of blood. Finally, we used the AMVN to show that the optimal hematocrit – i.e., the hematocrit at which oxygen transport effectiveness is maximized – is dependent on the pressure differential applied across the AMVN.

CHAPTER 2 General background

2.1 Sickle cell disease

2.1.1 Overview

Sickle cell disease (SCD) is an inherited blood disorder which affects hemoglobin (Hb). Unlike normal adult Hb, sickle hemoglobin (HbS) deforms and polymerizes under low oxygen conditions, forming long, rigid fibers which cause structural and functional abnormalities in affected red blood cells (RBCs).[1] These abnormalities lead to life-long SCD-specific morbidities, complicate numerous comorbidities and ultimately result in premature death. SCD affects millions of individuals worldwide, with approximately 300,000 individuals with SCD born each year and with the majority of affected births occurring in sub-Saharan Africa, South America, Central America, southern Asia, the Mediterranean basin and Saudi Arabia.[2,3] Children under 5 years of age are at a particularly high risk of death due to opportunistic infections associated with SCD.[4] The severity of SCD varies greatly from person to person, but for individual SCD patients the rate of adverse events, such as vaso-occlusive crisis or stroke, is strongly correlated with intraerythrocytic HbS concentration. The frequency and severity of these adverse events can be reduced by maintaining an intraerythrocytic HbS concentration below a target value (typically below 30%).[5,6] As such, the early detection and accurate quantification of HbS are essential for providing high quality treatment of SCD.[4,6] The following chapter provides a brief general background covering the aspects of SCD pathophysiology and of the current state of the art for diagnosing, quantifying and treating SCD which are necessary for putting the research described in this dissertation in context.

2.1.2 Pathophysiology

Genetics

Sickle cell disease is a recessively inherited hemoglobinopathy which results from a single nucleotide mutation (i.e., adenine to thymine; GAG to GTC; glutamic acid to valine) of the β-globin gene (HBB) encoding the beta-globin protein chain subunits which make up hemoglobin.[7] Sickle cell disease follows the classic autosomal recessive pattern of inheritance. If a single copy of the gene coding for sickle

hemoglobin (HbS) and single copy of the gene coding for normal adult hemoglobin (HbA) are inherited (i.e., heterozygous; HbAS), the resulting condition is termed sickle cell trait (SCT).[7] Individuals with SCT typically have HbS concentrations of 20-40% and are generally non-symptomatic, except in extreme cases of overexertion or oxygen deprivation, but are carriers of the sickle gene and have a chance of having children with SCT and/or SCD.[1,6,8] If two copies of the gene coding for HbS are inherited (i.e., homozygous; HbSS), the resulting condition is termed sickle cell anemia (SCA) – the main form of sickle cell disease (approximately 70% of cases).[6,9] Those with sickle cell disease typically have HbS concentrations of 60-100%, are symptomatic and require clinical care to manage symptoms.[1,3] Other forms of sickle cell disease occur when an individual inherits one copy of the gene coding for HbS in conjunction with another gene coding for a different aberrant form of hemoglobin – such as $Hb\beta^{+}$, $Hb\beta^{0}$, HbO-Arab, HbD Punjab, HbC, HbC Harlem, or HbS Antilles.[3,10] The typical HbS concentration ranges and degrees of symptoms of these other varieties of SCD vary by disease type as well as between individuals with the same disease type, with lower HbS concentrations typically associated with lower incidences of adverse events.[6] Those with these other forms of SCD are also carriers of the sickle gene and therefore may also potentially have offspring with SCT and/or SCD. Sickle cell anemia (SCA; HbSS) accounts for approximately 70% of all cases of SCD and is one of the most severe forms of SCD, therefore for the purposes of this dissertation when we say sickle cell disease we refer only to the main form of sickle cell disease – sickle cell anemia – unless otherwise indicated.

Sickle hemoglobin

Hemoglobin (Hb) is the iron-containing protein found in human red blood cells (RBCs) which enables transport of oxygen from the lungs to tissues and organs throughout the body. Normal adult hemoglobin (HbA) is composed of two alpha- and two beta-globin protein chain subunits which contain iron-based heme groups.[7] Sickle hemoglobin (HbS) is an aberrant form of normal adult hemoglobin resulting from a point mutation of the β-globin gene (HBB). This point mutation of HBB occurs at codon 6 (codon 7 if start codon is counted) of chromosome 11 and results in the replacement of glutamic acid with valine, which, importantly, is hydrophobic.[1,7] Under oxygenated conditions, this replacement does not result in any significant changes to Hb structure or function, but under low oxygen conditions deoxy-Hb exposes a

hydrophobic region which is attracted to the hydrophobic region introduced by valine in HbS. This attraction between hydrophobic regions causes multiple HbS molecules to stick together and form long polymers under low oxygen conditions (**Fig. 2.1.1**; reproduced with permission from Bunn[1] Copyright Massachusetts Medical Society). These long rod-like HbS polymers cause red blood cells to deform and assume characteristic sickle shapes.

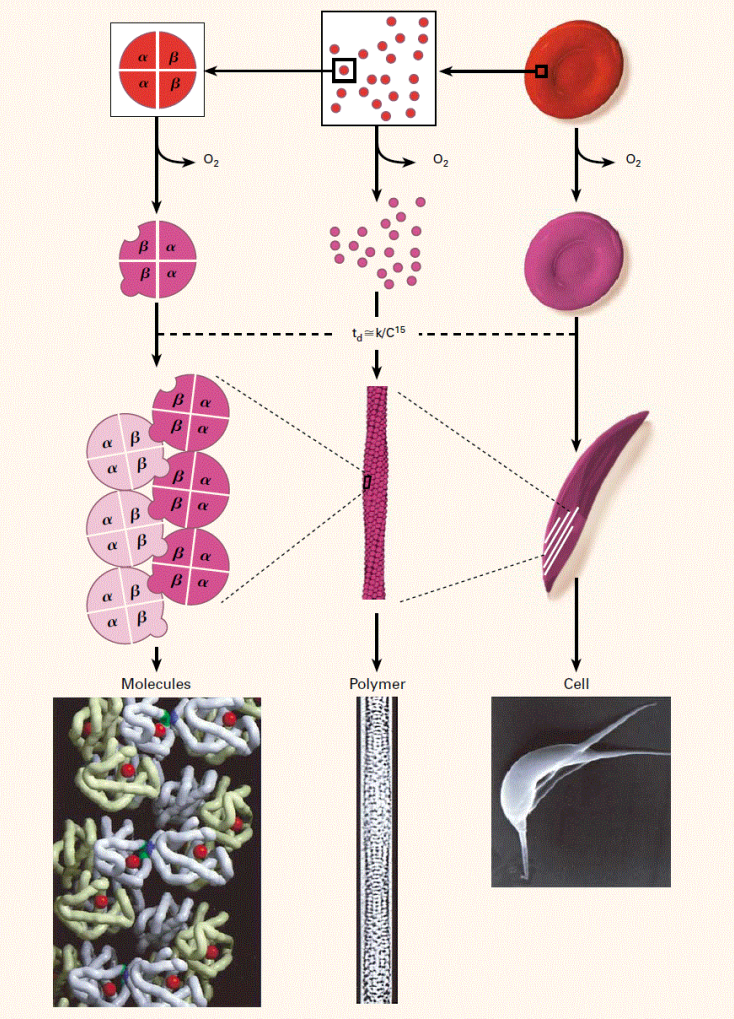

Figure 2.1.1 Schematic illustration of sickle hemoglobin polymerization at the molecular, polymer and cellular level.

Sickle red blood cells

Healthy, normal human red blood cells (RBCs; erythrocytes) are anucleated, flexible biconcave discs with diameters of 6 to 8 μm and thicknesses of 2 to 2.5 μm (**Fig. 2.1.2**; reproduced from Bessis[11]). RBCs with this characteristic morphology (discocytes) have high ratios of cell membrane to cell volume.

This high surface area to volume ratio enables normal, discocytic RBCs to deform and pass through microcapillaries with diameters that are much smaller than the RBCs themselves (as small as 2 to 3 micrometers in diameter).[12] The long, rigid polymers formed by deoxy-HbS aggregates cause affected RBCs to deform into characteristic sickle shapes (**Fig. 2.1.3**; reproduced from Bessis[11]).[1] Sickle-shaped RBCs are both less deformable and more fragile than normal discocytic RBCs.[13] Because deoxygenated sickle RBCs cannot deform to the same extent as healthy normal RBCs, they are more likely to become stuck in microcapillaries under hypoxic conditions, particularly at vessel constrictions, contortions and bifurcations.[6] The structural and functional abnormalities of sickle RBCs also make them more likely to undergo intravascular lysis as they travel throughout the circulator system.[1,13] Additionally, the spleen senses the decreased deformability of sickle RBCs and retains them, leading to an increased rate of RBC destruction.[12] The high levels of lysis and destruction of sickle RBCs result in chronic hemolytic anemia (from which sickle cell anemia derives its name). Hb released into the circulation via hemolysis contributes to inflammation and endothelial cell dysfunction.[6] Of note, non-homozygous recessive forms of sickle cell disease are not all characterized by this type of hemolytic anemia.[10]

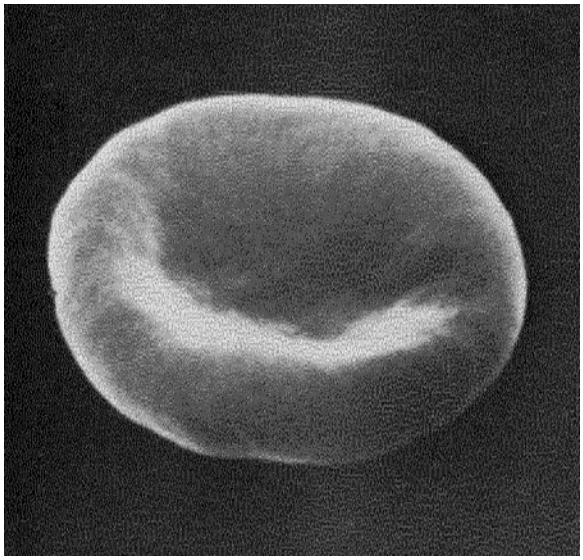

Figure 2.1.2 Characteristic scanning electron microscope image of a human red blood cell with normal discocytic morphology.

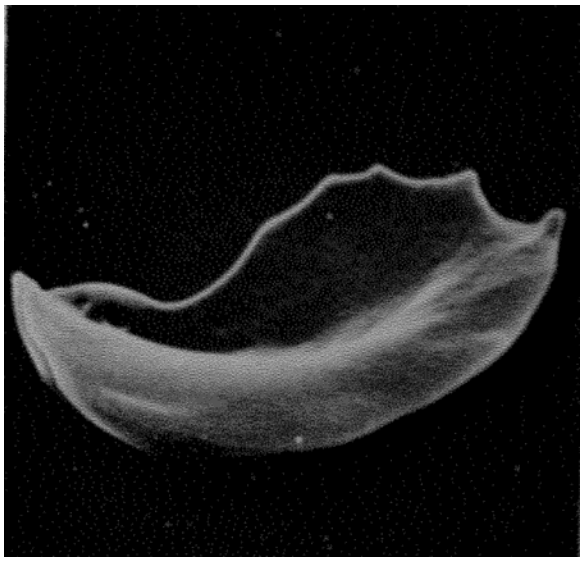

Figure 2.1.3 Characteristic scanning electron microscope image of a human sickle red blood cell.

Pathogenesis and clinical outcomes

During gestation, 90-95% of all hemoglobin molecules produced are fetal hemoglobin (HbF), which is unaffected by the sickle mutation. Hemoglobin production switches from fetal to predominantly adult variants after 34-36 weeks of fetal development, with individuals reaching typical adult expression profiles by age 8-12 months.[14,15] At birth, the cord blood of normal healthy newborns contains 14.3 ± 5.3% HbA, while the blood of SCT carriers contains 9.5 ± 4.2% HbA and 6.5 ± 2.8% HbS, and the blood of those with SCD contains 10.2 ± 3.9% HbS.[16] Fetal hemoglobin is known to inhibit HbS polymerization and provide a protective effect against SCD. As a result, young children with SCD do not typically experience adverse vaso-occlusive events characteristic of SCD before hemoglobin production reaches adult levels. However, children with SCD remain highly susceptible to opportunistic bacterial infection and sepsis.[6]

The abnormal structural and functional properties of sickle RBCs result in increased interaction between RBCs and vascular endothelial cells as well as increased intravascular RBC lysis.[1] This persistent lysis of RBCs results in a chronically lower than normal hematocrit which prevents organs and tissue from receiving adequate oxygenation. Individuals with SCD experience many of the typical symptoms of hemolytic anemia.[1,6] Intravascular lysis of sickle RBCs also increases free iron levels, which increases susceptibility to infection, generates reactive oxygen species, and can contribute to iron overload – especially in patients receiving chronic RBC transfusion.[17] The decreased deformability and increased degree of RBC

membrane-endothelium interaction of sickle RBCs can cause episodic occlusion of blood vessels in the microcirculation, leading to tissue ischemia. Blood vessel blockage by rigid sickle RBCs and subsequent ischemia-reperfusion injury are the underlying causes of many of the acute and chronic adverse clinical outcomes associated with SCD.[1,6,7]

Individuals with SCD experience both acute and chronic pain. Acute painful crises can occur when deoxygenated sickle RBCs obstruct capillaries and prevent blood from reaching organs and tissues, resulting in ischemia, necrosis, organ damage and extreme pain.[1] Stroke is one of the most serious complications of vaso-occlusion in SCD. In addition to overt stroke, vaso-occlusion in the brain can cause so called 'silent' strokes which are not outwardly obvious but are associated with neuropsychological deficits and impaired cognitive performance.[18,19] A subset of these vaso-occlusive painful crises present as acute chest syndrome (ACS).[20] In ACS, pain presents in the chest and is accompanied by pulmonary infiltrate, fever, hypoxia, cough and respiratory problems.[13] Importantly, the pulmonary symptoms of acute chest syndrome result in decreased oxygen levels and therefore have an exacerbating effect on polymerization of deoxy-HbS. Sickle cell crises can also manifest as aplastic crises where the degree of anemia acutely increases due to cessation of RBC production. Rapid decreases in the number of RBCs in blood (i.e., hematocrit) can result in fatigue, weakness, shortness of breath, confusion, thirst and pallor.[13]

SCD can also result in chronic pain, progressive organ dysfunction and organ failure. Repeated ischemia-reperfusion insults increasingly damage organs over time, ultimately leading to organ failure if sickle hemoglobin is not maintained at sufficiently low levels. Specifically, the spleen often becomes blocked by poorly deformable sickle RBCs, leading to splenomegaly and failure within the first several years of life for individuals with sickle cell disease.[14] Over time this cycle of vaso-occulsion, ischemia-reperfusion injury and hemolytic anemia can also result in chronic inflammation, hypercoagulability and generalized vascular dysfunction.[5,6] The chronic hemolytic anemia associated with SCD also predisposes individuals to ulceration, cholithiasis, priapism and pulmonary hypertension. Even with early diagnosis and intervention, the chronic anemia, ischemia, organ dysfunction and vascular dysfunction characteristic of individuals with SCD result in premature death.[14] The median age at death for individuals with SCD in the United States was 38 years for males and 42 years for females as of 2005.[21]

2.1.3 Diagnosis and monitoring techniques

High-performance liquid chromatography

High-performance liquid chromatography (HPLC) is a quantitative technique which uses the differences in attraction between various forms of hemoglobin (e.g., HbA, HbS, HbF, HbC) and an adsorbent material to separate, identify and quantify the types of hemoglobin present in a blood sample.[16] To perform a measurement using HPLC, hemoglobin is suspended in a mixture of solvents and pumped through a column of porous adsorbent material at high pressure. Different forms of hemoglobin are attracted to the adsorbent material to different degrees and therefore take different amounts of time to pass through the column. Forms of hemoglobin with weak attraction to the adsorbent material pass through the column more quickly, while forms of hemoglobin with strong attractions to the adsorbent material take longer to pass through the column.[22] The different flow rates of different forms of hemoglobin through the column separates the hemoglobin into groups which exit the column at different times. The amount of hemoglobin exiting the column is measured continuously over time, providing a quantitative assessment of the concentrations of each form of hemoglobin present in the sample as it exits the column.[16] HPLC is typically limited to centralized clinical laboratories in resource-rich regions because it requires electricity, specialized equipment, expensive materials and reagents and trained technicians to perform.[23] At the time of this writing, HPLC is widely considered to be the 'gold standard' method for diagnosing SCD and monitoring HbS concentration.

Hemoglobin electrophoresis and isoelectric focusing

Hemoglobin electrophoresis (HE) is an application of standard gel electrophoresis which uses the differences in charge between various forms of hemoglobin to semi-quantitatively determine the types and relative amounts of hemoglobin present in a blood sample.[24] Applying an electric current across a two-dimensional porous agarose gel causes hemoglobin to migrate through the gel from the cathode to the anode. The speed with which different forms of hemoglobin move through the agarose gel depends on the charge of the hemoglobin molecules. Different forms of hemoglobin are separated into bands within the gel due to the different speeds of their travel (**Fig. 2.1.4**). Densitometric scanning of the resulting bands can be used to semi-quantitatively calculate the percentages of various forms of hemoglobin present in the sample.[24] Like

HPLC, hemoglobin electrophoresis requires specialized equipment and materials as well as electricity and trained technicians.[23] However, recent innovations have enabled the process to be performed accurately in both capillaries and in microfluidic devices, providing potentially easier-to-use and lower-cost alternatives to traditional methods.

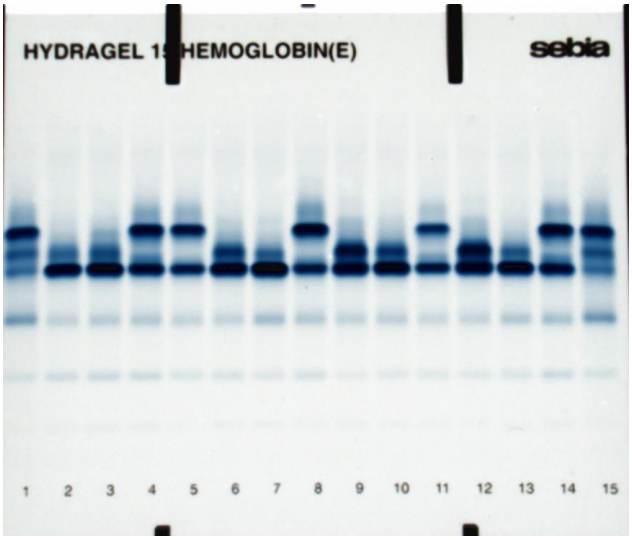

Figure 2.1.4 Characteristic image of the bands formed by various forms of hemoglobin (from top to bottom: HbA, HbF, HbS, HbA2/C) in an agarose gel after performing hemoglobin electrophoresis on blood samples.

Isoelectric focusing (IEF) is a form of electrophoresis, similar to hemoglobin electrophoresis, which uses the differences in the isoelectric points between various forms of hemoglobin to semi-quantitatively determine the types of hemoglobin present in a blood sample.[25] Isoelectric point refers to the pH at which a molecule has no net electrical charge. By applying an electric current to hemoglobin loaded into a porous gel which contains a pH gradient along the same axis as the electric current, the hemoglobin migrates through the gel in the direction of the cathode to the anode and comes to rest at the position where the pH results in no net charge for the hemoglobin molecule. The positions at which different forms of hemoglobin come to rest in the gel depends on the charge of the hemoglobin molecules. As such, different forms of hemoglobin are separated into distinct bands within the gel due to their different isoelectric points.[26] Absorbance scanning of the resulting gel can be used to semi-quantitatively calculate the percentages of various forms of hemoglobin present in the sample. IEF also requires specialized equipment and materials as well as electricity and trained technicians.[23] Most HE and IEF machines are inexpensive compared to HPLC machines, and

several low-cost HE and IEF machines are commercially available. HE and IEF are used in clinical laboratories for the diagnosis of SCD as well as in many research laboratories for the identification and quantification of hemoglobin. Pilot SCD screening programs which utilize IEF have been implemented in some resource-limited clinical settings of developing regions such as sub-Saharan Africa.[4] However, IEF remains prohibitively complex and expensive for most clinics in developing regions with the highest incidence of SCD.

Sickle hemoglobin solubility assay

Solubility-based methods utilize the difference in solubility of deoxygenated HbS and other forms of hemoglobin to detect HbS. HbS polymerizes and becomes insoluble in high osmolality solutions when deoxygenated, while normal adult hemoglobin remains soluble under the same conditions.[27] To perform this technique, whole blood is added to a hemoglobin solubility buffer containing agents which lyse RBCs and deoxygenate freed Hb. The turbidity (i.e., cloudiness) of the mixture is then evaluated by eye, with a highly turbid appearance indicating the presence of insoluble HbS.[28] Solubility-based assays for HbS are not quantitative and cannot distinguish between individuals with SCT and individuals with SCD; solubility-based tests are only capable of determining whether any HbS is present. Numerous conditions – including malaria, hyperlipidemia, malnutrition and pregnancy – can alter the turbidity of the hemoglobin solubility buffer and whole blood mixture, causing false positive results.[27] Additionally, the limit of detection of solubility-based assays is not sufficiently low to detect newborn levels of HbS, and as such solubility assays cannot be used to perform newborn screening for SCD.[16] Solubility assays are relatively low-cost (<$10 per test) and do not require any specialized equipment, electricity or trained technicians, so they are practical for use in resource-limited settings, but have limited clinical utility due to the limitations described above.[23,27] Solubility assay are typically used as a primary screen for SCD with positive results indicating the need for testing using more accurate laboratory-based methods.

Approaches currently under development

In addition to the research described in this dissertation, several other novel technologies for SCD diagnosis and monitoring are currently under development by other groups. An aqueous multi-phase system

which exploits the difference in density between normal and sickle RBCs is currently being developed. However, this approach is not quantitative, requires centrifugation (i.e., requires equipment and electricity) and cannot distinguish between normal individuals and individuals with SCT.[29,30] Methods based on differences in hemolysis between normal and sickle RBCs,[31] a magnetic levitation-based smartphone platform,[32] and lower-cost implementations of conventional laboratory methods,[33-35] have been proposed and are currently under development, but require further validation to determine their feasibility, relative clinical utility and cost effectiveness. Finally, rapid diagnostic tests for SCD based on conventional lateral flow immunoassay technology are currently being developed. These lateral flow assays are instrument- and electricity-free and show much potential, but may not be significantly less expensive than other approaches because they rely on proprietary antibodies.[36-38]

2.1.4 Treatment

Prophylaxis

Individuals with SCD are at increased risk for infection and sepsis due to chronic intravascular RBC lysis and associated hemolytic anemia. Prophylactic penicillin has been shown to be an effective means of reducing mortality from pneumococcal sepsis in infants with SCD.[39] Conjugated pneumococcal vaccines and influenza vaccines are also especially important prophylactic precautions for individuals with SCD.[39,40] In regions where malaria is endemic, it is also recommended that individuals with SCD receive daily malaria prophylaxis. Folic acid supplements, which aids in hemoglobin production, are also recommended to counteract anemia. Mosquito nets and parental education have also been shown to be effective means of preventing adverse events related to SCD.[4]

Acute care

SCD can present with severe acute symptoms, most notably in cases of vaso-occlusive crisis, aplastic crisis and acute chest syndrome. Severe acute symptoms often require hospital admission and analgesic administration to prevent patient suffering and potential escalation of symptoms.[6] Degree of pain and duration of crisis vary significantly between patients and for individual patients over time. Typically non-opioid pain medication in combination with an adjuvant is appropriate for treating mild pain, while

opioid pain medication and adjuvant(s) are recommended for treating severe pain.[41] Non-steroidal anti-inflammatory drugs (NSAIDs), alone or in combination with opioids, are recommended for mild to moderate acute painful crises. However, NSAIDs are not appropriate for patients with known liver failure and should be used with caution in patients with asthma, peptic ulcers, renal failure or clotting problems.[42] Morphine and diamorphine are the most commonly prescribed drugs used to treat severe acute painful crises in SCD.[5] All precautions typically taken when prescribing opioids should be followed when using opioids to manage pain in sickle cell disease. Prophylactic administration of antibiotics and anticoagulants is also recommended during the management of acute painful crises.[43] Supplemental oxygen, acute blood transfusion and fluid replacement theory have also been shown to be effective techniques for managing acute painful crises.[44]

Hydroxyurea therapy

At the time of this writing, hydroxyurea (HU; also known as hydroxycarbamide) is the only drug approved for treatment of SCD.[45,46] Hydroxyurea was initially approved in 1967 for the treatment of neoplastic diseases, specifically solid tumors, and has since been used for the treatment of chronic myelogenous leukemia, psoriasis, melanoma, polycythemia vera and recurrent, metastatic or inoperable carcinoma of the ovary.[46] Hydroxyurea acts primarily by inhibiting ribonucleotide reductase activity which interrupts DNA replication as well as the repair of damaged DNA, however the full mechanism of action of HU is incompletely understood.[45,47] Hydroxyurea is used to treat SCD because it has been shown to suppress erythroid precursor maturation in the bone marrow and thereby induce increased production of fetal hemoglobin (HbF).[48,49] Increased HbF production dilutes the relative concentration of sickle hemoglobin present within RBCs, which decreases the likelihood of RBC sickling under low oxygen conditions. HbF is also known to directly inhibit the formation of HbS polymers. In addition to increasing the production of fetal hemoglobin, hydroxyurea increases the water content of red blood cells, decreases patient neutrophil count, and modulates RBC adhesion the endothelium.[50] Hydroxyurea therapy requires frequent monitoring of HbS concentration to assess therapy efficacy – i.e., to ensure that relative HbS concentration is maintained below the target therapeutic value at the current HU dosage. Several studies have demonstrated the long term efficacy of HU as a therapy for SCD.[51,52] HU therapy is a promising, accessible alternative to blood

transfusion therapy for regions which currently lack the infrastructure for safe blood banking and transfusion practices.

Blood transfusion

Chronic blood transfusion is one of the most widespread and effective treatments for SCD. Transfusion of normal healthy RBCs directly decreases the relative concentration of sickle RBCs via dilution and thereby reduces the fraction of RBCs in the circulation which are prone to hemolysis and sickling under hypoxic conditions.[53,54] Simple transfusion consists of the infusion of RBCs from a donor into the SCD patient without the removal of patient blood and is typically less than or equal to 300 mL in volume.[55,56] Whereas exchange transfusion consists of the infusion of RBCs from a donor paired with the removal of the patients own red blood cells via apheresis and is typically more than 300 mL in volume. The primary goals of chronic RBC transfusion therapy are to: (i) increase overall Hb concentration ([Hb]) to improve the oxygen-carrying capacity of blood; (ii) dilute HbS concentration (to <30%) to decrease the viscosity and increase the oxygen saturation of blood; and (iii) increase tissue oxygenation to suppress the occurrence of sickle RBCs and prevent chronic organ damage.[53,54,57] Chronic transfusion therapy can be used as a means of treating and/or preventing recurrent stroke, primary stroke, complicated pregnancy, chronic renal failure, frequent pain crisis, recurrent acute chest syndrome, priapism, pulmonary hypertension and leg ulcers. Acute RBC transfusion can be used as a means of treating symptomatic anemia, aplastic crisis, splenic or hepatic crisis, stroke, acute chest syndrome, multi-organ system failure and severe infection.[58] In current clinical practice, transfusion frequency and volume are typically determined empirically based on patient [Hb], body weight and clinical condition, and are not based on direct measurement of patient HbS concentration. As a result, SCD patients receiving RBC transfusions may not necessarily receive optimal volumes of RBCs for maintaining HbS concentrations below 30% and simultaneously minimizing risks of adverse side effects of over-transfusion.

Individuals receiving frequent RBC transfusions – e.g., SCD patients on chronic transfusion therapy regimens – are at risk of developing transfusion-related iron overload as well as alloimmunization to RBC blood group antigens.[17] SCD patients receive blood transfusions more frequently and over longer periods (i.e., lifelong transfusion regimens) than almost any other group of patients. Over time, SCD patients receiving frequent transfusions become sensitized to an increasing number of minor and variant blood group

antigens from different donors, despite donor and patient blood type cross-matching.[59] This increasing sensitization over time limits the potential RBC donor pool and increases the risk of hemolytic transfusion reactions.[60] It is of extreme importance to transfuse SCD patients with only the highest quality, most well-preserved RBCs available, so as to limit hemolytic transfusion reactions, sensitization and iron overload. RBCs progressively accumulate damage during hypothermic storage, resulting in heterogeneous populations of well and poorly preserved cells within individual blood units.[61] The properties of stored blood units are known to vary significantly due to natural donor to donor variability and differences in storage conditions and duration.[62] Poorly-preserved, irreparably damaged RBCs are known to not survive longer than 24 hours following transfusion, and therefore may provide little therapeutic benefit while instead directly contributing to iron overload via intravascular lysis.[63] However, in current clinical practices RBC quality is not routinely assessed prior to transfusion; instead, RBC units are given an expiration date of 42 days (6 weeks) from the time of donation and are considered safe for transfusion up until that date. The relationship between RBC unit age and patient outcomes – in SCD as well as other conditions – remains an area of intense debate in the clinical community.[64-69] RBC transfusion requires a safe pool of donor blood as well as stable infrastructure for RBC collection, processing and storage. These requirements currently prevent the use of RBC transfusion therapy in resource-limited settings such as in sub-Saharan Africa where the incidence of SCD is highest.

Bone marrow transplant

The transplantation of hematopoietic stem cells from donors with identical human leukocyte antigen (HLA) typing has been shown to cure a number of nonmalignant hematologic disorders including aplastic anemia, beta-thalassemia, metabolic problems, congenital immunodeficiency disorders and SCD.[70] HbS is produced in the bone marrow of individuals with SCD due to a mutation of the HBB gene which codes for the beta globin protein chain subunits which make up hemoglobin. This underlying source of pathology in SCD – HbS – can be eliminated by replacing bone marrow from an individual with SCD with compatible hematopoietic stem cells from healthy donors known to produce normal adult hemoglobin.[71] Patients with SCD who have not previously undergone chronic transfusion therapy and who do not already have severe complications related to SCD (e.g., organ damage, chronic inflammatory disease) are optimal candidates for bone marrow transplantation as a cure for sickle cell disease.[72] Patients with SCD receiving bone marrow

transplants are at risk for infection, rejection, graft-versus-host disease and hemorrhage.[73] Patients must be HLA-A, HLA-B and HLA-DR compatible in order to avoid potential graft rejection – with most compatible donors being closely related siblings.[70] It is not uncommon to be unable to identify a compatible donor, and even when a compatible donor is available the technical complexity of the transplant procedure limits its use to resource-rich hospital settings and precludes use in resource-limited settings such as sub-Saharan Africa where the incidence of SCD is highest. Bone marrow transplants are currently the only known cure for SCD, however novel gene therapies aimed at correcting the underlying mutation responsible for SCD are currently being developed and validated.[74]

CHAPTER 3 Engineering and validating a paper-based test capable of screening newborns for sickle cell disease

3.1 Paper-based newborn SCD screening test

The following research has previously been published and much of the following text is reprinted with permission from: Scientific Reports, 7, Piety NZ, George A, Serrano S, Lanzi MR, Patel PR, Noli MP, Nirenberg D, Camanda JF, Airewele G, Shevkoplyas SS, "A Paper-Based Test for Screening Newborns for Sickle Cell Disease," Article number 45488, Copyright 2017 The Author(s).

3.1.1 Introduction

Universal newborn screening, in combination with early intervention for affected infants, has nearly eliminated early childhood mortality due to sickle cell disease (SCD; HbSS) in high-income developed countries.[39,40,75] In contrast, a majority of children born with SCD in low-income developing countries die before the age of 5 due to lack of early diagnosis and comprehensive care.[2,76] Recent estimates suggest that implementation of wide-spread screening and follow-up care in countries affected most by the disease (e.g., Nigeria, Democratic Republic of the Congo, India) could save the lives of nearly 10 million children by 2050.[77] Data from pilot screening and treatment programs in sub-Saharan Africa demonstrate >95% survival for affected infants enrolled in inexpensive follow-up care, such as penicillin prophylaxis, pneumococcal immunizations, malaria bed nets, and family education about the disease.[4]

The major barriers limiting the expansion of these highly successful pilot screening programs are the high cost and technical complexity of conventional diagnostics methods (e.g., HPLC, high-performance liquid chromatography[22], or IEF, isoelectric focusing electrophoresis[26]), and their dependence on specialized equipment, stable infrastructure and well-trained laboratory personnel.[2,76,78] Because of these limitations, newborn screening for SCD remains confined to only a few specialized clinical laboratories in major population centers, almost entirely missing the majority of all births occurring out of hospital.[4,79,80] Importantly, the results of screening with conventional laboratory methods are rarely available before postnatal discharge, reducing the all-important follow-up rate to as low as 50% of identified newborns.[4,79]

There is therefore an urgent need for a screening test that is sufficiently inexpensive, portable, simple and rapid enough to enable universal screening of newborns for SCD in resource-limited settings lacking established infrastructure, specialized equipment or trained personnel.

We have previously described the development and clinical validation of a rapid, low-cost paper-based diagnostic test for SCD that permits the diagnosis of adults and children older than 6 months of age.[81-83] We now describe a test based on the same principles which is optimized to detect the low levels of sickle hemoglobin (HbS) present in the blood of newborns, allowing the direct screening of newborns for SCD and sickle cell trait (SCT; HbAS). We also report on the feasibility and diagnostic accuracy of the paper-based newborn test as performed by local health workers in a resource-limited clinical setting in Cabinda, Angola.

3.1.2 Methods

Study design and participants

All experimental protocols involving human blood samples were approved by the institutional review boards at the Universidade Onze de Novembro Medical School (Cabinda, Angola), Baylor College of Medicine (Houston, USA) and University of Houston (Houston, USA). Informed consent was obtained from all subjects. All experiments were performed in accordance with guidelines and regulations established by the University of Houston, Baylor College of Medicine and the U.S. Department of Health and Human Services for the protection of human study subjects. After obtaining informed consent from the newborns' mothers, local health workers collected blood samples from newborns at the obstetric center of the Primero de Maio hospital in Cabinda. Eligibility criteria included gestation of greater than 30 weeks and uncomplicated delivery (judged by local clinical staff). Samples were collected from n = 160 newborns, a convenience sample. We successfully screened 160 newborn samples with the paper-based test, and performed successful IEF testing on 159 of these samples (**Fig. 3.1.1**).

Blood sample collection, storage, and processing

For initial development of the paper-based newborn SCD screening test, blood samples were collected from SCD (HbSS) patients at the Texas Children's Hematology Center and from healthy volunteers (HbAA) into Vacutainer vials (K_2EDTA, BD Diagnostics, USA) using standard venipuncture technique.

Samples were stored at 4°C until use. Artificially reconstituted samples with a range of HbS levels were created by mixing ABO/Rh-matched, equal-hematocrit HbAA and HbSS blood samples at various ratios.

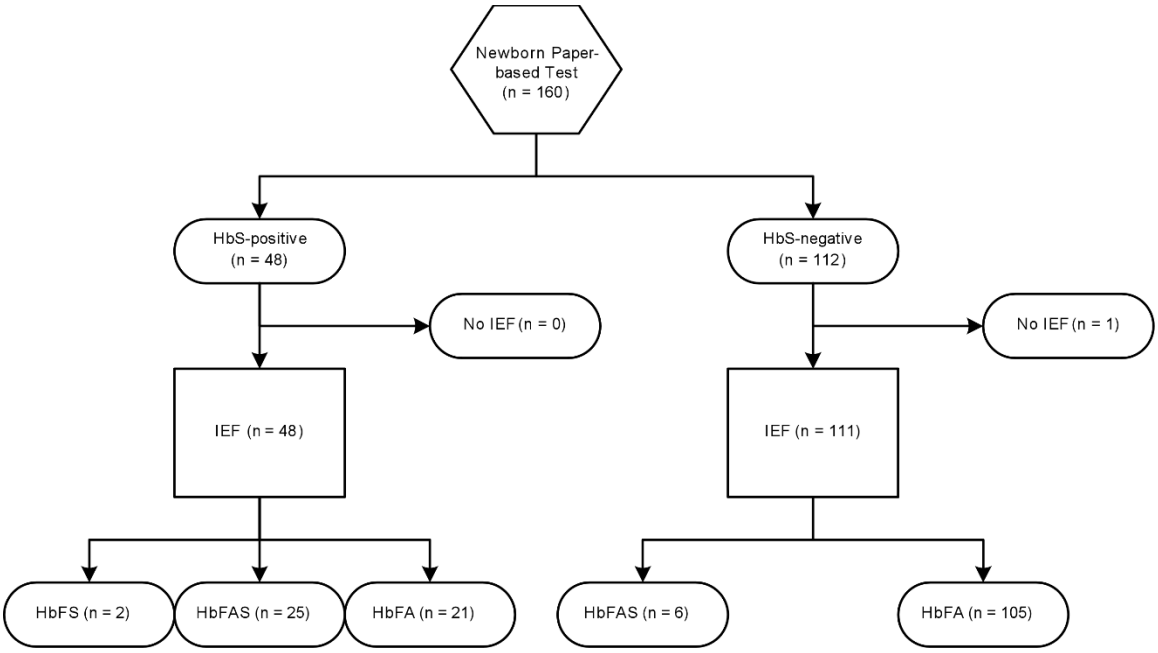

Figure 3.1.1 Classification flowchart for newborn samples evaluated with the paper-based SCD newborn screening test and isoelectric focusing (IEF).

For test validation in Cabinda, blood samples were collected from newborns by heel-stick onto blood collection cards (Whatman 903 Protein Saver Card, GE Healthcare, USA) and into capillary blood collection tubes (Microvette, K_2EDTA, Sarstedt AG & Co, Germany). Eluted dried blood spot samples were tested with isoelectric focusing (IEF) following existing standard operating procedures.[4] Liquid blood samples were refrigerated and used to perform the paper-based test within 7 days of collection. For all patients, the paper-based test was completed before IEF analysis. Local health workers interpreted the results of the paper-based test visually, using reference images of HbS-positive and HbS-negative bloodstains.

Statistical analysis

Mean, standard deviation, p-values, and confusion matrices were calculated using built-in functions in MATLAB 2014b (The Math Works Inc., Natick, MA). 95% confidence intervals (CI) were calculated using the Wilson method.[84] Fleiss' kappa calculations were performed to determine inter-operator agreement

for visual scoring of bloodstains.[85] Performance metrics were calculated as: sensitivity = TP / (TP + FN); specificity = TN / (FP + TN); positive predictive value = TP / (TP + FP); negative predictive value = TN / (TN + FN); and accuracy = (TP + TN) / (TP + FP + TN + FN); where TP = true positive, FP = false positive, TN = true negative and FN = false negative.

3.1.3 Results

Design and operation of the paper-based newborn screening test

The design and operation of a paper-based SCD test capable of diagnosing SCD in adults and children older than 6 months have been described previously in detail (**Fig. 3.1.2a**).[81-83] When evaluated visually, the limit of detection (LOD) for the *adult* test was about 15% HbS,[83] which was insufficient for detecting the very low percentages of HbS typically found in newborn samples – 6.5 ± 2.8% for SCT (HbFAS) and 10.2 ± 3.9% for SCD (HbFS).[16] The reason for the relatively high LOD was the faint center spot in the center of the stain formed by cellular debris of lysed red blood cells even in the complete absence of any HbS (**Fig. 3.1.2b, inset**).[82]

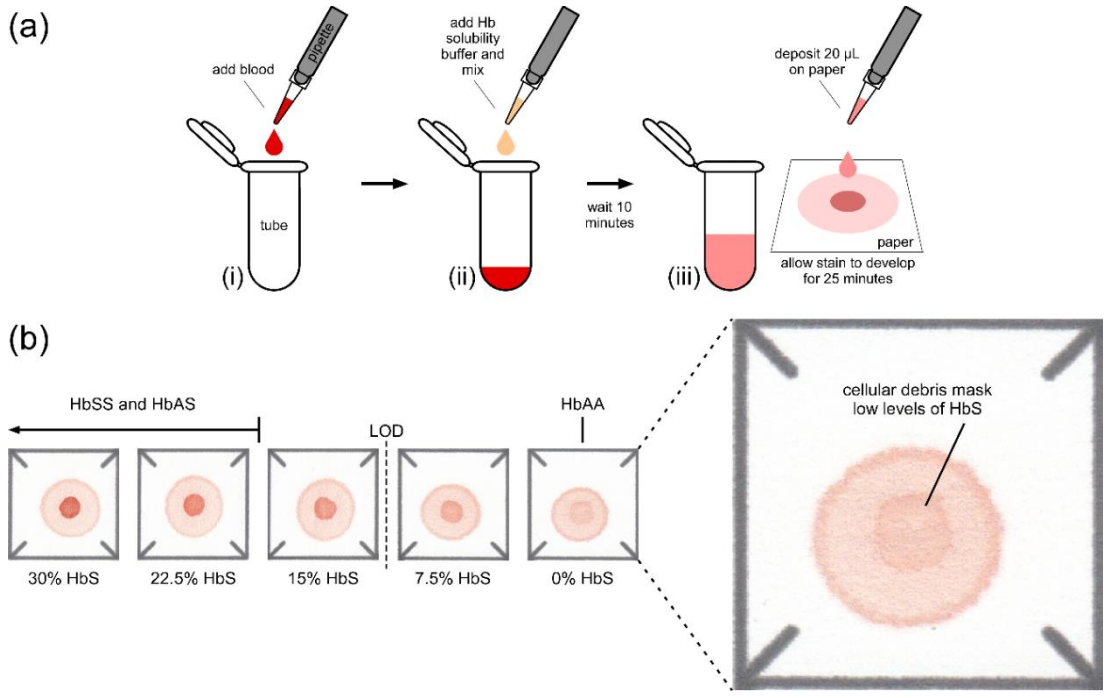

Figure 3.1.2 Previously developed paper-based SCD diagnostic test for adults and older children. (**a**) Schematic illustration of test steps (**b**) Representative bloodstains for samples with less than 30% sickle hemoglobin (HbS) and typical adult HbS ranges for different genotypes.

To address this limitation and further lower the LOD of the test, we introduced a filtration step for removing cellular debris from the blood lysate prior to deoxygenation (**Fig. 3.1.3a**). This *newborn* paper-based test is performed by first mixing 40 µL of blood with 200 µL of lysis buffer (8 g/L saponin in phosphate buffer) in the bottom chamber of a disposable syringe-less filter (0.2 µm PES Whatman Mini-Uniprep™, GE Healthcare, USA). After 5 minutes, the filter top is compressed until the solution is filtered into the top chamber. An approximately equal volume (75 µL) of the deoxygenation buffer (200 g/L sodium hydrosulfite in phosphate buffer) is then added to the top chamber and mixed with the filtered solution. After 10 minutes, a 20 µL drop of the mixture is deposited onto chromatography paper (Whatman™ 1 Chr, GE Healthcare, USA) and allowed to dry for up to 25 minutes (**Fig. 3.1.3a**). The characteristic bloodstain pattern, indicative of the presence or absence of HbS in the blood sample, is formed by polymerized deoxy-HbS, which becomes trapped in the pores of the chromatography paper substrate in the area where the drop was deposited, and soluble forms of hemoglobin which wick laterally through the pores of the paper towards the periphery. The inherent red color of hemoglobin is sufficient for visual evaluation of the bloodstain pattern, with no additional signal amplification necessary.

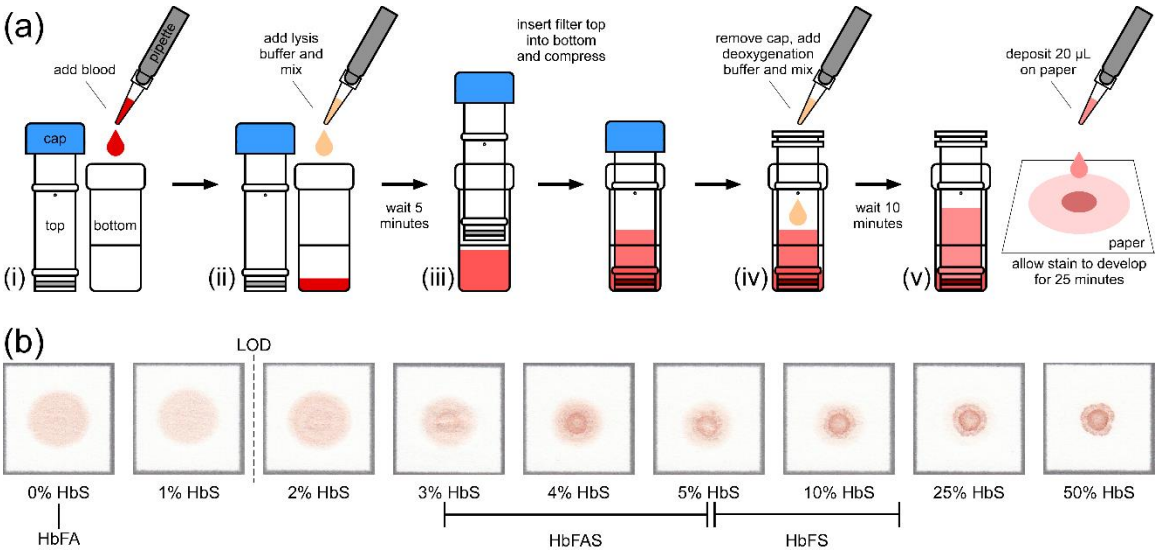

Figure 3.1.3 Paper-based newborn SCD screening test. (**a**) Schematic illustration of test steps. (**b**) Representative bloodstains for blood samples with various sickle hemoglobin (HbS) levels and typical newborn HbS ranges for different genotypes. Limit of detection (LOD) = 2%.

Figure 3.1.3b shows characteristic bloodstain patterns for artificially reconstituted samples with 0, 1, 2, 3, 4, 5, 10, 25 and 50% HbS that were used to determine the LOD of the newborn test. Novice scorers (n = 5) with no previous experience performing or evaluating the test were provided with reference images of bloodstain patterns formed by samples with and without HbS and asked to score a set of stains (n = 45) as positive or negative for the presence of HbS. All users correctly scored all stains with >1% HbS as HbS-positive (LOD = 2% HbS). The test was independently performed 5 times for each sample in order to determine reliability of visual scoring. All users made the same diagnosis for all 5 tests at every HbS concentration, indicating that visual scoring of the test is highly reliable. The scoring process was also repeated 3 times for the same bloodstains (presentation order randomized) and scores were perfectly consistent between trials, further supporting that the visual scoring of the test is highly repeatable. The Fleiss' kappa value over all scored stains was 1.0, suggesting a perfect agreement between all five scorers in interpreting the set of bloodstain patterns.

Clinical validation of the newborn paper-based screening test in a resource-limited setting

To evaluate the performance of the newborn paper-based screening test in the real-world environment of a resource-limited clinical setting, we deployed the test at the pilot newborn screening program in Cabinda, Angola. The rationale for this field testing was that newborn screening with the paper-based test should identify all samples positive for HbS (i.e., from both SCD and SCT newborns) and should therefore capture all newborns at risk for either disease or trait for confirmatory IEF testing. We trained local health workers to collect capillary blood samples from newborns via heel-stick, process the samples using the paper-based test, and score the result of the test visually as either HbS-positive or HbS-negative (**Fig. 3.1.4a**). The results of paper-based testing were then compared with those of IEF testing performed on the same samples as part of the current standard screening practice.[4]

Figure 3.1.4b shows the confusion matrix for the paper-based test performed by the local health workers on samples from 159 newborns with unknown SCD status. The test was able to identify HbS-positive samples with a sensitivity of 81.8% (95% confidence interval: 75.1 – 87.0%), specificity of 83.3% (CI: 76.8 – 88.3%), positive predictive value of 56.3% (CI: 48.5 – 63.7%), negative predictive value of 94.6% (CI: 89.9 – 97.2%) and overall diagnostic accuracy of 83.0% (CI: 76.4 – 88.1%). The relatively high number of

false-positives for the newborn test – samples from normal (HbFA) newborns misidentified as HbS-positive – was due to occasional filter malfunction resulting in incomplete removal of cellular debris from the whole blood lysate, thus allowing the formation of a faint center spot which was misinterpreted as HbS-positive. All of the false HbS-negatives (4%) for the newborn test (i.e., samples containing some HbS misidentified as HbS-negative) were from SCT (HbFAS) newborns (**Fig. 3.1.4b**). Importantly, the newborn paper-based test was able to identify SCD (HbFS) newborns with a sensitivity of 100.0% (CI: 97.6 – 100.0%), specificity of 70.7% (CI: 63.2 – 77.2%), positive predictive value of 4.2% (CI: 2.0 – 8.5%), negative predictive value of 100.0% (CI: 97.6 – 100.0%) and overall diagnostic accuracy of 71.1% (CI: 63.6 – 77.6%).

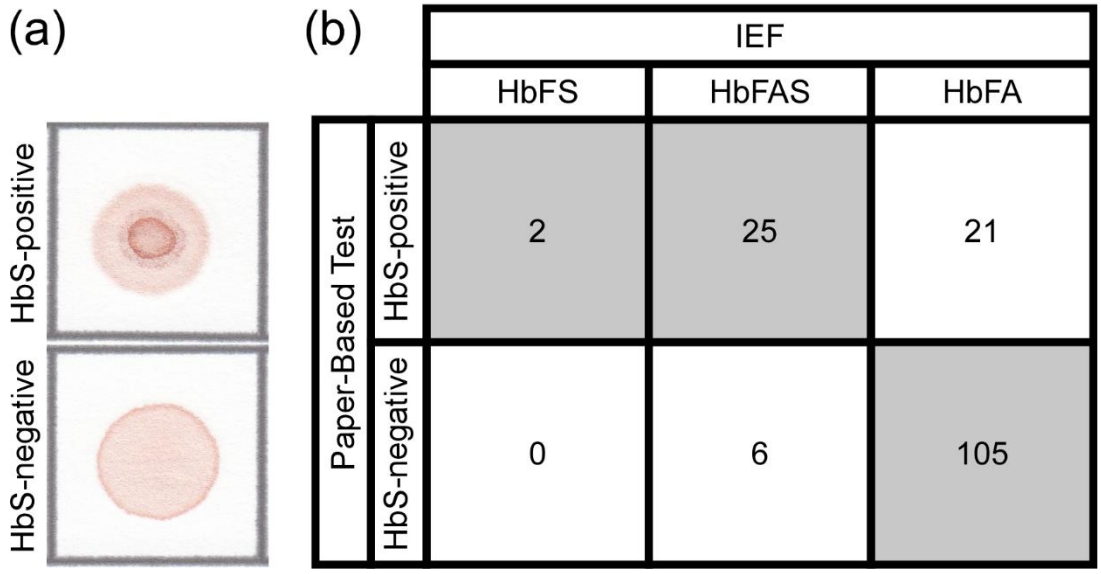

Figure 3.1.4 Accuracy of the paper-based newborn SCD screening test. (**a**) Representative bloodstains for HbS-positive and HbS-negative newborn samples. (**b**) Confusion matrix of the results of tests performed in Cabinda, Angola. Shaded cells contain correctly screened newborns.

The paper-based test deployed in Angola employed a reusable pipette with disposable pipette tips (4 per test) for liquid metering. The cost per test for all test specific consumables (i.e., chromatography paper, reagents, syringeless filter, tubes and pipette tips) of the paper-based test deployed in Angola was $2.16. **Figure 3.1.5** shows a self-contained, distributable version of the test kit comprised of off-the-shelf components, with about the same cost per test. For the self-contained test kit, the reusable pipette with disposable tips was replaced with disposable plastic pipettes and droppers. The total cost per test kit comprised of off-the-shelf materials is $2.12. The retail-priced syringeless filter and disposable plastic

components constitute the majority of test cost (reagents and chromatography paper cost <$0.07 per test), and as such the per test cost can be expected to decrease significantly if the test kits are produced in large quantities using non-marked-up plastic components. The per test cost estimates for both versions of the paper-based newborn SCD screening test do not include the cost of consumables which would be common to any blood test (e.g., gloves, alcohol swab, lancet, collection tube and bandage), as these materials are not typically included in retail test kits.

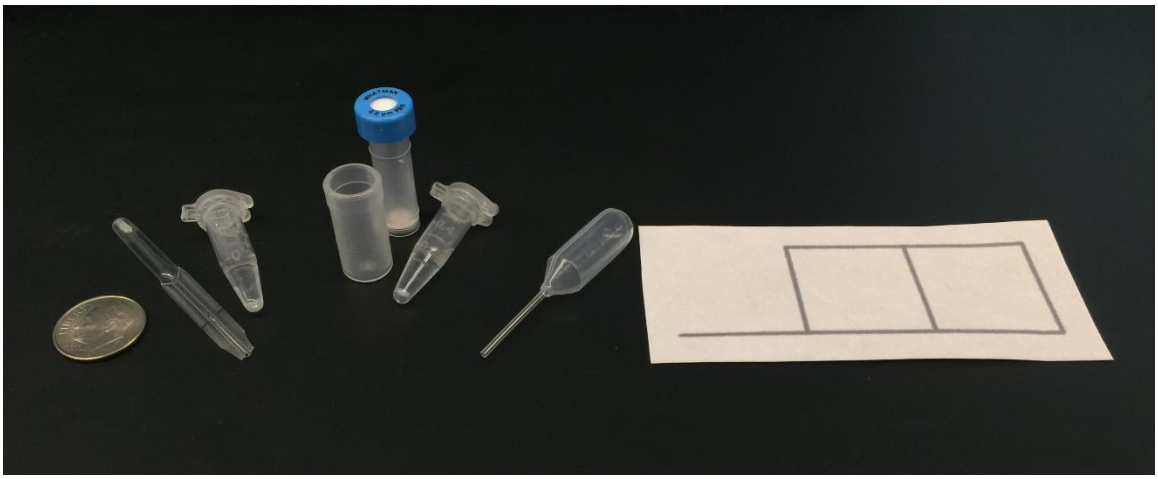

Figure 3.1.5 Self-contained version of the paper-based SCD newborn screening test kit. The kit consists of one exact volume pipette, two tubes containing lysis and deoxygenation buffers, one syringeless filter, one dropper and one piece of chromatography paper. Coin (17.9 mm).

Table 3.1.1 shows the potential cost savings from using the paper-based test as a preliminary screen-in test prior to confirmatory IEF testing of positive samples, based on the previously published cost per sample of $4.94 for IEF in Angola.[4] For our cohort of 159 newborns, screening all samples by IEF alone would cost $785.46 (cost per sample = $4.94). In contrast, screening using the paper-based test followed by IEF testing only of positive samples would cost an estimated $343.44 for the paper-based testing and $237.12 for subsequent IEF testing of positive samples, for a total cost of $580.56 (cost per sample = $3.65); a potential cost reduction of 29%. The relatively low incidence of SCD and SCT in the general population and consequently the relatively low ratio of confirmatory IEF to paper-based screening tests which will need to be performed, suggest that the potential cost savings from such a two-stage, screen-in program would increase proportionally with the number of newborns screened.

Table 3.1.1 Potential cost savings from using the paper-based SCD newborn screening test as a preliminary screen, followed by confirmatory diagnosis of only screened-in HbS-positive newborns via isoelectric focusing (IEF).

	IEF alone	**Paper-based test + IEF**
Cohort size	159	159
Number screened by paper-based test	0	159
Total cost of paper-based screening (at $2.16 / test)	$0	$343.44
Number requiring IEF testing	159	48
Total cost of IEF testing (at $4.94 / test)	$785.46	$237.12
Total cost of all testing	$785.46	$580.56
Average cost per sample	$4.94	$3.65

3.1.4 Discussion

Two major barriers to successful implementation of universal newborn screening for SCD in low-income developing countries are the cost and logistical complexity of conventional diagnostic methods and the delayed availability of screening results.[86] In Angola, for example, the cost of newborn screening using IEF is reported as $4.94 per sample, and as a result screening remains limited to only the major urban centers of Luanda and Cabinda City.[4] The need to transport blood samples from birthing centers to a centralized testing laboratory for analysis also severely limits the ability to screen children at remote and rural facilities. In Angola, the results of IEF testing are rarely available less than 4 weeks after sample collection, and as a consequence, fewer than 55% of newborns with SCD identified through the IEF-based screening in Angola are successfully re-contacted and initiated on prophylaxis regimens.[4]

The current paradigm of universal newborn screening is to test *every* child for SCD at birth using a highly-accurate laboratory method such as IEF.[87] Given the relatively low incidence of SCD in the general population, most of the resources of such a screening paradigm are currently spent on diagnosing *healthy* children. A more cost-effective alternative could be to first identify newborns at the highest risk for having SCD using a rapid and low-cost screening test with a low false-negative rate, and then perform higher-cost confirmatory testing only for these screened-in high-risk newborns.

The paper-based SCD newborn screening test described here successfully addresses many of the technical and logistical impediments of the conventional approaches described above. Firstly, the per test cost of the self-contained, distributable paper-based test using off-the-shelf components purchased at retail prices is $2.12, already less than half the per test cost of conventional IEF currently employed in the pilot newborn screening program in Angola ($4.94 per sample). Additionally, the per test cost of the finalized test kit could potentially be lower than the current version as it will employ integrated sample collection and processing components, produced by a contract manufacturing partner, which are projected to be less expensive than the sum of the current retail prices for the multiple commercially available components comprising the current test. Secondly, the paper-based test is lightweight, completely electricity-free, requires no specialized equipment or instrumentation and is simple enough for a user with no previous experience performing the test to learn to operate and interpret the test with expert proficiency in under one hour. Therefore the paper-based test would not be limited to centralized laboratories with specialized equipment and trained technicians, but rather could be deployed to remote facilities and operated by health workers with any level of experience. In this study the results of the test were typically available within one hour or less of initiating the test. This rapid turnaround time, compared to conventional laboratory methods, could therefore potentially enable counseling of families with high-risk newborns before postpartum discharge (usually within 6-12 hours of delivery at the Primero de Maio obstetric center). Finally, our data show that a two-stage approach consisting of preliminary screening of all infants and confirmatory testing of only the high-risk subset could reduce the number of newborns requiring IEF testing by at least 70%, thus significantly reducing the overall cost of the screening program. More importantly, accurate identification of newborns at the highest risk for SCD could help focus limited available resources on establishing proper longitudinal care for this much smaller cohort.

The paper-based test offers important advantages over existing technologies designed to enable low-cost SCD diagnostics in resource-limited settings. Conventional hemoglobin solubility tests (e.g., SickleDex™) are not sensitive enough to detect the low levels of HbS typically found in newborn blood samples, are notoriously difficult to standardize and interpret, and are confounded by numerous comorbidities which effect the turbidity of blood samples.[88] Various modifications of conventional laboratory methods (e.g., lower-cost implementation of IEF[33], or a microfluidics-based HE[89]) as well as novel diagnostic

approaches (e.g., density-based separation of sickle RBCs in capillaries[29,30], or magnetic levitation-based smartphone platforms[32]) may reduce the cost of testing and/or may be performed at the point-of-care but continue to require highly trained personnel and rely on complex specialized equipment and electricity to operate. Rapid diagnostic tests for SCD based on conventional lateral flow immunoassay technology are instrument- and electricity-free and show great potential.[36,90,91] However, these tests still require extensive field-testing to determine real-world performance for newborn samples and for tests performed in resource-limited settings, and are subject to well-known limitations of all antibody-based assays, such as limited shelf-lives when ambient temperatures exceed recommended ranges for even short periods of time during shipping, storage or usage – a scenario which is highly likely in resource-limited setting such as sub-Saharan Africa.[92] Additionally, because these tests rely on proprietary antibodies, their cost per test may not be significantly lower than the cost of conventional testing methods such as IEF, and the rates and scale at which these tests can be manufactured may be limited by the rates at which the proprietary antibodies can be produced.

There are three major limitations to the paper-based newborn SCD screening test. The first is that the paper-based test cannot yet distinguish between SCT and SCD in newborns, and therefore must be used as a *screening*, rather than a *diagnostic* test. To make a definitive diagnosis, the screening results must be confirmed with a laboratory test (such as IEF) or later in life using the previously developed adult version of the paper-based test.[81,83] The second limitation is the relatively high incidence of false-positives observed in this study. This problem was due to the occasional malfunction of the filter used to remove cellular debris from the blood lysate, resulting in a false central spot mimicking that produced by HbS. The volume of blood and lysis buffer used in the filtration step has since been decreased in order to reduce the rate of false-positive results due to filter malfunction. Finally, we had a small but significant rate of false-negative results (4%) with the paper-based test, all of which were from newborns with SCT. A retrospective analysis of these samples and bloodstains revealed that the blood samples had clotted before processing or were otherwise inadequate, suggesting that these false-negatives were due to improper sample handling, rather than a malfunction of the paper-based test itself. Quality control standards for blood samples to be used with the paper-based test and obligate IEF analysis of samples deemed inadequate for the paper-based test could prevent these false negatives in further iterations of this two-stage testing protocol.

In summary, we demonstrate that the paper-based newborn SCD screening test, optimized to detect the low levels of sickle hemoglobin present in newborn blood, enables the direct screening of newborns for sickle cell trait and sickle cell disease. We also demonstrate that this test is feasible and has a high diagnostic accuracy when performed by local health workers in a resource-limited clinical setting. These results demonstrate the potential utility of the newborn paper-based test for identifying high-risk newborns in the immediate postnatal period and reducing the overall cost of screening newborns for sickle cell disease, thus increasing the practicality and effectiveness of universal newborn SCD screening programs in resource-limited settings.

CHAPTER 4 Engineering and validating a paper-based assay capable of quantifying sickle hemoglobin concentration in blood samples from patients with sickle cell disease

4.1 Paper-based HbS quantification assay

The following research has previously been published and much of the following text is reprinted with permission from: the American Journal of Hematology, 90(6), Piety NZ, Yang X, Lezzar D, George A, and Shevkoplyas SS, "A rapid paper-based test for quantifying sickle hemoglobin in blood samples from patients with sickle cell disease," pages 478 – 482, Copyright 2015 Wiley Periodicals, Inc.

4.1.1 Introduction

Sickle cell disease (SCD) is a common recessively inherited blood disorder caused by a point mutation of the β-globin gene.[7] Unlike normal adult hemoglobin (HbA), sickle hemoglobin (HbS) polymerizes and becomes insoluble under hypoxic conditions, causing a number of structural and functional abnormalities in affected red blood cells (RBCs). Sickled RBCs have increased fragility and rigidity that render them prone to early breakdown and occlusion of blood vessels. Patients with SCD experience chronic hemolytic anemia, episodic pain crises and abnormal blood flow to critical organs that cumulatively result in significant illness and shortened lifespans.[6] Although, the severity of the disease varies greatly among patients, for each individual patient the rate of adverse events is strongly correlated with the intraerythrocytic concentration of HbS.[7]

The two main therapeutic options for SCD, hydroxyurea and chronic transfusion, both rely primarily on a reduction of the relative HbS level for their beneficial effect. Hydroxyurea induces the expression of hemoglobin F (HbF) in erythrocytes, reducing the intraerythrocytic HbS concentration and making the erythrocyte less likely to sickle in hypoxic conditions. Chronic transfusion therapy does not affect intraerythrocytic HbS concentration but reduces the overall proportion of sickle erythrocytes and partially corrects the anemia of SCD, improving organ perfusion and oxygenation.[93] The main goal of chronic RBC transfusion for SCD patients is to maintain a low level of HbS (<30%) in order to decrease the rate of adverse clinical outcomes, in particular the risk of primary or secondary stroke.[94-96] Generally, the transfusion of 2-3

RBC units or 10-15 mL/kg every 3-5 weeks is sufficient to keep the %HbS below 30% and the [Hb] at 9-10 g/dL and minimize the risk of progressive complications.[97]

Both hydroxyurea and chronic transfusion therapy require frequent monitoring of the relative HbS concentration to assess effectiveness of therapy. The monitoring of %HbS in patients on these therapies using conventional laboratory methods (e.g., Hb electrophoresis[24] and HPLC[22]) is impeded by the high cost and long processing time usually associated with these methods.[24] Typically, results are not available rapidly enough to guide clinical decision-making at the time of the clinic visit. Additionally, since HbS levels are not routinely measured during or after transfusions, relatively little is known about the evolution of HbS levels in SCD patients on chronic transfusion therapy. A rapid, inexpensive assay for measuring HbS concentration in patient blood samples could be useful in monitoring the effectiveness of hydroxyurea and transfusion therapy by enabling more frequent testing than currently possible with conventional laboratory methods, thereby providing additional information that could inform clinical decision making.

Our research group has recently developed a low-cost paper-based test for diagnosing SCD in resource-limited settings.[98] This test utilizes the separation of HbS and non-sickle hemoglobin by differential wicking in a paper matrix to qualitatively diagnose SCD. We postulated that a similar test could be capable of quantifying the sickle component of total hemoglobin in patient blood samples. In this study, we demonstrate that this paper-based test can be used to rapidly and accurately quantify the HbS content in SCD patients on chronic transfusion and hydroxyurea therapy, as well as in infants with a relatively high endogenous level of Hb F.

4.1.2 Methods

Blood samples

Venous blood samples were collected from patients with SCD, after informed consent following an IRB-approved protocol, during clinic visits (January 2013 – September 2014) at the Texas Children's Hematology Center (Houston, TX). Healthy, consenting volunteers donated normal venous blood samples. Blood samples were collected in Vacutainer tubes (K_2EDTA, BD, Franklin Lakes, NJ), stored between 4-25°C and analyzed within 21 days after collection (mean storage time before analysis = 6.4 ± 3.6 days). Sample storage time up to 21 days was only weakly correlated with assay performance ($R^2 = 0.09$, $p < 0.01$).

Hemoglobin Electrophoresis

Hemoglobin A, F, C and S for each sample were measured using conventional Hb electrophoresis performed on the semi-automated Sebia Hydrasys 2 Scan system (Sebia Inc., Norcross, GA). All materials were prepared and run according to manufacturer specifications. Phoresis curve editing software (Sebia Inc., Norcross, GA) was used to calculate hemoglobin composition. For post-transfusion samples, the expected %HbS was calculated using the following method: Post-transfusion %HbS = Total HbS (g) x 100 / (Total post-transfusion Hb (g)); Total HbS = Pre-transfusion [Hb] x pre-transfusion %HbS x Total blood volume (dl); Total post-transfusion Hb = (Pre-transfusion [Hb] x total blood volume (dl)) + (Total transfused volume (dl) x $[Hb]_{Transfused\ blood}$).

Hemoglobin solubility buffer

The Hb solubility buffer was a mixture of a hemolytic agent (saponin), a reducing agent (sodium hydrosulfite) and a high-phosphate buffer. The high-phosphate buffer (2.49M) consisted of 1.24M (169 g/L) monobasic and 1.25M (217 g/L) dibasic potassium phosphate dissolved in deionized water. The saponin (4 g/L) permeabilizes red cell membranes, releasing Hb into the solution. The sodium hydrosulfite (30 g/L) converts the released Hb into deoxy-Hb. Converted HbA, HbE, HbF and HbC remain soluble in the high-phosphate buffer, while deoxy-HbS polymerizes and precipitates.[99,100]

Quantification of the blood stain color intensities

The blood stains on patterned chromatography paper were digitized by scanning the paper with a portable flatbed scanner (CanoScan LiDE110, Canon USA Inc, Lake Success, NY). The digitized blood stains were analyzed with a custom image analysis algorithm (MATLAB, The Math Works Inc, Natick, MA). The algorithm automatically isolates features of the blood stain via contrast stretching and thresholding, then calculates the mean color intensity of each feature using RGB color data from the Blue (B) channel of each pixel within the feature (color intensity = 255 – B).[101]

The relationship between the quotient of relative mean color intensities of the standardized blood stains and HbS content in patient samples was determined using a series of reconstituted blood samples with %HbS artificially adjusted from 0 - 75%. These calibration samples were created by mixing ABORh-

matched, equal-hematocrit normal (HbAA) and SCD (HbSS) blood samples at various ratios to achieve the desired HbS concentrations. %HbS of artificially adjusted samples was verified by Hb electrophoresis. **Figure 4.1.2b** shows this calibration curve relating the quotient of mean color intensities to %HbS, an exponential curve was fit to the data, where estimated $\%\text{HbS} = 0.332 * \ln(0.639 * I_C/I_R)$. This calibration curve was used throughout the rest of this study to convert I_C/I_R to estimated %HbS.

4.1.3 Results

The design and operation of the paper-based assay for SCD has been previously described in detail.[98] Briefly, to perform the assay 20 μL of whole blood was added to 200 μL of solubility buffer, mixed by inversion, and allowed to sit for 10 minutes, to allow RBC lysis and hemoglobin deoxygenation. At the end of this period, 20 μL of the lysate was pipetted onto chromatography paper and allowed to wick laterally and dry for 25 minutes (**Fig. 4.1.1a**). The entire assay was performed indoors, in ambient conditions (temperature 15°C to 25°C, 20% to 70% humidity, fluorescent lighting). The difference in transport of soluble and insoluble variants of hemoglobin (Hb) through the paper substrate produces a blood stain consisting of two parts: the area of the initial drop where polymerized deoxy-HbS is retained (center spot), and the area where all soluble forms of Hb are wicked laterally (peripheral ring). The color intensity of the center spot relative to that of the peripheral ring is indicative of the HbS level in the blood sample. **Figure 4.1.1b** shows representative blood stains for samples artificially reconstituted with %HbS varying from 0 to 75%. As expected, increasing HbS content results in increased color intensity of the center spot and decreased intensity of the peripheral ring. The absolute color intensity of the stain is dependent on the Hb concentration of the sample, but the relative color intensities of the center spot and peripheral ring are independent of Hb concentration. The resulting blood stain is digitized using a portable flatbed scanner (in reflected light) and analyzed with a custom image analysis algorithm. The entire assay can be performed for up to 20 samples in less than 35 minutes.

Figure 4.1.2 describes the process of estimating %HbS based on the relative color intensity of the center spot and the peripheral ring areas of the blood stain. First, the custom image analysis algorithm applies a standard contrast stretching and thresholding routine to the digitized image of the blood stain to determine the center of the stain (**Fig. 4.1.2a-i**). A standardized binary mask[102] is then used to isolate the appropriate

parts of the blood stain image to calculate, I_C, the mean color intensity of the center spot (**Fig. 4.1.2a-ii**) and, I_R, the mean color intensity of the peripheral ring (**Fig. 4.1.2a-iii**). For each sample, the quotient of these two values (I_C/I_R) is then converted to estimated %HbS using the equation (estimated %HbS $= 0.332 * \ln(0.639 * I_C/I_R)$) derived from the calibration curve (**Fig. 4.1.2b**).

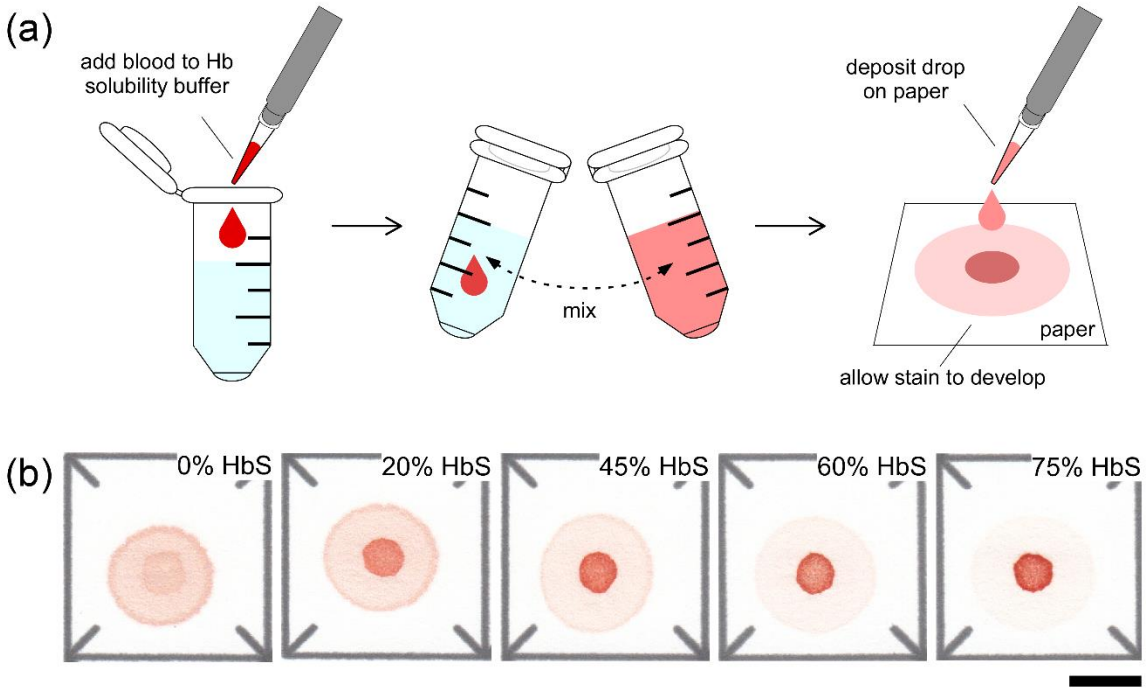

Figure 4.1.1 Paper-based sickle hemoglobin (HbS) quantification assay. (**a**) Schematic illustration of test steps (**b**) Representative bloodstains produced on paper by samples with various %HbS. Scale bar is 1 cm.

To test the accuracy of our paper-based quantification method, we then compared the value of %HbS in individual patient samples measured by conventional Hb electrophoresis (Sebia Hydrasys 2 Scan, Sebia Inc., Norcross, GA) and by the paper-based assay. Of the 88 samples used in this analysis, 55 were from patients on hydroxyurea therapy, 25 were from patients on chronic transfusion therapy, and 8 were from infants. The ages of the patients ranged from one month to 18.8 years, hemoglobin concentrations ranged from 5.6 to 12.9 g/dL, and %HbS ranged from 10 to 97%. Five patients had the SC genotype, 3 patients had the $S\beta^0$ genotype, and 2 patients had the $S\beta^+$ genotype. As shown in **Figure 4.1.3a**, the values of %HbS estimated using the paper-based assay (Estimated %HbS) and measured using conventional hemoglobin electrophoresis (Actual %HbS) were highly correlated ($R^2 = 0.86$). When broken down by sample type, the

correlation between %HbS measured by electrophoresis and that measured by the paper-based assay remained high, although the correlation was weaker for patients undergoing hydroxyurea therapy ($R^2_{hydroxyurea}$ = 0.61, $R^2_{transfusion}$ = 0.87, R^2_{infant} = 0.83), indicating that the accuracy of the paper-based assay was not affected by significant variations in %HbS and %HbA, and %HbF or by the relative distribution of these hemoglobin complexes within erythrocytes. The lower correlation for patients undergoing hydroxyurea therapy resulted from decreased accuracy of the test at very high %HbS levels (the samples from patients undergoing hydroxyurea therapy tended to have the highest HbS concentrations) rather than from inherent differences between patient groups.

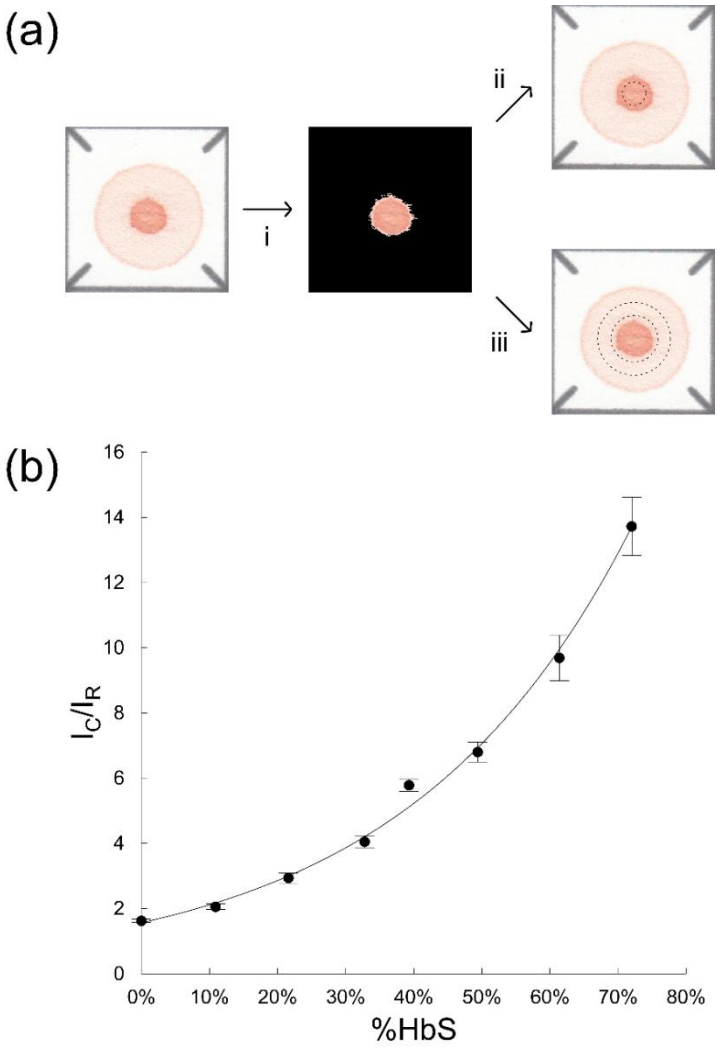

Figure 4.1.2 Using a blood stain to estimate %HbS. (**a**) Schematic illustration of image analysis algorithm. (**b**) Dependence of mean color intensities of center spot (I_C) and peripheral ring (I_R) on %HbS for a series of reconstituted blood samples (calibration curve = solid line).

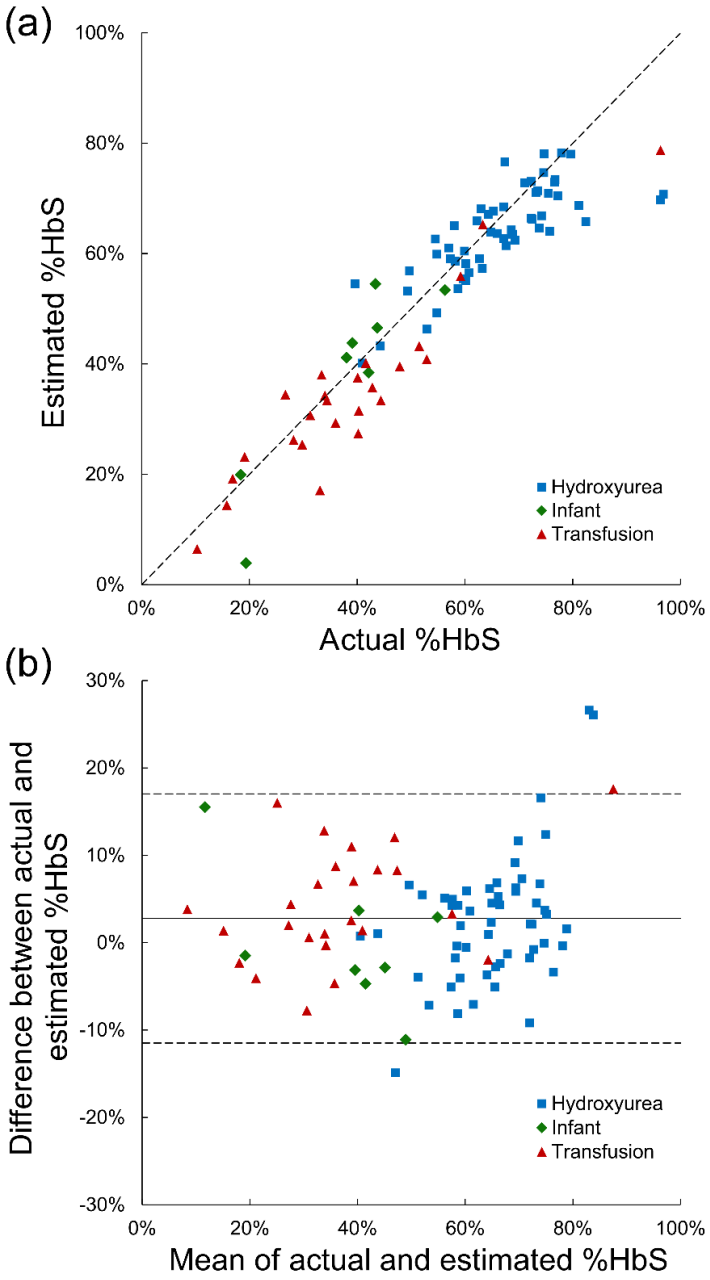

Figure 4.1.3 Paper-based assay performance. (**a**) %HbS measured using the paper-based assay (Estimated) vs. electrophoresis (Actual). (**b**) Bland–Altman plot shows strong agreement (SD difference = 7 %HbS) between estimated and actual %HbS.

Figure 4.1.3b shows a Bland-Altman plot[103] of the %HbS values obtained using both methods. The values of %HbS for patient samples estimated using the paper-based assay and measured using conventional hemoglobin electrophoresis show strong agreement. The standard deviation of the differences between different %HbS values obtained using both methods was 7 %HbS. The majority (95.5%) of the differences

between actual and estimated %HbS are within 2 standard deviations of the mean of the differences. The limits of agreement between the paper-based HbS assay and conventional hemoglobin electrophoresis were -11.5 %HbS and 17.0 %HbS. The paper-based HbS assay agreed with the hemoglobin electrophoresis system within 5 %HbS 58.0% of the time, overestimating %HbS by >5 %HbS in 10.2% of subjects and underestimating %HbS by >5 %HbS in 31.8% of subjects.

We tested the repeatability of the paper-based method for quantifying HbS by repeatedly measuring (n = 5) the %HbS for a series of blood samples with HbS content of approximately 10, 20, 30, 40, 50, 60, 70 and 80 %HbS. The standard deviation for the %HbS measurements performed with different droplets of the same blood sample was consistently < 1.5 %HbS for all values of %HbS measured: 0.9 %HbS (CV 6.3%) for the sample with 10 %HbS; 1.0 %HbS (CV 4.8%) for 20 %HbS; 1.3 %HbS (CV 4.1%) for 30 %HbS; 1.1 %HbS (CV 2.6%) for 40 %HbS; 0.7 %HbS (CV 1.3%) for 50 %HbS; 1.3 %HbS (CV 2.1%) for 60 %HbS; 1.1 %HbS (CV 1.6%) for 70 %HbS; and 1.5 %HbS (CV 1.9%) for 80 %HbS. For comparison, the standard deviations for the %HbS measurements performed by the manufacturer of the Sebia Hydrasys 2 Scan system for blood samples with %HbS ranging from 8.8 – 83.6 %HbS was 0.2 – 0.6 %HbS (CV 0.7 – 2.1%).

Finally, to assess the utility of the paper-based assay in measuring the change in %HbS with transfusion therapy, we compared the change in %HbS in five patients based on pre- and post-transfusion measurements made using Hb electrophoresis to the same measurements made using the paper-based assay and to an estimate of post-transfusion %HbS made using a formula currently used to guide clinical transfusion practices (based on patient weight, Hb concentration and initial %HbS). As presented in **Table 4.1.1**, the change in %HbS with transfusion measured by Hb electrophoresis was very close to both that estimated by the clinical formula (mean difference 3.3 %HbS) and that measured with the rapid assay (mean difference 3.9 %HbS) for all five patients, indicating that our paper-based assay is capable of accurately determining changes in %HbS following transfusion therapy.

4.1.4 Discussion

In this report, we present a novel paper-based method of quantifying HbS levels in blood samples from patients with sickle cell disease. Our method is based on the previously described qualitative diagnostic test for sickle cell disease that relies on the differential wicking of insoluble HbS and soluble non-sickle

hemoglobins on a paper substrate to produce characteristic blood stain patterns. We now extend this method to permit the quantification of sickle hemoglobin using the patterns produced by this diagnostic test. This quantification is effected by digitization of the rapid test paper containing the blood stain and measurement of the relative color intensity of the center spot, composed of trapped, precipitated sickle hemoglobin, and the peripheral ring, composed of free, soluble hemoglobins. As indicated by the data presented above, quantification of %HbS by this method is highly accurate and reproducible relative to conventional hemoglobin electrophoresis. This method is also accurate across a wide range of HbS levels and hemoglobin concentrations and is unaffected by high levels of endogenous HbF or exogenous HbA. As such, it is potentially applicable to monitor any therapeutic modality that alters the relative level of HbS, including acute or chronic transfusion therapy and hydroxyurea therapy.

Table 4.1.1 %HbS information of patients (n = 5) receiving transfusion therapy.

	Hb electrophoresis			***Clinical estimation***			***Paper-based assay***		
Patient	**Initial %HbS**	**Final %HbS**	**Change in %HbS**	**Initial %HbS**	**Final %HbS**	**Change in %HbS**	**Initial %HbS**	**Final %HbS**	**Change in %HbS**
1	41.2	27.8	-13.4	41.2	32.1	-9.1	34.3	22.8	-11.5
2	30.5	20.2	-10.3	30.5	22.4	-8.1	26.3	20.4	-5.9
3	43.5	30.4	-13.1	43.5	34.4	-9.1	30.4	24.7	-5.7
4	33.7	23.2	-10.5	33.7	21	-12.7	32.3	22.1	-10.2
5	33.3	19.7	-13.6	33.3	23.4	-9.9	21.8	13.6	-8.2

Our paper-based assay offers several advantages over conventional methods for the quantification of HbS. The first and most prominent is the low cost of our assay. The cost of consumable materials and reagents for our test is less than $0.25 per sample, and the initial investment for a computer and scanner for image digitization is less than $400. By contrast, the cost of required supplies for the conventional hemoglobin electrophoresis system used as a reference standard in our laboratory is $1,800 annually for system solutions and controls, plus an additional $5.77 to $12.07 per sample for consumable materials and reagents, and the initial investment for the system is more than $20,000. The estimated cost per sample of both IEF and HPLC at our collaborating center is approximately $60. Our rapid assay thus offers significant cost savings compared to other methods of HbS quantitation.

A second advantage of our paper-based assay is the ease of use of the system. Processing of blood samples to develop the blood stain is a simple operation requiring only two steps (mixing and sample deposition). Subsequent digitization and quantification of the blood stain itself is also straightforward and is largely accomplished by the automated image analysis algorithm. The overall process of blood stain development, image scanning, and HbS quantification can therefore be performed with minimal technical training by any operator with basic laboratory skills.

A final advantage of the paper-based assay is the rapidity of the assay. Conventional laboratory methods of hemoglobin quantification can be completed rapidly, but due to the limited availability of clinical technicians and costs associated with sample processing, samples are often grouped to be run in large batches, delaying the availability of results. In contrast, our paper-based assay does not require batching and has an extremely low per-test cost, even for single samples. A sample obtained from a patient can be processed, digitized, and quantified within less than 35 minutes, permitting rapid clinical assessment of a patient's HbS burden and the adjustment of therapeutic interventions. This capability could be especially useful for patients on chronic transfusion therapy since, unlike conventional measures of %HbS, the paper-based test could determine the current %HbS level in time to assist the clinician in making decisions about current transfusion volume and subsequent transfusion frequency to maintain a target HbS level.

The paper-based assay for HbS quantification offers obvious advantages for resource-limited settings. The low cost of the assay and its technical simplicity are major advantages in environments in which clinical resources, a reliable stream of specialized supplies for complex medical testing, and training for clinical and laboratory personnel are deficient. This assay is highly portable and can be set up quickly in any clinical setting, including those in which the supply of electricity may be uncertain. A major barrier to the implementation of transfusion and hydroxyurea therapies in resource-limited settings is the inability to monitor their efficacy in a timely manner that could influence patient care. The use of this assay could therefore make chronic transfusion therapy targeting a specific %HbS level, such as for primary or secondary stroke prophylaxis, more feasible in such settings. It can also be used in conjunction with other simple measurements (e.g., hemoglobin concentration and patient clinical status) to indirectly monitor the efficacy of HbF induction with hydroxyurea therapy since the reduction of %HbS in patients on hydroxyurea correlates with the degree of HbF induction.

There are a few technical limitations to the paper-based assay. The most prominent of these is that conditions resulting in clotting of blood samples can affect the quantification of HbS in the sample. In our validation cohort of 88 patient samples, the presence of clots in the samples resulted in greater deviation of the value for %HbS determined by the paper-based assay from that measured by hemoglobin electrophoresis. Secondly, the paper-based assay is not as accurate as more technically complex methods of HbS quantitation, especially at very high HbS levels, though this inaccuracy is relatively minor. Thirdly, very high levels of HbF (such as those found in newborns) may interfere with the polymerization of HbS and therefore decrease the accuracy of the assay. Finally, the assay in its current form cannot distinguish between non-pathological soluble hemoglobins, such as HbA, HbA_2, and HbF, and those that can cause SCD in association with HbS, such as HbC or HbD. As such, the utility of this assay is currently limited to patients with homozygous sickle cell disease and $S\beta^0$ thalassemia. Of note, however, patients with homozygous sickle cell disease and $S\beta^0$ thalassemia constitute the majority of all sickle cell patients (>70% in the United States and over 95% in many sub-Saharan African countries[104]) and are also the two most severe forms of the disorder with the most pressing need for clinical intervention.

In summary, we have developed a new, rapid, inexpensive paper-based assay for the quantification of %HbS in blood samples from patients with sickle cell disease. The assay determines %HbS across a wide range of values with a high degree of accuracy relative to hemoglobin electrophoresis and is unaffected by variations in overall hemoglobin concentration or the presence of HbA or HbF in the patient sample. Our assay has obvious applications in resource-limited settings and could be an important step towards making chronic transfusion therapy and hydroxyurea therapy feasible in such settings. The assay could also be useful in resource-rich settings by permitting more rapid and less expensive monitoring of response to these therapies, thus improving clinical care and reducing costs associated with the management of sickle cell disease.

CHAPTER 5 Engineering and validating a microfluidic device for high-throughput analysis of stored red blood cell morphology

5.1 Microfluidic device for high-throughput analysis of stored red blood cell morphology

The following research has previously been published and much of the following text is reprinted with permission from: Vox Sanguinis, 109(3), Piety NZ, Gifford SC, Yang X, and Shevkoplyas SS, "Quantifying morphological heterogeneity: a study of more than 1 000 000 individual stored red blood cells," pages 221 – 230, Copyright 2015 International Society of Blood Transfusion.

5.1.1 Introduction

Normal, healthy red blood cells (RBCs) are highly-deformable biconcave discs with a diameter of ~8 μm, thickness of ~2.5 μm and volume of ~90 fL (**Fig. 5.1.1a**).[11,105,106] High surface membrane area to volume ratio enables RBCs to deform and fit into even the narrowest capillaries, such as those in the spleen.[12,107] During *ex vivo* hypothermic storage, RBCs accumulate significant oxidative damage and shed microparticles via vesiculation, progressively losing membrane surface area, cell volume and physiologically relevant deformability.[61,62,108] As a result of the storage-induced biochemical changes and microvesiculation, stored RBCs undergo a gradual morphological transformation from healthy, flexible discocytes through reversible intermediate forms to irreversibly-damaged, rigid spherocytes with the smallest surface area to volume ratio allowed by geometry, before ultimately undergoing lysis (**Fig. 5.1.1c**).[109,110]

Individual RBCs are extraordinarily heterogeneous with respect to this morphological transformation – after the first 2-3 weeks of storage, the population of stored RBCs in a single unit consists of a complex mixture of relatively well-preserved cells, reversibly damaged intermediate cells and an increasing fraction of irreparably damaged cells (**Fig. 5.1.1b**). A manual evaluation of individual RBC morphology in 9 units previously found that after 6 weeks of storage the units consisted of 23.3 ± 4.3 % discocytes, 46.8 ± 6.7 % reversibly damaged RBCs and 29.9 ± 4.0 % irreversibly damaged RBCs.[109] The variation between units is likely the result of intrinsic inter-donor differences, post-collection processing practices and storage conditions. Unlike RBC biochemical properties (e.g., levels of ATP or 2,3-BPG) that

are known to recover following infusion,[111] the transformation of stored RBCs into spherocytes is irreversible because the total surface area of the cell membrane lost due to vesiculation is too large for the cell to return to the discoid form.[109,112] These irreparably damaged RBCs are dysfunctional, non-deformable cells, potentially capable of obstructing capillaries and causing ischemia.[113] They are removed from the circulation by the phagocytic cells of the recipient's spleen shortly after transfusion, provided they did not lyse in the blood bag or bloodstream before reaching that organ.[12,114] The infusion and subsequent destruction of a large number of these cells may accelerate iron overload in chronically transfused patients.[61,115] The non-transferrin-bound iron released due to the extra- or intravascular lysis of these cells may predispose the recipient to inflammation and infection.[116,117]

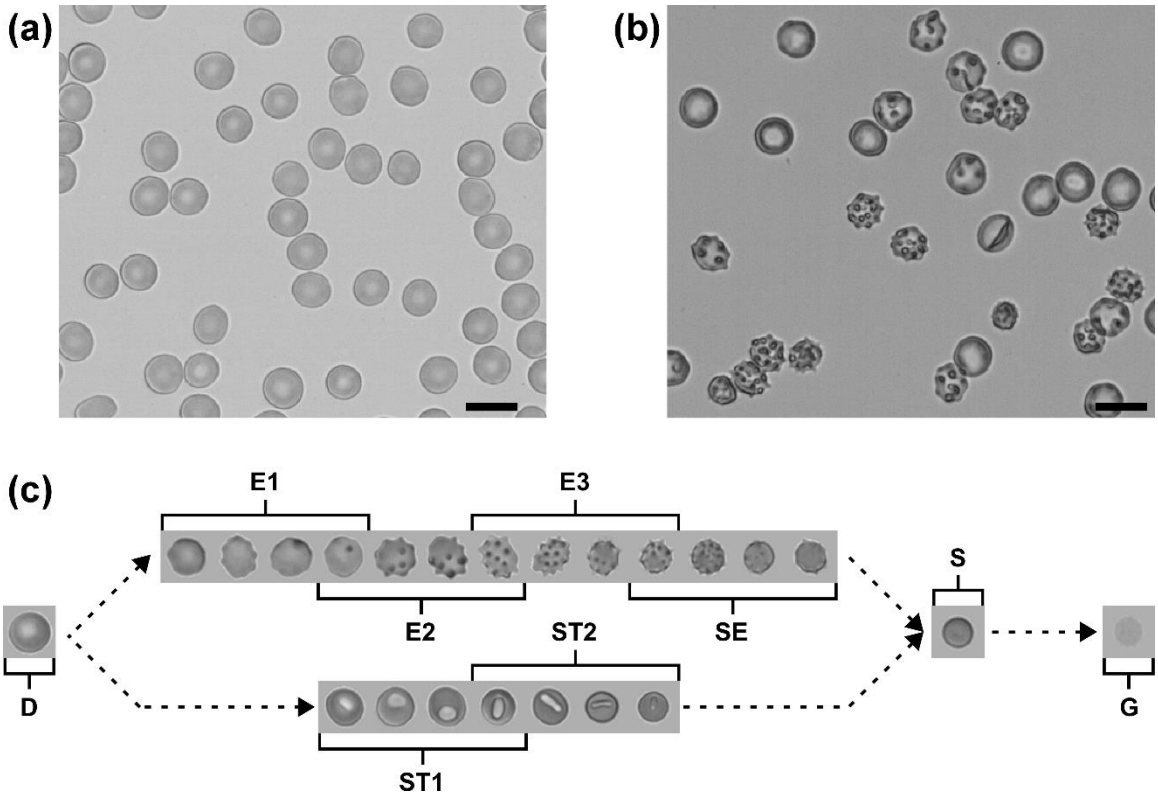

Figure 5.1.1 Morphological heterogeneity of individual (**a**) fresh and (**b**) stored RBCs. Scale bars are 10 µm. (**c**) Morphological transformation of stored RBCs: discocyte (D), echinocyte 1-3 (E1-3), sphero-echinocyte (SE), stomatocyte 1-2 (ST1-2), spherocyte (S), ghost (G).

In current research and clinical practice, the morphology of individual stored RBCs is evaluated by visually matching and assigning cells to predefined morphological classes based on each cell's overall

appearance (e.g., size, shape, surface texture).[11] The extent of RBC morphological deterioration induced by hypothermic storage for each unit is then quantified by determining the percentage of cells in the RBC population that belong to each of the predefined morphological classes and/or calculating a weighted-average "morphology score".[118,119] A conventional approach to performing the measurement is to fix the RBCs in the sample, spread them on a glass slide and acquire several non-overlapping images of the cells in the blood smear via bright-field digital microscopy[120,121] or using a scanning electron microscope.[109,119,122] Individual RBCs captured in the acquired images are then visually classified via manual counting.[123,124] The highly laborious nature of this manual approach has limited the number of individual cells that are normally counted in a single morphological measurement to a very small number, varying from only 200 to 1500 cells.[109,119-122] This technical limitation may introduce a significant sampling error,[124,125] particularly when attempting to quantify the morphological heterogeneity of nearly 2×10^{12} cells contained in a single RBC unit.

The objective of this study was to develop and validate a simple, automated system for morphological classification of single stored RBCs at high-throughput and to use this system to analyze a statistically meaningful number of individual cells. Once loaded into the microfluidic device, individual RBCs (arranged in a single-cell, non-overlapping layer) were continuously passed through the field-of-view of a microscope equipped with a digital camera. The morphological appearance of individual RBCs was determined via automated segmentation, feature extraction and classification of the acquired images. The use of the microfluidic device alleviated the need for skilled sample preparation and, in combination with the image analysis algorithm, reduced subjectivity and eliminated the need for tedious manual counting. We demonstrated the performance of this automated system by simultaneously classifying the morphology and measuring the diameter of 1,367,852 individual stored RBCs; the largest set of such paired data known to date.

5.1.2 Methods

Microfabrication

The microfluidic devices used in the study were fabricated using soft lithography.[126] Silicon wafers (University Wafer, South Boston, MA) were spin-coated with a 7 μm layer of SU-8 negative photoresist (MicroChem Corp, Newton, MA). The wafers were then exposed to near-UV light

(ETI/6/350/NUV/DCCD/M mask aligner, Evergreen Technology Inc., San Jose, CA) through a transparency photomask (FineLine Imaging, Colorado Springs, CO) and developed. Large domed structures at the inlet and the outlet port were fabricated by depositing small droplets (23 µL) of SU-8 photoresist onto the circular regions outlining the inlet and the outlet, soft-baking at 55°C for 8 hours, exposing to near-UV light (3x 100 seconds) and post-baking at 95°C for ~5 hours.[127,128] Patterned wafers were treated for 8 hours with (tridecafluoro-1,1,2,2-tetrahydrooctyl) trichlorosilane (Gelest Inc., Morrisville, PA) in a vacuum chamber.

The patterned wafers served as templates for replicating the microfluidic devices in polydimethylsiloxane (PDMS) (Sylgard 184, Dow Corning Corp, Midland, MI). Inlet and outlet ports were created by punching 4 mm holes through the PDMS replicas using biopsy punches (Acuderm Inc., Fort Lauderdale, FL). A ~1 mm thick slab of PDMS and the patterned surface of the PDMS replica of the device were exposed to air plasma (PDC-3xG, Harrick Plasma, Ithaca, NY) for 100 seconds then sealed together. The resulting devices were filled with 1% (w/v) aqueous solution of mPEG-silane (MW 5000, Laysan Bio Inc., Arab, AL) and let sit for at least 15 minutes before being flushed with GASP buffer (1.3 mM NaH_2PO_4, 9 mM Na_2HPO_4, 140 mM NaCl, 5.5 mM glucose, 1% bovine serum albumin; osmolality 290 mmol/kg; pH 7.4) in order to prevent unwanted RBC adhesion to the walls of the microchannels.[129-131] The combined cost of materials needed to fabricate a single PDMS device for our system was less than $0.25. The microfluidic devices were discarded after a single use.

Preparation of stored RBC samples

Six units of packed RBCs were purchased from regional blood centers (The Blood Center, New Orleans, LA; Gulf Coast Regional Blood Center, Houston, TX). RBC units were stored in a blood bank refrigerator (Helmer iB111 i.Series, Helmer Scientific, Noblesville, IN) at 2-6°C for 8 weeks. Prior to sampling, RBC units were removed from the refrigerator and placed on a rocking platform (model 100, VWR, West Chester, PA) for 15 minutes. 5mL RBC samples were withdrawn from each unit after 6, 7 and 8 weeks of storage, using the aseptic technique with a sterile syringe (BD, Franklin Lakes, NJ) through a sampling site coupler (Fenwal Inc., Lake Zurich, IL). Whole blood samples from healthy, consenting volunteers were collected by venipuncture into 4 mL plastic Vacutainer tubes spray-coated with K_2EDTA (BD, Franklin Lakes, NJ). A hematology analyzer (Medonic M-Series, Boule Medical AB, Stockholm, Sweden) was used

to verify the initial hematocrit and cell count of the blood samples. The samples were diluted to ~1% hematocrit with GASP buffer prior to introduction into the devices. 40μL aliquots of the diluted RBC samples were used for each experiment. Experiments were repeated six times for each unit at each time point.

Imaging and analysis

The imaging system consisted of an inverted microscope (IX71, Olympus America Inc., Center Valley, PA) and a digital camera (MC1362, Mikrotron GmbH, Germany). The microscope was manually focused on the microchannel at a magnification of 64x. The camera was programmed to acquire an image every 5 seconds for 30 minutes (100 fps, 9.617 ms exposure, global shutter). Image sequences were analyzed using a custom algorithm developed in MATLAB (The Math Works Inc., Natick, MA) for automated classification of individual stored RBC morphology in accordance with standard classification.[11,109] The algorithm first standardized the brightness of captured grayscale images, then created a binary mask separating objects from the background via a combination of contrast stretching, erosion, dilation and thresholding. Partial cells, overlapping cells and image artifacts were removed from the binary mask, and a composite image of the brightness-adjusted grayscale image and the binary mask was then used to measure features of individual RBCs, and a binary decision tree was then used to assign RBCs into morphology categories based on these features.[132]

5.1.3 Results

Design of the microfluidic device

The design of the microfluidic device is illustrated schematically in **Figure 5.1.2**. The device was symmetrical, with two identical cylindrical through-holes serving as the inlet and the outlet ports. To prevent screening of cells based on their shape and size in the inlet, the through-holes lead into a smooth, curved slope allowing for a less abrupt transition into the microchannel.[128] The microfluidic part of the device (**Fig. 5.1.2a**) comprised a relatively wide (1.5 mm) and long (7.5 mm) but shallow (7 μm) channel connecting the inlet and the outlet of the device. The channel contained a sparse array of 30 μm × 30 μm square pillars oriented to conform to the field-of-view of the microscope (280 μm × 225μm) (**Fig. 5.1.2a, inset**). The pillars (i) prevented spontaneous collapse of the shallow microchannel,[133] (ii) simplified alignment of the field-of-

view of the microscope with the direction of flow through the device, and (iii) provided a high-definition standard for microscope focusing to ensure consistency of images obtained from different devices.

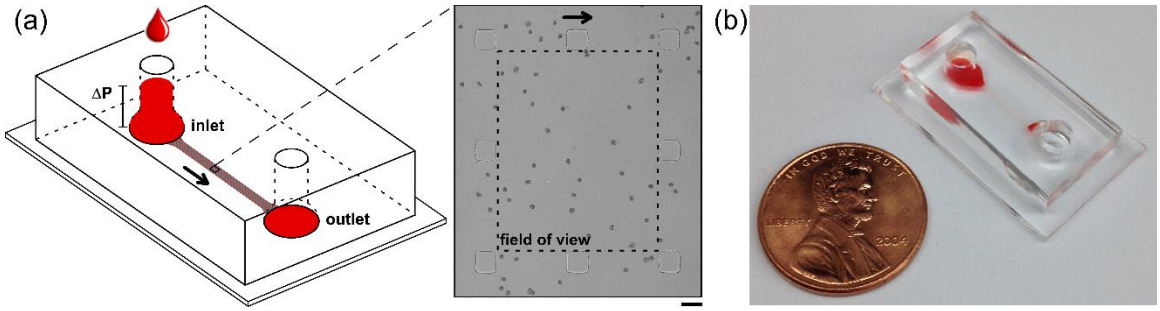

Figure 5.1.2 Schematic illustration of the microfluidic morphology device. (**a**) Pressure differential (ΔP) drives flow through the device. Inset shows 280 µm × 225 µm field of view surrounded by 30 µm × 30 µm pillars. Scale bar is 30 µm. (**b**) Photograph of the assembled device.

To perform the measurement, 40 µL of diluted RBC sample was added to the inlet, the microscope was focused on the microchannel (such that the square pillars were outside the margins of the field-of-view) and image acquisition was initiated. The height of sample in the inlet created a sufficient pressure difference between the inlet and the outlet of the device to drive the flow of sample through the device. Because of the very small rate of flow through the device (~0.5 nL/s), the level of liquid in the inlet did not change significantly during the measurement and, consequently, the driving pressure difference remained relatively constant. The sample flow through the 7 µm microchannel transported thousands of individual RBCs through the field-of-view of the microscope in a single-cell layer, without significant cell flipping, overlap or evidence of morphology-based selection bias at the inlet. The image acquisition was timed with the rate of cells entering and exiting the field-of-view to prevent possible bias due to double-counting. The recorded images were processed off-line to classify the morphology of each individual RBC.

Automated classification of individual RBC morphology

The uniform, high quality images acquired using the microfluidic system enabled consistent extraction of basic cellular features and complex subcellular features. Cell form factor, cross-sectional area, spicule presence, spicule coverage, pallor intensity and pallor aspect ratio were extracted from each isolated RBC image. Individual cells were automatically classified based on these features. The RBCs were

categorized at two levels: into 8 specific ("high-resolution") categories (D, discocyte; E1, echinocyte 1; E2, echinocyte 2; E3, echinocyte 3; SE, sphero-echinocyte; ST1, stomatocyte 1; ST2, stomatocyte 2; S, spherocyte) and into 4 broad ("low-resolution") categories (D; E [E1, E2, E3, SE]; ST [ST1, ST2]; S) based on Bessis's general classification.[11] Two levels of precision (high-resolution and low-resolution) were calculated in order to avoid limiting the utility of the system. Some applications (e.g., study of RBC deformability, fragility or morphology recovery) may require high-resolution classification because the number of spicules an echinocyte has is an indicator of the degree of membrane loss due to microvesiculation during storage and therefore of functionally relevant RBC surface area to volume ratio. However, other applications (e.g., microfluidic cell sorting) may only require distinctions between broad categories of RBCs (e.g., D, E and ST vs. S) in order to separate reversibly and irreversibly damaged RBCs.

Figure 5.1.3 shows the logic of the simple binary decision tree used to structure the RBC classification algorithm. The layout of the tree was modeled after the decision making process used for manual RBC classification. A multiparameter cluster analysis algorithm employed all six cellular features at each branch point to classify each individual RBC; weighting factors for each feature, and a threshold level with which to classify the result of their combination, at each branch point were determined via previously-described numerical methods.[132] The final categorization was determined by the terminal branch reached by each individual RBC. The RBC classification algorithm was capable of automatically classifying single RBCs at a rate of >10,000 cells per hour (CPU time). After the algorithm is initiated, it does not require user input, so the operator is free to perform other tasks while the algorithm is running – a significant improvement compared to manual classification which requires active user involvement. The cell classification algorithm was optimized using a manually-categorized training set of 1000 randomly-selected individual RBCs, taken from the entire set (n = 1,367,852) of images of single stored RBCs acquired using the system.

Figure 5.1.4 shows a *confusion matrix* (a method commonly used for evaluating the accuracy of automated classifications)[134,135] for the morphology classifications based on the multi-parameter cluster analysis algorithm. To produce the confusion matrix, we selected a random set of images of 1000 single stored RBCs (test set) from the set of all images and classified the morphology of each individual RBC via visual examination ("True Class") and by applying the automated classification ("Algorithm Predicted Class"). The overall accuracy was calculated as the quotient of the number of correctly classified RBCs (i.e.

cells in which the true class was the same as algorithm predicted class) and the total number of analyzed RBCs. The overall accuracy of the RBC classification algorithm was 91.9% for low-resolution classification (D, E, ST, S) and 75.3% for high-resolution classification (D, E1, E2, E3, SE, ST1, ST2, S). The overall accuracy for high-resolution sub-classifications (E1, E2, E3, SE) of RBCs classified as echinocytes (E) at low-resolution was 77.5%. The overall accuracy for high-resolution sub-classifications (ST1, ST2) of RBCs classified as stomatocytes (ST) at low-resolution was 66.7%.

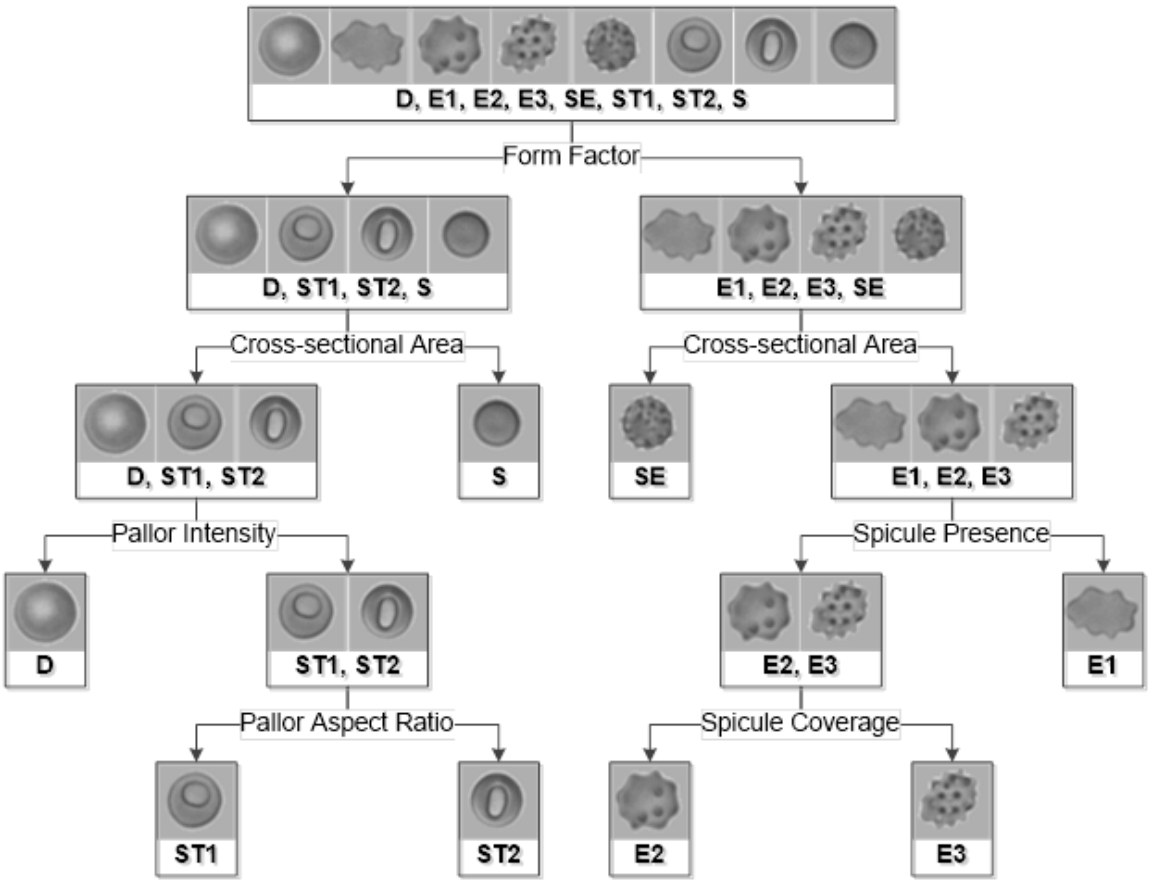

Figure 5.1.3 Schematic illustration of binary decision tree for morphology classification algorithm. The feature specified at each bifurcation informed the structure of the tree. Final morphology classification is determined by the terminal branch reached by each sorted cell.

To evaluate the reproducibility of the system, we performed 5 measurements of the same stored blood unit and compared the distributions of morphologies among all individual RBCs analyzed for each measurement. A total of 66,161 RBCs were used to evaluate reproducibility (n = 16,217 – measurement 1, n = 12,262 – measurement 2, n = 12,943 – measurement 3, n = 10,213 – measurement 4 and n = 14,526 –

measurement 5). The means and standard deviations of the proportions of the samples composed of each morphology class are as follows: 3.50 ± 0.26 % (CV 7.5%) - D, 25.50 ± 3.40 % (CV 13.3%) - E1, 13.20 ± 1.05 % (CV 8.0%) - E2, 19.16 ± 4.10 % (CV 21.4%) - E3, 16.48 ± 0.65 % (CV 4.0%) - SE, 21.25 ± 1.07 % (CV 5.1%) - S, 0.90 ± 0.19 % (CV 21.2%) - ST1 and 0.01 ± 0.01 % (CV 122.9%) - ST2. The low standard deviation between experiments suggests that the system is highly reproducible. The coefficient of variation for ST2 is very high because very few RBCs with this morphology were present in this unit compared to all other morphologies.

		Algorithm-Predicted Class							
		D	**E1**	**E2**	**E3**	**SE**	**ST1**	**ST2**	**S**
True Class	**D**	68	16	0	0	0	1	0	1
	E1	16	240	16	4	15	0	0	1
	E2	1	34	64	34	8	1	0	0
	E3	0	8	21	198	18	0	0	0
	SE	0	3	4	0	67	0	0	18
	ST1	3	2	1	0	2	2	0	2
	ST2	0	0	0	1	0	1	0	0
	S	2	1	0	0	11	1	0	114

Figure 5.1.4 Confusion matrix for the automated stored RBC morphology classification algorithm. Cells along the diagonal contain correct high-resolution morphology classifications, and all shaded cells contain correct low-resolution morphology classifications.

Measurement of the diameter of individual RBCs with different morphologies

The data from all experiments (6 units × 3 weeks per unit × 6 experiments per week) was combined to form a single representative set of single stored RBCs (n = 1,367,852). We used our system to automatically classify the morphology of these individual stored RBCs and to determine the mean effective diameter ($d = (4A/\pi)^{0.5}$, where A is the total cross-sectional area of the cell) of individual RBCs belonging to different stages of storage-induced RBC morphology deterioration. **Figure 5.1.5** shows the distribution of the diameters of individual RBCs by morphology class for all stages of echinocytosis. A distribution of sizes

for fresh RBCs (D0 in **Fig. 5.1.5**) is given for reference. With respect to discocytes from fresh blood samples, stored discocytes were slightly larger (D: 7.80 ± 0.49 µm vs. D0: 7.69 ± 0.43 µm), which is consistent with initial swelling of RBCs during storage, prior to loss of volume by vesiculation. There was significant overlap of the size distributions for individual stored RBCs in various stages of echinocytosis (**Fig. 5.1.5**), which is indicative of the practical difficulty with making a sharp distinction between echinocyte subtypes. Sphero-echinocytes and spherocytes had a virtually identical size distribution (SE: 6.01 ± 0.26 µm vs. S: 6.02 ± 0.27 µm). The mean diameters for all high-resolution and low-resolution morphology categories are summarized in **Table 5.1.1**.

Table 5.1.1 Diameter data by morphology class. (**a**) Diameter mean and standard deviation data for high-resolution multiparameter cluster analysis classification. (**b**) Diameter mean and standard deviation data for low-resolution multiparameter cluster analysis classification.

(a)	D0 (n = 22,985)	D (n = 124,229)	E1 (n = 395,472)	E2 (n = 174,836)	E3 (n = 321,762)	SE (n = 162,648)	S (n = 154,570)	ST1 (n = 11,193)	ST2 (n = 157)
Diameter mean ± standard deviation (µm)	7.69 ± 0.43	7.80 ± 0.49	7.61 ± 0.63	7.02 ± 0.61	6.47 ± 0.42	6.01 ± 0.26	6.02 ± 0.27	6.95 ± 0.61	7.32 ± 0.47

(b)	D0 (n = 22,985)	D (n = 124,229)	E (n = 1,054,718)	S (n = 154,570)	ST (n = 11,350)
Diameter mean ± standard deviation (µm)	7.69 ± 0.43	7.80 ± 0.49	6.92 ± 0.80	6.02 ± 0.27	6.96 ± 0.61

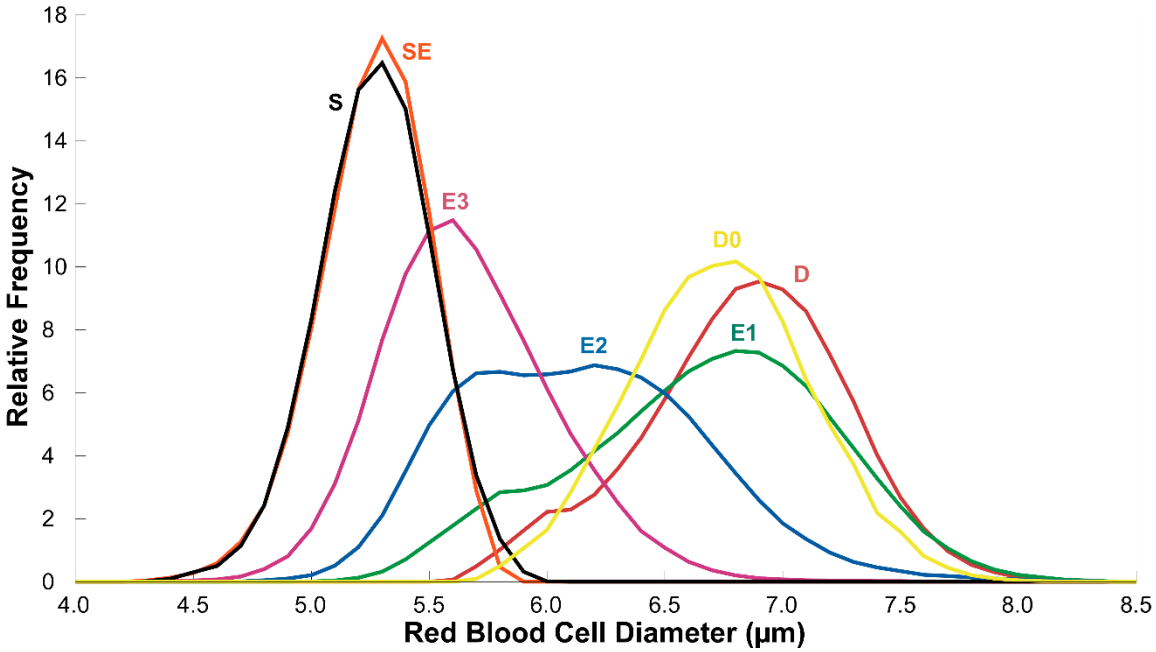

Figure 5.1.5 Distribution of individual stored RBC diameters by morphology class. Cells were categorized automatically by multiparameter cluster analysis. The distribution of a sample (unpaired) of fresh discocytes (D0) is shown for comparison.

5.1.4 Discussion

The majority of individual stored RBCs are well-preserved cells (discocytes or early stages of echinocytosis), which largely recover their properties post-transfusion and survive a normal lifespan in circulation [111,136]. A relatively small fraction of individual stored RBCs, however, is damaged irreversibly, entering into the terminal stages of echinocytosis (sphero-echinocytes, spherocytes) and ultimately undergoing lysis either during storage or soon after transfusion. Conventional approaches to improving the quality of stored blood have focused on optimizing storage conditions (e.g., composition of the anticoagulant-preservative solution,[136] or reduction of oxygen in the storage bag[111]). Given the highly heterogeneous response of individual RBCs to hypothermic storage, however, further fine-tuning of the overall storage conditions may not produce a significant improvement in quality.[136] In this context, a more successful approach could be to simply remove the irreparably damaged cells from the unit before transfusion (e.g., using one of the methods recently developed in the field of high-throughput microfluidics [137-139]). To enable this approach, we need to quantify morphology, size and other properties that could potentially inform the design of microfluidic devices to be used for separating the populations of well-preserved and irreparably damaged cells. Existing manual methods for evaluating morphology of single stored RBCs severely limit the number of cells that can be analyzed and are impractical for making simultaneous measurements of morphology and other properties (e.g., size) for a meaningful number of cells with required precision. The simple, automated system we developed in this study enabled us to accomplish this task for >1,000,000 individual cells.

The most common conventional procedure for measuring the morphology of individual stored RBCs involves preparation of a blood smear, best-effort focusing of the microscope on the cells in the smear, a search for good working areas of correctly oriented cells by repeatedly moving the blood smear preparation in the field-of-view of the microscope (with a possible need for re-focusing), image acquisition, and visual classification of a few hundred individual RBCs (all normally manually performed by a skilled technician). These manual operations are very laborious, highly dependent on the technical skills and experience of the operator performing the measurement and are notoriously difficult to standardize between different laboratories. The primary advantage of our automated approach is its simplicity. To perform the RBC morphology measurement with our approach, an operator only needs to load the diluted RBC sample into the

inlet of the microfluidic device, focus the microscope using the support pillars as a high-definition standard, and initiate the automated image acquisition and analysis processes. The microfluidic device completely eliminated the need for preparation of the blood smear and search for good working areas by creating a *dynamic* blood smear (**Fig. 5.1.2**) which allowed acquisition of numerous unique images of single optimally oriented, non-overlapping RBCs, without moving the blood smear preparation in the field-of-view of the microscope or re-focusing. The automated morphology analysis algorithm eliminated the need for subjective visual classification of individual RBCs. Our approach significantly reduced the time and user-input required to perform the morphological study and simultaneously increased the consistency and quality of the images. A secondary advantage of our approach is it's relatively low cost, and lack of a need for specialized equipment – the disposable microfluidic devices are compatible with any sufficiently powerful bright field microscope equipped with a digital camera, which may already be in place in many laboratories. Because of these properties, our system could also be useful for studying the impact of different storage conditions, naturally occurring inter-donor variation and various rejuvenation strategies on the morphology of stored RBCs.

The approach to morphometric image analysis described in this paper represents a significant departure from conventional paradigms that emphasize development of ever more complex image analysis algorithms capable of compensating for images with inconsistent quality instead of improving the consistency and quality of images. Recent efforts in developing new analytical methods attempt to counterbalance the physical limitations of poor sample preparation by circumventing the issue of poor image quality through additional layers of complex code. Several clever methods (e.g., the pulse-coupled neural network approach) have been developed that can efficiently de-noise and segment blood cell images, selectively eliminating objects that may confound subsequent analysis steps, and extract specific cells from the image background.[140,141] However, because these improved methods do not resolve the inherent problem of poor quality images, complex additional codes are required each time new features need to be extracted from the same images, severely limiting the versatility of these systems. The approach implemented in this paper utilizes automated sample preparation and imaging to produce standardized RBC images with consistently-high quality (minimal cell clumping, overlapping and non-standard orientation), thereby eliminating the need for complex image analysis techniques.

By resolving the problem of poor image quality, our system significantly reduced the complexity of the code required for cell feature extraction and measurement, creating a versatile, easily adaptable platform for high-throughput morphometric analysis of single cells. Here, paired stored RBC morphology and diameter data was chosen as a useful demonstration of the capabilities of the system, however the system is capable of extracting other complex cellular and subcellular features (e.g., number of spicules, form factor or central pallor aspect ratio) with single cell resolution. The image analysis algorithm could easily be adapted for use in quality control procedures (e.g., after blood collection and processing) or for the automated detection of RBC pathologies (e.g., sickle cell disease). As such, this simple, versatile, low-cost system has applications in both clinical and research environments.

The overall accuracy of the automated RBC classification algorithm was 91.9% for low-resolution and 75.3% for high-resolution. This compares favorably with the general accuracy of automated image analysis methods throughout other areas, particularly for the low-resolution classification.[134,142] Interestingly, the majority of incorrectly categorized cells (high-resolution) in the test set were categorized as one of the neighboring morphologies along the transition from discocyte to spherocyte (e.g., E1 identified as D or E2). These 'off-by-one' errors likely occurred because the transition from discocyte to spherocyte is a continuous spectrum spanning a range of intermediate forms between these more distinct morphological endpoints. Even experienced technicians have to make subjective judgments regarding how to classify each individual cell, and thus could potentially classify the same cell differently. Manual classification of RBCs, which in itself is not perfectly objective, was used to define 'true' classes in the training and test sets. The observed deviation of the diameter distributions from normal distributions for some of the morphological classes (particularly E2) likely reflects these classification inaccuracies.

In summary, we developed an easy-to-use system for automated and high-throughput measurement of the morphology of individual stored RBCs by combining a simple microfluidic device and a morphometric image analysis. Our system completely eliminated the need for laborious manual preparation and visual examination of blood smears, and thus enabled classification of the morphology of more than one million individual cells, the largest dataset of stored RBC morphology data known to date. Using these data, we were able to quantify the distribution of cell diameter across a heterogeneous population of single stored RBCs in various stages of morphological deterioration. This information will be useful for developing technologies

aimed at eliminating the irreparably damaged cells (particularly spherocytes and sphero-echinocytes) from stored blood units before transfusion. The ability to evaluate the morphology and other properties of individual RBCs automatically, rapidly and in statistically significant numbers could also improve our ability to assess the quality of stored blood in clinical and research settings.

CHAPTER 6 Using microfluidic tools to quantitatively assess the quality of stored and/or rejuvenated red blood cells

6.1 Comparison of conventionally (aerobically) and anaerobically stored red blood cells

6.1.1 Introduction

Conventionally, red blood cells (RBCs) are separated from donated whole blood then suspended in anticoagulant-preservative solution and stored in oxygen permeable polyvinylchloride (PVC) bags for up to 6 weeks at 2-6 °C prior to transfusion.[143] During this hypothermic storage period the biochemical and mechanical properties of stored RBCs deteriorate progressively, resulting in heterogeneous RBC damage collectively referred to as storage lesion.[113,144] Damage accumulated during storage is known to impair the rheological properties of stored RBCs, most importantly their ability to perfuse microvascular networks *in vitro*,[128,145-147] *ex vivo*,[148] and *in vivo*.[149,150] This decreased ability to traverse the microcirculation suggests that RBCs damaged during storage may have a reduced ability to perform their primary function – the delivery of oxygen to tissues and vital organs.

Oxidative damage to RBCs is believed to be one of the primary mediators of this storage induced deterioration.[62,109,151] Hemoglobin oxidation during storage is known to precipitate damage to the lipids and proteins comprising the RBC membrane and cytoskeleton.[152] As such, the reduction of oxidative damage during storage has become a major focus of research efforts aimed at improving the quality of stored RBCs.[152,153] One approach to reducing oxidative damage to RBCs during hypothermic storage is to reduce the availability of oxygen within the RBC unit. Donated RBCs can be deoxygenated and stored under anaerobic conditions to maintain a low concentration of oxygen within the unit throughout storage. Storage of RBCs under anaerobic conditions has previously been shown to decrease hemolysis and phosphatidylserine exposure and to increase adenosine triphosphate and 2,3-diphosphoglycerate levels as well as 24-hour post transfusion recovery.[153-155] However, the differences in rheological properties between conventionally and anaerobically stored RBCs have not yet been studied in detail.

There is no single metric which defines the rheological fitness of a cell, and as a result numerous techniques for measuring rheological properties have been devised. For this study we employed two

conventional ektacytometers,[156,157] which measure average RBC deformability in response to shear stress, as well as two custom microfluidic devices, the artificial microvascular network (AMVN) and the multiplexed microcapillary network (MMCN).[128,147] The AMVN device evaluates the rate at which RBCs perfuse a network of microchannels inspired by the layout of rat mesentery microvasculature.[128] The MMCN device evaluates the ability of individual RBCs to deform and pass through narrow constrictions, thus enabling the detection of poorly deformable single RBCs. Additionally, we evaluated the morphology of the stored RBCs, using a simple microfluidic system.[158] Here we describe a comprehensive split-unit comparison study of conventionally (aerobically) and anaerobically stored RBCs over the course of 6 weeks of hypothermic storage.

6.1.2 Methods

Microfluidic device fabrication

The design and validation of the artificial microvascular network (AMVN) microfluidic device (**Fig. 6.1.1a**) and the multiplexed microcapillary network (MMCN) microfluidic device (**Fig. 6.1.1b**) have previously been described in detail.[128,145,146,159] In brief, the AMVN device consists of three parallel, identical networks of interconnected channels inspired by the layout of rat mesentery microvasculature. Each network is connected to a separate 4 mm diameter domed inlet and a shared 2 mm diameter domed outlet by 70 µm wide channels. The MMCN device consists of two parallel, identical networks of 32 microcapillaries. Each microcapillary consisted of a 330 µm long and 5 µm wide straight portion, followed by a 45 µm long portion that tapered in width from 5 µm to 3 µm and finally a 125 µm long and 3 µm wide straight portion. Each network is connected to a separate 4 mm diameter domed inlet and a shared 2 mm diameter domed outlet by 70 µm wide channels and series of bifurcating channels. All device channels are 5 µm deep.

AMVN and MMCN devices were constructed from polydimethylsiloxane (PDMS) molds of wafers fabricated via soft lithography as described previously.[128] Inlet and outlet ports were fabricated using biopsy punches (Acuderm, Inc., Fort Lauderdale, FL) of the same diameter. AMVN and MMCN devices were sealed to PDMS coated glass slides after exposure to air plasma for 100 seconds. Assembled microfluidic devices were treated with a solution of 1% mPEG-silane (Laysan Bio, Inc., Arab, AL) in GASP buffer (1.3 mmol/L NaH_2PO_4, 9 mmol/L Na2HPO4, 140 mmol/L NaCl, 5.5 mmol/L glucose, 1% bovine serum albumin;

osmolality 290 mmol/kg; pH 7.4) for at least 8 hours.[128] GASP buffer was removed from the device before use.

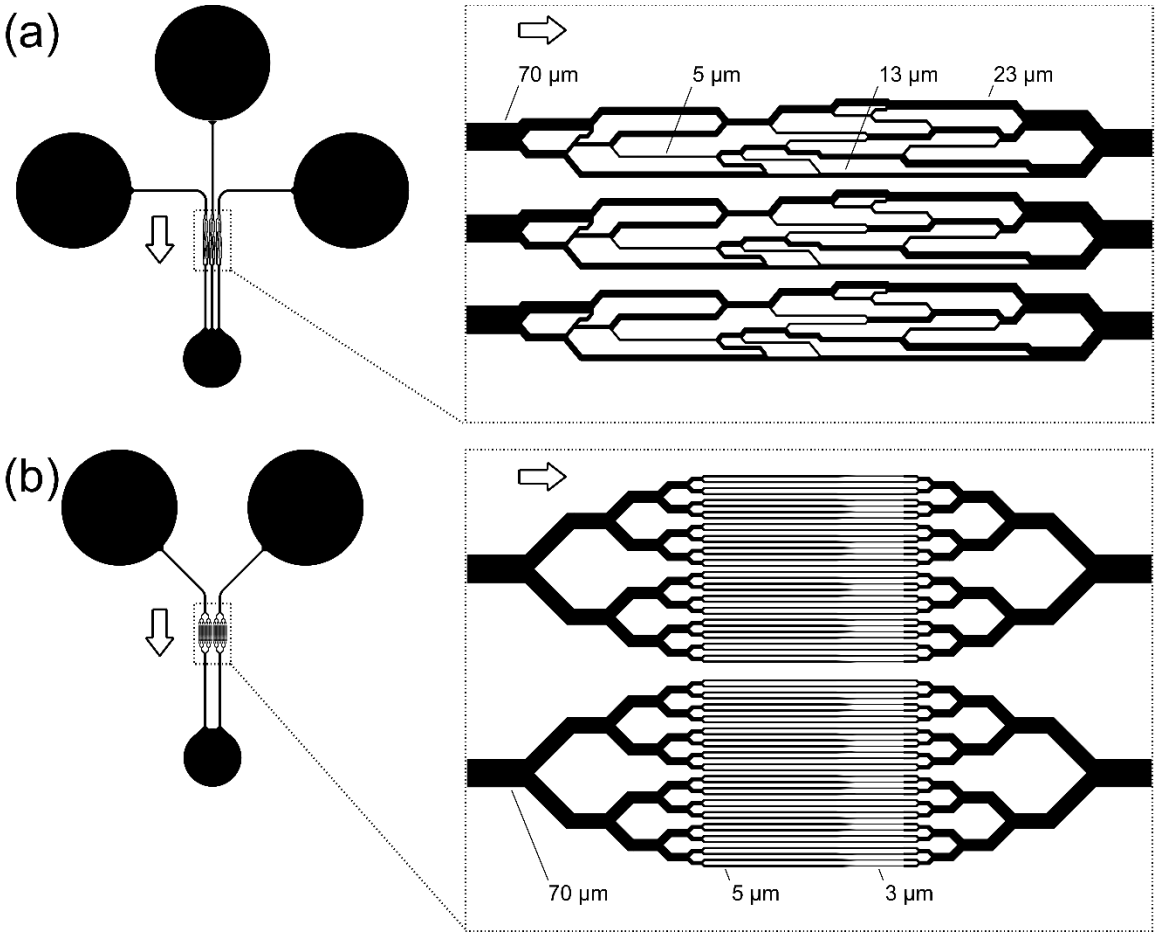

Figure 6.1.1 Schematic illustrations of microfluidic devices. (**a**) The artificial microvascular network (AMVN) microfluidic device. (**b**) The multiplexed microcapillary network (MMCN) microfluidic device. All channels were 5µm deep; arrows indicate direction of net flow.

RBC sample preparation

Whole blood was collected from healthy, consenting volunteers (n=9) into citrate phosphate double dextrose (CP2D) anticoagulant solution (Pall Medical, Covina, CA). The blood was centrifuged (2,000×g for 3 minutes) and mixed with 100 mL of AS-3 (Nutricel, Pall Medical). All units were leukoreduced by filtration (RC2D, Pall Medical) and split into two smaller units; one to be stored conventionally and one anaerobically. RBC units to be stored anaerobically were deoxygenated by passing the RBCs through a neonatal membrane oxygenator (Sorin D100, Sorin Group USA, Arvada CO) under nitrogen. Conventionally and anaerobically

stored RBCs were stored in 150 mL capacity PVC blood bags (Teruflex T-150, Terumo Corp., Tokyo, Japan). Each anaerobically stored RBC unit was further packaged in an oxygen-impermeable bag (Rollprint Z, Addison, IL, USA) containing 4 oxygen sorbent sachets (AGELESS, Mitsubishi Gas Chemical America, Inc., New York, NY). Processed RBC units were stored in a blood bank refrigerator (Helmer iB111 i.Series, Helmer Scientific, Noblesville, IN) at 2-6 °C in blood bag holders (Blood Shoe, Genesis BPS, Ramsey, NJ) for the duration of 6 weeks.

Corresponding anaerobically and conventionally stored RBCs of the same storage duration were evaluated side-by-side at weekly intervals. RBC units were removed from the refrigerator and mixed by inversion, then 2 mL aliquots were collected from each unit using the aseptic technique. After the anaerobically stored unit was sampled, the oxygen sorbent sachets were replaced with fresh sachets and the outer bag was resealed with a plastic film sealer. The hematocrit of each RBC aliquot was adjusted to 40.0 ± 1.0 % by adding a calculated volume of normal saline (9.0 g/L sodium chloride). Sample hematocrit was verified with an automated hematology analyzer (Medonic M-series, Boule Medical AB, Stockholm, Sweden). Hematocrit adjusted samples were kept at 2-6 °C until use, at which point they were allowed to reach room temperature and mixed by inversion prior to use.

Microfluidic device measurements

Driving pressure across the AMVN and MMCN was controlled with an adjustable water column connected to device outlets via tubing and a barbed tube fitting (L420/410-6, Value Plastics, Fort Collins, CO). Images were captured of the 70 μm downstream channels using an inverted bright-field microscope (IX71, Olympus America Inc., Center Valley, PA) equipped with a high-speed digital camera (Flea3, Point Grey Research, Inc., Richmond, Canada). Image sets were analyzed offline using a custom image analysis algorithm implemented in MATLAB (The Math Works Inc., Natick, MA, USA).[128,145]

To perform bulk perfusion rate measurements, 25 μL hematocrit adjusted RBC samples were added to each device inlet and allowed to fully perfuse the microfluidic network. Image capture was initiated with driving pressure set to 0 cmH_2O, then after 30 seconds the driving pressure was set to -20 cmH_2O, and bursts of 10 images at 150 fps were collected at 10 second intervals for the duration of each 6 minute measurement. The procedure for performing MMCN capillary plugging measurements was similar to that for bulk perfusion

measurements, however images were captured of the capillary portion of the device and 750 images were captured continuously at 150 fps. Capillary plugging was defined as a decrease in RBC flow rate within a MMCN microcapillary below a cutoff value of the mean RBC flow rate at week 0 minus two standard deviations.

Ektacytometer measurements

To perform deformability measurements with the RheoScan-D ektacytometer (RheoMeditech, Republic of Korea) the RBC sample was diluted to 1% by volume in polyvinylpyrrolidone (PVP) solution included in the RheoScan-D Test Kit (RSD-K02, RheoMeditech).[157,160,161] 500 μL of the diluted sample was then loaded into the disposable microfluidic chip included in the RheoScan-D Test Kit (RSD-K02, RheoMeditech) and the chip was inserted into the RheoScan-D instrument and evaluated automatically. Samples were evaluated at shear stresses from 0.5 to 20.0 Pa.

To perform deformability measurements with the Maxsis Osmoscan Laser Optical Rotational Cell Analyzer (LORRCA, Mechatronics Instruments, The Netherlands) the RBC sample was diluted to 0.5% by volume in isosmolar PVP solution included in the LORRCA reagents.[156,161-163] 800 μL of the diluted sample was then loaded into the instrument and analyzed automatically. Samples were evaluated at shear stresses from 0.3 to 30.0 Pa at 37.0°C and camera gain level 301. For both ektacytometers, the elongation index (EI) was calculated as $EI = (A - B)/(A + B)$, where A and B represent the major and minor axes of the ellipse-shaped RBC diffraction pattern.[157]

Morphology measurements

Images of RBCs were obtained using a simple microfluidic device, as described previously.[158] To perform a morphology measurement a RBC sample was diluted to 1% hematocrit in normal saline, then 40 μL of the diluted sample was loaded into the device inlet. The pressure difference between the device inlet and outlet was sufficient to drive flow through the device. Images of the single layer of RBCs in the 1.5mm × 7.5mm × 7μm microchannel were captured using an inverted bright-field microscope (IX73, Olympus America Inc.) equipped with a digital camera (MC1362; Mikrotron GmbH, Germany) at a magnification of 64×. The camera acquired one image every 5 seconds for 20 minutes. A randomly selected set of 200 images

of individual RBCs from each experiment was analyzed offline by a blinded expert scorer. RBCs were scored as discocyte (D), echinocyte I (E1), echinocyte II (E2), echinocyte III (E3), sphero-echinocyte (SE), spherocyte (S), stomatocyte I (ST1) or stomatocyte II (ST2). Morphology Index (MI) was calculated using the equation: MI = [-2(#ST2) + -1(#ST1) + 0(#D) + 1(#E1) + 2(#E2) + 3(#E3) + 4(#SE) + 5(#S)] / #total.[11,164]

Statistical analysis

Statistical analysis was performed using built-in functions of MATLAB 2014b Statistics Toolbox (The Math Works Inc., Natick, MA). A paired, two-tailed t-test was used for the comparison between two groups. A p-value of < 0.05 was considered statistically significant.

6.1.3 Results

Microfluidic device perfusion rates

Figure 6.1.2 shows the bulk RBC perfusion rates for the AMVN and MMCN devices measured at the 70μm wide outlet channel. The bulk AMVN and MMCN perfusion rates decreased progressively over the course of 6 weeks of hypothermic storage for both anaerobically and conventionally stored RBCs, however perfusion rates were consistently higher for anaerobically stored RBCs than for conventionally stored RBCs. For conventionally stored RBCs, the bulk AMVN perfusion rate decreased by 27.5% between week 0 and week 6 of storage, while for anaerobically stored RBCs, the bulk AMVN perfusion rate decreased by only 24.5%. At the beginning of storage, there was not a statistically significant difference in AMVN perfusion rate between conventionally and anaerobically stored RBCs, but after one week of storage the AMVN perfusion rates diverged and anaerobically stored RBCs perfused the AMVN significantly faster than conventionally stored RBCs at weeks 1, 2, 4 and 6. At the end of six weeks of hypothermic storage, the bulk AMVN perfusion rate for anaerobically stored RBCs was 5.0% higher than for conventionally stored RBCs. For conventionally stored RBCs, the bulk MMCN perfusion rate decreased by 49.0% between week 0 and week 6 of storage, while for anaerobically stored RBCs, the bulk MMCN perfusion rate decreased by only 42.4%. At the beginning of storage, there was not a statistically significant difference in MMCN perfusion rate between conventionally and anaerobically stored RBCs, but after one week of storage the MMCN perfusion rates diverged and anaerobically stored RBCs perfused the MMCN significantly faster than

conventionally stored RBCs for the remainder of storage (weeks 1–6). At the end of six weeks of hypothermic storage, the bulk MMCN perfusion rate for anaerobically stored RBCs was 15.0% higher than for conventionally stored RBCs.

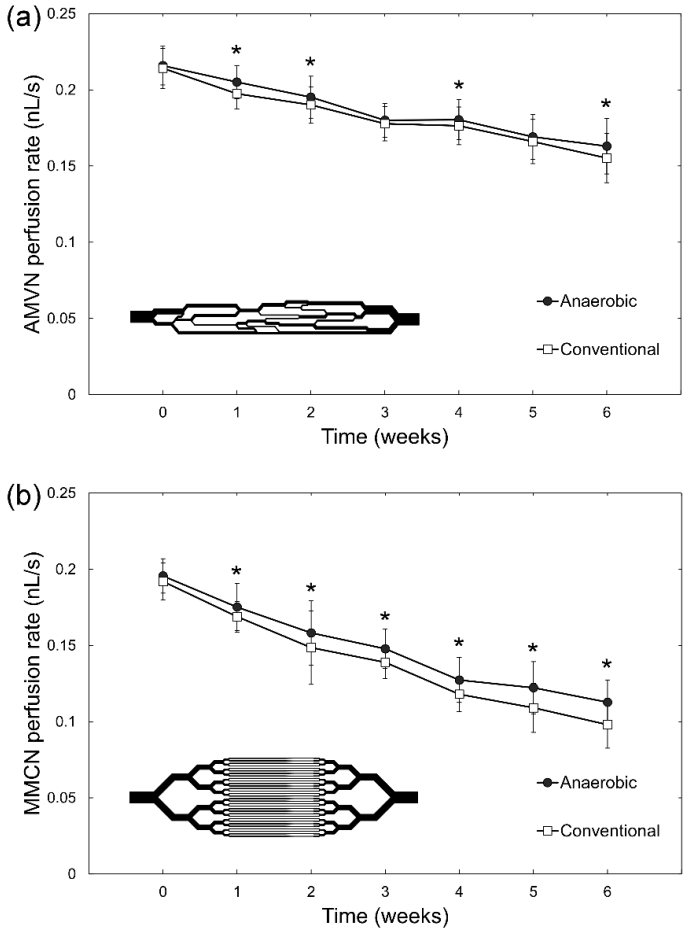

Figure 6.1.2 Bulk AMVN and MMCN perfusion rates for anaerobically and conventionally stored RBCs over the course of 6 weeks of hypothermic storage. (**a**) n = 4. (**b**) n = 9. Mean values ± SD. Statistically significant differences ($p < 0.05$) are marked by an asterisk (*).

MMCN Plugging

We measured the flow rate of RBCs through the 32 microcapillaries comprising the MMCN in order to determine the number of times individual poorly deformable RBCs "plugged" the capillary (**Fig. 6.1.3a**) and the percentage of time the capillaries spent in a "plugged" state (**Fig. 6.1.3b**). Overall, the number of MMCN plugging events as well as the percentage of time MMCN capillaries spent in a plugged state increased progressively throughout storage for both anaerobically and conventionally stored RBCs. The

number of MMCN plugging events and percentage of time MMCN capillaries spent in a plugged state was generally lower for anaerobically stored RBCs than for conventionally stored RBCs; except for week 0 when the number of plugging events was slightly (but not significantly; $p > 0.05$) higher for anaerobically stored RBCs, potentially due to the extra stresses imparted on the RBCs by the deoxygenation process. The mean number of plugging events increased 2.9 fold by week 6 for conventionally stored RBCs but only 2.5 fold for anaerobically stored RBCs. The percentage of time the MMCN capillaries spent in a plugged state diverged after 1 week of storage and conventionally stored RBCs spent significantly more time in a plugged state for the remainder of storage (weeks 1 – 6). After 6 weeks of storage, conventionally stored RBCs spent 8.0% more time in a plugged state than anaerobically stored RBCs.

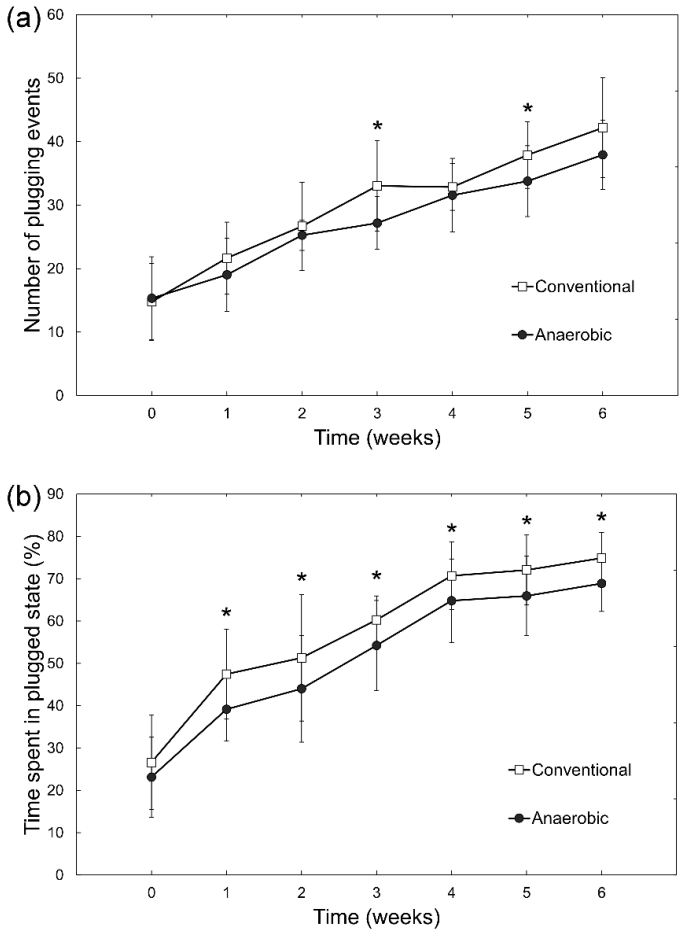

Figure 6.1.3 Plugging of individual microcapillaries in the MMCN. (**a**) Number of 'plugging' events. (**b**) Total percent of time all MMCN microcapillaries spent in a plugged state. Mean values ± SD, n = 9. Statistically significant differences ($p < 0.05$) are marked by an asterisk (*).

Conventional ektacytometry

Figure 6.1.4 shows RBC elongation index (EI) measurements made using two commercially available ektacytometers; the RheoScan-D (RheoMeditech Inc.) and LORRCA (Mechatronics Instruments BV). The EI of conventionally and anaerobically stored RBCs, as measured by both ektacytometers at low (3 Pa) and high (17 Pa) shear stresses, decreased progressively over the course of 6 weeks of hypothermic storage. Between week 0 and week 6 the EI measured by RheoScan-D decreased by 7.1% for conventionally stored RBCs and 6.2% for anaerobically stored RBCs at 3 Pa, and decreased by 5.8% for conventionally stored RBCs and 5.8% for anaerobically stored RBCs at 17 Pa. Between week 0 and week 6, the EI measured by LORRCA decreased by 7.0% for conventionally stored RBCs and 6.9% for anaerobically stored RBCs at 3 Pa, and decreased by 6.9% for conventionally stored RBCs and 5.4% for anaerobically stored RBCs at 16.87 Pa. There was not a consistent trend or statistically significant difference in EI, measured by RheoScan-D or by LORRCA, between anaerobically and conventionally stored RBCs at either low or high shear stresses (i.e., changes in EI were not consistent across different shear stresses or ektacytometers), despite the clear patterns observed for all measurements made using the AMVN and MMCN microfluidic devices for the same samples at the same time points (**Fig. 6.1.4**).

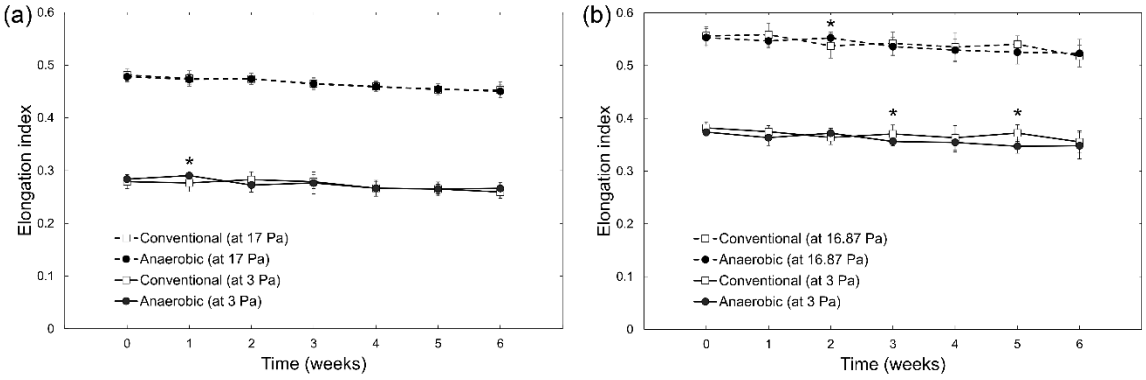

Figure 6.1.4 Elongation index (EI) measured using conventional ektacytometry. (**a**) EI measured using RheoScan-D, n = 5. (**b**) EI measured using LORRCA, n = 4. Mean values ± SD. Statistically significant differences ($p < 0.05$) are marked by an asterisk (*).

RBC morphology

Figure 6.1.5 shows morphology data for conventionally and anaerobically stored RBCs over the course of 6 weeks of hypothermic storage. The morphology of RBCs deteriorates progressively during

hypothermic storage, resulting in a heterogeneous population of cells within each unit. Stored RBCs can be categorized, based on their morphology, as well-preserved (Stomatocyte, Discocyte and Echinocyte 1), poorly preserved (Echinocyte 2 and Echinocyte 3), and irreparably damaged (sphero-echinocyte and spherocyte).[11] Overall, the fraction of well-preserved RBCs decreased and the fractions of poorly preserved and irreparably damaged RBCs increased for both conventionally and anaerobically stored RBC units over the course of storage (**Fig. 6.1.5c**). The morphology index (MI), which indicates the balance between well preserved, poorly preserved and irreparably damaged RBCs (lower is better), of conventionally stored RBC units was significantly higher than the MI of anaerobically stored RBCs from weeks 2 through 6 (**Fig. 6.1.5a**). Most importantly, there was a statistically significantly lower percentage of irreparably damaged RBCs (sphero-echinocytes and spherocytes) in anaerobically stored RBC units compared to conventionally stored units by week 6 (**Fig. 6.1.5b**).

6.1.4 Discussion

Under normal physiological conditions, RBCs are hemoglobin filled biconcave discs with high cell membrane area to cell volume ratios that enable them to deform through narrow capillaries much smaller than the resting diameter of RBCs (6-8μm).[11,158] It is well known that numerous mechanical and biochemical changes to RBCs occur during *ex vivo* hypothermic storage, which cumulatively result in the progressive degradation of RBC properties.[113,144] Oxidative damage is known to be a primary mediator of the storage-induced deterioration of the RBC membrane and cytoskeleton.[61,62,108] As RBCs accumulate these so called storage-lesions, they gradually undergo a process called echinocytosis, where the cells progressively lose membrane and volume via microvesiculation, resulting in an increasingly irregular, spiculated RBC morphology, until achieving the lowest surface area to volume ratio allowed by geometry (i.e., sphere) and ultimately undergoing lysis.[11,61,108] These changes to RBCs during storage result in a decreased ability to deform and traverse microcapillaries.[145] Changes to the RBC membrane are readily observable, with different degrees of degradation reflected by different cell morphologies.[11,158] Interestingly, individual RBCs within the same unit are known to have variable susceptibility to storage-induced deterioration, hence the well documented heterogeneity of RBC populations after only days of hypothermic storage.[158] We hypothesized that by storing RBCs anaerobically we could limit the amount of oxidative damage to RBCs which would

normally become irreparably damaged over the course of storage without adversely affecting RBCs which would normally remain well preserved.

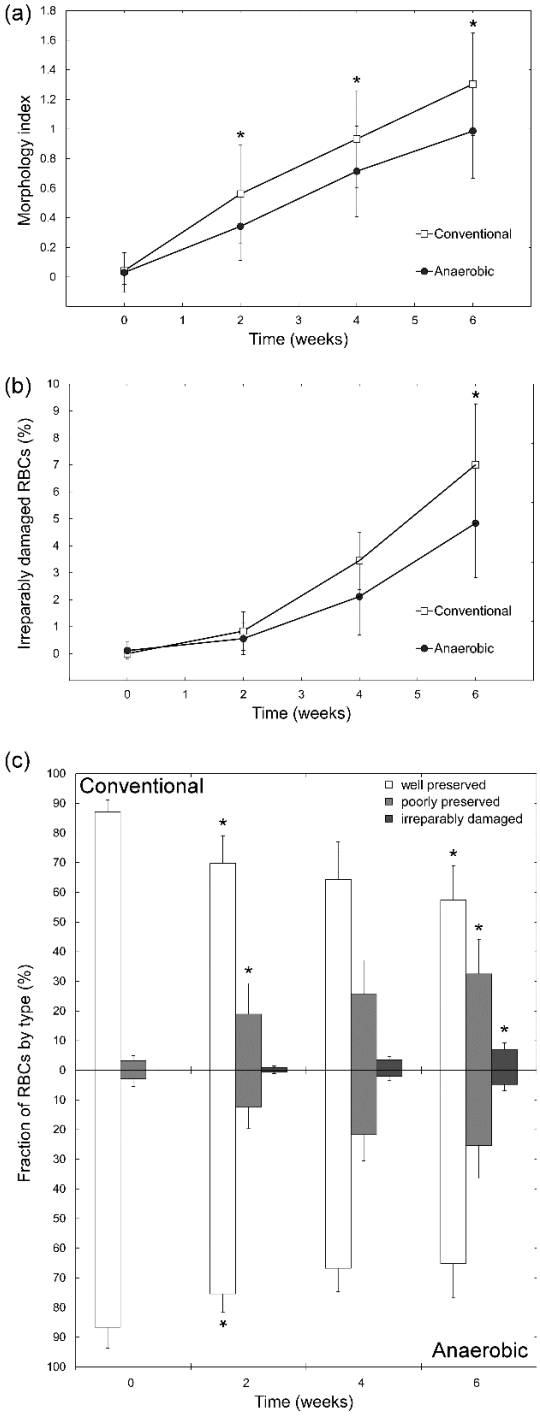

Figure 6.1.5 Morphology of anaerobically and conventionally stored RBCs. (**a**) Morphology index. (**b**) Percent irreparably damaged RBCs. (**c**) Well preserved, poorly preserved and irreparably damaged RBCs. Mean ± SD, n = 9. Significant differences are marked by an asterisk (*).

The key finding of this study is that anaerobic storage conditions preserve the rheological properties of RBCs more effectively than conventional (aerobic) conditions during *ex vivo* hypothermic storage. The overall rate at which anaerobically stored RBCs were able to perfuse two distinct microfluidic networks (AMVN and MMCN) was consistently faster than that of conventionally (aerobically) stored RBCs (**Fig. 6.1.2**), which suggests that the overall rheological fitness of anaerobically stored RBCs is superior to that of conventionally (aerobically) stored RBCs. Specifically, anaerobic storage appeared to decrease the number of RBCs which accumulated irreparable damage to the RBC membrane and cytoskeleton over the course of six weeks of hypothermic storage. This conclusion was supported by the lower number of plugging events and lower percentage of time spent in a plugged state by individual poorly deformable RBCs in the MMCN (**Fig. 6.1.3**). This conclusion was further supported by direct morphological analysis of anaerobically and conventionally stored RBCs, which found that the morphology index of anaerobically stored RBCs was consistently better than that of conventionally stored RBCs, largely because the fractions of poorly preserved and irreparably damaged RBCs were lower for anaerobically stored RBCs (**Fig. 6.1.5**). Interestingly, the deformability measurements made by both conventional ektacytometers (RheoScan-D and LORRCA) indicated no consistent, statistically significant difference between conventionally and anaerobically stored RBCs (**Fig. 6.1.4**), however we believe that this lack of a difference (which would contradict all other measurements) is a result of the lower sensitivity of the ektacytometers compared to the microfluidic devices (please see discussion below), which is in agreement with our previous comparison of ektacytometer and microfluidic technology.

During the planning phase of this study we anticipated that the impact of anaerobic storage on the rheological properties of stored RBCs may not be obvious for aggregate measurements which generate an average deformability value over a population of RBCs (e.g., conventional ektacytometer), but may become apparent when measuring the properties of individual RBCs. We reasoned that by removing oxygen, we may alter the balance between well preserved, poorly preserved and irreparably damaged RBCs, which could result in significant changes within various subpopulations of RBCs (e.g., least deformable RBCs) without drastically impacting the average properties of the unit. Therefore, in addition to conventional ektacytometers, we chose to utilize several microfluidic devices which are highly sensitive to changes to

individual RBCs in order to detect minor differences within units from week to week and between conventionally and anaerobically stored units of the same storage duration.

The AMVN has previously been validated as a robust *in vitro* system for detecting a wide range of changes to the rheological properties of blood.[128,145-147,159] However, the AMVN has several limitations including: (1) it is constructed of PDMS, which does not reproduce the mechanical or biochemical properties of microvasculature *in vivo*, (2) the microchannels have rectangular cross-sections, which is not realistic,[165] and (3) the layout of microchannels is biologically-inspired, but is simplified and is not representative of all possible configurations of human microvasculature. The MMCN has previously been used to assess the deformability of stored RBCs and shares limitations (1) and (2) with the AMVN but is intentionally not biologically-inspired.[147] Additionally, there are limitations to the plugging event measurements made using the MMCN device; while this metric accurately measures frequency of plugging, it does not account for the duration of these events. This prompted the inclusion of an additional metric, the percentage of time spent in plugged state, which provides a measure of the duration of the plugging events. The microfluidic device used to facilitate imaging of RBCs for morphological analysis has been validated previously.[158] RBC shape, independent of any other factors, has previously been correlated with the ability of RBCs to perfuse an artificial microvascular network,[145] which supports the use of RBC morphology as an indicator of RBC rheological fitness. A final, unavoidable limitation of this study was that all RBC units were removed from the blood bank refrigerator, mixed and sampled weekly throughout storage. This extra manipulation of the units could potentially have resulted in unknown changes to RBC properties compared to undisturbed units. However, because the sampling procedure was identical for anaerobically and conventionally stored units, these potential changes are unlikely to have affected the outcomes of this study.

The primary purpose of collecting and storing RBCs is to later transfuse them, and the primary goal of most RBC transfusions is to increase the ability of the cardiovascular system to deliver oxygen to tissues and organs. Therefore, it is essential to store RBCs in a manner which best preserves their rheological properties, so that they can efficiently perfuse the microvasculature upon transfusion. Here we showed that anaerobic conditions decreased the rate at which rheological properties of the RBCs deteriorated during hypothermic storage and that anaerobically stored RBC units contained a smaller fraction of irreparably damaged RBCs than conventionally (aerobically) stored RBC units. It has previously been shown that

transfusion of younger RBC units, which on average contain fewer poorly preserved and irreparably damaged RBCs, improved cardiac surgery patient outcomes.[64,68,166] However, these results were not replicated in a more recent study.[69] While the net result of most RBC transfusions is undoubtedly beneficial, certain subpopulations of the transfused cells, which accumulated irreparable damage during storage and cannot deform sufficiently to traverse the microcirculation, may actually provide no therapeutic benefit to the patient. Our *in vitro* results suggest that the number of irreparably damaged, poorly deformable RBCs within otherwise well-preserved RBC units may significantly alter microvascular blood flow *in vivo* and could therefore contribute to differential patient outcomes. Even if microcapillary networks *in vivo* are better able to deal with poorly deformable RBCs (e.g., via biochemically regulated vasomotion) than the comparatively rigid PDMS microfluidic devices, the impact of these damaged RBCs on the overall rheology of stored blood remains clinically significant.[145]

The subpopulation of poorly deformable, irreparably damaged RBCs identified in this study most likely constitutes the majority of the RBCs which are known to not survive beyond the 24 hours immediately after transfusion.[136,167] RBCs which lyse or are removed from circulation via sequestration by the spleen soon after transfusion do not serve their intended purpose of perfusing the microvasculature and oxygenating tissue, but instead contribute to negative side effects of transfusion (e.g., iron overload).[148] This suggests that it would be beneficial to avoid transfusing the most irreparably damaged RBCs within individual RBC units. Importantly, it has previously been shown that the rheological properties and morphology of well and poorly preserved RBCs can be recovered prior to transfusion via cell washing,[128,146] but that irreparably damaged RBCs cannot be fully recovered, as they have lost too much membrane area to reassume normal, healthy morphologies and rheological function. Therefore a primary goal of RBC storage should be to prevent RBCs from accumulating enough storage lesions to become irreparably damaged. Because storage under anaerobic conditions decreases the amount of irreparably damaged RBCs and results in a statistically significant improvement in AMVN and MMCN perfusion as well as MMCN plugging, we conclude that anaerobic storage increases the quality and efficacy of stored RBCs.

6.2 Washing stored red blood cells in an albumin solution

The following research has previously been published and much of the following text is reprinted with permission from: Transfusion, 55(80), Reinhart WH, Piety NZ, Deuel JW, Makhro A, Schulzki T, Bogdanov N, Goede JS, Bogdanova A, Abidi R, Shevkoplyas SS, "Washing stored red blood cells in an albumin solution improves their morphologic and hemorheologic properties," pages 1872 – 1881, Copyright 2015 AABB

6.2.1 Introduction

The transfusion of red blood cells (RBCs) stored for a longer period of time, is associated with an increased morbidity and mortality.[64,168-171] The underlying pathophysiological mechanisms have not been fully elucidated, but are likely to be multifactorial. Of major concern is the fact that RBC properties degrade progressively during storage.[172] These so-called storage lesions are of various origin:[144,173] lipid peroxidation,[174] exposure of the thrombogenic phosphatidylserine on the membrane surface,[175] clustering[174] and degradation[176] of the transmembraneous anion channel protein band-3 have been described.

A frequently underestimated storage lesion is the progressive echinocytic shape transformation of RBCs.[166,177-180] Echinocytes have decreased membrane[181] and whole cell[175,182] deformability, they increase blood viscosity[166,180,183] and impair microcirculatory blood flow,[128] which may contribute to poor clinical outcomes after massive transfusion.

Albumin is capable of reversing this storage-induced echinocytic shape transformation, i.e., higher degrees of echinocytosis become less frequent, while normal discocytic shapes become more abundant.[183,184] The aim of this study was to determine whether such a recovery of RBC shape improves the rheological behaviour of RBCs and hence improves blood flow properties.

6.2.2 Methods

Preparation of RBC samples

Units of RBC concentrates were obtained from local blood banks (Red Cross Blood Bank, Kantonsspital Graubünden for experiments in Switzerland; Gulf Coast Regional Blood Center, Houston for

experiments in the USA). They had been produced from whole blood drawn in citrate-phosphate-dextrose (CPD) and had been leukocyte-depleted. These RBCs had been stored either in SAGM (NaCl, adenine, glucose, mannitol) or PAGGSM (NaCl, adenine, glucose, guanosin, Na_2HPO_4/NaH_2PO_4, mannitol) for 6 and 7 weeks, respectively, in Switzerland, or in AS-1 (NaCl, adenine, glucose, mannitol) for 6 weeks in the USA. Fresh blood was collected from healthy volunteers using EDTA as an anticoagulant. Fresh blood was either passed through a leukocyte reduction filter (Purecell NEO, Pall Corp., Port Washington, USA) or the buffy coat and adjacent RBC layer were removed after centrifugation.

For RBC washing, one part stored RBCs (hematocrit 50-60%) was diluted with 9 parts 1% human serum albumin (HSA) solution. For the experiments in Switzerland, a human serum albumin solution with a concentration of 20 g/L (Albumin CSL, Behring, Bern, Switzerland) was diluted to 1% in phosphate buffered saline (PBS); in the USA, human serum albumin (Sigma-Aldrich, St. Louis, MO, USA) was dissolved at 1% in normal saline. After 10 min of washing under gentle mixing, the samples were centrifuged at 2500×g for 5 min. Packed RBCs were prepared from all samples by discarding the supernatant. They were resuspended in PBS or in saline for further experiments. Blood cell counts, RBC indices and hematocrit were measured with a hematology analyser.

Analysis of the RBC morphology

For the assessment of the RBC morphology, 20 µL of the RBC suspensions were fixed by addition of 1000 µL 1% glutaraldehyde. The specimens were analysed by light microscopy in wet preparations using a Neubauer counting chamber. For each sample, at least 200 RBCs were classified on the basis of the nomenclature of Bessis.[11] Thereby, a discocyte has a score of 0, an echinocyte I (an irregularly contoured discocyte with up to 5 protrusions) has a score of +l, an echinocyte II (a flat RBC with several spicules) has a score of +2, an echinocyte III (ovaloid or spherical RBC with multiple spicules) has a score of +3, an echinocyte IV or sphero-echinocyte (a sphere with multiple short and thin spicules) has a score of +4, a stomatocyte I (convex-concave instead of biconcave RBC) has a score of -1, etc. The morphological index was calculated according to Ferrell and Huestis[185] as the sum of all scores divided by the number of analysed RBCs. Some glutaraldehyde-fixed samples were also prepared for scanning electron microscopy according to standard procedures (e.g., see[183]).

Cell density fractionation in Percoll density gradients

RBCs were mixed with 90% isotonic Percoll solution prepared by mixing a 90 mL aliquot of sterile Percoll (GE Healthcare, density 1.130 g/mL) with 10 ml x10 phosphate buffered saline (PBS, Sigma-Aldrich) and 11 mL x1 PBS (Sigma-Aldrich). This mixture was centrifuged using a Sorvall RC 5C plus centrifuge (Thermo Fisher Scientific, Inc.) equipped with an SM-24 rotor at 4ºC for 30 min at 45,000×g.

Cell water and ion detection

RBCs were placed in pre-weighed pre-dried Eppendorf tubes washed three times at 4ºC with a Na/K/Cl-free solution containing 100 mM of $Mg(NO_3)_2$ and 10 mM imidazol-HCl buffered when cooled. The obtained cell pellets were weighed before and after drying at +80ºC for 72 h. The water content was calculated between the wet and dry pellet weights.

Cell ATP, reduced (GSH) and oxidized (GSSG) glutathione levels

Aliquots of RBC suspensions (200µL) were deproteinized by suspending in ice-cold 5% aqueous solution of trichloracetic acid. The protein pellet was discarded and the supernatant used for ATP detection and GSH/GSSG measurements as described elsewhere.[186] Briefly, ATP was measured using a luciferine-luciferase assay (FLAA ATP Bioluminescent Assay Kit, Sigma-Aldrich). GSH and GSSG were detected using Ellmanns reagent either in the presence or absence of glutathione reductase and NADPH. The values were normalized for the hematocrit.

Ektacytometry

RBC deformability was analyzed by laser diffraction with an ektacytometer (Technikon, Bayer, Leverkusen, Germany) in the osmoscan mode.[187] Aliquots of 500µL of either stored RBCs or stored RBCs washed in 1% HSA as described above, were added to 3mL of a hyperviscous 20% dextran 70 solution (Sigma-Aldrich). They were inserted into the ektacytometer for measurement of RBC deformability in a continuous osmolality gradient generated by the addition of sodium chloride. Digitized osmoscans were obtained, on which the following parameters were calculated: P_{max}: the highest value of the deformability index (DI) and P_{min}: the lowest deformability reached on the hypoosmolar branch of the curve, representing

the inflection point where hemolysis occurs. In addition the osmolalities were determined at which half of the P_{max} was seen on the hypoosmolar (P'A) and hyperosmolar branch (P'B) of the osmoscan curve.

Measurement of suspension viscosity

Suspension viscosities were measured with a Couette-type viscometer (Contraves LS-30, ProRheo, Althengstett, Germany) at room temperature (21.6 ± 0.7 °C) at shear rates ranging from 0.11 to 128 s^{-1}. In the first set of experiments, RBCs were suspended with a hematocrit of 45% in PBS containing 3% dextran 70 (Sigma-Aldrich), which allows RBC aggregation. RBCs stored for 6 weeks in SAGM were used, either unwashed or washed in the 1% HSA solution and were compared with freshly drawn RBCs from healthy volunteers. In the second set of experiments, RBCs stored for 7 weeks in PAGGSM were used, either unwashed or washed in 1% HSA. Washed RBCs were suspended in saline, unwashed RBCs either in saline or resuspended in their own storage medium with a hematocrit of 40 %.

Measurement of the RBC ability to perfuse an artificial microvascular network

Artificial microvascular network (AMVN) devices were fabricated from polydimethylsiloxane (PDMS) using previously described methods.[128,131,188,189] Each AMVN device consisted of three identical networks of microchannels; each of the network units had a separate inlet and all converged into a common outlet.[128,188] RBCs stored for 6 weeks in AS-1 were used. A 60 µL sample of each type (stored, washed, fresh) with hematocrit adjusted to 40% was loaded into one of the three inlets in of the AMVN device. To perform the measurement, the driving pressure was set to 0 cmH_2O, image acquisition was initiated, and after 30 seconds the driving pressure was increased to 20 cmH_2O and image acquisition continued until 10 minutes had elapsed. Images were acquired on an inverted bright field microscope (IX71, Olympus America Inc., Center Valley, PA, USA) equipped with a high-speed camera (MC1362, Mikrotron GmbH, Unterschleissheim, Germany). Images were captured in bursts of 10 frames at 100 fps every 10 seconds using a custom image capture program. Images were analysed offline with a custom algorithm in MATLAB (The Math Works Inc., Natick, MA, USA) that computed mean cell velocity in the postcapillary venule (exit microchannel) for each network unit in the device. Each sample was measured in triplicate, using three separate AMVN devices.

Statistical analysis

Statistical analysis was performed with STATISTICA for Windows, Version 9.1 (Statsoft Inc., Tulsa, OK, USA). A one way analysis of variance (ANOVA) was used for the comparison of more than two groups, a paired t-test for two groups, as appropriate. The results are presented as mean values ± standard deviation (SD). A p-value of < 0.05 was considered statistically significant.

6.2.3 Results

Storage of RBCs in any available conservation medium (SAGM, PAGGSM, or AS-1) for the allowed blood banking period of 6 weeks (SAGM and AS-1) or 7 weeks (PAGGSM) led to an echinocytic shape transformation, which is illustrated in **Figure 6.2.1a**. A marked heterogeneity of shape changes was observed intra-individually, with RBC shapes ranging from discocytes to sphero-echinocytes, as well as inter-individually, ranging from 43% discocytes and only 12% higher degrees of echinocytosis (E II-E IV) in the best donor to 8% discocytes and 69% E II-E IV in the worst case. Washing stored RBCs in a 1% HSA solution reversed echinocytosis towards discocytosis, which is shown in **Figure 6.2.1b**. Note that even higher degrees of echinocytosis became less frequent.

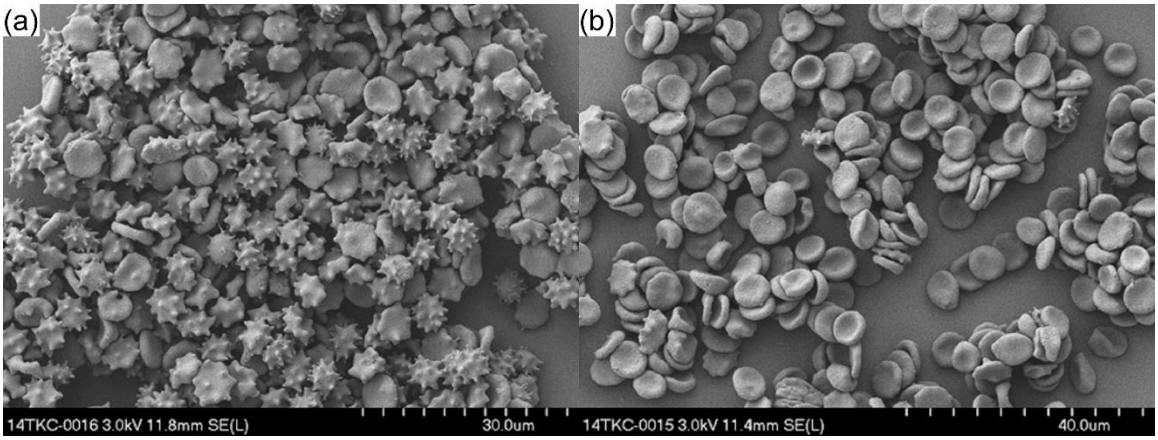

Figure 6.2.1 Scanning electron micrographs of stored and washed RBCs. (**a**) RBCs stored in SAGM for 6 weeks. (**b**) The same, stored RBCs as in (a) washed in a 1% human serum albumin solution.

The quantitative assessment of RBC shape transformation at the end of storage in either SAGM or PAGGSM and the shape restoration after washing these RBCs in a 1% HSA solution is shown in **Figure**

6.2.2. After washing, the strongly echinocytic RBC shapes shifted back towards discocytosis, i.e., the percentage of discocytes increased, while higher degrees of echinocytosis were decreased (ANOVA: $p < 0.001$). This shape recovering effect remained stable for at least 24 h (data not shown). As shown in **Table 6.2.2**, the morphological index (MI) decreased from 1.72 ± 0.32 to 0.29 ± 0.18 and from 1.52 ± 0.38 to 0.66 ± 0.43 for RBCs stored in SAGM and PAGGSM, respectively. It was a specific effect of the HSA solution, since the same washing procedure either in PBS alone or in saline had no shape recovering effect; the morphological index (MI) was 1.38 ± 0.44, and 1.40 ± 0.38, respectively. A resuspension of stored RBCs in fresh frozen plasma, or even washing in plasma as described (ten times the volume), had no shape recovering effect, the MI remained at 1.63 ± 0.29 and 1.68 ± 0.42, respectively.

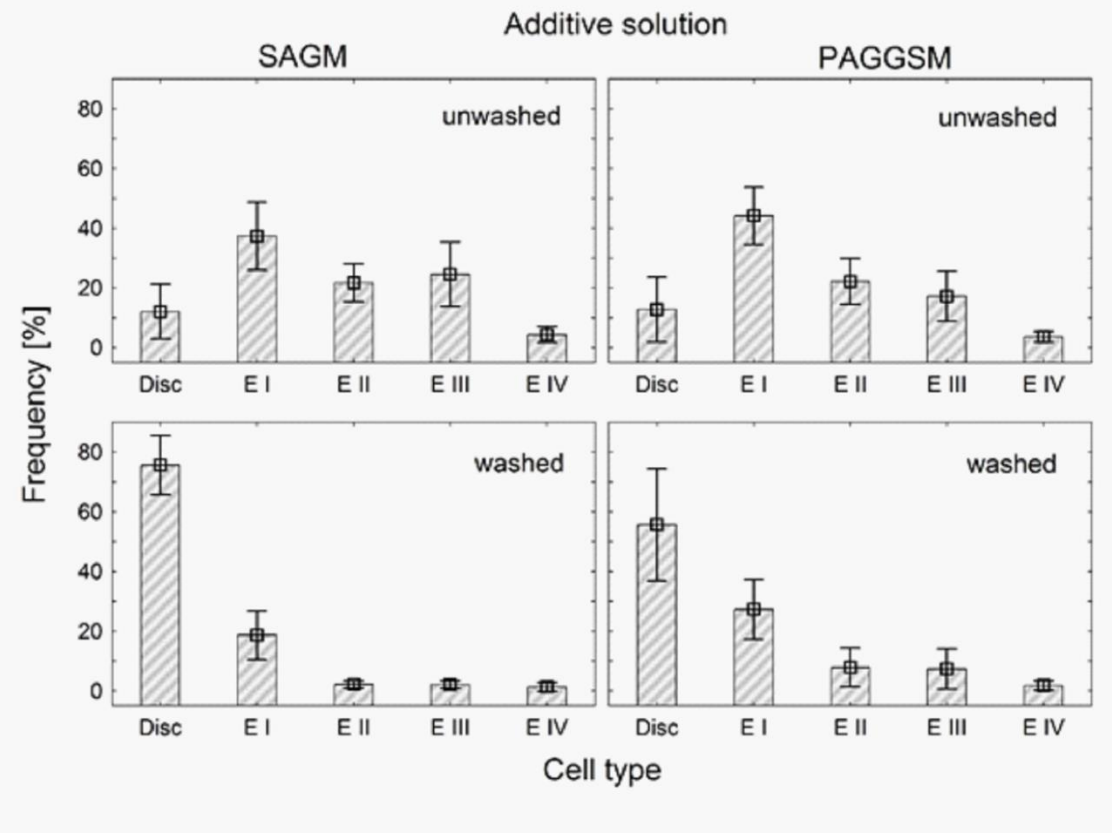

Figure 6.2.2 Histograms of stored RBC morphology before and after washing. 6 weeks in SAGM (left) or 7 weeks in PAGGSM (right); before washing (above) and after washing in a 1% human serum albumin solution (below). Mean values ± SD, n = 11 (SAGM), n = 9 (PAGGSM).

Storage of RBCs in SAGM conservation medium at 4°C for 6 weeks increased the mean corpuscular volume (MCV) as shown in **Table 6.2.1**. This indicates RBC swelling during storage. Washing stored RBCs

in a 1% HSA solution reduced the MCV and increased the MCHC as shown in **Table 6.2.2** for SAGM and PAGGSM, respectively. The MCV reached values similar to those measured before storage (see **Table 6.2.1**).

Table 6.2.1 Hematological parameters at the beginning and end of 6 week storage in SAGM at 4°C.

Parameter	Day 1	Day 42
RBC (x10/µL)	6.60 ± 0.29	6.56 ± 0.30
Hb (g/L)	201 ± 8	201 ± 8
Hct (%)	58.6 ± 1.9	61.5 ± 1.7 *
MCV (fL)	88.3 ± 2.6	93.8 ± 3.2 *

*indicates $p < 0.001$ (paired t-test)

A water loss from the RBCs subjected to washing with HSA-containing PBS, monitored as a decrease in MCV and up-regulation of MCHC, was confirmed by the measurement of RBC density and cell water content (**Fig. 6.2.3**). RBCs stored for 42 days underwent swelling and decrease in density compared to fresh RBCs. The upward shift of overhydrated RBCs forming medium (M) and light (L) fractions in Percoll gradient was not any more observed after the stored RBCs had been washed with a HSA-containing solution. Note that hemolysis observed in stored RBCs as free hemoglobin solution above the Percoll gradient did not occur in cells washed in HSA-containing solution. Water content was measured in packed, stored RBCs, either untreated (control) or washed with HSA-containing solution. As shown in **Figure 6.2.3B**, stored and washed RBCs contained significantly less water than stored control RBCs. This finding is in line with the decrease in MCV and increase in MCHC observed upon washing with HSA-containing solution.

Washing RBCs in a 1% HSA solution resulted in a subtle increase in intracellular ATP levels from 2.96 ± 0.24 to 3.73 ± 0.43 mmol/L packed RBCs ($p=0.0002$). Reduced glutathione levels were not affected by the washing (1.04 ± 0.16 and 1.13 ± 0.18 mmol/L packed RBCs for control and washed samples, respectively). Oxidized glutathione levels, however, decreased after washing from 7.1 ± 2.9 to 4.5 ± 2.8% ($p=0.045$).

Table 6.2.2 Influence of washing procedure with 1% human serum albumin solution on morphological parameters of RBCs stored for 6 weeks in SAGM (n = 11) or 7 weeks in PAGGSM (n = 9). Mean values ± SD are given, p-value is for a paired t-test.

Parameter	Stored RBCs	Stored RBCs, washed in 1% albumin	p
Stored in SAGM			
MCV (fL)	93.2 ± 3.5	87.9 ± 3.2	< 0.005
MCHC (g/dL)	34.5 ± 1.1	38.6 ± 1.2	< 0.005
MI	1.72 ± 0.32	0.29 ± 0.18	< 0.005
Stored in PAGGSM			
MCV (fL)	94.5 ± 8.7	88.3 ± 6.4	< 0.005
MCHC (g/dL)	32.8 ± 2.1	35.0 ± 1.2	< 0.0005
MI	1.52 ± 0.38	0.66 ± 0.43	< 0.00005

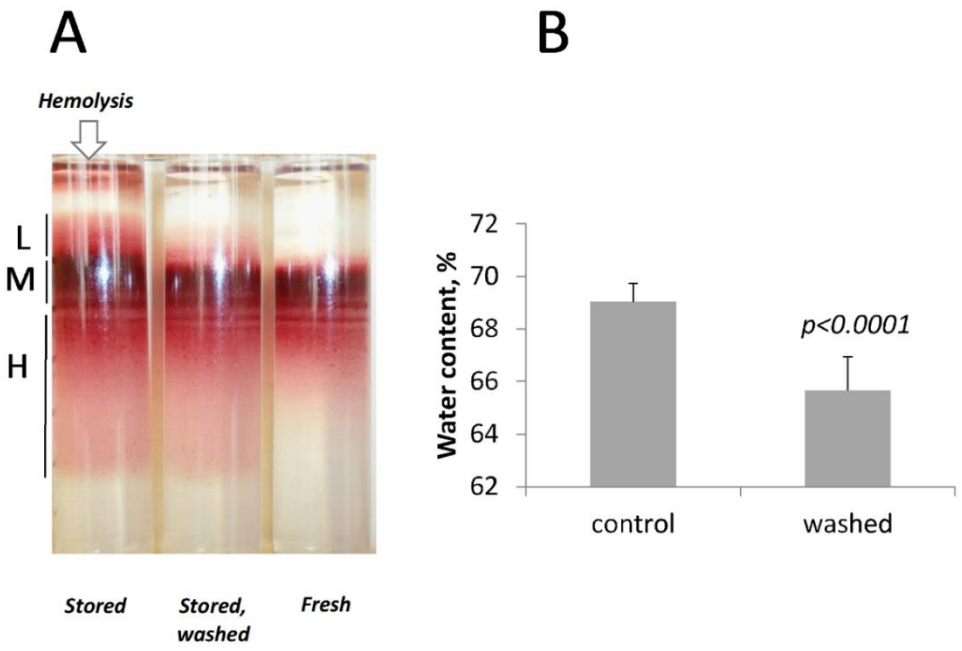

Figure 6.2.3 Changes in stored (6 weeks; SAGM) red cell density and water content upon washing with 1% HSA. (**a**) Distribution in Percoll density gradients; low (L), medium (M) and high (H) density fractions. (**b**) Stored RBC water content measured gravimetrically, n = 11.

RBC deformability measured with ektacytometry is shown in **Figure 6.2.4**. Compared with the deformability index of fresh RBCs, stored RBCs were less deformable. The maximum DI of stored RBCs,

which had been washed in 1% HSA, was similar to the maximum DI of stored, but unwashed RBCs (0.567 ± 0.013 and 0.563 ± 0.013, respectively). At low osmolality, the curves were also similar (DI_{min} 0.056 ± 0.041 and 0.043 ±0.025 at 132 ± 8 mOsm/kg and 133 ± 6 mOsm/kg for washed and unwashed RBCs, respectively). At high osmolalities, the osmoscan curves of RBCs washed in 1% HSA were slightly shifted to the left, i.e., to lower osmolality; the half maximum DI (P'B) was at 379.8 ± 10.4 mOsm/kg compared with 393.7 ± 10.7 mOsm/kg, respectively (p =0.003). These results are in agreement with the reduced water content of RBCs after washing (**Fig. 6.2.3**) and resulting decrease in MCV and increase in MCHC (**Table 6.2.2**).

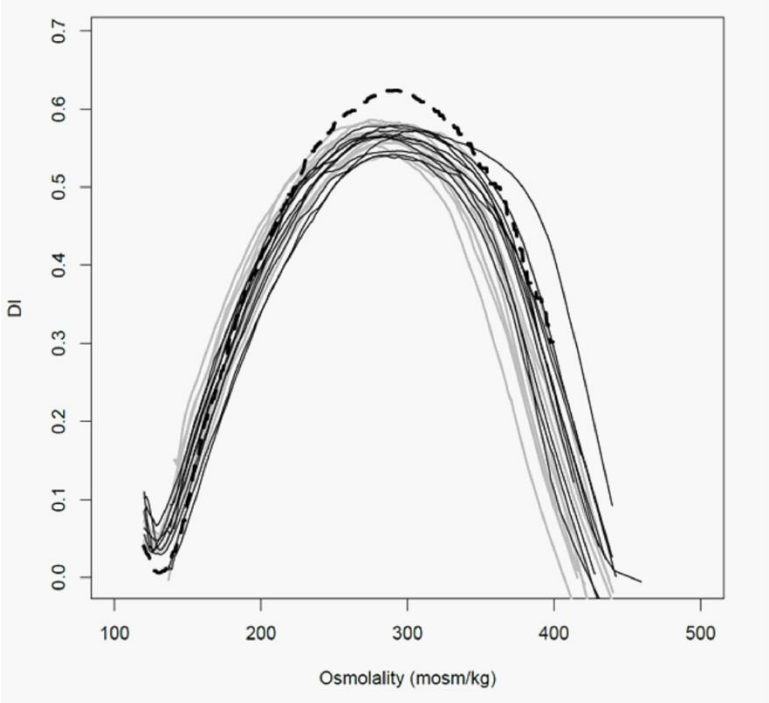

Figure 6.2.4 Osmotic gradient ektacytometry (osmoscans) of RBCs stored for 6 weeks in SAGM, either unwashed (grey lines) or after washing in a 1% human serum albumin solution (black lines). The dashed line represents mean values of fresh control RBCs.

Figure 6.2.5 shows the viscosities of RBCs stored for 6 weeks in SAGM, which were resuspended in a 3% dextran 70 solution. The suspension viscosities increased with decreasing shear rates, which reflects the RBC aggregating properties of dextran 70. The suspension viscosities of stored RBCs were much higher than that of fresh RBCs. However, washed and unwashed, stored RBCs had similar viscosities, with a tendency for higher values of washed RBCs at high shear rates and lower values at low shear rates. When the data, which were obtained at a standardized hematocrit, but differences in RBC count due to differences in

MCV (see **Table 6.2.2**), were normalized for the differences in RBC count, the suspension viscosities of washed RBCs were significantly lower at shear rates < $1s^{-1}$ (data not shown).

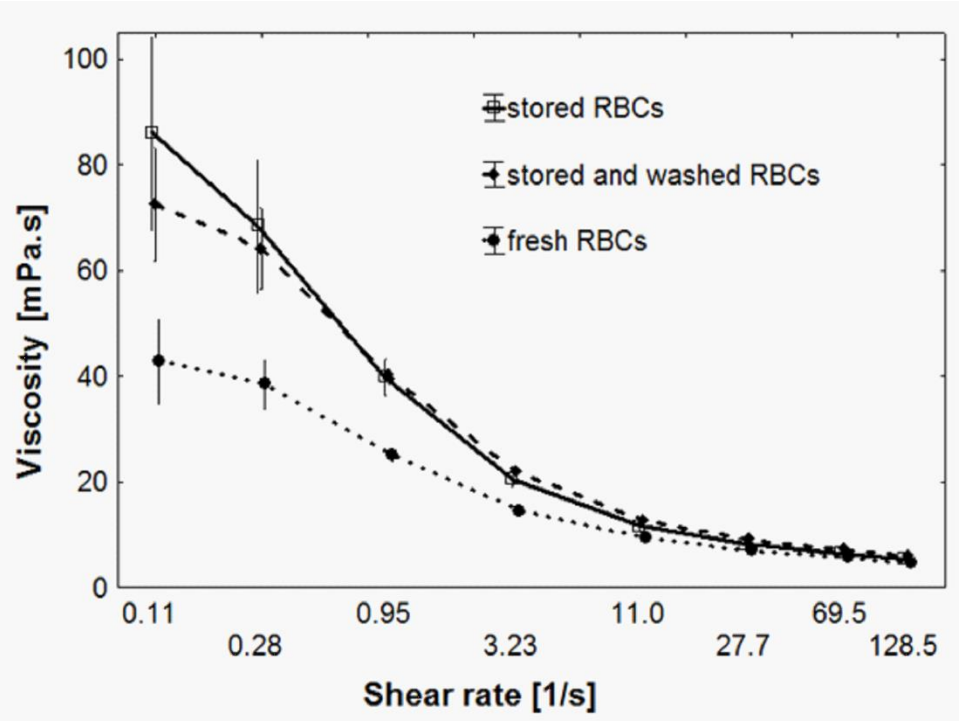

Figure 6.2.5 Log-linear plot of suspension viscosities of fresh, stored (6 weeks; SAGM) and washed (1% HSA solution) RBCs at 37°C. RBCs suspended in a 3% dextran 70 solution with a hematocrit of 45%. Mean values ± SD, n = 11.

Figure 6.2.6 shows the suspension viscosities of RBCs stored for 7 weeks in PAGGSM. These RBCs were resuspended either in their storage medium or in saline, or they were washed in 1% HSA as described above, and then resuspended in saline. The hematocrit was adjusted to 40%, which resulted in a difference in the RBC count due to the difference in MCV (RBC count: 3.74 ± 0.36 and 3.99 ± 0.29 $x10^6/\mu L$ for stored RBCs and stored/washed RBCs, respectively, $p < 0.005$). The viscosity of all suspensions increased gradually with decreasing shear rate, indicating that this so called shear thinning effect is not only caused by RBC aggregation, which does not occur in saline as used in this study. RBCs washed in a 1% HSA solution had a lower suspension viscosity than unwashed RBCs (ANOVA for repeated measures: $p \leq 0.01$), a phenomenon which was more pronounced at lower shear rates. The morphological index of RBCs correlated with low shear viscosity at 0.11 s^{-1} ($y = 5.06 + 1.03x$, $r = 0.529$, $p < 0.05$). The osmolality and pH of the

supernatant were similar. They were 307 ± 4 mOsm/kg, 293 ± 10 mOsm/kg and 290 ± 3 mOsm/kg and 6.85 ± 0.22, 7.00 ± 0.112, and 6.87 ± 0.08 for the conservation medium, and the suspending medium of stored and stored/washed RBCs, respectively.

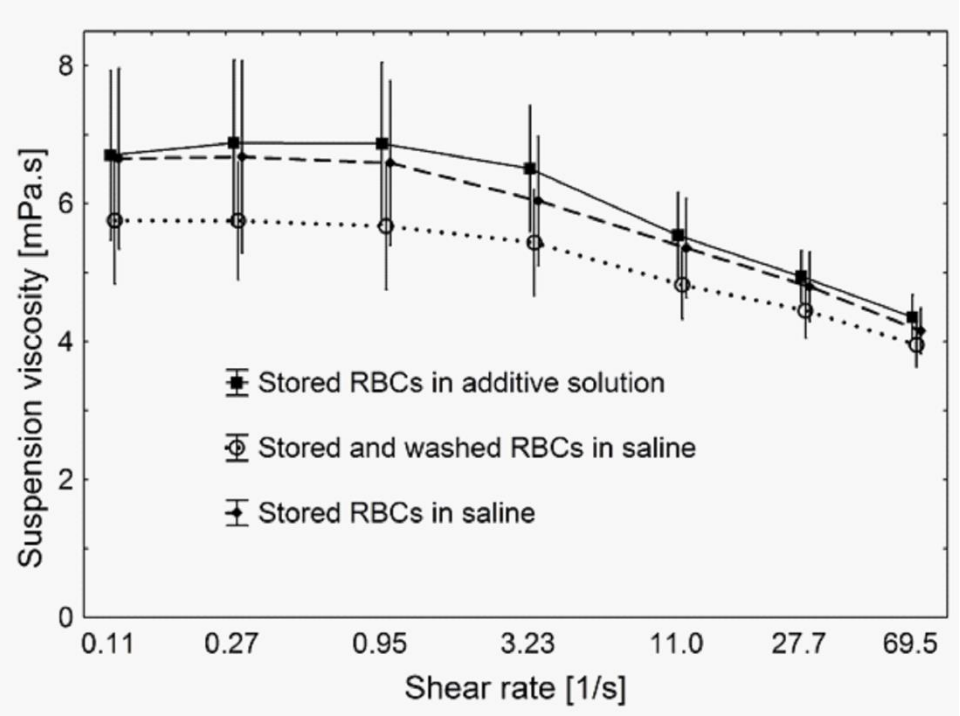

Figure 6.2.6 Log-linear plot of suspension viscosities at room temperature of RBCs stored for 7 weeks in PAGGSM. RBCs were either resuspended in their storage medium, in saline, or in saline after washing in 1% human serum albumin before resuspension. Mean values ± SD, n=9.

Figure 6.2.7 shows the analysis of the ability of stored and washed RBCs to perfuse an artificial microvascular network. The morphological index of RBCs stored for 6 weeks in AS-1 decreased from 1.82 ± 0.07 to 1.19 ± 0.11 after washing in a 1% HSA solution ($p = 0.004$). **Figure 6.2.7a** shows perfusion rate traces that are characteristic of the data acquired for fresh, stored and washed RBCs using the AMVN device. Each trace initially started at ~0 nL/s when the driving pressure was 0 cmH_2O, increased as the driving pressure was increasing, and plateaued after the 20 cmH_2O target driving pressure was reached. The mean perfusion rate for each sample was calculated as the average of the first 10 data points of the plateau region common to all traces. **Figure 6.2.7b** shows normalized (with respect to fresh RBCs) perfusion rates for stored and washed RBCs. RBCs from all stored units experienced an increase in AMVN perfusion rate after

washing, however the degree of improvement varied significantly between units. It is tempting to speculate that the inter-donor differences in storage-induced shape transformation may have been the reason. The minimum increase in perfusion rate due to washing was 4.84 % of fresh (unit 2) while the maximum increase was 10.49 % of fresh (unit 1). Increase in perfusion rate after washing appeared to be inversely proportional to the perfusion rate of the stored RBCs prior to washing. The improvement of perfusion rate for washed RBCs was limited to approximately 90 % of fresh for all units, regardless of the initial (stored) perfusion rate. The mean perfusion rate for stored RBCs was 81.4 ± 3.0 % of the perfusion rate for fresh RBCs suspended in saline. A single washing of stored RBC samples with 1% HSA solution before resuspension reduced the morphological index and improved the mean perfusion rate to 88.0 ± 2.0 % of the perfusion rate for fresh RBCs. The mean increase in perfusion rate after washing with 1% HSA solution was 6.7 ± 1.9 %. Additionally, RBC transit in the artificial microvascular network at the level of 5 µm capillaries was observed to occasionally experience RBC plugging with stored RBCs, which did not seem to occur with fresh RBCs. Washing of stored RBCs in 1% HSA did not improve this plugging rate visibly.

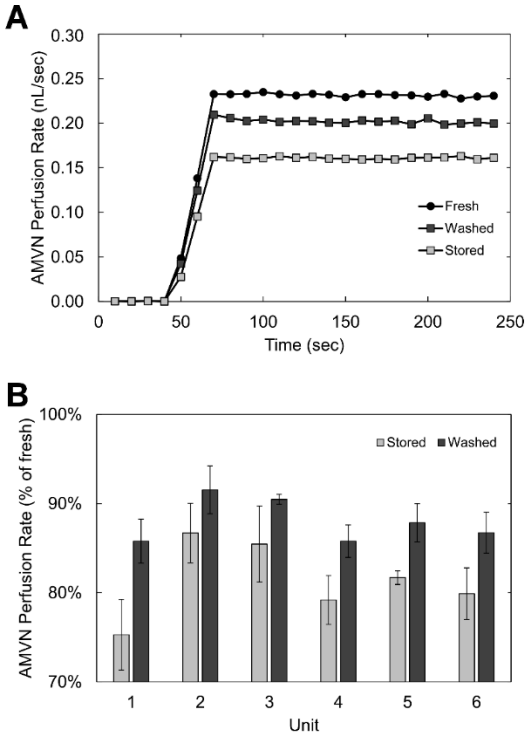

Figure 6.2.7 Ability of RBCs to perfuse the AMVN. (**a**) Representative perfusion rate traces for fresh (●), stored (■) and 1% HSA washed stored RBCs (■). (**b**) Normalized (with respect to fresh RBC) AMVN perfusion rates for stored and washed RBCs, n = 6.

6.2.4 Discussion

The results of the present study confirm that HSA has the unique capacity to reverse storage-induced echinocytosis.[183,184] This shape recovering effect depends on the concentration of HSA and is inversely related to the hematocrit.[184] Based on these data we had decided in the present study to wash stored RBCs with a tenfold dilution in 1% human serum albumin solution, which lowered the hematocrit temporarily to about 5%. This effect of HSA was not due to differences in osmolality because 1% HSA did not affect the osmolality of the suspending medium. The effect was specific to HSA, since it was not seen when stored RBCs were washed in either PBS, saline, or even plasma. The latter indicates that recovery of RBC shape should not be expected after transfusion to patients, but that these abnormally shaped RBCs could circulate in the recipient until they are removed by the reticulo-endothelial system, primarily the spleen.[190]

Why does the shape recovery occur only in 1% HSA solution, but not in plasma which has a higher HSA concentration? In plasma, albumin binds avidly to many different types of molecules such as calcium, fatty acids, hormones, and drugs,[191] which may diminish available binding sites for interactions with RBC membrane. Furthermore, plasma contains echinocytogenic molecules (e.g., globulins), which may interact with the RBC membrane[192] and induce dose-dependent echinocytosis,[193] thus counteracting the shape-recovering action of albumin.

The mechanism behind this action of HSA has not been elucidated so far. Echinocytosis is induced when molecules are intercalated in the outer half of the membrane lipid bilayer, which leads to a relative expansion of the membrane towards the outside and the formation of membrane protrusions or spicules according to the bilayer couple theory.[194] One may postulate that HSA is capable of removing molecules from this outer half of the membrane lipid bilayer, which leads to a shape normalisation. We have shown previously that HSA-induced shape restoration is a rapid process,[184] which suggests extraction of responsible agents from the membrane. Membrane-derived lysophosphatidylcholine (lysolecithin) generated during RBC storage[195-197] induces echinocytosis.[198-200] HSA is known to interact with RBC membrane[201] and to be able to remove lysophosphatidylcholine from the membrane,[200,202] which could explain its shape-recovering action.

RBC swelling during storage leads to an increase of MCV and a decrease of MCHC.[166,180] It is interesting that the partial shape recovery induced by washing in 1% HSA also reduced MCV. This was not an artefact of the aperture impedance analyser, which may overestimate the effective volume of a particle

with less deformability and/or an odd shape,[203] but was confirmed by a loss of cell water and increased density (**Fig. 6.2.2**). As discussed above, this effect was not due to osmolality of the HSA solution, which was not different from that of saline or PBS. The underlying mechanism, therefore, remains to be elucidated.

Oxidation triggers the formation of protein band 3 aggregates in the RBC membrane, which has an impact on the RBC shape. These band 3 aggregates serve as scaffolds for the recognition and binding of naturally occurring antibodies (NAF) against band 3 and complement.[204] Our observation of a reduction of oxidized glutathione after washing in a 1% HSA solution suggests that HSA may function as a scavenger for reactive oxygen intermediates originating from membrane-bound degraded hemoglobin fragments.[205] Membrane-bound hemoglobin induces protein band 3 oxidation and polymerisation. It is tempting to speculate that HSA could act as an antioxidant, reducing protein band 3 clustering and RBC shape alterations. This antioxidative effect is likely to be related to observed recovery of ATP, which improves pump activities.

The main topic of this study was to compare the rheological properties of stored RBCs before and after washing in a 1% HSA solution. Osmotic gradient ektacytometry was chosen to analyse RBC deformability under high shear stress conditions (**Fig. 6.2.4**). Compared with normal fresh RBCs, stored RBCs were less deformable, which is in agreement with earlier reports using laser-assisted analysis of RBC elongation under high shear stress conditions on stored samples[166,206] and blood drawn from patients after transfusion.[207,208] The decreased RBC elongation is probably due to the cell swelling described above and potential loss of membrane surface area by exovesiculation of echinocytes, which leads to increased sphericity of stored RBCs[182] and hence reduces their ability to elongate. Washing stored RBCs in 1% HSA did not improve ektacytometric deformability. This could suggest that the remaining degree of echinocytosis after washing was still relevant in comparison with the discocytic shape of normal RBCs. Another explanation is that storage lesions other than the echinocytic shape transformation, such as membrane alterations,[174,176] are not reversible by washing and, therefore, keep RBC deformability at a lower level.

Suspension viscosities of stored RBCs in a 3% dextran solution, which allowed RBC aggregation, showed higher suspension viscosities than normal RBCs at all shear rates. This is opposite to what might be expected from the fact that echinocytes undergo much less aggregation,[209,210] but echinocytes have been shown to increase low shear viscosity irrespective of RBC aggregation.[182,211] Washing stored RBCs had no beneficial effect at high shear rates and slightly decreased the viscosities at low shear rates. Suspended stored

and washed RBCs in saline, i.e., without RBC aggregation, showed a lower viscosity of washed compared with unwashed RBCs. The hematocrit of these suspensions was adjusted to 40%. Since washed RBCs had a lower MCV, the RBC count was higher at the given hematocrit of 40%. In other words, the suspension viscosity was lower despite a higher number of RBCs, which is beneficial from a physiological point of view.

Although washing of stored RBCs in 1% HSA did not recover ektacytometric deformability, it improved the ability of washed RBCs to perfuse the artificial microvascular network (AMVN). The AMVN represents a novel tool, which allows a closer approximation of *in vivo* microcirculation than any other available instrument for measuring RBC rheological properties *in vitro*.[128,188] We have shown before that the AMVN perfusion rate for stored RBCs is lower than that for fresh RBCs, and that washing and re-suspending stored RBCs in saline instead of the storage medium increases their ability to perfuse the artificial microvascular network.[128] Here we further showed that washing in a 1% HSA solution can improve the ability of stored RBCs to perfuse the microvasculature. The degree of improvement appeared to be dependent on the initial quality of individual blood units. Units with lower perfusion rates for unwashed RBCs improved more after washing than units with higher perfusion rates for unwashed RBCs. The perfusion rate for all of the RBC units after washing did not exceed 92 % of fresh, which may suggest a natural limit as to the level of improvement one can expect for any stored RBCs using washing as the rejuvenation strategy.

These differences in rheological data – obtained either using ektacytometry or the AMVN – highlight the fact that a single *in vitro* measurement may be not sufficient to predict the flow behaviour of RBCs *in vivo*. Each rheological *in vitro* test examines only a limited spectrum of deformation experienced by a RBC in the circulation *in vivo*. While RBC elongation under high shear conditions in the ektacytometer was not affected, the perfusion of an AMVN was improved by the washing procedure, which indicates that AMVN may be the most comprehensive rheological test available at the moment.

These observations may have clinical implications, suggesting that older RBC units stored until the end of their shelf life could be “rejuvenated” by a simple washing procedure in a 1% HSA solution. After washing, storage-induced echinocytosis decreases and *in vitro* microvascular perfusion increases. This may improve blood circulation after massive blood transfusion and eventually result in better clinical outcomes. Since a considerable donor-to-donor variability in RBC storage exists,[167,212] washing of stored RBCs in 1% HSA before transfusion could probably be limited to those RBC units with a high degree of echinocytosis.

CHAPTER 7 Using microfluidic tools to elucidate how physiologically relevant processes impact the rheological properties of red blood cells

7.1 Morphology

The following research has previously been published and much of the following text is reprinted with permission from: Transfusion, 56(4), Piety NZ, Reinhart WH, Pourreau PH, Abidi R, Shevkoplyas SS, "Shape matters: the effect of red blood cell shape on perfusion of an artificial microvascular network," pages 844 – 851, Copyright 2015 AABB

7.1.1 Introduction

Under resting conditions, the human red blood cell (RBC) assumes the shape of a biconcave disc, called *discocyte*. This unique shape is explained by a state of least total curvature (and thus minimum bending energy) of RBC membrane.[213] The RBC membrane consists of a lipid bilayer with a spectrin-based membrane cytoskeleton underneath. When either the structural properties of the cytoskeleton or the equilibrium between the two hemi-leaflets of the lipid bilayer are disturbed, the normal discocyte morphology is lost.[214] Genetic defects with membrane protein abnormalities lead to spherocytosis or elliptocytosis.[215] Disturbances in the lipid bilayer lead to stomatocytosis when the inner half of the bilayer is expanded relative to the outer half, and to echinocytosis or RBC crenation when the outer half is expanded relative to the inner half.[194] Lipid bilayer disturbances may occur when certain molecules or drugs intercalate either into the inner or outer hemi-leaflet.[213]

The most common type of RBC shape transformation is *echinocytosis*, which has been observed under various circumstances *in vitro* and *in vivo*. Certain drugs may induce echinocytosis: radiocontrast media,[216,217] propofol,[218] fish oil,[219] 5-fluorouracil,[220] antiepileptic drugs,[221,222] non-steroidal anti-inflammatory drugs[223] and particularly sodium-salicylate (SA), which has been used extensively to study echinocytosis *in vitro*.[182,224,225] Hemodialysis[226] and extracorporeal circulation during open heart surgery[227] induce some degree of echinocytosis as well. Perhaps the most important instance of echinocytosis occurs during hypothermic storage of RBCs.[166,175,228] The morphology of stored RBCs progressively deteriorates

due to oxidative damage, biochemical changes and microvesiculation.[61,144,174,176,229] Microvesiculation results in a disproportionately larger loss of cell membrane than cell volume, increasing sphericity of the cell. Stored RBCs gradually transition from normal, biconcave discocytes, through distinct intermediate echinocytic stages (echinocyte I, echinocyte II, echinocyte III, sphero-echinocyte) to spherocytes and ultimately undergo lysis.[230] The rate and degree of this morphological deterioration varies greatly between individual RBCs, resulting in a highly heterogeneous population of cells with different morphologies within each stored RBC unit.

It is well known that hypothermic storage impairs RBC deformability, as evidenced by the increasing suspension viscosities[166,228] as well as decreasing ability of stored RBCs to perfuse an artificial microvascular network.[228] It is however not yet known whether RBC *shape* directly and independently affects microvascular perfusion. In this study we investigated the impact of various degrees of echinocytosis (induced by increasing concentrations of sodium salicylate) on perfusion of an artificial microvascular network (AMVN).

7.1.2 Methods

Device Preparation

A master silicon wafer containing the pattern of the AMVN device was fabricated using soft lithography as described previously.[128,131,188,189] The AMVN device consisted of three parallel identical microchannel networks, each with a separate domed inlet port and all converging to the same domed outlet port.[128] The AMVN comprised a system of microchannels with a depth of 5 μm and range of widths from 5 μm to 70 μm connected in a pattern inspired by the layout of the microvasculature of rat mesentery.[131] Polydimethylsiloxane (PDMS, Sylgard 184, Dow Corning Corp., Midland, MI) was poured over the wafer and cured at 65°C for 3 hours to create a cast of the device. Biopsy punches (Acuderm, Inc., Fort Lauderdale, FL) were used to create access ports for the inlets (4 mm) and outlet (1.5 mm) through the PDMS cast. The AMVN device and a glass slide (VWR, West Chester, PA) spin-coated with a ~50 μm layer of PDMS were then plasma oxidized (100 seconds, air plasma) and bonded to one another. The assembled devices were filled with a 1% solution of mPEG-silane (Laysan Bio, Inc., Arab, AL) in GASP buffer (1.3 mM NaH_2PO_4, 9 mM Na_2HPO_4, 140 mM NaCl, 5.5 mM glucose, 1% bovine serum albumin; osmolality 290 mmol/kg; pH

7.4)[128] and incubated at ambient temperature for at least 8 hours to prevent cell adhesion to the walls of the microchannels. The mPEG-silane solution was flushed from the microchannel with GASP buffer prior to performing experiments.

Sample Preparation

Whole blood was collected from healthy consenting volunteers (n = 5) via venipuncture into Vacutainer tubes containing K_2EDTA anticoagulant (BD, Franklin Lakes, NJ). Blood samples were leukoreduced using a high-efficiency pediatric leukocyte reduction filter (Purecell NEO, Pall Corp., Port Washington, USA).[189] Samples were adjusted to 40% hematocrit (Hct) with normal saline (osmolality 290 mOsm/kg). To create RBC samples with various induced morphologies, 1 mL aliquots of leukoreduced, 40% Hct samples were centrifuged at 2500 x g for 5 minutes at ambient temperature (Microfuge 22R, Beckman Coulter, Fullerton, CA) to separate RBCs from the supernatant. Various volumes of supernatant were removed from the aliquoted samples and replaced with equal amounts of an isotonic stock solution of sodium salicylate (SA) in saline (290 mOsm/kg), to create solutions with final SA concentrations of 0, 9, 18, 27, 36 and 54 mM.[182] The samples were mixed by inversion on a sample tube rotator (Labquake, Barnstead Thermolyne, Dubuque, IA) for 30 minutes prior to use. For each sample, RBC count and mean corpuscular hemoglobin (MCH) were measured with a hematology analyzer (Medonic M-series, Boule Medical AB, Stockholm, Sweden). Hct was measured from the relative fractions of packed RBCs and plasma in untreated plastic 75 mm microcapillary tubes (n = 4; Fisherbrand, Thermo Fisher Scientific, Waltham, MA) centrifuged for 15 minutes at 11,500 × g in a micro-hematocrit centrifuge (PowerSpin BX, UNICO, Princeton, NJ). Hct, measured by microcentrifugation, was used to calculate mean corpuscular volume, MCV = Hct × 10/RBC count. This calculated MCV was then used to calculate mean corpuscular hemoglobin concentration, MCHC = 100 × MCH/MCV.

Imaging and Analysis

An inverted bright-field microscope (IX71, Olympus America Inc., Center Valley, PA, USA) equipped with a high-speed camera (MC1362, Mikrotron GmbH, Unterschleissheim, Germany) was used to acquire images of the post-AMVN (venous) channels at 20x magnification. A band-pass blue-violet filter

(394 ± 50 nm, B-390, Hoya Corp. USA, Fremont, CA) was placed between the microscope lamp and condenser in order to improve contrast (RBCs appear dark in blue light). A custom image capture application implemented in Microsoft Visual Studio (Microsoft Corp., Redmond, WA) was used to capture bursts of 10 frames at 100 fps every 10 seconds for the duration of 5 minutes. A custom image analysis algorithm implemented in MATLAB (The Math Works Inc., Natick, MA, USA) was used to analyze the image sequences and calculate the RBC velocity (V_{RBC}; μm/s) in the channels at each time point based on the shift in RBC position between images. Perfusion rate was defined as the product of the cross sectional area of the post-AMVN microchannel ($A_{channel}$; 350 μm^2) and the measured RBC velocity (perfusion rate = $V_{RBC} \times A_{channel}$; $\mu m^3/s = 1 \times 10^{-6}$ nL/s). For each sample, the perfusion rate was normalized with respect to the perfusion rate of a control sample (normal, untreated RBCs) run through the same device.

Experimental Setup

Figure 7.1.1 demonstrates the components of the AMVN measurement system. A water reservoir fixed to a vertical linear motion stage (Series A40 UniSlides, Velmex Inc., Bloomfield, NY) connected with flexible plastic tubing (Tygon R-3603, VWR, West Chester, PA) and a barbed tube fitting (L420/410-6, Value Plastics, Fort Collins, CO) to the outlet of the AMVN device (**Fig. 7.1.1a,b**), was used to control the driving pressure of the system by adjusting hydrostatic pressure between the AMVN inlets and the reservoir.[131,189] The microscope field-of-view was then aligned with the post-AMVN venule microchannels and a best-effort manual focusing was performed using the walls of the microchannels as high-contrast standard. To perform the measurement, GASP buffer was removed from the inlets of the AMVN device and 25 μL of RBC sample was deposited in each inlet. The system driving pressure was then set to approximately -10 cmH_2O and the RBCs were allowed to perfuse the system until RBCs from all three inlets reached the outlet port. The water column was then adjusted such that flow through the device stopped (0 cmH_2O driving pressure) and the image capture application was initiated. A baseline perfusion rate (~0 nL/s) was established for 30 seconds, and then the driving pressure was set to -20 cmH_2O for the remainder of the 5 minute image capture period.

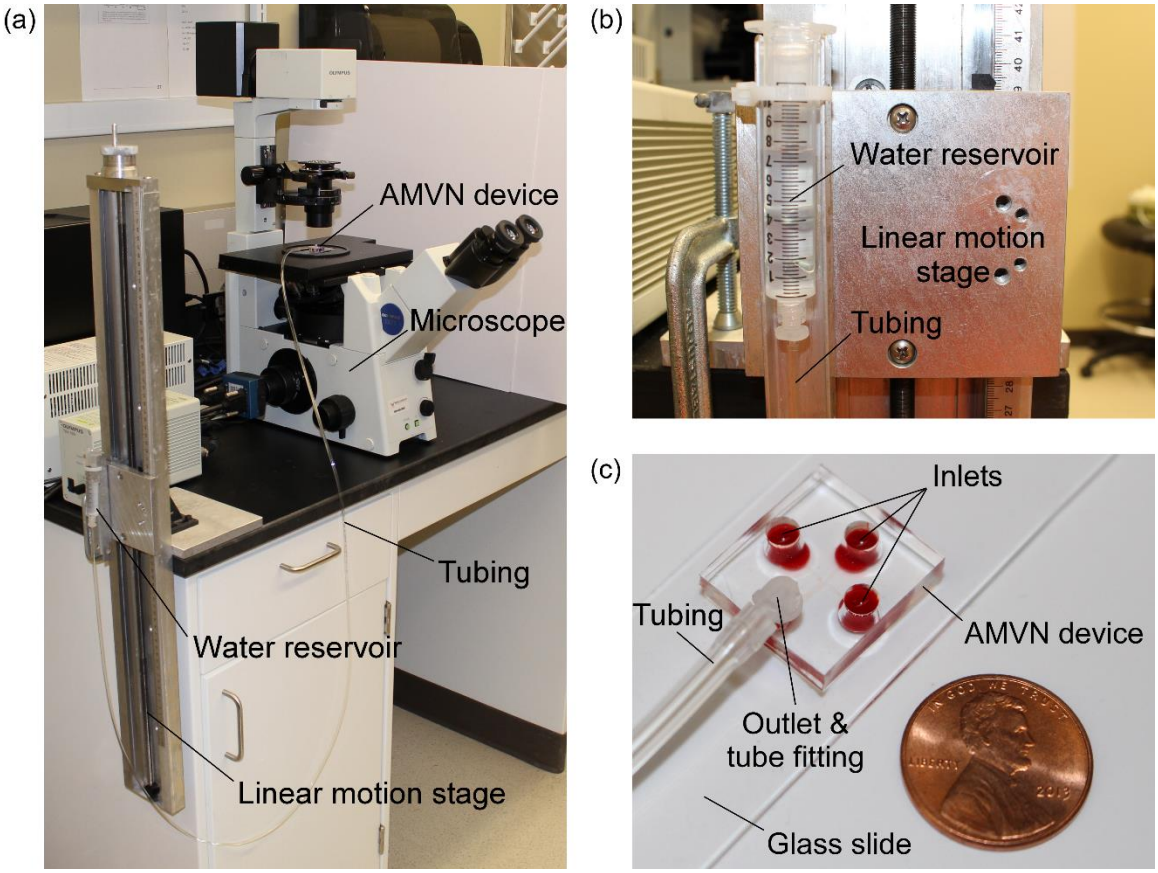

Figure 7.1.1 Setup for measuring the AMVN perfusion rate. (**a**) Complete AMVN system. (**b**) Water reservoir attached to vertical linear motion stage is used to control the driving pressure of the AMVN system. (**c**) Photograph of the AMVN device (coin shown for size reference).

The AMVN device consisted of three identical networks of microchannels, each with their own inlet port, converging to the same outlet port (**Fig. 7.1.1c**). Three samples (two experimental and one control) were run in parallel through identical networks within each device. The variation in AMVN perfusion rate between microchannels within a single device is <1%, and the variation between microchannels in different devices is <2%, as previously shown.[128] Samples treated with appropriate concentration of SA to induce each distinct RBC morphology were run in multiple channels within a single device, and in multiple separate devices to minimize potential bias due to minor fabrication irregularities.

Statistical Analysis

Statistical analysis was performed using built-in functions of MATLAB 2014b Statistics Toolbox (The Math Works Inc, Natick, MA). A paired t-test was used for the comparison between two groups. The

results are presented as mean values ± standard deviation. A p-value of < 0.01 was considered statistically significant.

7.1.3 Results

Figure 7.1.2 illustrates the changes in RBC morphology induced by exposure to different SA concentrations. The specific concentrations of SA were chosen so that the resulting morphologies approximated different degrees of echinocytosis,[11,230] namely: echinocyte I (an irregularly contoured discocyte with up to 5 protrusions) for 9 mM SA; echinocyte II (a flat RBC with a few spicules) for 18 mM SA; echinocyte III (an ovaloid or spherical RBC with many spicules) for 27 mM SA; sphero-echinocyte (a spherical RBC with multiple short and thin spicules) for 36 mM SA; and finally spherocyte (a completely spherical RBC) for 54 mM SA.

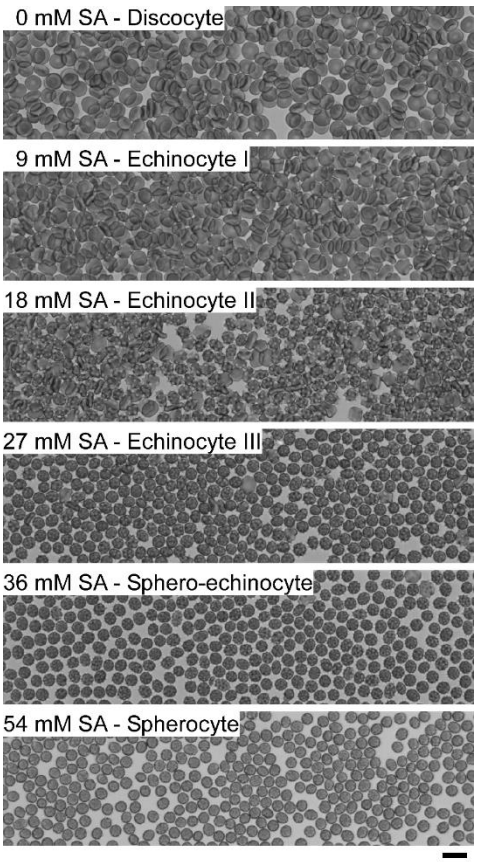

Figure 7.1.2 Representative images of RBCs treated with sodium salicylate (SA). Exposure to SA changed the shape of RBCs in a dose-dependent fashion, approximating the increasing degrees of echinocytosis. Scale bar is 10 μm.

Figure 7.1.3 shows the characteristic images of RBCs (**Fig. 7.1.3b**) with each of the induced morphologies as they perfused the arteriole and capillary portions of the AMVN (**Fig. 7.1.3a**). Our visual phenomenological observations showed that morphology of RBCs influenced their flow, packing and deformation characteristics within the AMVN. Echinocytic RBCs were unable to form the characteristic bullet shapes as they traversed microcapillaries (**Fig. 7.1.3b**). The spherical geometry of sphero-echinocytes and spherocytes severely limited the number of RBCs which could simultaneously pass through individual microchannels (**Fig. 7.1.3b**).

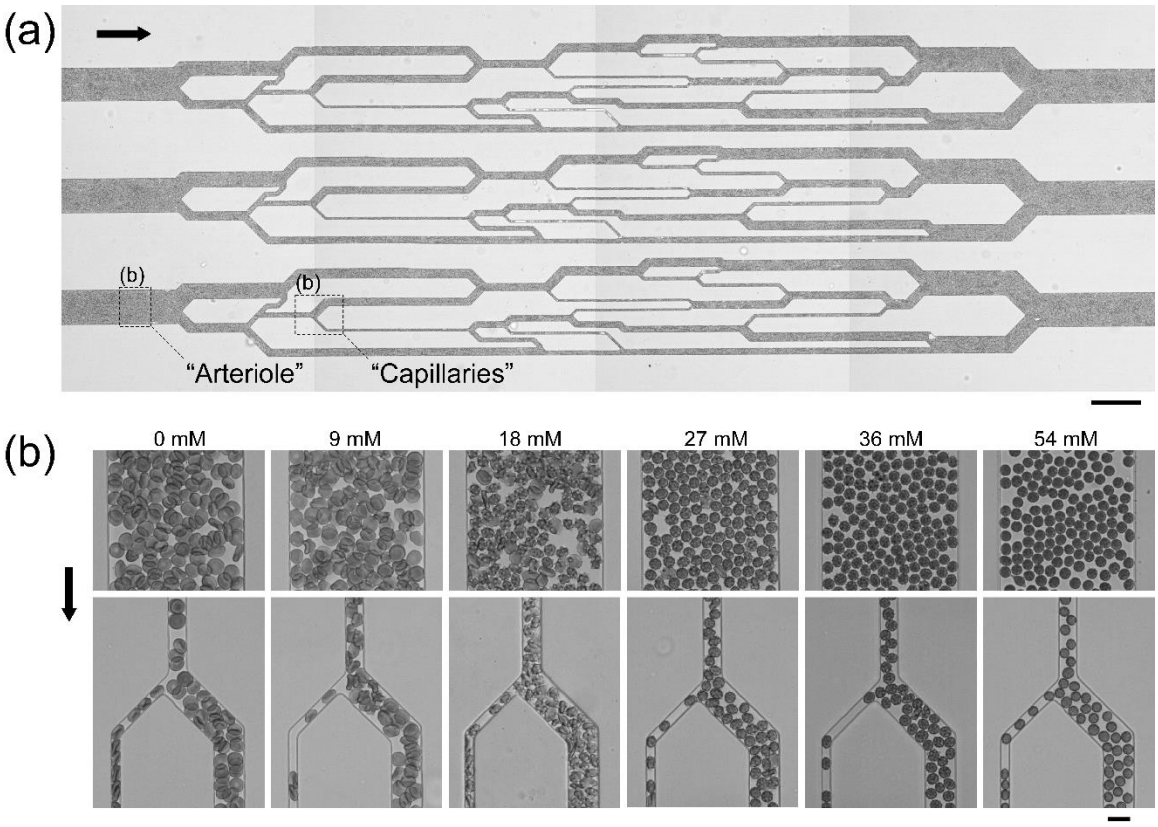

Figure 7.1.3 Flow patterns of RBCs with different shapes in the AMVN. (**a**) Bright-field micrograph of AMVN, scale bar is 100 µm. (**b**) RBCs in 70 µm AMVN 'arteriole' (upper) and in 10 µm split into 5 µm and 15 µm AMVN 'capillaries' (lower), scale bar is 10 µm.

Figure 7.1.4 shows the normalized AMVN perfusion rates for RBCs with different shapes. For each trial, a control, untreated RBC sample (0 mM SA; Hct = 39.6 ± 0.8 %; MCV = 85.6 ± 1.7 fL; MCHC = 32.2 ± 0.6 g/dL) and two experimental, treated RBC samples were analyzed using the three identical channels comprising each AMVN device. RBC samples from each of the five volunteers were used to evaluate each

SA concentration independently (50 experiments for untreated samples, 0 mM; n = 19 experiments for each of the samples exposed to 9, 18, 27, 36, and 54 mM of sodium salicylate). The AMVN perfusion rate decreased as the degree of echinocytosis increased. There was only a minor, non-significant decrease in perfusion rate from discocyte to induced echinocyte I (0.1% of discocyte; $p = 0.837$). The perfusion rate then drastically decreased from echinocyte I to echinocyte II (8.8% of discocyte; $p = 0.0000414$), more so from echinocyte II to echinocyte III (15.9% of discocyte; $p = 0.00000000495$), and even further from echinocyte III to sphero-echinocyte (5.8% of discocyte; $p = 0.000580$). The decrease in the AMVN perfusion rate from sphero-echinocyte to spherocyte (3.0% of discocyte; $p = 0.00690$) was noticeable but less drastic. Overall, there was a decrease in the AMVN perfusion rate of 33.6% as the RBC shape progressively changed from discocyte to spherocyte (**Fig. 7.1.4**). For context, a previous study found that the overall decrease in AMVN perfusion rate for hypothermically stored RBC units between week 0 and week 6 of storage is approximately 20 – 25%.[128,228]

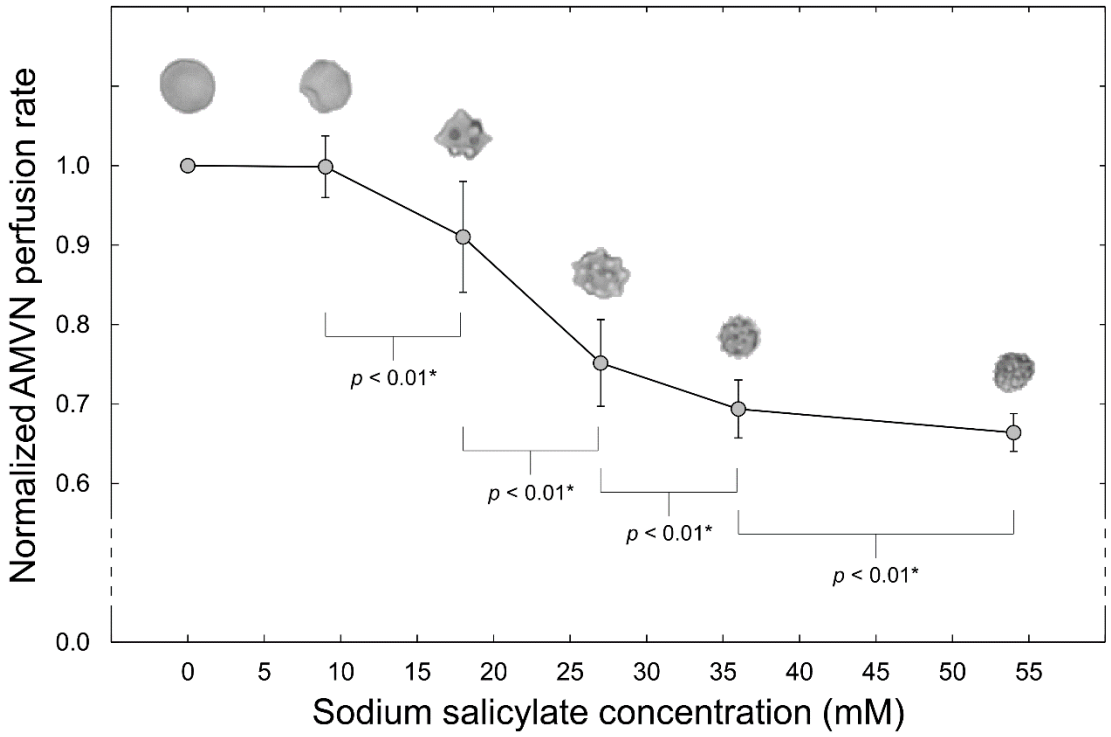

Figure 7.1.4 Dependence of AMVN perfusion rate on RBC shape. Inset images show representative RBC morphologies. Perfusion rates normalized with respect normal RBCs (0 mM). Mean values ± standard deviation, n = 50 (0 mM), n = 19 (9, 18, 27, 36 and 54 mM).

We found that exposure to SA resulted in small decrease of MCV (up to 5.2 fL) and a modest increase of MCHC (up to 2.0 g/dL) compared to normal discocytes (**Table 7.1.1**), which is in agreement with earlier observations.[182] The decrease in MCV (1.7% of discocyte; $p = 0.252$) and increase in MCHC (5.0% of discocyte; $p = 0.0105$) between discocytes (0 mM SA) and induced spherocytes (54 mM SA) were not statistically significant. The decrease in Hct between discocytes and induced spherocytes, potentially due to lysis, was statistically significant (5.7% of discocyte; $p = 0.00499$). For all of our samples, MCHC ranged from 32.0 to 34.0 g/dL, and the maximum decrease in AMVN perfusion rate was 0.084 nL/s (or 33.6% of the perfusion rate for discocytes). We have previously shown that changes in MCHC of up to 7.8 g/dL produce a decrease in the AMVN perfusion rate of <0.016 nL/s (or 6.6% of discocyte).[159] The decreases in AMVN perfusion rate experienced by induced echinocyte II (9.0% of discocyte), echinocyte III (24.9% of discocyte), sphero-echinocytes (30.6% of discocyte) and spherocytes (33.6% of discocyte) were all significantly greater than would be expected based on change in MCHC alone.

Table 7.1.1 Summary of hemorheological parameters at different sodium salicylate concentrations (mean values ± SD, n = 5). Measured non-normalized AMVN perfusion rate (mean values ± SD, n = 50 for 0 mM, n = 19 for 9, 18, 27, 36 and 54 mM).

	Sodium salicylate concentration (mM)					
	0	**9**	**18**	**27**	**36**	**54**
Hct (%)	39.6 ± 0.8	39.7 ± 0.9	38.9 ± 0.3	39.0 ± 0.6	38.8 ± 0.6	37.4 ± 0.5
RBC count (10^{12}/L)	4.63 ± 0.00	4.58 ± 0.00	4.63 ± 0.00	4.79 ± 0.00	4.64 ± 0.00	4.44 ± 0.00
MCV (fL)	85.6 ± 1.7	86.6 ± 2.0	84.0 ± 0.7	81.4 ± 1.3	83.7 ± 1.4	84.2 ± 1.0
MCHC (g/dL)	32.2 ± 0.6	32.0 ± 0.7	33.0 ± 0.3	34.0 ± 0.5	33.8 ± 0.5	33.9 ± 0.4
AMVN perfusion rate (nL/s)	0.268 ± 0.022	0.261 ± 0.025	0.237 ± 0.021	0.198 ± 0.012	0.187 ± 0.011	0.182 ± 0.012

7.1.4 Discussion

SA produced a concentration-dependent echinocytic shape transformation comparable to earlier studies.[181,182,209,211,224,225] The influence of SA-induced echinocytosis on rheological parameters has been extensively studied in the past. RBC suspension viscosity is increased, due to mechanical hindrance between spiculated RBCs.[182,211,224] RBC aggregation is drastically reduced because spiculated RBCs are unable to make large enough surface area contact with neighboring cells to form stable aggregates.[209,211] The passage

of narrow filter pores with a nominal diameter of 3µm (i.e., smaller than the diameter of the smallest capillary in our AMVN device) was not hindered, but even facilitated by SA-induced echinocytosis of higher degree, explained by a preserved or even increased surface area to volume ratio of echinocytes, which is the most relevant parameter for the passage of very narrow pores.[182] On the level of membrane deformability, micropipette experiments have shown that echinocytes induced by SA had a slightly increased resistance to membrane extension.[181] Shape normalization by the addition of a counteracting stomatocytogenic agent such as chlorpromazine normalized these rheological alterations, indicating that the shape matters and not the drug interaction with the RBC membrane itself.[181,211] Taken together, these divergent rheological results make it difficult to anticipate the role of the RBC shape in microvascular perfusion, which is most important in (patho)physiological and clinical terms and has prompted the present study.

We found that perfusion of the artificial microvascular network (AMVN) was maximized for RBCs of normal biconcave discoid and echinocyte I shape. These results suggest that although discocytes are best for microvascular perfusion, some degree of RBC shape deterioration such as the initial stages of echinocytosis could be well-tolerated by the microvasculature. Further progression of RBCs along the path of the echinocytic transformation towards spherocytosis gradually decreased the AMVN perfusion in our experiments. The maximum average drop of the AMVN perfusion rate we measured in this study was approximately 30% for the sample that mostly consisted of spherocytes (the end point of the echinocytic transformation). Echinocytosis is by far the most common type of RBC shape deterioration occurring during hypothermic storage,[230] and therefore our results could have particularly important implications in the context of blood storage and transfusion. Interestingly, in our previous studies we measured a 20-25% difference in the AMVN perfusion rate between fresh RBC (mostly discocytes) and RBC stored hypothermically for 6 weeks.[128,228] Because 6-week old blood is a heterogeneous mixture composed predominantly of cells in early stages of echinocytosis (which may recover their shape *in vivo*, post-transfusion[231] or via washing[228]), some discocytes and a sizable fraction of irreparably damaged late stage echinocytes and spherocytes,[230] the shape change could explain a large fraction of the decline in the AMVN perfusion rate we have previously measured for hypothermically stored blood.

During flow in the circulation, RBCs are exposed to a large variety of shear stresses, ranging from very small, such as in the axis of a large vessel, where the shear stress approaches zero, to very large shear

stresses, such as in capillaries, where the strongest RBC deformation occurs. The deformation into a bullet-like shape in smaller capillaries is only possible because RBCs have a high surface area to volume ratio, which is a geometric prerequisite for this deformation.[232] When the surface area to volume ratio is decreased (i.e., RBCs become more spherical as seen in hypotonic swelling) RBC deformability in capillaries is reduced, which reduces the AMVN perfusion rate.[159] The present data and earlier observations[182] indicate that echinocytosis induced by SA does not decrease the surface area to volume ratio of RBCs, thus allowing an unhindered passage of smallest capillaries (5 μm) within the AMVN (or even narrower channels such as 3 μm filter pores[182]) despite the fact that echinocytes have an increased resistance to membrane deformation as measured by the micropipette aspiration technique,[181] and an increased suspension viscosity due to the entanglement among spiculated RBCs.[166,182] We conclude, therefore, that the decrease in the ability of echinocytic RBCs to perfuse the AMVN was not caused by a deformability-dependent reduced capacity of single RBCs to pass through the smallest capillaries, but was caused primarily by an impaired flow in arteriole/venule-sized channels (13-70 μm).

Our present data suggest that deterioration of RBC shape occurring during hypothermic storage is likely a significant cause of the storage-induced decline of RBC deformability, particularly as reflected by a reduction in the ability of stored RBCs to perfuse an artificial microvascular network. It has been shown that RBC units stored for less than 2 weeks (and therefore containing on average less echinocytes[166]) decrease post-transfusion morbidity and mortality in patients undergoing cardiac surgery,[64,68] which has, however, not been confirmed by a more recent study.[69] Our data suggest that the degree of storage-induced echinocytosis in each particular RBC unit could influence microcirculatory blood flow *in vivo* and thus contribute to different clinical outcomes.[233] We had previously shown that severe echinocytosis after prolonged hypothermic storage can be partially reversed towards discocytosis by washing stored RBCs in a 1% human serum albumin (HSA) solution, a procedure that also significantly improves the ability of stored RBCs to perfuse the AMVN.[228] We reason therefore that if the echinocytic transformation of RBC shape due to hypothermic storage could be either completely prevented, or arrested in its earliest stages (e.g., echinocyte I), or reversed through some kind of treatment right before transfusion (e.g., washing in 1% HSA) the microvascular perfusion in the recipient may be improved.

Our results may have important implications in other clinically-relevant contexts. For example, it is well-known that radiographic contrast media may induce echinocytosis *in vivo*.[234] Angiography (e.g., of the brain, heart, or leg) may induce echinocytosis, which could, at least temporarily, reduce microvascular perfusion and by doing so deteriorate critical peripheral ischemia further. It is, therefore, advisable to use the smallest possible volume of contrast medium and choose one with low echinocytogenic properties.[216,234] Although our results cannot be easily generalized for other, similar shape abnormalities (e.g., acanthocytosis[235,236]), it is very likely that they might be disadvantageous as well.

We conclude that normal discocytes represent the optimum RBC shape for AMVN perfusion and that the echinocytic shape transformation leads to a progressive decrease of AMVN perfusion rates. RBC shape is an indicator of the rheological performance of RBCs in the microvasculature and therefore could be used as a measure of the quality of stored blood units.

7.2 Osmolality

The following research has previously been published and much of the following text is reprinted with permission from: Microvascular Research, 98, Reinhart WH, Piety NZ, Goede JS, Shevkoplyas SS, "Effect of osmolality on erythrocyte rheology and perfusion of an artificial microvascular network," pages 102 – 107, Copyright 2015 Elsevier Inc.

7.2.1 Introduction

Plasma osmolality is primarily determined by the plasma sodium concentration. It is held within narrow limits under normal physiological conditions. Alterations in plasma osmolality are readily sensed by hypothalamic receptors in the brain, which initiates compensatory mechanisms such as water intake in the case of hyperosmolality or water excretion in the case of hypoosmolality. In hypoosmolality, the secretion of antidiuretic hormone ADH is suppressed, which leads to decreased water reabsorption in the collecting tubules of the kidney and thereby increases water excretion. In hyperosmolality, the body reacts with thirst-driven water ingestion and an increased ADH secretion leading to water retention in the kidney.[237,238]

This normal homeostasis of plasma sodium concentration and osmolality can be disturbed under pathophysiological conditions and represents the most common clinical electrolyte disorder,[237] which is associated with a considerable morbidity and mortality when severe.[239,240] However, even mild hypoosmolality caused by hyponatremia is associated with a poor outcome in chronic heart failure.[241] Hyponatremic hypoosmolality of severe degree can occur in the syndrome of inappropriate ADH secretion (SIADH), e.g., after brain injury, or when an excess of free water is either ingested or infused during medical treatment. Symptoms are nausea, malaise and headache, followed by lethargy, disorientation, seizure, coma and even death in severe hyponatremia.[242] On the other hand, hypernatriemic hyperosmolality, which is much less common, is seen in diabetes insipidus due to either a lack of ADH or an unresponsiveness of the kidney to ADH. Symptoms of hypernatriemic hyperosmolality are similar to symptoms of hyponatremic hypoosmolality: initial unspecific symptoms such as anorexia, restlessness, nausea and vomiting are followed by more severe neurological symptoms such as lethargy, stupor or coma.[237,243]

The neurological symptoms are caused by an osmotic gradient, which is generated between the extracellular space and the intracellular compartment of brain cells. In case of hypoosmolality, water moves into neuronal cells and causes cell swelling and tissue edema,[244,245] in hyperosmolality, water is lost from the cells which leads to cell shrinkage. Both conditions impair cell function. Cell swelling and shrinkage is induced in every cell exposed to osmotic gradients, including blood cells.[246] In hypoosmolality, the red blood cells (RBCs) increase their volume and thereby sphericity and at the same time reduce the cellular viscosity determined by the intracellular hemoglobin concentration.[247] On the other hand, hyperosmolality leads to a volume reduction but increased cellular viscosity.[247] These opposing changes could have an influence on RBC deformability, and thus on microvascular blood flow. It was the aim of the study to investigate the role of osmolality of the suspending medium on RBC deformability, RBC suspension viscosity and the ability of RBCs to perfuse an artificial microvascular network.

7.2.2 Methods

Sample Preparation

Solutions with different osmolalities were prepared as follows. Saline (0.9% NaCl, 277mOsm/kg H_2O) was used as a basis. For hypoosmolar solutions it was diluted 1:1 and 2:1 with distilled water, which

resulted in measured osmolalities of 136 and 182 mOsm/kg H_2O, respectively. Higher osmolalities were obtained by adding either 30 mg or 60mg sodium chloride (Sigma-Aldrich, St. Louis, MO, USA) to 10 mL of saline, yielding osmolalities of 373 and 466mOsmol/kg, respectively. Osmolalities were measured with a vapor pressure osmometer (Vapro 5520, Wescor Inc., South Logan, Utah, USA). All experiments described below were completed within 2 h.

Blood was taken by venipuncture from healthy volunteers (age range 20-65 years), who gave their informed consent to the *in vitro* study. Tubes containing 1.8mg/mL K_2EDTA as an anticoagulant were used. Routine hematological analyzers (Sysmex XT-1800i, Sysmex Digitana Co, Horgen, Switzerland; Medonic M-series, Boule Medical AB, Stockholm, Sweden in the USA) were used to determine RBC count and mean cellular hemoglobin (MCH). Hematocrit (Hct) was determined by microcentrifugation. For each sample 3 uncoated hematocrit glass tubes (length 75 mm) were filled and centrifuged for 5 min in a micro-hematocrit centrifuge (IEC MB Centrifuge, Damon), the Hct was determined (Hawksley Micro-hematocrit Reader, Lancing, Sussex, UK) and the mean value calculated. The Hct was used to calculate the mean cellular volume in the actual suspension with a given osmolality (MCV = Hct*10/RBC count). This MCV was then used to calculate the MCHC (MCHC = MCH/MCV). Samples of RBCs incubated at high and low osmolality were fixed in 1% glutaraldehyde and prepared for scanning electron microscopy as described previously.[183]

Ektacytometry

RBC deformability was analyzed by laser diffraction in an ektacytometer (Technicon, Bayer, Leverkusen, Germany) using an osmoscan mode.[187] Blood from 6 healthy volunteers (age range 28-50 years) anticoagulated with EDTA as described above was used. Aliquots of 500 µL whole blood were mixed with 3 mL of an isotonic 20% dextran 70kDa solution and inserted into the ektacytometer. RBC elongation as a measure of deformability was then registered continuously while the osmotic conditions were gradually changed, going from hypoosmolality to hyperosmolality. The osmotic gradient was generated by adding sodium chloride to the solution in one compartment of the gradient mixer. The osmolality of the suspension was measured by determining the conductivity of the solution close to the diffractometer of the instrument, which had been calibrated by a series of different osmolalities by cryoscopic osmometry (Osmomat 030, Gonotec GmbH, Berlin, Germany). RBC deformability was plotted against the suspension osmolality. The

analog output was digitized using a 12-bit A/D-converter (NI USB-6008, National Instruments, Austin, TX, USA). The deformability index (DI) was calculated at given osmolalities used in the other experiments (179, 213, 283, 354, and 420 mOsm/kg H_2O).

Viscometry

EDTA-blood from 8 healthy volunteers was centrifuged at 1500 x g for 5 min. The plasma and buffy coat were discarded. Volumes of 500 µL packed RBCs were added to 750 µL of NaCl solutions with increasing osmolalities (see above). The RBC count and hematocrit of these samples were measured. The hematocrit was then adjusted to 40% in the isotonic aliquot (283 mOsm/kg H_2O) by removing a calculated volume of suspending medium. The resulting actual RBC count in the 283 mOsmolar (isosmotic) sample was then used to adjust the same RBC count in the other samples. The final centrifuged hematocrit values of the different osmolality samples were calculated accordingly. RBC suspension viscosities were measured with a couette viscometer (Contraves LS 30, ProRheo, Althengstett, Germany) at room temperature (20-22^o C) at shear rates of 69.5, 27.7, 11.0, 3.23, 0.95, 0.28, and 0.11 s^{-1}.

Perfusion of artificial microvascular networks

Artificial microvascular network (AMVN) devices were fabricated using previously described methods.[128,131,188,189] Each polydimethylsiloxane (PDMS) AMVN device consisted of three identical networks of microchannels, each with a separate domed inlet (4 mm diameter), that all converged into a common domed outlet (1.5 mm diameter) connected to an adjustable water column.[128,188] The interconnected microchannels making up the AMVN had a depth of 5 µm and ranged in width from 5 to 70 µm. The layout of the AMVN was inspired by the microcapillary architecture of rat mesentery and has been described in detail previously.[128]

Fresh blood antricoagulated with EDTA from 5 healthy volunteers was centrifuged at 1500 x g for 5 min. 100 µL packed RBCs were then resuspended in 150µL NaCl solutions (target hematocrit 40% at isotonicity) of increasing osmolalities (see above). To perform the measurement, 60 µL samples of resuspended RBCs were loaded into the inlets of the AMVN device with a conventional 10-100 µL pipette tip, image acquisition was initiated and the driving pressure was increased to 20 cmH_2O. Image acquisition

continued for 10 minutes. An inverted bright field microscope (IX71, Olympus America Inc., Center Valley, PA, USA) equipped with a high-speed camera (MC1362, Mikrotron GmbH, Unterschleissheim, Germany) were used to acquire images. The camera was programmed to acquire sets of 10 frames at 100 fps every 10 seconds. A custom algorithm in MATLAB (The Math Works Inc., Natick, MA, USA) computed mean cell velocity in the microchannel exiting each network unit from the average change in cell position between consecutive timed images for each image set. AMVN perfusion rate was then calculated as the product of mean cell velocity and the cross-sectional area of the exit microchannel (350 μm^2).[14]

7.2.3 Results

The initial osmolalities of the suspending solutions were 138, 183, 277, 376, and 468 mOsm/kg H_2O. The suspension of RBCs in these solutions with a target hematocrit of 40% led to an osmotic equilibration between the suspending solution and the cytoplasm of RBCs. After centrifugation, the osmolalities in the supernatant were 179 ± 4, 213 ± 1, 283 ± 2, 354 ± 3, and 423 ± 5 mOsm/kg H_2O, respectively. Hypoosmolality induced water uptake by the discocytes leading to spherical swelling with a reduction of the cell diameter (**Fig. 7.2.1a**). On the other hand, hyperosmolar conditions dehydrated RBCs, which became more flattened discocytes (**Fig. 7.2.1b**). The difference in diameter seen in **Figure 7.2.1** may be exaggerated due to the isotonic glutaraldehyde fixing solution, which might have decreased osmotically the existing RBC volume in hypoosmolar medium. The influence of the different osmolalities on MCV and MCHC is shown in **Figure 7.2.2**. With increasing osmolality, MCV decreased, while MCHC increased. Correspondingly, the hematocrit for a given number of RBCs was inversely proportional to osmolality: it increased with lower and decreased with higher osmolality (**Fig. 7.2.2**).

The suspension viscosities at constant numbers of RBCs in solutions with different osmolalities for shear rates of 69.5, 11.0, 0.95, and 0.11 s^{-1} are shown in **Figure 7.2.3**. Hypoosmolality increased suspension viscosities, while hyperosmolality did not, or even tended to lower it compared with isotonicity. These differences increased with decreasing shear rates; at the lowest shear rate ($0.11s^{-1}$) suspension viscosity was more than doubled at 179 mOsm/kg H_2O in comparison with 283 mOsm/kg H_2O. Suspension viscosities at a shear rate of $27.7s^{-1}$ are given in **Table 7.2.1**; data obtained at 3.23 and 0.28 s^{-1} did not add value and are not shown.

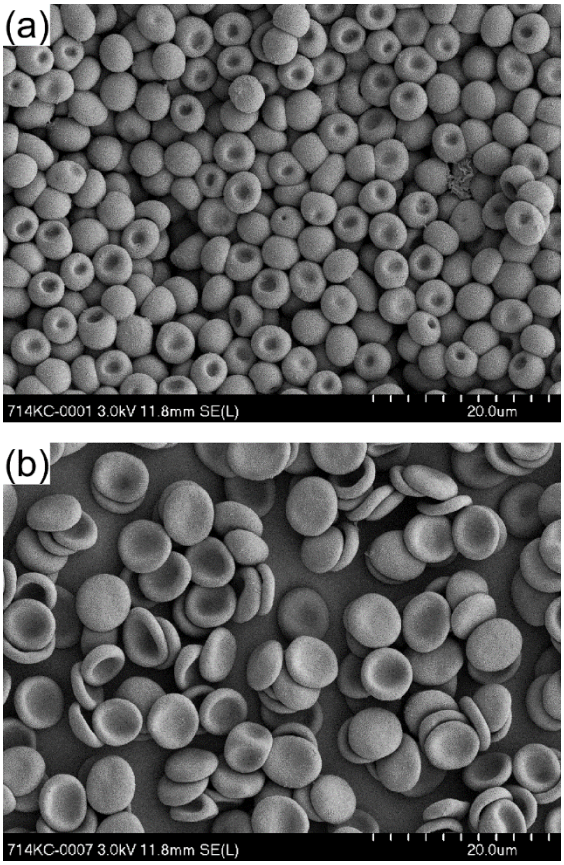

Figure 7.2.1 Scanning electron micrographs of RBCs. 2000x-magnification. (**a**) RBCs in hypotonic solution (189 mOsm/kg H_2O). (**b**) RBCs in hypertonic solution (431 mOsm/kg H_2O).

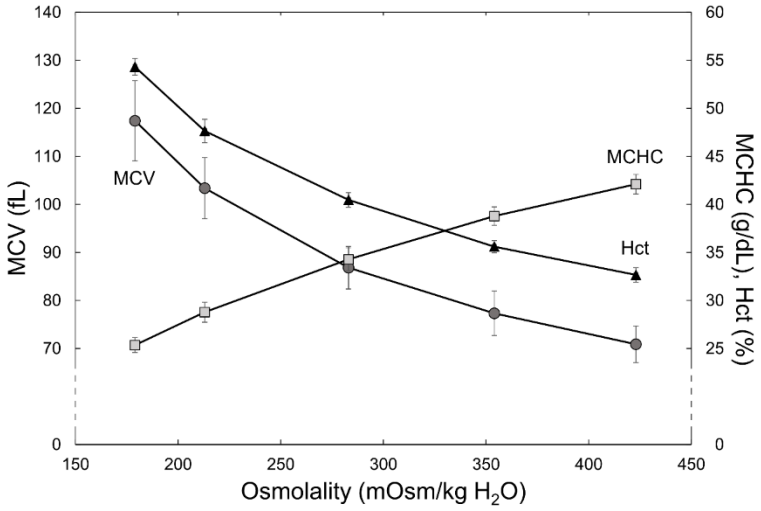

Figure 7.2.2 RBC indices. The centrifuged hematocrit – Hct_c (triangles) – and the calculated RBC indices – MCV (circles) and MCHC (rectangles) – for constant RBC numbers at different osmolalities. Mean values ± SD, n = 6.

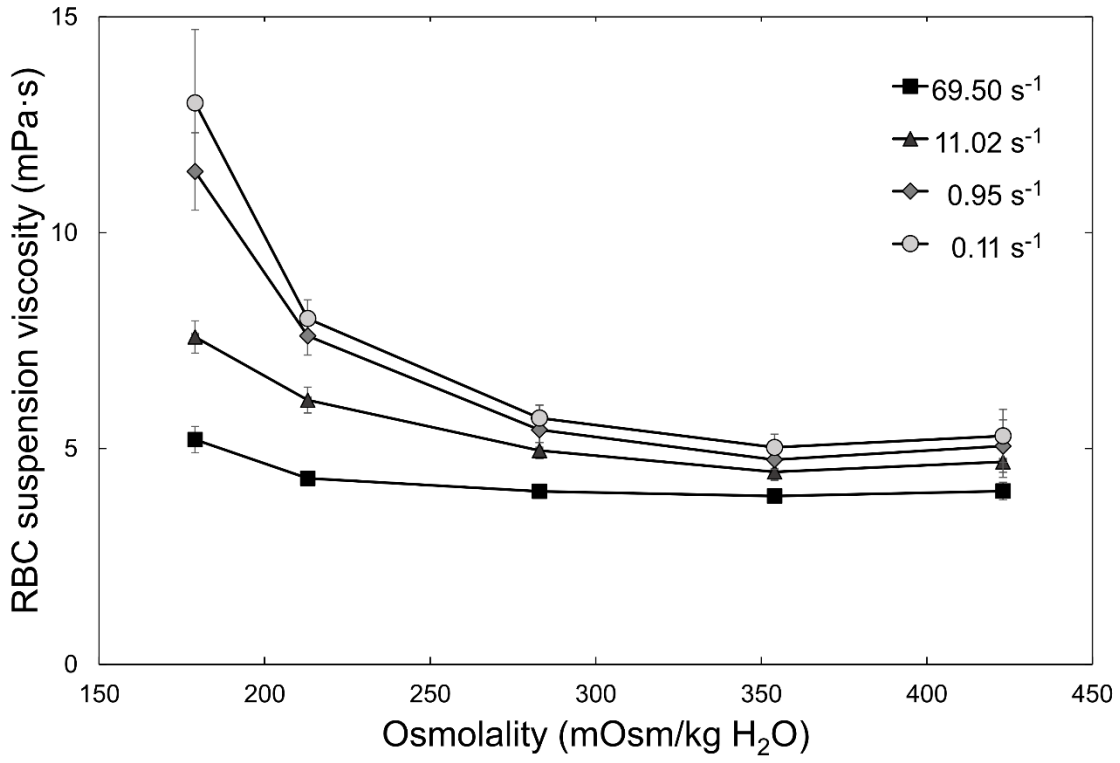

Figure 7.2.3 Viscosity of RBC suspensions at room temperature for a range of osmolalities measured at shear rates of 69.5, 11.02, 0.95 and 0.11 s^{-1} with a couette viscometer. Mean values ± SD, n = 8.

Table 7.2.1 Summary of hemorheological parameters at different suspension osmolalities (mean values ± SD).

Osmolality (mOsm/kg H_2O)	**179**	**213**	**283**	**354**	**423**
Ektacytometric DI (%)	31 ± 4	46 ± 5	62 ± 1	52 ± 8	33 ± 23
Suspension viscosity (mPa·s) at 27.7 s^{-1}	5.3 ± 0.2	5.1 ± 0.2	4.5 ± 0.2	4.3 ± 0.2	4.4 ± 0.3
AMVN perfusion rate (nL/s)	0.226 ± 0.003	0.230 ± 0.005	0.236 ± 0.008	0.226 ± 0.004	0.221 ± 0.011

Figure 7.2.4 shows the results of the osmotic gradient ektacytometry measurements. The ektacytometry curve had a characteristic bell shape (**Fig. 7.2.4**), with the highest RBC deformability corresponding to the isotonic conditions (283 mOsm/kg H_2O). Hypoosmolality and hyperosmolality both led to a decrease in RBC deformability as measured by osmotic gradient ektacytometry. The numeric values of the ektacytometric deformability index (DI) at the 5 investigated osmolalities is shown in **Table 7.2.1**.

Figure 7.2.5 shows microscopic pictures of RBCs suspended at different osmolalities flowing through the artificial microvascular network (AMVN). RBCs in a hypotonic solution (left side) appeared more spherical and were less dense, whereas in a hypertonic solution they appeared more dense (right side) than in isosmotic conditions (middle). Hypoosmotically swollen RBCs filled a 7 µm wide microchannel almost entirely. Because they were not completely spherical (see **Fig. 7.2.1**), however, they were able to deform during the passage of 5 µm channels into a sausage-like shape with two convex ends, which is in contrast to isoosmolality (middle) showing missile-like shapes with a convex front end and concave trailing end.

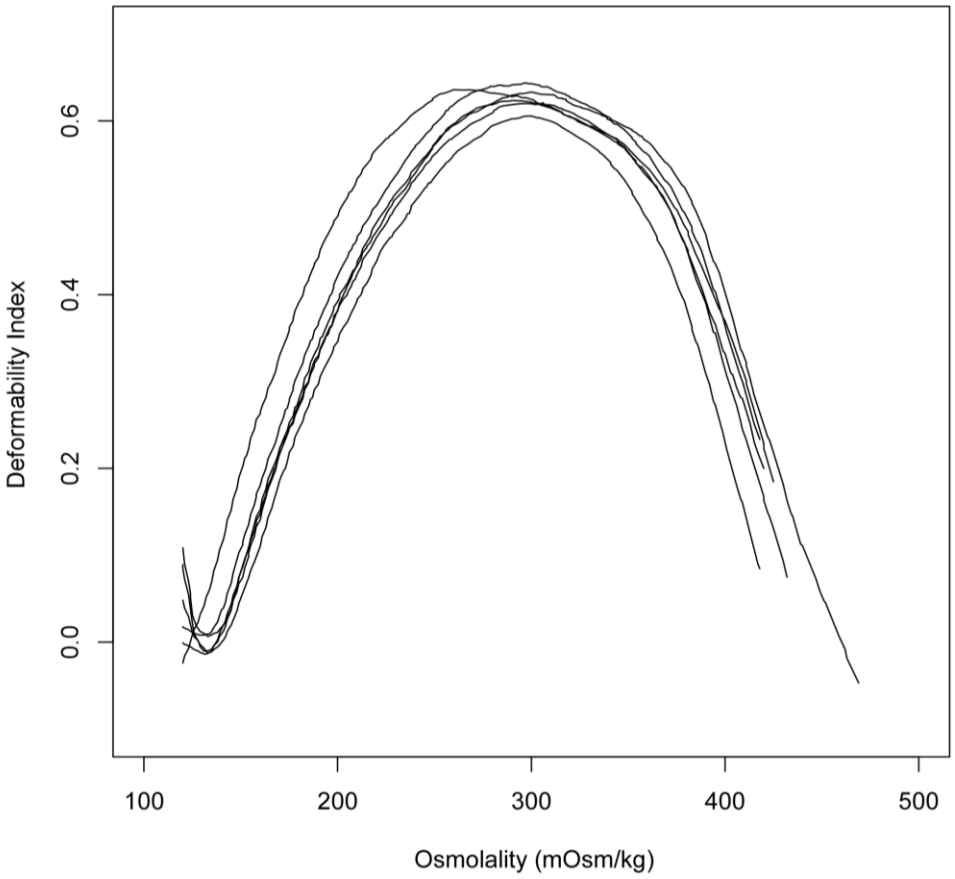

Figure 7.2.4 Deformability index (DI) measured by osmotic gradient ektacytometry for RBCs across a range of osmolalities. Each line (osmoscan) corresponds to a separate sample, n = 6.

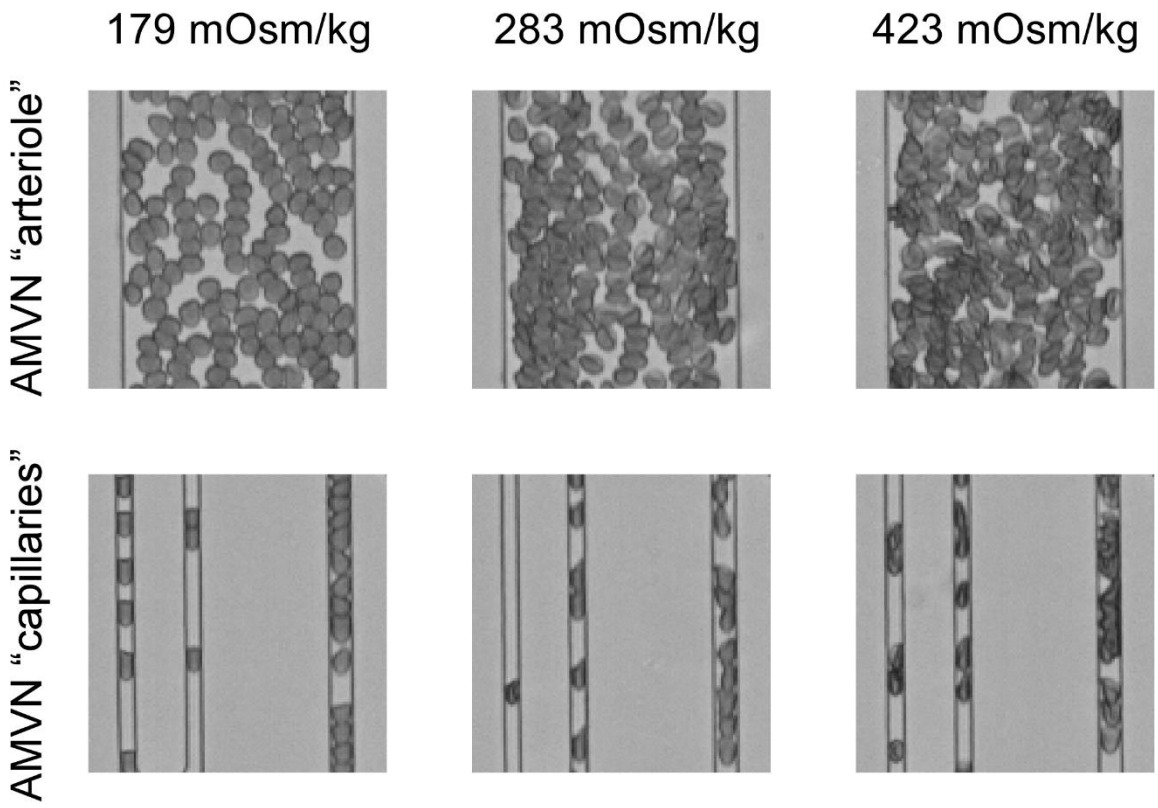

Figure 7.2.5 Bright-field micrographs of RBCs suspended in hypotonic (left), isotonic (middle) and hypertonic (right) solutions as they perfuse portions of the AMVN. 70 μm wide inlet 'arterioles' (upper) and 5-7 μm wide 'capillaries' (lower) are shown.

The effect of osmolality on the ability of RBCs to perfuse the AMVN is shown in **Figure 7.2.6**. The mean perfusion rate for each sample was calculated as the cross-sectional area (350 μm^2) multiplied by the average of the mean cell velocities in the venule of the AMVN for the first 10 sets of images after the three velocities plateaued (simultaneously) following the increase of the driving pressure to 20 cmH_2O (as previously described).[131,188,189] **Figure 7.2.6** shows normalized (with respect to isotonic conditions) perfusion rates for RBCs resuspended at constant RBC numbers (corresponding to 40% hematocrit in isotonic saline) in suspending solutions with initial osmolalities of 150, 200, 300, 400 and 500 mOsm/kg H_2O and measured average osmolalities in the supernatant of 189, 228, 293, 364, and 431 mOsm/kg H_2O. RBCs showed the maximum AMVN perfusion rate in isotonic conditions. Deviations from isoosmolality in either direction decreased the AMVN perfusion rate (maximum decrease in mean AMVN perfusion rate was 6.6%). The numeric data are given in **Table 7.2.1**.

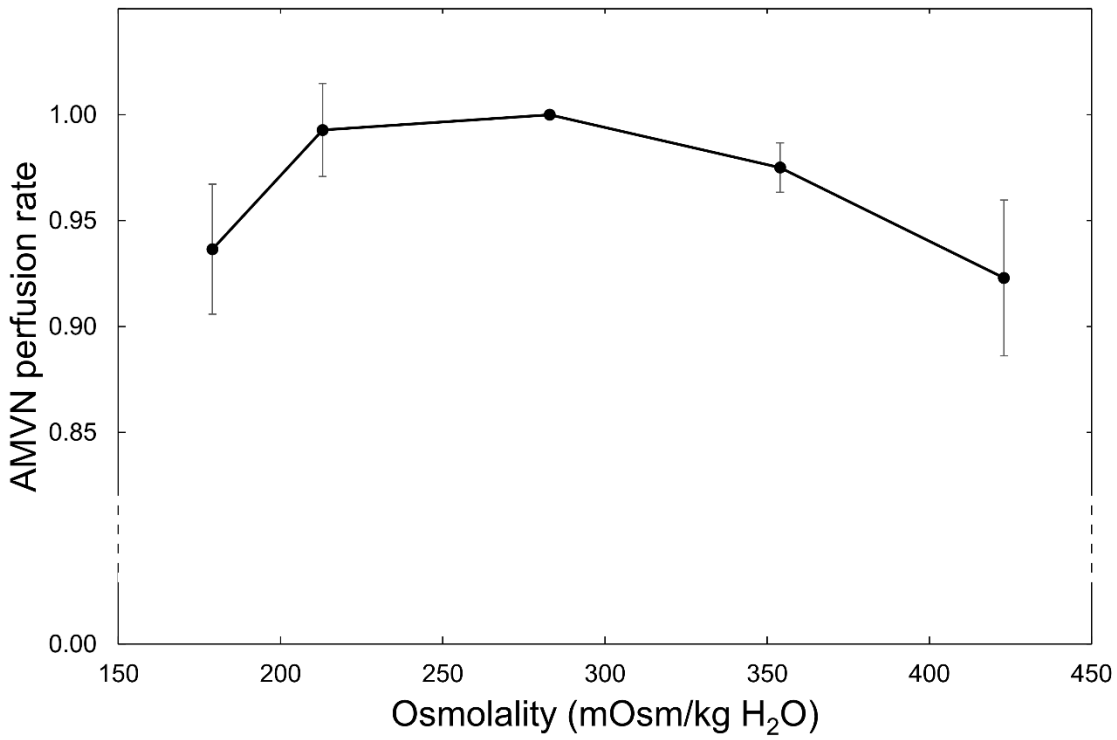

Figure 7.2.6 Normalized AMVN perfusion rates (relative to the AMVN perfusion rate under isosmotic conditions) for RBCs suspended in solutions with different osmolalities. Mean values ± SD, n = 5.

7.2.4 Discussion

The osmolality of the suspending medium affected RBC shape. As originally described by Evans and Fung,[248] hypoosmolality gradually increases RBC thickness and decreases the diameter, while the two opposing dimples persist until a spherical shape is reached. Our morphological analysis by scanning electron microscopy (**Fig. 7.2.1a**) at severe hypoosmolality indicates that one dimple persists until complete sphericity is reached, while the opposing dimple disappears, leading to an extreme form of cup-shaped RBC, which agrees also with earlier theoretical considerations.[213] The persistence of a marked dimple area in an otherwise almost spherical shape is remarkable, it is not an artifact of RBC fixation by glutaraldehyde or the sample preparation.[249] The biconcave RBC shape is explained by the principle of least total curvature of the membrane, which means that the bending energy is minimized.[213] The biophysical properties of the membrane are considered to be uniform over the surface,[213] with dimple areas moving over the membrane surface during the tank-treading motion in shear flow. That is, RBC deforms to an ellipsoidal shape and its membrane rotates steadily around the cell,[250] which also occurs in hypotonically swollen RBCs.[251] Our

scanning electron micrographs also show (**Fig. 7.2.1b**) that RBC shrinkage in hypertonic medium rarely induces RBC crenation (echinocytosis), which had been observed for higher osmolalities in earlier studies.[247,252]

Automated hematology analyzers used routinely in clinical practice cannot detect osmotically induced changes of RBC volume because a relatively large volume of isotonic solution is added to the sample in the instrument before measurement,[253] which reverses the RBC volume almost instantly.[254] Osmotically induced changes of RBC indices are therefore rarely reported in the literature. The RBC indices must be assessed with the help of centrifuged microhematocrit, which analyses RBCs at the actual suspension osmolality. It has been shown that osmolalities below 250 mOsm/kg increase the sphericity of RBCs to a point, where the trapping of suspending medium between RBCs during centrifugation gradually increases, which leads to an overestimation of MCV.[255] This may explain the non-linear increase of MCV and decrease of MCHC at very low osmolalities shown in **Figure 7.2.2**.

Osmotic gradient ektacytometry is an elegant way to measure RBC deformability by quantifying cell elongation under high shear conditions in a continuum of osmolalities.[187,256] We observed maximum elongation (deformability index) around 290 mOsm/kg H_2O. The osmolality with maximum RBC elongation varies among different species, for example, it is around 350 mOsm/kg H_2O in mice and pigs.[257] The maximum ektacytometric elongation index represents a balance in the adjustment of cell surface area-to-volume ratio, and intracellular viscosity. The deformability index declined at hypoosmolality because of the osmotically increased volume at constant surface area; at hyperosmolality, the deformability index decreases because of the increased intracellular viscosity due to osmotic loss of water and rising hemoglobin concentration.[256] Cell elongation during flow in an ektacytometer is one way to measure certain aspects of RBC deformability, which can, however, not be generalized for all types of RBC deformations present in the microcirculation. The capability of RBCs to pass narrow channels is determined by other factors, including the surface area/volume ratio (or sphericity) of the cells. Previous filtration experiments have shown that isoosmolality (290 mOsm/kg H_2O) does not necessarily maximize the measured RBC deformability. In filters with larger pores (7µm), 200 mOsm/kg H_2O generated the lowest filtration resistance, whereas in filters with very small pores (3µm) hyperosmolality around 400 mOsm/kg H_2O generated the lowest filtration

resistance.[247] These findings emphasize that RBC deformability cannot be sufficiently described by a single *in vitro* test, but needs to be accessed more comprehensively with several different methods.[188]

For the measurement of viscosity, RBCs were suspended at a constant cell number, but variable hematocrit. Hypoosmolality, which induced RBC swelling and by that increased hematocrit, increased suspension viscosity at all shear rates. The use of saline instead of plasma as a suspending medium eliminated RBC aggregation, which would have further increased low shear viscosity. Hypotonically swollen RBCs have been shown to aggregate less,[247] which may counterbalance to some extent the increased low shear viscosity at hypoosmolality *in vivo*.

We evaluated the ability of RBCs suspended in saline of different osmolalities to perfuse microvasculature by measuring the perfusion rate of an artificial microvascular network (AMVN). In the AMVN device, RBCs experience a wide range of physiologically relevant deformations, similar to those they experience *in vivo*, including folding deformations when entering the smallest capillary microchannels, and deformations due to shear and cellular collisions occurring in larger channels. Thus, because RBCs experience multiple types of deformation challenges, the measurement of the AMVN perfusion rate for a RBC suspension provides a much more comprehensive assessment of RBC rheological properties than conventional, single-parameter measurements of RBC deformability.[128,188] Here we showed that deviations in osmolality (±100 mOsm/kg H_2O) resulted in relatively minor decline in AMVN perfusion rates.

Although one must be cautious when directly extrapolating *in vitro* findings to *in vivo* conditions, our results may have significant clinical implications. First of all, they show that data from a single biorheological measurement may be misleading and induce inappropriate conclusions with regard to pathophysiology and ensuing therapeutic concepts. In the present study, ektacytometric RBC elongation suggested that isoosmolar conditions yielded best results and that even moderate deviations in osmolality should be avoided. On the other hand, suspension viscosity showed that not isoosmolar, but hyperosmolar conditions would be beneficial, indicating that for bulk viscosity hematocrit is more important than RBC deformability. Since viscosity determines blood flow in large vessels, it is tempting to speculate that some degree of plasma hyperosmolality could be beneficial for the macrocirculation and hypoosmolality would be detrimental. One has to keep in mind that not only blood cells, but also endothelial cells undergo swelling when exposed to a hypotonic solution, which would additionally increase flow resistance.[258] The concept of

a beneficial effect of hyperosmolality is corroborated by *in vivo* studies showing that hypertonic solutions improve cardiac function in children after open-heart surgery[259] and improve the outcome after hemorrhagic shock.[260-263]

The marked effect of osmolality on RBC deformability and suspension viscosity are in contrast to microvascular network perfusion, which changed only by a few percent in an osmolality range from 200 to 400 mOsm/kg H_2O. An appropriate perfusion of the microcirculation is pivotal for any organ function. The newly available AMVN is probably the best and most comprehensive way to analyze RBC flow in the microcirculation *in vitro*. Our results show that the microcirculation is relatively inert to changes in osmolality. This finding is physiologically and clinically relevant, because it explains how adequate organ perfusion could be maintained even under relatively harsh conditions such as in severe dehydration.

7.3 Aggregation

The following research has previously been accepted for publication and much of the following text is reprinted with permission from: Microcirculation, Reinhart WH, Piety NZ, Shevkoplyas SS, "Influence of red blood cell aggregation on perfusion of an artificial microvascular network," DOI: 10.1111/micc.12317, Copyright 2016 John Wiley & Sons Ltd.

7.3.1 Introduction

Red blood cells (RBCs) suspended in plasma tend to aggregate among each other, forming multi-cellular branched or linear aggregates called rouleaux.[264] RBC aggregation occurs under conditions with low shear rates during stagnant or low flow. It is a reversible process, i.e., aggregates are dispersed by higher shear forces and reform within seconds when those forces have ceased. RBC aggregation depends on the concentration of high molecular weight proteins such as fibrinogen in plasma.[264]

Increased RBC aggregation has been reported in many different diseases such as bacterial infections[265,266] and sepsis,[267] myocardial ischemia and infarction,[268,269] cerebral infarction,[270] peripheral

vascular disease,[271] hypertension,[272] diabetes mellitus,[273] metabolic syndrome,[274] hypergammaglobulinemias,[275] and inflammatory rheumatological diseases.[276,277]

Inflammatory disease is accompanied by a systemic acute phase reaction characterized by an increased production of C-reactive protein, fibrinogen, alpha-2-macroglobulin, and immunoglobulins.[278-280] Increased concentration of fibrinogen and other high molecular weight proteins in plasma leads to increased RBC aggregation[281] which becomes apparent through elevated RBC sedimentation rate, a very old and time-honored laboratory test in clinical medicine.[282] It is still a matter of controversy whether increased RBC aggregation is beneficial and contributes to recovery from a disease,[283,284] whether it is a harmful process and thus perhaps a mediator of disease,[285-287] or an irrelevant parameter and only a marker of disease.[288,289]

RBC aggregation affects hemorheology by increasing blood viscosity at low shear rates.[290] In tube flow, RBC aggregation occurs in the center axis of the tube, which leads to an increased cell-free layer near the wall.[291,292] Whether RBC aggregation also affects the flow of blood in the microvasculature is still a matter of debate. Current experimental data are confounded by the fact that a change in RBC aggregation is accompanied by a concomitant change in plasma viscosity, which itself is a major determinant of capillary blood flow.[289,293] In the present study we suspended normal human RBCs in two solutions of dextran with equivalent viscosities, but different capacity to cause RBC aggregation, namely dextran 70 as aggregating medium and dextran 40 as non-aggregating medium. We measured the ability of RBCs suspended in these to different media to perfuse an artificial microvascular network (AMVN). We also estimated the hematocrit in the "capillary" and "venular" portions of the AMVN for both suspensions, which in combination with the perfusion rate data, allowed us to test whether RBC aggregation increases or decreases tissue oxygenation capacity.

7.3.2 Methods

Dextran solutions

Dextrans with molecular weights of 70,000 Daltons (dextran 70) and 40,000 Daltons (dextran 40) were used (Tokyo Chemical Industry Co., Tokyo, Japan). Both dextran 70 and dextran 40 were dissolved in saline for measuring RBC aggregation and viscosity, or in GASP buffer (1.3 mM NaH_2PO_4, 9 mM Na_2HPO_4, 140 mM NaCl, 5.5 mM glucose, 1% bovine serum albumin; osmolality 290 mOsm/kg; pH 7.4) for measuring

AMVN perfusion rates. Dextran 70 was dissolved at a concentration of 35 g/L based on our previous experience studying RBC aggregation,[294] A series of dextran 40 concentrations was prepared and their viscosities were measured (see below). From these viscosity measurements it was calculated that 46.5 g/L dextran 40 solution matched the viscosity of the 35 g/L dextran 70 solution, and therefore these concentrations were used in all experiments.

Blood samples

Samples of whole blood were obtained from healthy consenting volunteers via venipuncture using EDTA as an anticoagulant (4 mL, 7.2 mg K_2EDTA, Vacutainer, Becton Dickinson, Franklin Lakes, NJ, USA). The collection of blood samples was approved by the institutional review board (IRB) at the University of Houston (Houston, TX). For measurements of RBC aggregation (n = 5) and suspension viscosity (n = 10), whole blood was centrifuged at 2500 × g for 5 min (Allegra X-15R, Beckman Coulter, Schaumburg IL, USA), and plasma, buffy coat and the uppermost RBC layer were discarded. The pelleted RBCs were washed twice in saline and then resuspended in either dextran 40 or dextran 70 solutions described above with final hematocrit adjusted to 30%.

For measuring AMVN perfusion (n = 7), whole blood was centrifuged at 1300 × g for 5 min, plasma was discarded, and pelleted RBCs were diluted with GASP buffer down to ~5% hematocrit. The diluted RBC suspension was passed through a high-efficiency pediatric leukocyte reduction filter (Purecell NEO, Pall Corp., Port Washington, USA). The filtrate was centrifuged at 3080 × g for 5 min, the supernatant was discarded, and packed RBCs were re-suspended in either dextran 40 or dextran 70 solution described above at 30% hematocrit. All measurements of hematocrit were performed in duplicate on a hematology analyzer (Medonic M-series, Boule Medical AB, Stockholm, Sweden). Samples were kept on a mixer (Labquake, Barnstead Thermolyne, Dubuque, Iowa, USA) until AMVN experiments were performed. Each RBC suspension was tested once then discarded, and all experiments were completed within 4 hours of drawing.

Viscosity measurements

A coaxial Couette-type viscometer (Contraves LS 30, ProRheo, Althengstett, Germany) was used to measure solution viscosities. Measurements of viscosity of dextran 40 and dextran 70 solutions were done

at a shear rate of 11 s^{-1}. Viscosities of RBC suspensions were measured over a wide range of shear rates in the following order: 69.5, 27.7, 11.0, 3.23, 0.95, 0.28 and 0.11 s^{-1}. Viscosity values were calculated from the plateau value of the stress-strain curve generated by the viscometer. All measurements were performed at room temperature within 4 hours.

Measurements of RBC aggregation

An aggregometer with a cone-plate shearing system and integrated infrared light transmission measurement (Myrenne MA-1, Roetgen, Germany) was used to quantify RBC aggregation. RBC aggregates were dispersed at a shear rate of 600 s^{-1} in an initial phase, which was followed by an integration of light transmission over 10 s either at stasis (M mode) or at a low shear rate of 3 s^{-1} (M1 mode). Measurements were performed at room temperature in triplicate.

Measurements of the AMVN perfusion rate

The scientific background, design and fabrication of the artificial microvascular network (AMVN) devices, and the methods used for measuring the AMVN perfusion rate have been described previously.[128,129,131,159,189,228] Each AMVN device contained three identical networks of "capillary" microchannels (widths 5-70 μm) arranged in a pattern inspired by rat mesentery microvasculature, and each having an independent inlet port connected to the "capillary" network via a 70 μm wide channel ("arteriole") and converging to a common outlet port by a 70 μm wide channel ("venule").[128] All microchannels comprising the AMVN were 5 μm deep. AMVN devices were manufactured using polydimethylsiloxane (PDMS; Sylgard 184, Dow Corning Corp., Midland, MI) replicas of a patterned silicon wafer fabricated using soft lithography as described previously.[128] Patterned casts were then sealed to PDMS coated glass slides after 100 second exposure to air plasma. The assembled AMVN devices were treated for 30 min with a 1% solution of mPEG-silane (Laysan Bio, Inc., Arab, AL) in GASP, and then flushed with GASP buffer prior to use.

GASP buffer was removed from the AMVN inlets by drying (Kimwipes, Kimberly-Clark Professional, Roswell, USA) and 25 μL of either dextran 40 or dextran 70 samples were deposited in each inlet. A 2 mm micro-stirring bar was inserted into each inlet, and a magnetic stirrer (Model 1060, Instech

Laboratories, Inc., Plymouth Meeting, USA) placed above the inlets was used to actuate micro-stirring bars in the inlets to prevent aggregation and sedimentation of RBCs within the inlets. The driving pressure applied to the system was controlled by a water column connected to the AMVN device outlet. RBCs were allowed to fully perfuse the AMVN device, then the driving pressure was set to 0 cmH_2O by adjusting the height of the water column until the RBCs came to a complete stop. Thereafter the system driving pressure was set to 60, 40, 20, 10 and 5 cmH_2O for 3 min at each pressure (Note: a driving pressure of 2.5 cmH_2O was attempted, however obstruction of microchannels, due to RBC adherence to channel walls – especially with dextran 70, resulted in inconsistent RBC velocities; therefore these data were not included in the final analysis).

Images were captured with a high-speed camera (100 fps, Flea3, Point Grey Research, Inc., Richmond, Canada) and analyzed offline with a custom image analysis algorithm implemented in MATLAB 2014b (The Math Works Inc., Natick, MA, USA).[128,159] The image analysis algorithm compared subsequent images to determine the change in position of RBCs between images, thereby enabling determination of RBC solution velocity. The AMVN perfusion rate was then calculated by multiplying the solution velocity by the cross-sectional area of the microchannel (5 μm × 70 μm = 350 μm^2 for "venules").

Estimation of hematocrit in microchannels

Microscopic observations of the flow through the AMVN suggested that the hematocrit was higher with dextran 70 suspensions than with dextran 40. This prompted a *post-hoc* analysis as follows. The same images used to measure AMVN perfusion rate were also used to estimate hematocrit in individual microchannels of the AMVN. To improve contrast and simplify the measurements of RBC velocity, we imaged the flow of blood through the AMVN in blue light (RBCs appear dark in blue light) using a band-pass blue-violet filter (394 ± 50 nm, B-390, Hoya Corp. USA, Fremont, CA). We reasoned that the hematocrit within each microchannel, therefore, was proportional to the intensity of light transmitted through the channel, based on the principles of spectrophotometry. The average grayscale color intensity (0 to 255 au) of the interior area within each microchannel and of the device background area around the microchannels was measured using a custom image analysis algorithm implemented in MATLAB (The Math Works Inc.). The average grayscale color intensity of each microchannel was subtracted from the average grayscale color intensity of the device background in order to correct for lighting variations resulting from the thickness of

the PDMS device and the microscope settings. The corrected average grayscale color intensities for individual microchannels were then compared to determine the differences in mean estimated hematocrit between different microchannels relative to one another. Importantly, while we were able to determine whether hematocrit in one channel was higher or lower than in another channel using this approach, we could not measure the absolute values of hematocrit in the channels. Therefore all hematocrit data in **Figure 7.3.6** and **Figure 7.3.7** is presented as the difference between the two estimated hematocrits (as a percent) and no absolute hematocrit values are given.

Statistical analysis

Statistical analysis was performed using built-in functions of MATLAB 2014b statistics toolbox. Paired Student's t-tests were used for comparisons of dextran 40 and dextran 70 data. The results are given as mean values ± standard deviations (SD). A p-value of < 0.01 was considered significant.

7.3.3 Results

The viscosities of 46.5 g/L solution of dextran 40 and 35 g/L solution of dextran 70 in saline were very similar (**Table 7.3.1**). Aggregometry revealed RBC aggregation in dextran 70 suspensions, but not in dextran 40 suspensions, both at stasis (M mode) and under low shear flow (M1 mode), which is also shown in **Table 7.3.1**. **Figure 7.3.1** shows viscosities of RBC suspensions in either dextran 40 or dextran 70 with a hematocrit of 30% for a wide range of shear rates. Whereas the viscosity of RBC suspensions in dextran 40 was almost independent of the applied shear rate (so called Newtonian behavior), the viscosity of RBC suspensions in dextran 70 increased exponentially with decreasing shear rates, indicating RBC aggregation.

Table 7.3.1 Viscosities of D40 and D70 solutions in saline and their effect on RBC aggregation in 30% hematocrit suspensions measured using a Myrenne aggregometer either at stasis (M mode) or at low shear rate (M1 mode). Mean values ± SD, n = 5.

	46.5 g/L dextran 40 (D40)	**35 g/L dextran 70 (D70)**
Solution viscosity (mPa·s)	2.13 ± 0.24	2.08 ± 0.20
RBC aggregation at stasis (M mode)	7.9 ± 2.6	23.9 ± 5.4
RBC aggregation at 3 s^{-1} (M1 mode)	15.2 ± 3.8	28.4 ± 7.0

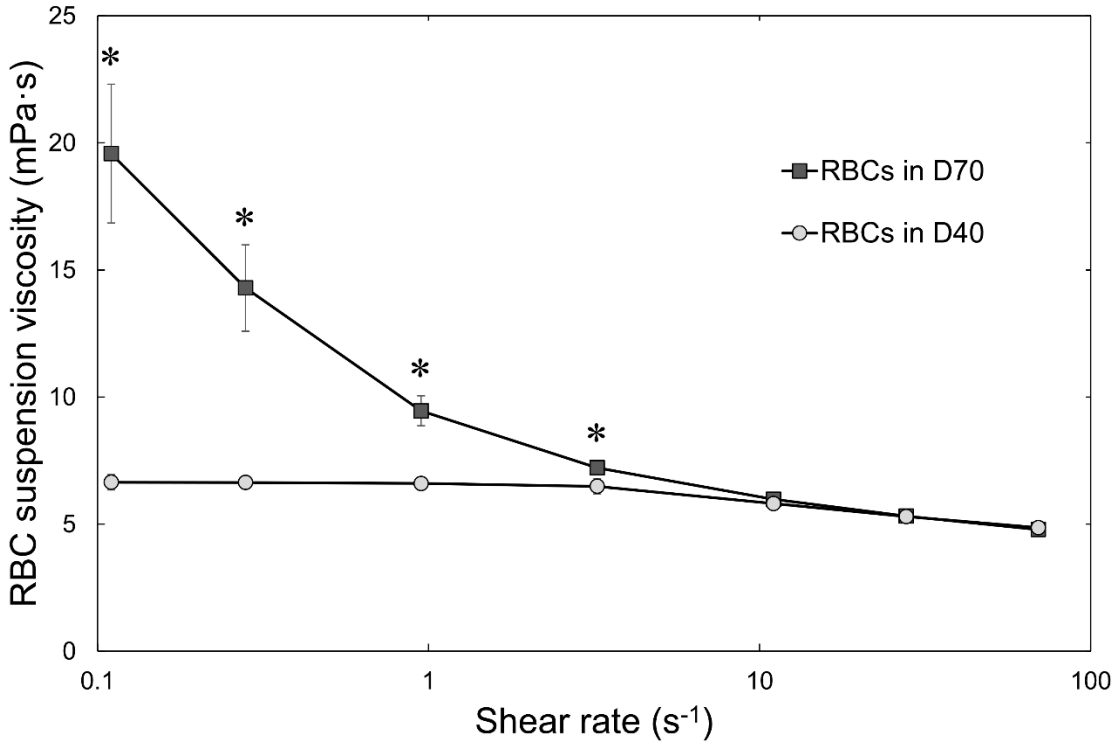

Figure 7.3.1 Viscosity of 30% hematocrit RBC suspensions in D40 (circles) or D70 (squares) for shear rates from 0.11 to 69.5 s^{-1}, at room temperature. Mean values ± standard deviation, n = 10. Statistically significant differences ($p < 0.01$) are marked by an asterisk (*).

Figure 7.3.2 illustrates the microscopic appearance of RBC aggregates in an AMVN at various driving pressures. In contrast to dextran 40, which did not exhibit RBC aggregation even at the lowest driving pressure (far left side **Fig. 7.3.2**), stacks of RBCs without apparent gaps between adjacent cells were seen for dextran 70 suspensions in "arterioles", "venules" and in "capillaries", best visible by single files of aggregated RBCs moving like trains into a first order "venule" (e.g., see right "capillary" at driving pressures of 10 – 40 cmH_2O in **Fig. 7.3.2**). A driving pressure of 60 cmH_2O resulted in such high velocities that we cannot make statements about the occurrence of RBC aggregation. Adhesion of RBCs to the mPEG-silane treated walls of the microchannel was very rarely observed, and was always transient, across all driving pressures evaluated.

Figure 7.3.3 shows characteristic traces of the AMVN perfusion rate, calculated from the mean RBC velocity in "venular" microchannels. The perfusion rate traces for RBCs suspended in dextran 40 (without aggregation) were relatively constant for any given driving pressure, while those for RBCs suspended in dextran 70 (with aggregation) showed a considerable undulating variation over time, which

most likely reflected the intermittent passage through the network of large aggregates with aberrant, rotational movements.

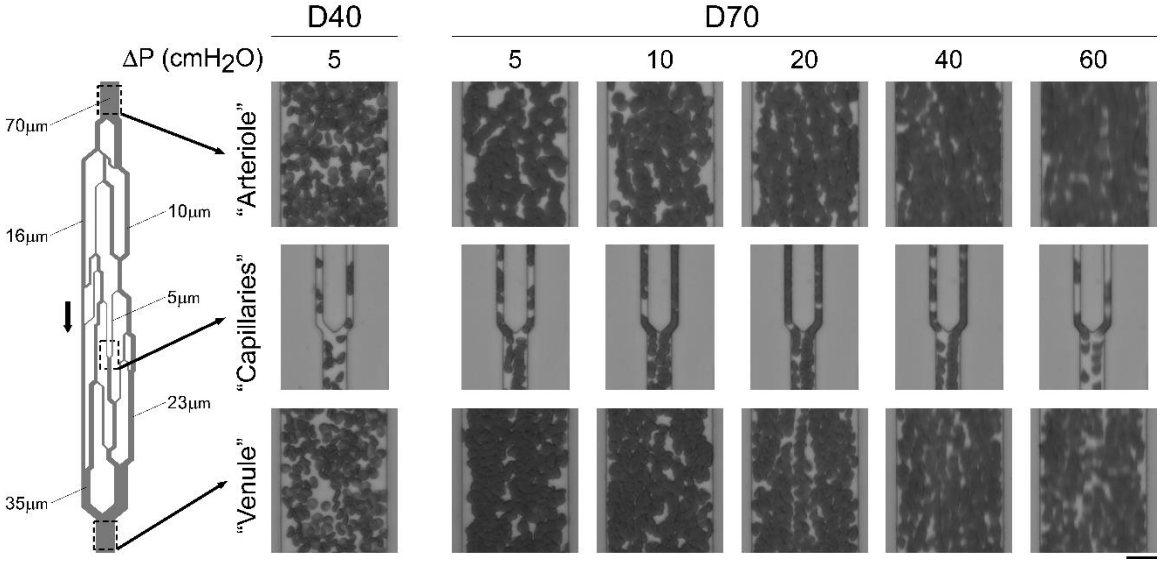

Figure 7.3.2 Photographs of RBC suspensions flowing through the AMVN, at the level of "arterioles" (top), "capillaries" (middle) and "venules" (bottom). Arrow indicates direction of flow. Scale bar is 20 μm.

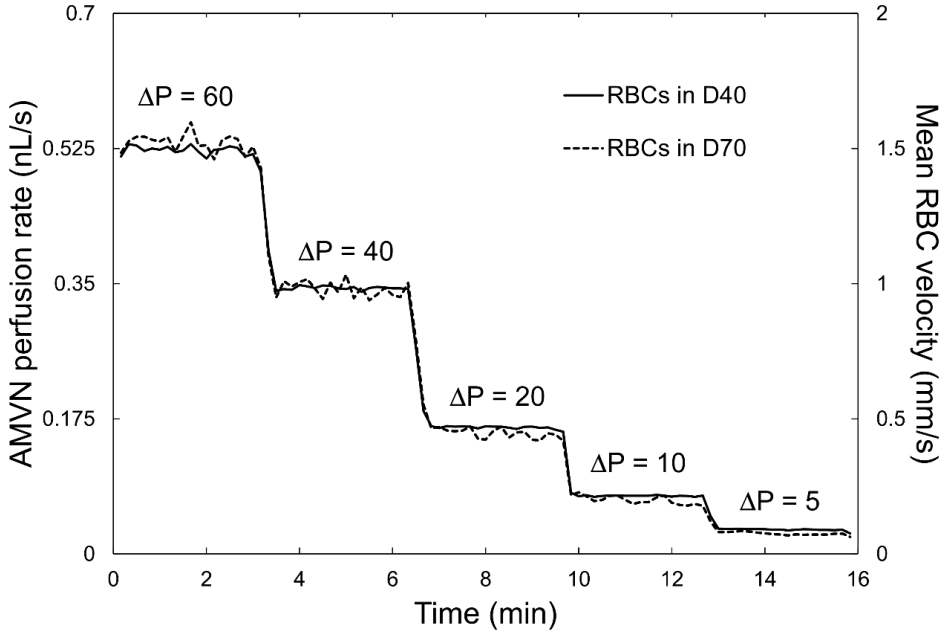

Figure 7.3.3 Typical traces of AMVN perfusion rate (left scale) and mean RBC velocity (right scale) obtained at the "venular" level for 30% hematocrit suspensions of RBCs in D40 (solid line) or D70 (dashed line) at decreasing driving pressures (ΔP).

Figure 7.3.4 shows the AMVN perfusion rates (calculated using the measured mean RBC velocities in "venular" microchannels) for RBC suspensions in dextran 40 and dextran 70, for a range of driving pressures. There was a linear relationship between the driving pressure applied to the AMVN and the AMVN perfusion rate. The AMVN perfusion rates were similar for RBC suspensions in dextran 70 (with aggregation) and in dextran 40 suspensions (without aggregation) for all driving pressures.

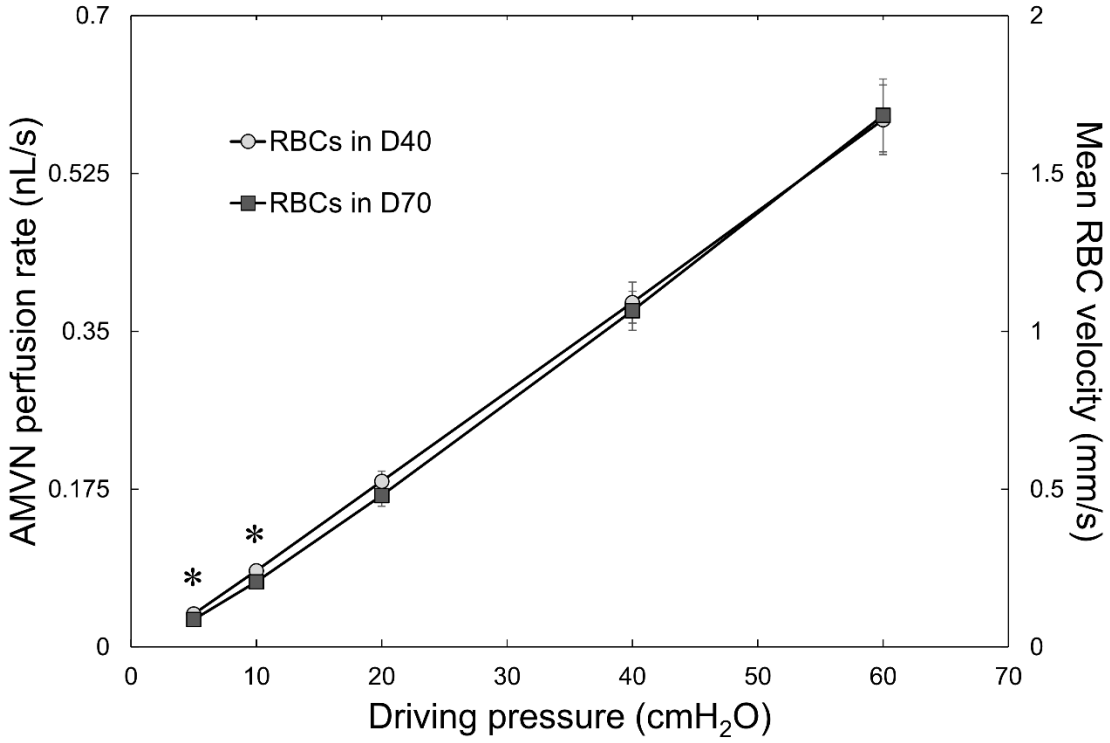

Figure 7.3.4 AMVN perfusion rate and mean RBC velocity measured in "venular" microchannels for 30% hematocrit RBC suspensions in D40 (circles) or in D70 (squares). Mean values ± SD, n = 7. Statistically significant differences ($p < 0.01$) are marked by an asterisk (*).

We also measured RBC velocities in two different 5 μm "capillaries". **Figure 7.3.5** shows the results of these measurements. The two "capillaries" (**Fig. 7.3.5 inset**) had very different RBC velocities despite having the same dimensions, because the right "capillary" branched from a larger feeding vessel than the left "capillary" (see schematic drawing of an AMVN on the left side of **Fig. 7.3.2**). A linear relationship between driving pressure and RBC velocity was also seen in these two different "capillaries", and no difference in RBC velocity was observed between RBC suspensions in dextran 70 with aggregation and in dextran 40

suspensions without aggregation, even at low pressures, when linear RBC aggregates were clearly visible within the "capillaries" (see **Fig. 7.3.2**).

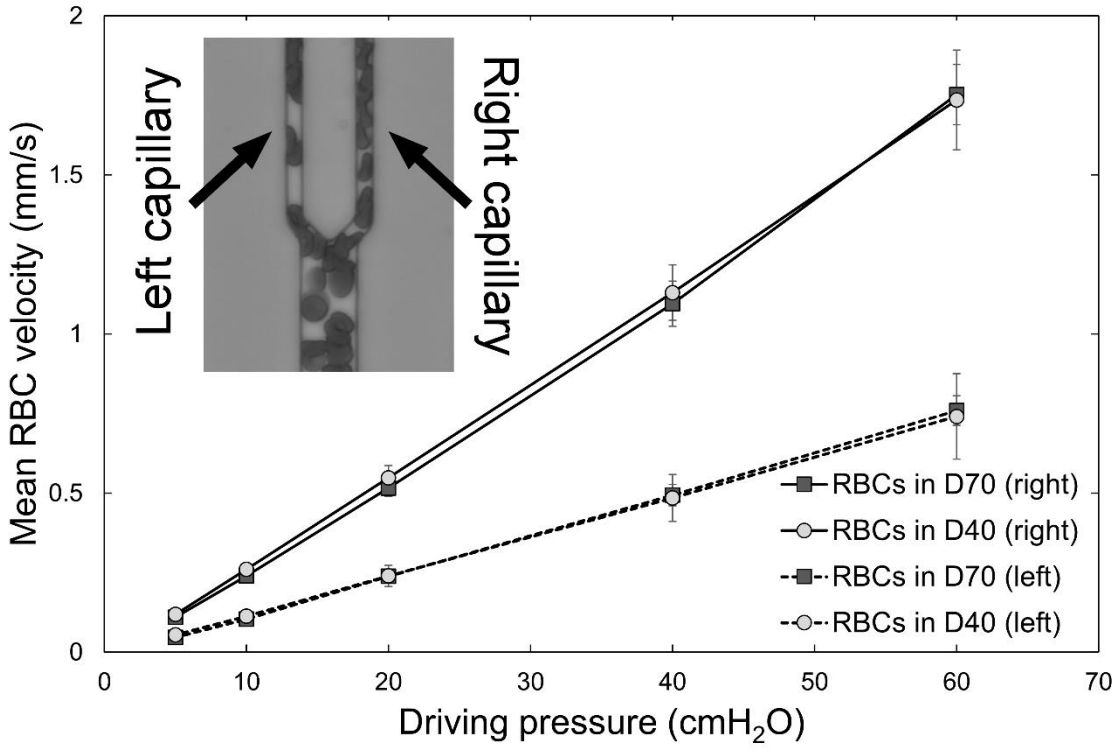

Figure 7.3.5 Mean RBC velocity measured in "capillary" microchannels – left capillary (dashed line) and right capillary (solid line) – for 30% hematocrit RBC suspensions in D40 (circles) or in D70 (squares). Mean values ± SD, n = 7.

Figure 7.3.6 shows the estimated hematocrits in "capillaries" and "venules" for RBCs suspended in dextran 70 with respect to RBCs suspended in dextran 40, across the same range of driving pressures at which AMVN perfusion rates were evaluated. There was no difference in hematocrit at high driving pressure (60 cmH_2O). With decreasing driving pressures down to 10 cmH_2O, estimated hematocrits in aggregating suspension medium dextran 70 became gradually higher with respect to non-aggregating dextran 40. This difference in estimated hematocrit was more pronounced in "capillaries" (up to 30 – 40% at driving pressures of 5 – 10 cmH_2O) than in "venules" (up to 10% at driving pressures of 10 – 20 cmH_2O).

Compared with feeding arterioles or draining venules, capillaries have a lower hematocrit, which is called the Fahraeus effect [272]. We have analyzed the difference in estimated hematocrit between "capillaries" and draining "venules" of the AMVN (**Fig. 7.3.7**). For RBCs in dextran 40, i.e., without RBC aggregation,

"capillary" hematocrit was 30 – 40% below "venular" hematocrit and showed a tendency to become more pronounced with decreasing driving pressure. In contrast, aggregation-inducing dextran 70 reduced the "capillary" hematocrit to only 20 – 25% of the "venular" hematocrit at driving pressures of 5 – 40 cmH_2O, where RBC aggregation was visually observed (**Fig. 7.3.2**).

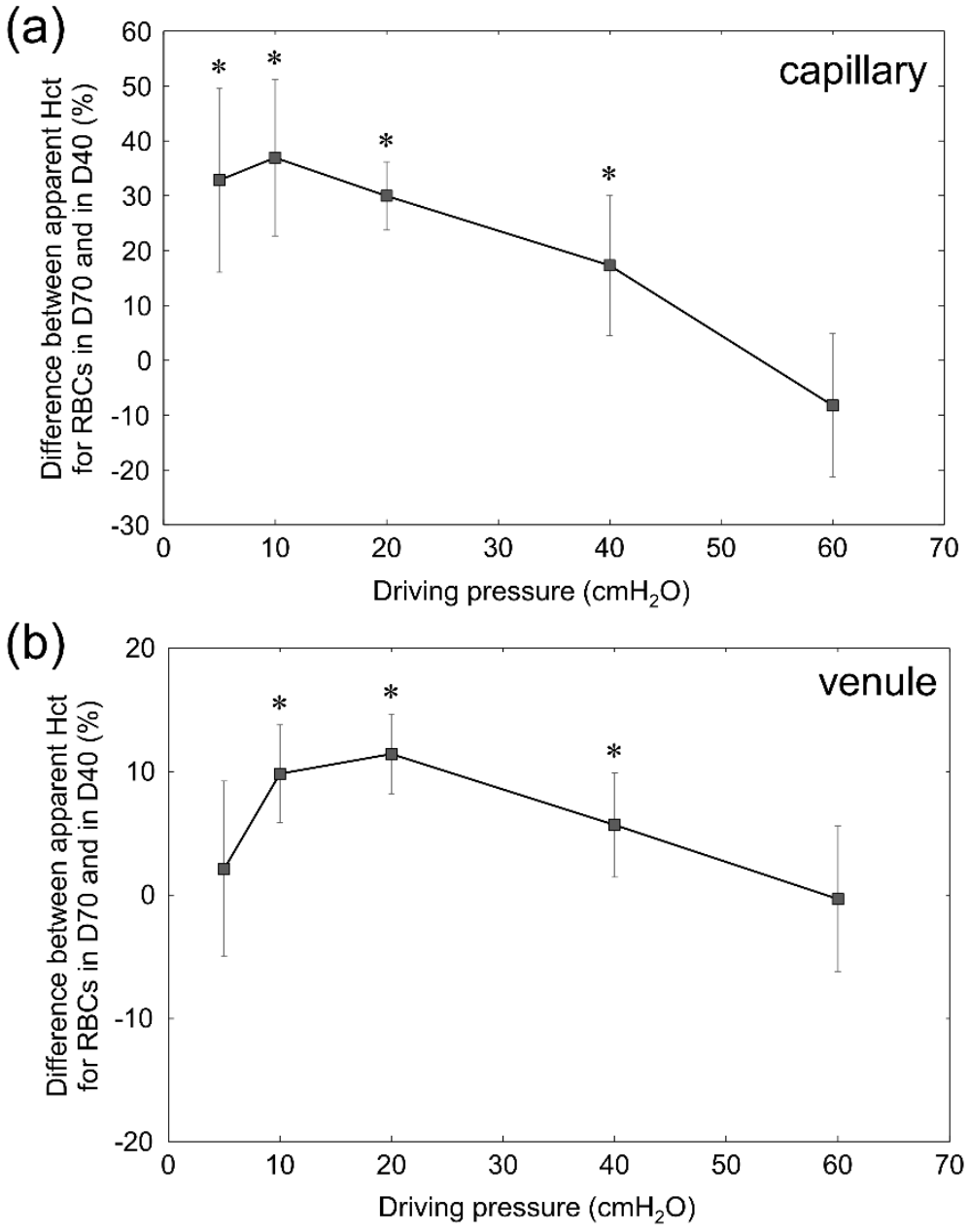

Figure 7.3.6 Difference between estimated hematocrit for RBCs in D40 and D70 for (**a**) "capillaries" and (**b**) "venules" of the AMVN. Asterisks denote a statistically significant difference (p-value < 0.01). Mean values ± SD, n = 7.

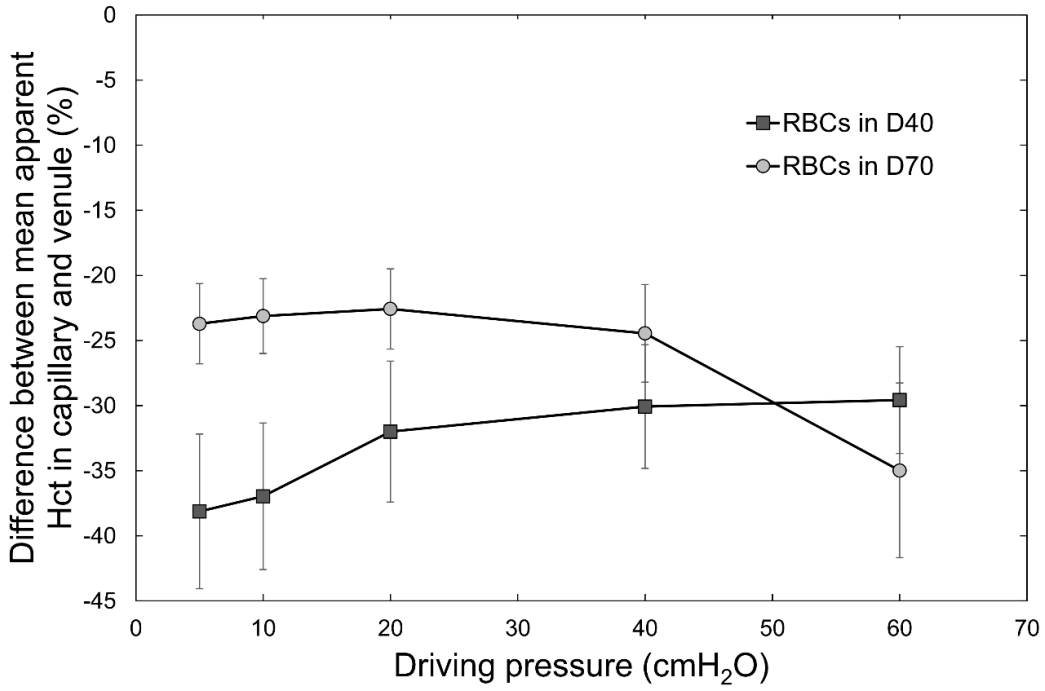

Figure 7.3.7 Difference between mean estimated hematocrit in "capillaries" and "venules" of the AMVN for RBCs suspended in D40 and D70, for driving pressures ranging from 5 to 60 cm H_2O (0.49 to 5.88 kPa).

7.3.4 Discussion

The key finding of this study is that RBC aggregation did not affect the RBC flow velocity through microchannels of the AMVN. Blood flow is determined by plasma viscosity, hematocrit, RBC deformability and RBC aggregation.[295] In our *in vitro* experiments, we kept every parameter except RBC aggregation constant, which allowed an appraisal of the influence of RBC aggregation by itself without confounding factors: 1) the viscosities of 46.5 g/L dextran 40 and 35 g/L dextran 70 solutions were equivalent, 2) the hematocrit was 30% for both suspensions, and 3) RBC deformability is not known to be affected by either version of dextran. The only difference between the two types of suspensions was presence of absence of RBC aggregation (**Table 7.3.1**), as documented by light transmission aggregometry either at stasis or at low flow (at a shear rate of 3 s^{-1}) as well as by the increased viscosity at low shear rates (**Fig. 7.3.1**). In contrast to RBC suspensions in dextran 40, strong RBC aggregation was found in dextran 70, which confirms the results of the many previous studies done with dextran 70.[264,294,296-300]

As expected, RBC aggregation affected suspension viscosities at shear rates <10 s^{-1}; in contrast to RBC suspensions in dextran 40, RBC suspensions in dextran 70 behaved as non-Newtonian fluids

characterized by a progressive increase of viscosity with decreasing shear rate. At shear rates ≥10 s^{-1}, suspension viscosities were similar for RBC suspensions in dextran 70 and dextran 40, indicating that RBC aggregates were disrupted at these higher shear rates. The shear rate threshold around 10 s^{-1} for RBC aggregation in a rotational viscometer is in agreement with earlier observations.[290,295,301]

So far it has not been clear whether RBC aggregation occurs at all in the microcirculation *in vivo*, which is known to be a high shear environment. We have calculated pseudo-shear rates at capillary walls for our AMVN as the quotient of mean RBC velocity in the channel and channel diameter.[302] For RBC suspensions flowing through the faster capillary (shown on the right in **Fig. 7.3.5 inset**), pseudo-shear rates of 22, 48, 104, 220, and 350 s^{-1} correspond to driving pressures of 5, 10, 20, 40 and 60 cmH_2O respectively. We observed RBC aggregates even at these high wall shear rates (**Fig. 7.3.2**). This observation could be explained by the fact that shear forces act differently on RBC aggregates in the relatively large gaps of rotational viscometers (500 µm) than in 5 µm microchannels. Shear forces disrupt aggregates only when they produce velocity gradients between neighboring cells, e.g., when one plane of flow is moved relative to the adjacent plane, as is the case in rotational viscometers. In the case of single-file flow through 5 µm microchannels, the velocity gradient between adjacent RBCs is virtually zero and hence shear forces are negligible. This could potentially explain how RBC aggregates may form during flow through the microcirculation.[302] The occurrence of RBC aggregation in microcirculatory flow under physiologically relevant flow rates agrees with observations *in vitro* in microfluidic channels with a diameter of 4.5 µm and in capillaries *in vivo*.[301,303]

RBC aggregation induced by dextran 70 did not affect RBC flow velocity in "capillaries" and "venules" of the AMVN, and thus had no influence on AMVN perfusion rates at any driving pressure. This observation is in agreement with the work of others,[283,284,288,304-308] but contradicts many studies, which suggested a negative influence of RBC aggregation on microvascular perfusion.[285,287,309-311] The difference could be due to the difference in experimental approaches. In the discordant studies, RBC aggregation was changed by the addition of an aggregating substance, which concomitantly also increased the viscosity of plasma or other suspending medium. Since the viscosity of the suspending medium is a major determinant of microvascular perfusion, these studies could not separate between the influence of RBC aggregation alone and viscosity of the suspending medium.[289,293,312] Carefully matching viscosity of both aggregating and non-

suspending media in our experiments allowed us to draw the conclusion that RBC aggregation induced by dextran 70 *per se* did not affect AMVN perfusion.

The microscopic impression of a lower hematocrit in AMVN microchannels for dextran 40 suspensions compared with dextran 70 prompted further investigations. To this end we estimated changes in hematocrit based on differences in color density in "capillaries" and "venules" of the AMVN. It was confirmed that the hematocrit was lower, for RBCs suspended in dextran 40 (i.e., without aggregation) as compared to aggregating dextran 70 suspensions, in "capillaries", and to a lesser degree also in "venules". RBC aggregation increases sedimentation rate and could theoretically explain higher hematocrit values with dextran 70 in AMVNs. RBC sedimentation is, however, characterized by a lag phase of several minutes (usually 10 – 20 min) before it becomes visible.[282] In addition, we prevented RBC sedimentation in the inlets of the AMVN devices with magnetically actuated micro-stirring bars. Furthermore, the fact that the changes in hematocrit were dissimilar in "capillaries" and "venules" (up to a 4-fold difference) make an artefact rather unlikely. These observations and data presented in **Figure 7.3.7** suggest that RBC aggregation may blunt to some extent the Fahraeus effect (i.e., the lowering of hematocrit during the passage of capillaries[313,314]).

The AMVN experimental setup has inherent limitations. It is an *in vitro* study on an idealized, artificial microvasculature comprised of rectangular microchannels 5 to 70 µm wide, but only 5 µm high. Thus, our device simulates the *in vivo* dimensions of arterioles and venules less well, allowing only the formation of two-dimensional, but not 3-dimensional aggregates, which occur in such vessels.[315] Furthermore, the AMVN lacks endothelial lining. *In* vivo, endothelial cells, coated by a glycocalix, interact with flowing RBCs and produce the vasodilatory active nitric oxide (NO). It has been recently shown that RBC aggregation reduces NO production.[306] Additionally, the AMVN device is constructed of PDMS, which is stiff and inert, unlike microvessels *in vivo* which are capable of dynamically altering vessel diameter in order to modulate blood flow.[128,189] However, spontaneous self-sustained oscillations of capillary blood flow, resulting solely from the non-linear rheological behavior of blood at the microscale, have previously been demonstrated in the AMVN system despite the lack of active regulatory input, such as vasomotion.[189] Last but not least, we studied only samples with a single standardized hematocrit and suspending medium viscosity. Our data, therefore, should only be used to draw conclusions about the hemodynamic effects of RBC aggregation induced by dextran 70 *in vitro*. They should not be directly and uncritically extrapolated to

the microcirculation *in vivo* since dextran solutions, although studied intensively, do not represent physiological suspensions. Nevertheless, the AMVN has been rigorously validated in several studies[128,129,131,145,147,159,228] and it is arguably the best available model system for measuring the influence of various properties of blood on microvascular perfusion *in vivo*.

Limitations notwithstanding, our data are not in favor of therapeutic reduction of RBC aggregation in patients, which has been attempted by lowering fibrinogen with the snake venom ancrod in acute stroke,[316,317] by infusing low molecular weight dextran (dextran 40) in critically ill patients,[318] hydroxyethyl starch (6% HAES 130/0.4) in severe sepsis[319,320] and during cardiopulmonary bypass operations.[321] It is noteworthy that the latter study showed that reduced RBC aggregation induced by HAES 130/0.4 resulted in an undesirable activation of endothelial cells.[321] One of these clinical studies on patients receiving either HAES 130/0.4 or saline also analyzed sublingual microcirculation and found an increased capillary flow index, percentage of perfused capillaries and perfused capillary density after HAES 130/0.4.[319] However, these therapeutic approaches have not been consistently successful, and are no longer recommended.[322-327] Our data show that the negative results of these clinical trials could be explained, at least in part, by RBC aggregation having no negative influence on tissue perfusion, and therefore lowering of RBC aggregation could not be expected – from this purely hemorheological point of view – to improve the clinical outcome of a disease.

RBC oxygen transport capacity, and thus tissue oxygenation, depends on both capillary hematocrit and blood flow velocity [328]. Our data of a higher "capillary" hematocrit and unchanged flow velocity for dextran 70 suspensions suggests that increased RBC aggregation during an acute phase reaction could be beneficial for tissue oxygenation. This is an intriguing finding, which, if confirmed, could contribute significantly to a better understanding of pathophysiological mechanisms.

7.4 Hematocrit

7.4.1 Introduction

Tissue oxygenation is determined by the product of oxygen carrying capacity of blood and the rate of blood flow through the tissue's microvasculature. Because the oxygen carrying capacity of blood depends on the number of red blood cells (RBCs) available to participate in the transport of oxygen, tissue oxygenation should theoretically increase with increasing hematocrit. However, increasing hematocrit also increases the apparent viscosity of blood, which diminishes the flow of blood through the microvasculature and therefore reduces tissue oxygenation. A value of hematocrit for which these two opposite effects balance each other represents the optimal hematocrit that maximizes tissue oxygenation.[329-331]

Under normal physiological conditions, hematocrit is maintained at 35-45% in women and at 40-50% in men.[332] These normal values, however, may not represent the optimal hematocrit, since an increase in hematocrit for healthy young athletes can elevate their exercise performance.[333,334] On the other hand, chronic inflammatory processes, infections, chronic kidney disease, heart failure and cancer are often associated with anemia (i.e., decreased hematocrit), and it is debated if anemia in these conditions is a marker or a mediator of disease.[335-340] Current guidelines recommend a restrictive transfusion strategy with a threshold value for hemoglobin at 7-8 g/dL, corresponding to a hematocrit of 20.6 – 23.5%.[341,342] This discrepancy between the apparently higher than normal optimal hematocrit in healthy young athletes, and lower than normal optimal hematocrit in patients is intriguing and deserves further investigation.

Previous *in vitro* studies have attempted to determine the optimal hematocrit using straight capillary tubes with different diameters, perfused at various shear stresses with whole blood or RBC suspensions.[329,343-348] In these prior studies, the optimal hematocrit was described by the dynamic relationship between hematocrit and apparent blood viscosity in the capillary tubes. Tissue oxygenation, calculated as the quotient of hematocrit and apparent blood viscosity, was plotted against hematocrit, creating a parabolic curve with the maximum at the optimal hematocrit. Several *in vivo* studies have also attempted to determine the optimal hematocrit in short, non-bifurcating segments of microvessels.[349,350] While these studies expanded upon the earlier *in vitro* studies (by introducing factors such as vaso-dilation/-constriction and RBC-endothelium interactions), they also could not account for the dynamic heterogeneity of hematocrit found in complex

networks of bifurcating capillaries[189,351,352] and thus could not properly describe the optimal hematocrit in the microvasculature.

The ability of the circulatory system to transport oxygen to tissues and organs is determined by both the rheology of blood and the architecture of the microvasculature. Microvascular networks generally consist of relatively short (<400 μm) capillary segments of various diameters interconnected in a branching pattern. Because of plasma skimming, in any non-symmetrical capillary bifurcation the daughter branch with the highest flow rate receives an even higher fraction of all RBCs entering the bifurcation, thus increasing the local hematocrit in this branch. Higher hematocrit increases the apparent viscosity of blood and therefore reduces the rate of blood flow through that branch, which in turn reduces the fraction of RBCs the daughter branch receives from the bifurcation.[353,354] This coupling between plasma skimming in capillary bifurcations and the dependence of blood viscosity on local hematocrit generates spontaneous oscillations of blood flow in capillary segments of microvascular networks, and produces a highly heterogeneous and dynamically changing distribution of hematocrit throughout the microvasculature.[189,351,352]

In this study we hypothesized that optimal hematocrit for capillary networks may differ from that for straight capillary tubes or short, non-bifurcating segments of microvessels, and that its value may depend on the overall pressure differential applied to the capillary network. We tested this hypothesis using the artificial microvascular network (AMVN), a microfluidic device composed of interconnected capillary microchannels arranged in a pattern inspired by the microvasculature of rat mesentery.[128,129,131] We have used the AMVN previously to measure the impact of RBC deformability,[131,188] shape,[145] aggregation,[355] and osmolality of the suspending medium[159] on perfusion of microvasculature *in vitro*, to demonstrate the occurrence of self-sustaining spontaneous oscillations of capillary blood flow in microvascular networks[189] and to document a significant improvement in rheological properties of RBCs stored anaerobically[147] and after washing in normal saline[128] or in 1% solution of human serum albumin.[146] Here, the AMVN enabled systematic evaluation of a range of hematocrits at a number of precisely controlled pressure differentials in a capillary network with complex architecture (**Fig. 7.4.1**).

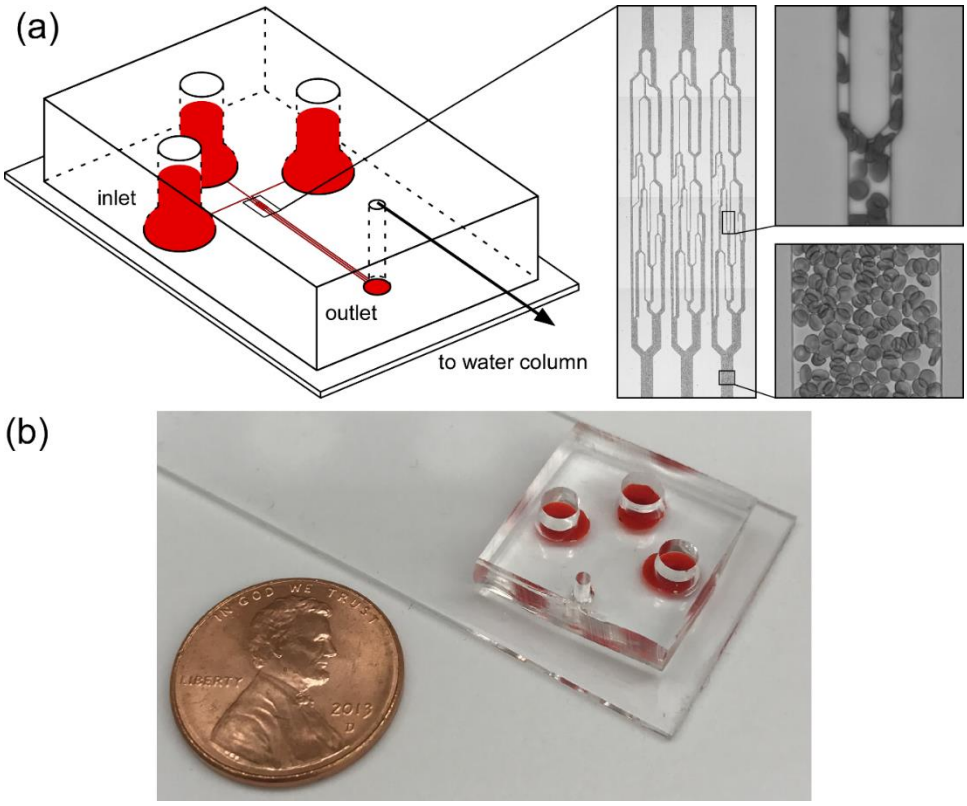

Figure 7.4.1 Artificial microvascular network (AMVN). (**a**) Schematic illustration and micrographs of the AMVN. Arrow indicates direction of flow through the device. (**b**) Photograph of assembled AMVN device (coin shown for size reference).

7.4.2 Methods

Fabrication of the AMVN devices

The design and fabrication of the AMVN devices has been previously described in detail.[128] Briefly, a patterned silicon wafer was used to mold the AMVN devices from polydimethylsiloxane (PDMS; Sylgard 184, Dow Corning, Midland, MI). Assembled devices were filled with GASP buffer (1.3 mM NaH_2PO_4, 9 mM Na_2HPO_4, 140 mM NaCl, 5.5 mM glucose, 1% bovine serum albumin; osmolality 290 mmol/kg; pH 7.4)[128] containing 1% mPEG-silane (Laysan Bio, Arab, AL) and incubated at ambient temperature for 8 hours.

Sample preparation for viscometry measurements

Whole blood was collected via venipuncture from healthy consenting volunteers (n = 10) into Vacutainer tubes (10 mL, K_2EDTA, BD, Franklin Lakes, NJ). Whole blood was centrifuged at 2500 × g for

5 minutes. Supernatant plasma centrifuged at 2500 × g for 10 minutes to remove any remaining cells. Residual plasma, leukocytes and the uppermost layer of RBCs were removed via aspiration. For suspensions in saline, packed RBCs were washed twice in saline and then re-suspended in saline at 60% hematocrit. For suspensions in autologous plasma, packed RBCs were re-suspended in autologous plasma at 60% hematocrit, verified with a hematology analyzer (XT-1800i, Sysmex, Kobe, Japan). Aliquots with hematocrits of 10, 20, 30, 35, 40, 45 and 50% were then prepared by diluting the stock suspensions with calculated volumes of saline or autologous plasma.

Sample preparation for the AMVN measurements

Whole blood was collected via venipuncture from healthy consenting volunteers (n = 7) into Vacutainer tubes (10 mL, K_2EDTA, BD, Franklin Lakes, NJ). Whole blood was centrifuged at 3000 × g for 5 minutes. Supernatant plasma was aspirated and centrifuged at 3000 × g for 10 minutes to remove any remaining cells. Residual plasma, leukocytes and the uppermost layer of RBCs were removed via aspiration. Packed RBCs were diluted with GASP buffer and leukocyte-depleted with a leukoreduction filter (Purecell NEO, Haemonetics, Braintree, MA). The leukoreduced filtrate was centrifuged at 3000 × g for 5 minutes, and the supernatant GASP and the uppermost layer of RBCs were removed via aspiration. For suspensions in GASP buffer, packed RBCs were re-suspended at 80% hematocrit, verified with a hematology analyzer (Medonic M-series, Boule Medical, Stockholm, Sweden). For suspensions in plasma, packed RBCs were diluted in autologous plasma and centrifuged at 3000 × g for 5 minutes (to ensure removal of residual GASP buffer), then re-suspended in autologous plasma at 80% hematocrit, verified by microcentrifugation performed in triplicate (PowerSpin BX, Unico, Dayton, NJ). Aliquots with hematocrits of 10, 20, 30, 35, 40, 45, 50, 55, 60, and 70% were then prepared by diluting the stock suspensions with calculated volumes of GASP buffer or autologous plasma.

Units of RBCs (n = 7) stored hypothermically for 6 weeks were purchased from a blood bank (CPD>AS-1, leukoreduced, Gulf Coast Regional Blood Center, Houston, TX). Stored RBCs were centrifuged at 3000 × g for 5 minutes. The supernatant storage solution and the uppermost layer of RBCs were removed via aspiration. Aliquots of stored RBCs in thawed fresh frozen plasma (AB, Gulf Coast

Regional Blood Center) were then prepared, and the hematocrits were verified as described above. All samples were evaluated within 4 hours.

Measurements of viscometry

A Couette-type coaxial rotational viscometer (Contraves LS30, ProRheo, Althengstedt, Germany) calibrated with H_2O (0.7 mPa·s at 37°C) was used. RBC suspension viscosities were measured at shear rates of 128.5, 69.5, 27.7, 11.0, 3.2, 0.95, 0.28 and 0.11 s^{-1}. All samples were incubated in a water bath at 37°C before completing the measurements, and all viscosity measurements were performed at 37°C.

Measurements of the AMVN perfusion rate

The measurements of the AMVN perfusion rate were performed as previously described in detail.[128,355] A water reservoir (30 mL syringe, BD) fixed to a linear motion stage (Series A40 UniSlides, Velmex, Bloomfield, NY) and connected to the AMVN outlet by flexible tubing was used to modulate the perfusion pressure differential across the AMVN. To perform the AMVN measurement, an AMVN device was secured to the stage of the microscope, connected to the water reservoir, and flushed with GASP buffer. A sample of 25 μL of RBC suspension was then pipetted into each AMVN inlet port, and a 2 mm magnetic stir bar (Spinbar, Bel-Art, Wayne, NJ) was inserted into each inlet. A magnetic stirrer (Model 1060, Instech Laboratories, Plymouth Meeting, PA) was used to actuate the stir bars. The RBC samples were allowed to fully fill the network, then the driving pressure was set to 0 cmH_2O, and imaging of the 70 μm wide "venule" channels downstream of the AMVN was initiated as described below. Three bursts of images were collected at 0 cmH_2O, then 18 bursts were collected at driving pressures of 60, 40, 20, 10, 5 and 2.5 cmH_2O, respectively.

Images of the AMVN were acquired with an inverted bright-field microscope (IX73, Olympus, Center Valley, PA) equipped with a high-speed CMOS camera (Flea3, Point Grey Research, Richmond, Canada). A band-pass blue filter (B-390, Hoya, Fremont, CA) was used to improve image contrast. Image sequences were acquired at 10 × magnification in bursts of 10 frames (at 150 fps) every 10 seconds for the duration of each measurement. Image sequences were analyzed offline with a custom algorithm implemented in MATLAB (MathWorks, Natick, MA).

Statistical analysis

Statistical analysis was performed using built-in functions of MATLAB 2014b Statistics Toolbox (MathWorks). Oxygen transport capacity datasets were fit with second degree polynomials and oxygen transport effectiveness datasets were fit with third degree polynomials.

7.4.3 Results

Figure 7.4.2 shows the viscosities of fresh RBC suspensions in saline (**Fig. 7.4.2a**) and in plasma (**Fig. 7.4.2b**) measured across a range of shear rates (0.3 – 128 s^{-1}) for various hematocrits. For all hematocrits, suspension viscosity increased with decreasing shear rate. Increases in suspension viscosity at decreasing shear rates were larger for higher hematocrits. The viscosity of RBC suspensions in plasma were higher than that of RBC suspensions in saline, which reflected higher viscosity of plasma and the ability of plasma proteins to induce RBC aggregation. Oxygen transport capacity (defined as sample hematocrit, *Hct*, divided by sample viscosity, η) increased with increasing shear rate and was generally higher for RBC suspensions in saline (**Fig. 7.4.2c**) than in plasma (**Fig. 7.4.2d**). In saline, oxygen transport capacity decreased almost linearly for all shear rates, while in plasma, oxygen transport capacity plateaued at intermediate hematocrits for high shear rates (11–128 s^{-1}) and decreased almost linearly for low shear rates (0.3–3.2 s^{-1}).

Figure 7.4.3 shows the AMVN perfusion rate for fresh RBCs suspended in GASP buffer (**Fig. 7.4.3a**) and in plasma (**Fig. 7.4.3b**) evaluated across a range of driving pressures (2.5 – 60 cmH_2O) for various sample hematocrits. The AMVN perfusion rate for RBC suspensions in GASP buffer (**Fig. 7.4.3a**) and in plasma (**Fig. 7.4.3b**) decreased approximately linearly with increasing hematocrit across all driving pressures evaluated, and was generally lower for RBCs suspended in plasma than in GASP buffer, for all corresponding driving pressures and hematocrits. We defined oxygen transport effectiveness as the product of the AMVN perfusion rate, Q_{AMVN}, and sample hematocrit, *Hct*, divided by the driving pressure, ΔP. The oxygen transport effectiveness reached maximum at intermediate hematocrits for both RBC suspensions in GASP buffer (**Fig. 7.4.3c**) and in plasma (**Fig. 7.4.3d**) across all driving pressures. The gradual shift of the maximal oxygen transport effectiveness towards higher hematocrits was more pronounced for suspensions in plasma than in GASP buffer (compare **Fig. 7.4.3d** and **Fig. 7.4.3c**). The oxygen transport effectiveness was generally lowest at the lowest hematocrit evaluated (10%) for both types of suspensions.

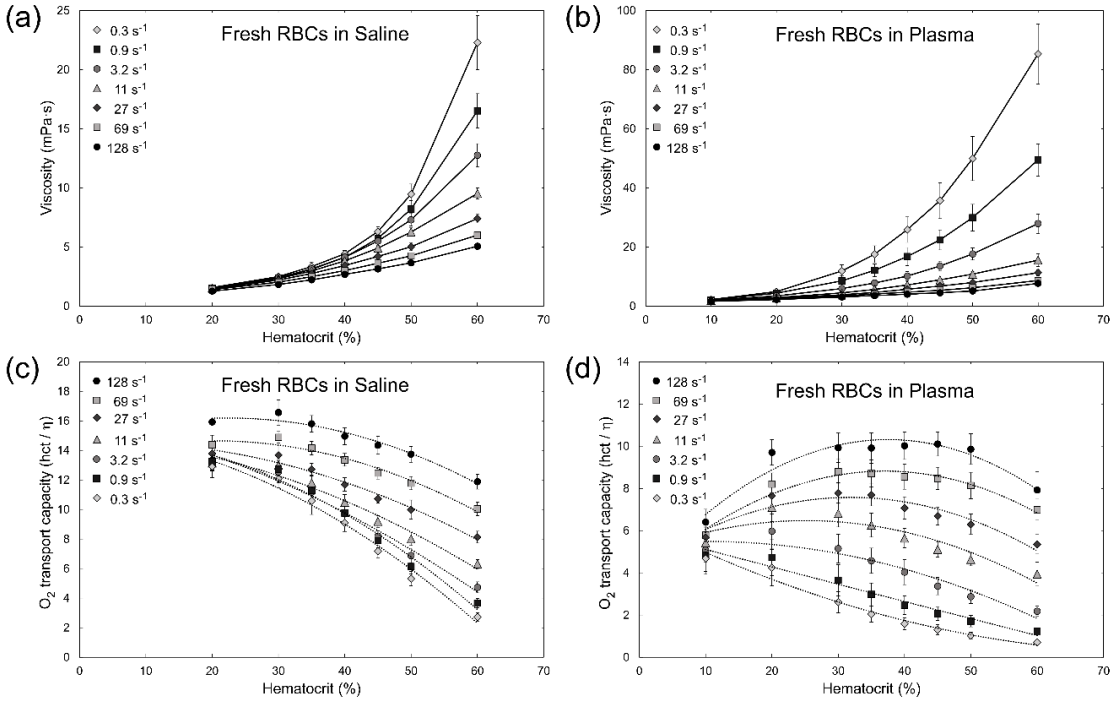

Figure 7.4.2 Estimation of optimal hematocrit based on viscometry. Viscosity of RBC suspensions in (**a**) saline and (**b**) plasma at ambient temperature. Oxygen transport capacity (hematocrit / viscosity) for RBC suspensions in (**c**) saline and (**d**) plasma. Mean values ± SD, n = 10.

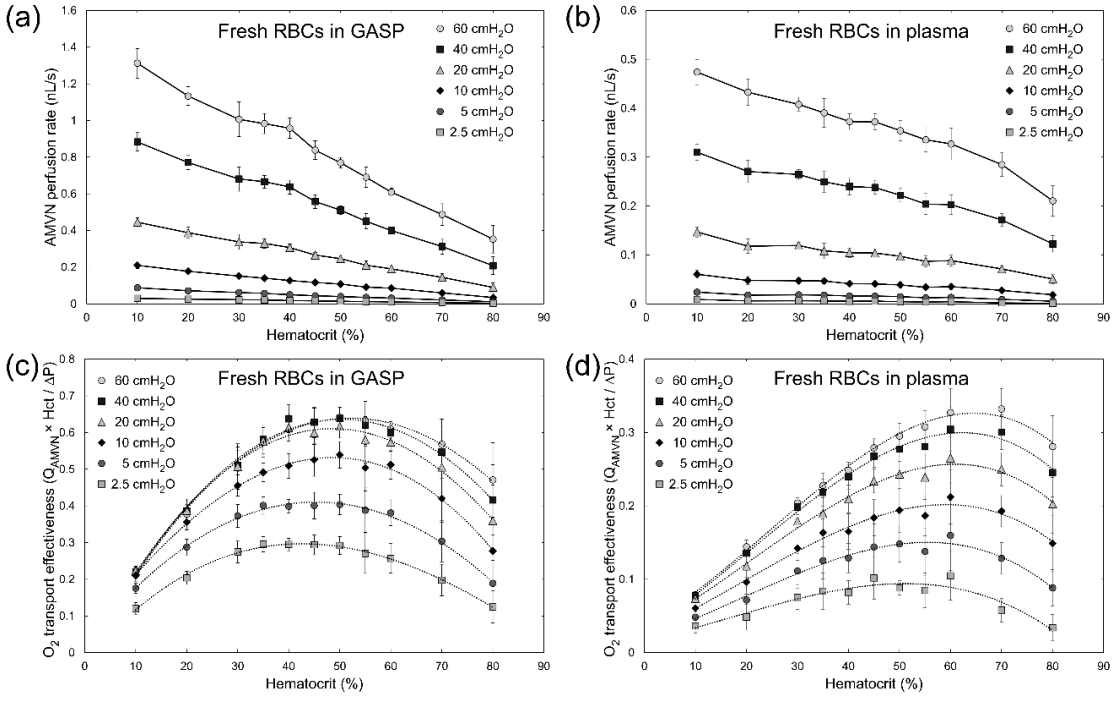

Figure 7.4.3 Estimation of optimal hematocrit based on AMVN perfusion. AMVN perfusion rate for RBC suspensions in (**a**) GASP buffer and (**b**) plasma. Oxygen transport effectiveness for RBC suspensions in (**c**) GASP buffer and (**d**) plasma. Mean values ± SD, n = 5-7.

Figure 7.4.4 illustrates the dependence of the AMVN perfusion rate (**Fig. 7.4.4a**) and of the oxygen transport effectiveness (**Fig. 7.4.4b**) on hematocrit for suspensions of stored RBCs (6 week storage duration) in plasma (ABORh-matched) at various driving pressures. Similarly to fresh RBCs (**Fig. 7.4.3b and d**), the AMVN perfusion rate for stored RBCs suspended in plasma declined approximately linearly with increasing hematocrit for all driving pressures (**Fig. 7.4.4a**), and the oxygen transport effectiveness was maximized at intermediate hematocrits with the maximum shifting towards higher hematocrits for higher pressures (**Fig. 7.4.4b**).

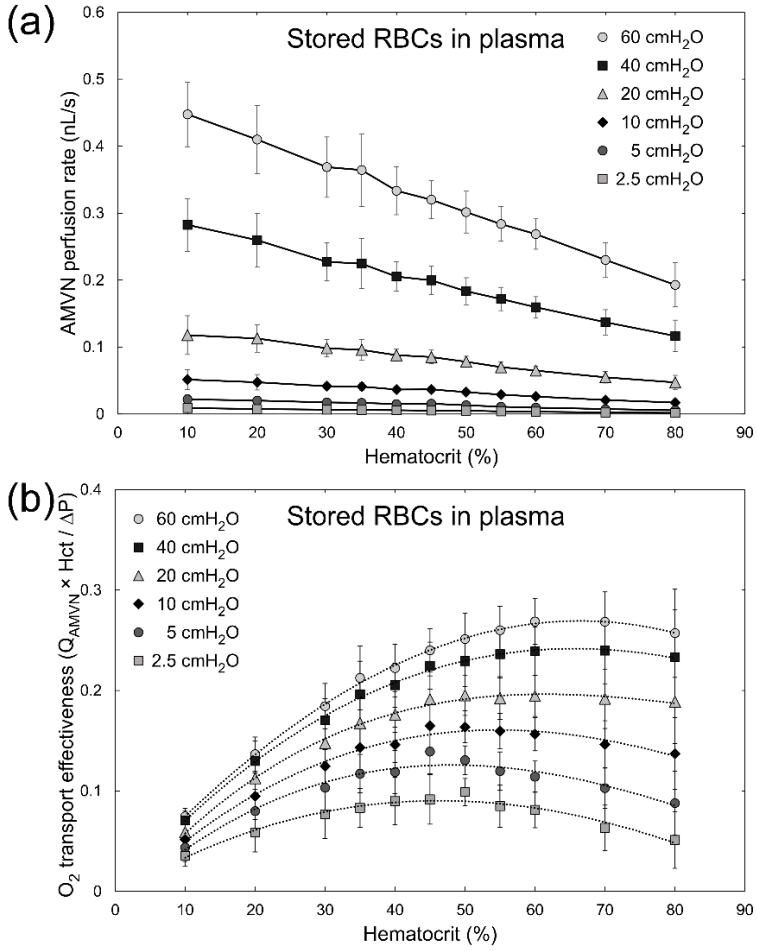

Figure 7.4.4 Estimation of optimal hematocrit for 6 week old, stored RBCs based on AMVN perfusion. (**a**) AMVN perfusion rate for stored RBCs in plasma. (**b**) Oxygen transport effectiveness for stored RBCs in plasma. Mean values ± SD, n = 7.

Figure 7.4.5 shows the dependence of optimal hematocrit (defined as the hematocrit at which oxygen transport capacity or oxygen transport effectiveness reached its maximum) on shear rate (**Fig. 7.4.5a**)

and on driving pressure (**Fig. 7.4.5b**) for all RBC suspensions studied. In case of viscometry, suspensions of fresh RBCs in saline had the optimal hematocrit consistently near the lowest value evaluated (20%). For suspensions of fresh RBCs in plasma, at low shear rates the optimal hematocrit was also near the lowest studied (10%), but then increased logarithmically with increasing shear rate, plateauing around 35% for the highest shear rates evaluated (10, 25.2, 31.9, 37.1 and 37.5% for shear rates of ≤3.2, 11.0, 27.7, 69.5, and 128.5 s^{-1}, respectively; **Fig. 7.4.5a**). For perfusion of the artificial microvascular network (AMVN), optimal hematocrit generally increased with increasing driving pressure (**Fig. 7.4.5b**): from 42.6% at 2.5 cmH_2O to 52.2% at 60 cmH_2O for fresh RBCs suspended in GASP buffer, from 51.1% at 2.5 cmH_2O to 64.5% at 60 cmH_2O for fresh RBCs suspended in plasma (51.1, 55.6, 59.2, 60.9, 62.3 and 64.6% for driving pressures of 2.5, 5, 10, 20, 40 and 60 cmH_2O, respectively), and from 46.4% at 2.5 cmH_2O to 66.5% at 60 cmH_2O for stored RBCs suspended in plasma (46.4, 48.1, 54.8, 61.4, 65.7 and 66.5% for driving pressures of 2.5, 5, 10, 20, 40 and 60 cmH_2O, respectively).

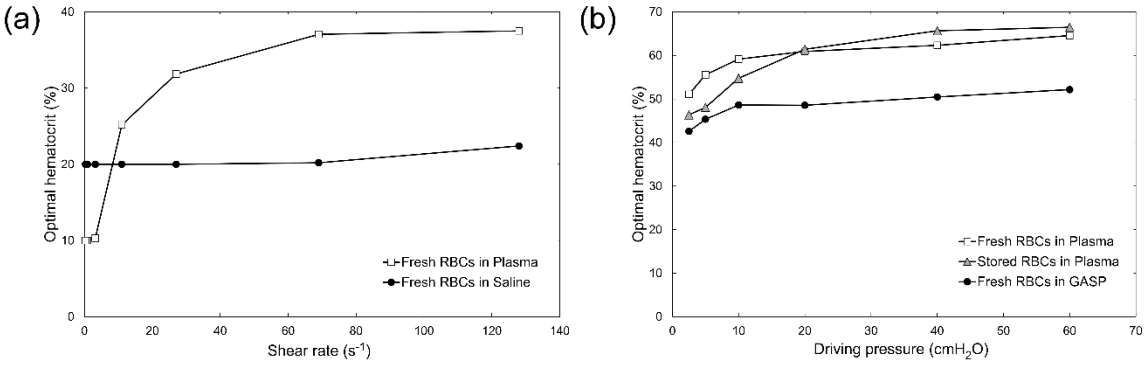

Figure 7.4.5 Dependence of optimal hematocrit on shear rate or on driving pressure. (**a**) Optimal hematocrit based on viscometry for each shear rate. (**b**) Optimal hematocrit based on AMVN perfusion for each driving pressure.

7.4.4 Discussion

Prior *in vitro* studies of optimal hematocrit in straight capillary tubes found that the capacity to deliver oxygen was maximized at intermediate hematocrit values, while low hematocrit suspensions lacked sufficient RBCs to effectively transport oxygen and high hematocrit suspensions were too viscous to effectively perfuse the capillary.[329,343-348] The optimum hematocrit values for tube diameters of 500 μm, 100 μm and 50 μm were found to be 38%, 44% and 51% respectively.[345] In this study, we first performed analysis

of the dynamic relationship between hematocrit and apparent suspension viscosity using a Couette-type viscometer.[356,357] Using the viscometry data we found that increasing hematocrits increased RBC suspension viscosities exponentially and that suspension viscosities were inversely related to applied shear rates (**Fig. 7.4.2a-b**). At high shear (129 s^{-1}), an increase in hematocrit from 20% to 60% increased the viscosity 3.5-fold for RBCs suspended in plasma and 4-fold for RBCs suspended saline. At the lowest shear rate investigated (0.3 s^{-1}), the dependence of viscosity on hematocrit was even more pronounced; viscosity increased 17.5-fold (plasma) and 14.3-fold (saline) between 20 and 60% hematocrit. The shear rate dependence of suspension viscosity was greater for RBCs suspended in plasma than in saline due to RBC aggregation in plasma; at 60% hematocrit, suspension viscosity increased 11.1-fold (plasma) and only 4.4-fold (saline) between shear rates of 129 and 0.3 s^{-1}.

Similar to prior *in vitro* studies, we calculated the capacity to deliver oxygen to the microvasculature (oxygen transport capacity) as the quotient of hematocrit and apparent suspension viscosity. Oxygen transport capacity increased with increasing shear rate, and was generally higher for RBCs suspended in saline than in plasma (**Fig. 7.4.2c-d**). In saline, oxygen transport capacity decreased almost linearly as hematocrit increased from 30 to 60%, and reached its maxima for optimal hematocrits ranging between 20% (0.3-27 s^{-1}) and 22.4% (128 s^{-1}) (**Fig. 7.4.2c**). For RBCs in plasma, at the highest shear rate (129 s^{-1}), the oxygen transport capacity plateaued between 20 and 50% hematocrit, with an optimal hematocrit of 37.5% (**Fig. 7.4.2d**). At a shear rate of 69 s^{-1}, a plateau between 20 and 50% also existed, but the optimal hematocrit was at 37.1%. At a shear rate of 27 s^{-1} a plateau was visible between 20 and 35%, and the optimal hematocrit was at 31.9%. At lower shear rates the plateau disappeared and optimal hematocrit shifted from 25.2% at 11 s^{-1} to 10% for all lower hematocrits. In other words, the value of optimal hematocrit assessed viscometrically shifted towards lower hematocrits with decreasing shear rates.

The estimates of optimal hematocrit derived from viscometric data are relevant primarily for blood flow in larger vessels. Our data suggest that for RBCs in plasma, at high shear rates hematocrit is optimal over a wide range with a plateau between 30 and 50% (**Fig. 7.4.5a**). With decreasing shear rates (that is decreasing blood pressure and hence blood flow, as seen in shock *in vivo*), the plateau effect may be lost and optimal hematocrits may become shifted towards lower values. This shift of the optimal hematocrit to lower values may even be aggravated *in vivo* by the infusion of large volumes of saline (so-called fluid

resuscitation), which is the cornerstone of shock therapy. In our study, the optimal hematocrit for RBCs in saline was about 20% (**Fig. 7.4.5a**), suggesting that dilution of plasma with saline could potentially shift the optimal hematocrit to even lower values.

We further investigated the relationship between hematocrit, driving pressure and perfusion rate in an artificial microvascular network (AMVN). We found that the AMVN perfusion rate decreased approximately linearly with increasing hematocrit and that the AMVN perfusion rate was proportional to applied driving pressure (**Fig. 7.4.3a-b**). At high driving pressures (60 cmH_2O), a decrease in hematocrit from 80% to 10% increased the AMVN perfusion rate 2.3-fold for RBCs suspended in plasma and 3.7-fold for RBCs suspended in GASP buffer. At the lowest driving pressure investigated (2.5 cmH_2O), the dependence of the AMVN perfusion rate on hematocrit was even more pronounced; as hematocrit decreased from 80 to 10%, the perfusion rate increased 8.5-fold (plasma) and 7.7-fold (GASP buffer). The dependence of the AMVN perfusion rate on driving pressure was substantially stronger for RBCs suspended in plasma than in GASP; at 80% hematocrit, as driving pressure increased from 2.5 to 60 cmH_2O the AMVN perfusion rate increased 200-fold for plasma and only 90-fold for GASP buffer.

Oxygen transport effectiveness in the AMVN increased with increasing driving pressure and was generally higher for RBC suspensions in GASP than in plasma. In GASP buffer, oxygen transport effectiveness had a parabolic relationship with hematocrit, reaching its maxima for optimal hematocrit values ranging between 42.6% (for 2.5 cmH_2O) and 52.2% (for 60 cmH_2O) (**Fig. 7.4.3c and Fig. 7.4.5b**). In plasma, oxygen transport effectiveness also had a parabolic relationship with hematocrit, however the highest values of oxygen transport effectiveness generally occurred at higher hematocrits than for GASP buffer – optimal hematocrit values for RBCs suspended in plasma ranged between 51.1% (for 2.5 cmH_2O) and 64.6% (for 60 cmH_2O) (**Fig. 7.4.3d and Fig. 7.4.5b**). Overall, the optimum hematocrit for oxygen transport in the artificial microvascular network shifted towards lower values for lower driving pressures. Our data suggests that plasma (as compared to GASP buffer) has the capacity to increase the optimum hematocrit and that optimum hematocrit, as measured by perfusion of the AMVN, is higher than that estimated by viscometric techniques.

Interestingly, when the AMVN was perfused with RBCs which had been stored hypothermically for 6 weeks and re-suspended in ABORh-matched plasma, optimal hematocrit values ranged from 46.4% (for 2.5 cmH_2O) to 66.5% (for 60 cmH_2O), a wider range with the lower bound extending well below what

we measured for *fresh* RBCs suspended in plasma (**Fig. 7.4.5**). We have previously shown that RBC shape and deformability are directly related to the rate at which RBCs can perfuse the AMVN.[145,146,158,159,355] These differences between fresh and stored RBCs are particularly important to the field of transfusion medicine because the optimal hematocrit, and thus the optimal transfusion target, could be impacted by RBC unit storage duration. In sickle cell disease, which is characterized by less deformable RBCs, it has been shown that increasing fractions of sickle cells progressively decrease the optimal hematocrit.[358] Oxygen transport effectiveness at low shear rates is adversely affected by RBC transfusions, which may explain why transfusion therapy may actually worsen complications in patients with sickle cell disease.[356]

There are several inherent limitations of the AMVN system. The AMVN is constructed of PDMS, which is inert and stiff, and therefore does not reproduce the biochemical or mechanical properties of microvasculature *in vivo*.[128,188,189] Additionally, the channels of the AMVN have rectangular cross-sections, which is not physiological, as microvessels *in vivo* have circular cross-sections.[165] Finally, the specific layout of the AMVN, which was inspired by the architecture of rat mesentery microvasculature, is only one possible configuration of microchannels and is not necessarily representative of all human microvasculature.[128,131] Therefore, the specific values of optimal hematocrit we found using the AMVN may not be universally applicable across different microvascular networks and should not be directly extrapolated to all microvascular networks *in vivo*. Nevertheless, the AMVN has previously been used to investigate various rheological and hemodynamic phenomena and has proven to be a robust *in vitro* model for microvascular perfusion.[128,131,145-147,159,188,189,355]

The AMVN data suggest that the optimal hematocrit for tissue oxygenation could be higher than the physiological range, which is in contrast to the viscometric results. This exemplifies that blood flow properties in the circulation are complex and cannot be defined by any single measurement. The high optimal hematocrit seen in AMVN experiments is in agreement with *in vivo* observations in healthy young athletes, but not with clinical data in patients.[334] Both of our *in vitro* methods indicated that for high shear rates or perfusion pressures (and hence higher rate of blood flow), the optimal hematocrit is shifted towards higher values. Well-trained athletes meet such conditions, which could explain why blood doping and erythropoietin administration improve exercise performance.[333] Higher than normal hematocrits also exist in polycythemia vera, but hematocrit reduction to values <45% is recommended because it reduces cardiovascular morbidity

and mortality.[359] Lower than normal hematocrits frequently accompany chronic diseases such as kidney disease, heart failure, critical illness, sepsis and cancer. Many of these patients are older and may have decreased blood flow and thus decreased microvascular perfusion pressures, either systemically, by an impaired pump function of the heart (e.g., in chronic heart failure), or locally, distal of arterial stenosis (e.g., in peripheral arterial disease). Our data suggest that at lower pressure differentials across the microcirculation, the optimal hematocrit would be shifted towards lower values. Anemia in chronic disorders may therefore be a beneficial response with regard to tissue oxygenation. This hypothetical notion allows a better understanding of why many clinical studies, which attempted to correct such anemias, yielded disappointing results. A normalization of anemia in chronic kidney disease did not reduce the risk of cardiovascular events and did not improve quality of life,[335,336,338,360] but increased the risk of stroke and death.[339,361] In septic shock,[362,363] critical care,[364,365] and acute upper gastrointestinal bleeding,[366] a restrictive transfusion regimen was as effective or even superior to a liberal transfusion regimen. Treatment of anemia in chronic heart failure had no clinical benefit.[340,367] Although preoperative anemia was associated with postoperative morbidity and mortality in cardiac and non-cardiac surgery,[368,369] a preoperative correction of anemia did not result in improved clinical outcomes.[370-372] Correction of anemia in cancer patients was associated with increased mortality.[337,373] Current guidelines, therefore, recommend a restrictive RBC transfusion strategy with a hemoglobin threshold of 7-8 g/dL.[341] In locally decreased perfusion pressure, such as in peripheral arterial disease, a lower than normal hematocrit has been shown to be beneficial.[374-376]

We conclude that the optimal hematocrit for oxygen transport *in vitro* decreases with decreasing flow rate. For flow in larger vessels, viscometry suggests that it is lower than the normal hematocrit, while for microvascular perfusion it may be higher than the normal value. By balancing those opposing effects, the normal physiological hematocrit may represent an optimal hematocrit for normal conditions, whereas it may be lower in diseases with low systemic or local blood flow. Our observations thus shed light on an old question; suggesting that a universally valid optimal hematocrit value may not exist, but may rather depend on underlying pathophysiological conditions.

CHAPTER 8 Conclusions

In Chapter 3 we described the development of a paper-based test optimized to detect the low levels of sickle hemoglobin present in newborn blood and demonstrated that this paper-based test enables the direct screening of newborns for sickle cell trait and sickle cell disease. We also demonstrated that this test is feasible and retains high diagnostic accuracy when performed by local health workers without specialized training, in a resource-limited clinical setting in Angola. These results demonstrated the potential clinical utility and cost savings of the paper-based test for identifying newborns likely to have SCD in the immediate postnatal period before families leave birthing centers. If adopted, the paper-based newborn sickle cell disease screening test could increase the practicality and effectiveness of universal newborn screening programs in resource-limited settings.

In Chapter 4 we described the development of a rapid, low-cost paper-based assay for the quantification of sickle hemoglobin in blood samples from patients with sickle cell disease. The assay was shown to accurately measure sickle hemoglobin across a wide range of values and with a high degree of accuracy relative to conventional hemoglobin electrophoresis. The assay was also shown to be unaffected by overall hemoglobin concentration or the relative fractions of other forms of hemoglobin in the sample. This novel assay, which enables inexpensive and accurate sickle hemoglobin concentration without specialized equipment, has obvious applications in resource-limited settings and could constitute an important step towards making chronic red blood cell (RBC) transfusion therapy and hydroxyurea therapy feasible in these settings. The paper-based assay could also be utilized in resource-rich settings to permitting more rapid and less expensive monitoring of sickle hemoglobin concentration during therapy, thus improving clinical care and reducing costs associated with the management of sickle cell disease.

In Chapter 5 we described the development of a simple system for automated, high-throughput quantification stored RBC morphology. The system, which was comprised of a microfluidic device and associated image analysis algorithm, completely eliminated the need for laborious manual preparation and visual examination of blood smears, and thereby enabled objective morphology classification. We validated the system by analyzing the morphologies and diameters of more than one million individual stored RBCs. If adopted, the ability to automatically evaluate the morphology of individual RBCs quickly and in

statistically significant numbers could enable selection of the most well-preserved RBC units for transfusion into vulnerable patients – such as individual with sickle cell disease who are chronically transfused and therefore at higher risk for negative transfusion-related side-effects.

In Chapter 6 we showed that anaerobic conditions decreased the rate at which the rheological properties of RBCs deteriorated over the course of hypothermic storage and that anaerobically stored RBC units contained smaller fractions of irreparably damaged RBCs than conventionally (aerobically) stored RBC units. In this chapter we also showed that washing stored RBCs in a 1% human serum albumin solution improved their ability to perfuse an artificial microvascular network – with the degree of improvement appearing to be dependent on the initial quality of individual RBC units. Both studies suggested that microfluidic devices are capable of more sensitive measurements or RBC properties than current commercially available ektacytometers, and demonstrated how microfluidic devices could potentially be used to assess the impact of novel RBC storage and/or rejuvenation methods on RBC quality.

Finally, in Chapter 7 we used microfluidic devices to show that normal discocytes represented the optimum RBC shape for perfusion of an artificial microvascular network and that the echinocytic shape transformation led to a progressive decrease of perfusion rate. We showed that RBC shape, independent of any other factor, is an indicator of the rheological performance of RBCs in the microvasculature which suggested that RBC shape could therefore be used as a measure of the quality of stored blood units. We also demonstrated that RBC deformability was maximized at isosmotic conditions and that the optimum osmolality for RBC suspension viscosity was shifted towards hyperosmolality. However, we also showed that the rate of perfusion of the artificial microvascular network changed by less than 10% over a wide range of osmolalities. Additionally, we demonstrated that the presence or absence of RBC aggregation did not affect artificial microvascular network perfusion rate, but that aggregation resulted in higher capillary hematocrit, which suggested that aggregation may increase the overall oxygen transport capacity of blood. Lastly, we showed that the exact values of optimal hematocrit may depend on specific microvascular architecture, that optimal hematocrit for oxygen delivery in the microvasculature depends on perfusion pressure, and that the optimal hematocrit for oxygen transport *in vitro* decreases with decreasing flow rate. Taken together, these findings made using novel microfluidic devices contribute to the basic understanding of blood rheology in health and disease, and may have significant implications for clinical practice.

REFERENCES

1. Bunn, H.F. "Pathogenesis and Treatment of Sickle Cell Disease." *N Engl J Med* 1997;**337**: 762-9.
2. Modell, B., Darlison, M. "Global Epidemiology of Haemoglobin Disorders and Derived Service Indicators." *Bull World Health Organ* 2008;**86**: 480-7.
3. Frenette, P.S., Atweh, G.F. "Sickle Cell Disease: Old Discoveries, New Concepts, and Future Promise." *The Journal of clinical investigation* 2007;**117**: 850-8.
4. McGann, P.T., Ferris, M.G., Ramamurthy, U., Santos, B., de Oliveira, V., Bernardino, L., Ware, R.E. "A Prospective Newborn Screening and Treatment Program for Sickle Cell Anemia in Luanda, Angola." *American journal of hematology* 2013;**88**: 984-9.
5. Rees, D.C., Olujohungbe, A.D., Parker, N.E., Stephens, A.D., Telfer, P., Wright, J., British Committee for Standards in Haematology General Haematology Task Force by the Sickle Cell Working, P. "Guidelines for the Management of the Acute Painful Crisis in Sickle Cell Disease." *Br J Haematol* 2003;**120**: 744-52.
6. Rees, D.C., Williams, T.N., Gladwin, M.T. "Sickle-Cell Disease." *Lancet* 2010;**376**: 2018-31.
7. Stuart, M.J., Nagel, R.L. "Sickle-Cell Disease." *Lancet* 2004;**364**: 1343-60.
8. Tsaras, G., Owusu-Ansah, A., Boateng, F.O., Amoateng-Adjepong, Y. "Complications Associated with Sickle Cell Trait: A Brief Narrative Review." *Am J Med* 2009;**122**: 507-12.
9. Weatherall, D.J. "The Inherited Diseases of Hemoglobin Are an Emerging Global Health Burden." *Blood* 2010;**115**: 4331-6.
10. Ashley-Koch, A., Yang, Q., Olney, R.S. "Sickle Hemoglobin (Hbs) Allele and Sickle Cell Disease: A Huge Review." *Am J Epidemiol* 2000;**151**: 839-45.
11. Bessis, M. "Red Cell Shapes. An Illustrated Classification and Its Rationale." *Nouv Rev Fr Hematol* 1972;**12**: 721-45.
12. Deplaine, G., Safeukui, I., Jeddi, F., Lacoste, F., Brousse, V., Perrot, S., Biligui, S., Guillotte, M., Guitton, C., Dokmak, S., Aussilhou, B., Sauvanet, A., Cazals Hatem, D., Paye, F., Thellier, M., Mazier, D., Milon, G., Mohandas, N., Mercereau-Puijalon, O., David, P.H., Buffet, P.A. "The

Sensing of Poorly Deformable Red Blood Cells by the Human Spleen Can Be Mimicked in Vitro." *Blood* 2011;**117**: e88-95.

13. Bartolucci, P., Brugnara, C., Teixeira-Pinto, A., Pissard, S., Moradkhani, K., Jouault, H., Galacteros, F. "Erythrocyte Density in Sickle Cell Syndromes Is Associated with Specific Clinical Manifestations and Hemolysis." *Blood* 2012;**120**: 3136-41.
14. Ryan, K., Bain, B.J., Worthington, D., James, J., Plews, D., Mason, A., Roper, D., Rees, D.C., de la Salle, B., Streetly, A. "Significant Haemoglobinopathies: Guidelines for Screening and Diagnosis." *Br J Haematol* 2010;**149**: 35-49.
15. Edoh, D., Antwi-Bosaiko, C., Amuzu, D. "Fetal Hemoglobin During Infancy and in Sickle Cell Adults." *Afr Health Sci* 2006;**6**: 51-4.
16. Kutlar, A., Kutlar, F., Wilson, J.B., Headlee, M.G., Huisman, T.H. "Quantitation of Hemoglobin Components by High-Performance Cation-Exchange Liquid Chromatography: Its Use in Diagnosis and in the Assessment of Cellular Distribution of Hemoglobin Variants." *American journal of hematology* 1984;**17**: 39-53.
17. Ballas, S.K., Lieff, S., Benjamin, L.J., Dampier, C.D., Heeney, M.M., Hoppe, C., Johnson, C.S., Rogers, Z.R., Smith-Whitley, K., Wang, W.C., Telen, M.J., Investigators, C.S.C.C. "Definitions of the Phenotypic Manifestations of Sickle Cell Disease." *American journal of hematology* 2010;**85**: 6-13.
18. Powars, D., Wilson, B., Imbus, C., Pegelow, C., Allen, J. "The Natural History of Stroke in Sickle Cell Disease." *Am J Med* 1978;**65**: 461-71.
19. Ohene-Frempong, K., Weiner, S.J., Sleeper, L.A., Miller, S.T., Embury, S., Moohr, J.W., Wethers, D.L., Pegelow, C.H., Gill, F.M. "Cerebrovascular Accidents in Sickle Cell Disease: Rates and Risk Factors." *Blood* 1998;**91**: 288-94.
20. Vichinsky, E.P., Styles, L.A., Colangelo, L.H., Wright, E.C., Castro, O., Nickerson, B. "Acute Chest Syndrome in Sickle Cell Disease: Clinical Presentation and Course. Cooperative Study of Sickle Cell Disease." *Blood* 1997;**89**: 1787-92.
21. Lanzkron, S., Carroll, C.P., Haywood, C., Jr. "Mortality Rates and Age at Death from Sickle Cell Disease: U.S., 1979-2005." *Public Health Rep* 2013;**128**: 110-6.

22. Head, C.E., Conroy, M., Jarvis, M., Phelan, L., Bain, B.J. "Some Observations on the Measurement of Haemoglobin A2 and S Percentages by High Performance Liquid Chromatography in the Presence and Absence of Alpha Thalassaemia." *J Clin Pathol* 2004;**57**: 276-80.

23. Weatherall, D.J., Clegg, J.B. "Inherited Haemoglobin Disorders: An Increasing Global Health Problem." *Bull World Health Organ* 2001;**79**: 704-12.

24. Clarke, G.M., Higgins, T.N. "Laboratory Investigation of Hemoglobinopathies and Thalassemias: Review and Update." *Clin Chem* 2000;**46**: 1284-90.

25. Rodriguez-Diaz, R., Wehr, T., Zhu, M. "Capillary Isoelectric Focusing." *Electrophoresis* 1997;**18**: 2134-44.

26. Jenkins, M.A., Ratnaike, S. "Capillary Isoelectric Focusing of Haemoglobin Variants in the Clinical Laboratory." *Clin Chim Acta* 1999;**289**: 121-32.

27. Schmidt, R.M., Wilson, S.M. "Standardization in Detection of Abnormal Hemoglobins. Solubility Tests for Hemoglobin S." *JAMA* 1973;**225**: 1225-30.

28. Chen, K., Ballas, S.K., Hantgan, R.R., Kim-Shapiro, D.B. "Aggregation of Normal and Sickle Hemoglobin in High Concentration Phosphate Buffer." *Biophys J* 2004;**87**: 4113-21.

29. Kumar, A.A., Patton, M.R., Hennek, J.W., Lee, S.Y., D'Alesio-Spina, G., Yang, X., Kanter, J., Shevkoplyas, S.S., Brugnara, C., Whitesides, G.M. "Density-Based Separation in Multiphase Systems Provides a Simple Method to Identify Sickle Cell Disease." *Proc Natl Acad Sci U S A* 2014;**111**: 14864-9.

30. Kumar, A.A., Chunda-Liyoka, C., Hennek, J.W., Mantina, H., Lee, S.Y., Patton, M.R., Sambo, P., Sinyangwe, S., Kankasa, C., Chintu, C., Brugnara, C., Stossel, T.P., Whitesides, G.M. "Evaluation of a Density-Based Rapid Diagnostic Test for Sickle Cell Disease in a Clinical Setting in Zambia." *PLoS One* 2014;**9**: e114540.

31. Milligan, C., Rees, D.C., Ellory, J.C., Osei, A., Browning, J.A., Hannemann, A., Gibson, J.S. "A Non-Electrolyte Haemolysis Assay for Diagnosis and Prognosis of Sickle Cell Disease." *J Physiol* 2013;**591**: 1463-74.

32. Knowlton, S.M., Sencan, I., Aytar, Y., Khoory, J., Heeney, M.M., Ghiran, I.C., Tasoglu, S. "Sickle Cell Detection Using a Smartphone." *Sci Rep* 2015;**5**: 15022.

33. Hajer, S., Neila, T., Sondess, H.F., Fekria, O., Nabila, A., Mahbouba, K., Melika, D., Faida, O., Amina, B., Raja, B., Hedi, R., Sadok, M., Naima, K., Slaheddine, F., Taieb, M. "A Lower-Cost Protocol for Sickle Cell Disease Neonatal Screening in Tunisia." *Ann Saudi Med* 2012;**32**: 49-52.

34. Alapan, Y., Kim, C., Adhikari, A., Gray, K.E., Gurkan-Cavusoglu, E., Little, J.A., Gurkan, U.A. "Sickle Cell Disease Biochip: A Functional Red Blood Cell Adhesion Assay for Monitoring Sickle Cell Disease." *Transl Res* 2016;**173**: 74-91 e8.

35. Alapan, Y., Fraiwan, A., Kucukal, E., Hasan, M.N., Ung, R., Kim, M., Odame, I., Little, J.A., Gurkan, U.A. "Emerging Point-of-Care Technologies for Sickle Cell Disease Screening and Monitoring." *Expert Rev Med Devices* 2016;**13**: 1073-93.

36. McGann, P.T., Schaefer, B.A., Paniagua, M., Howard, T.A., Ware, R.E. "Characteristics of a Rapid, Point-of-Care Lateral Flow Immunoassay for the Diagnosis of Sickle Cell Disease." *American journal of hematology* 2016;**91**: 205-10.

37. Quinn, C.T., Paniagua, M.C., DiNello, R.K., Panchal, A., Geisberg, M. "A Rapid, Inexpensive and Disposable Point-of-Care Blood Test for Sickle Cell Disease Using Novel, Highly Specific Monoclonal Antibodies." *Br J Haematol* 2016;**175**: 724-32.

38. Kanter, J., Telen, M.J., Hoppe, C., Roberts, C.L., Kim, J.S., Yang, X. "Validation of a Novel Point of Care Testing Device for Sickle Cell Disease." *BMC Med* 2015;**13**: 225.

39. Quinn, C.T., Rogers, Z.R., Buchanan, G.R. "Survival of Children with Sickle Cell Disease." *Blood* 2004;**103**: 4023-7.

40. Claster, S., Vichinsky, E.P. "Managing Sickle Cell Disease." *BMJ* 2003;**327**: 1151-5.

41. Geller, A.K., O'Connor, M.K. "The Sickle Cell Crisis: A Dilemma in Pain Relief." *Mayo Clin Proc* 2008;**83**: 320-3.

42. Niscola, P., Sorrentino, F., Scaramucci, L., de Fabritiis, P., Cianciulli, P. "Pain Syndromes in Sickle Cell Disease: An Update." *Pain Med* 2009;**10**: 470-80.

43. Wolters, H.J., ten Cate, H., Thomas, L.L., Brandjes, D.P., van der Ende, A., van der Heiden, Y., Statius van Eps, L.W. "Low-Intensity Oral Anticoagulation in Sickle-Cell Disease Reverses the Prethrombotic State: Promises for Treatment?" *Br J Haematol* 1995;**90**: 715-7.

44. Emre, U., Miller, S.T., Gutierez, M., Steiner, P., Rao, S.P., Rao, M. "Effect of Transfusion in Acute Chest Syndrome of Sickle Cell Disease." *J Pediatr* 1995;**127**: 901-4.

45. Strouse, J.J., Heeney, M.M. "Hydroxyurea for the Treatment of Sickle Cell Disease: Efficacy, Barriers, Toxicity, and Management in Children." *Pediatr Blood Cancer* 2012;**59**: 365-71.

46. Segal, J.B., Strouse, J.J., Beach, M.C., Haywood, C., Witkop, C., Park, H., Wilson, R.F., Bass, E.B., Lanzkron, S. "Hydroxyurea for the Treatment of Sickle Cell Disease." *Evid Rep Technol Assess (Full Rep)* 2008: 1-95.

47. Steinberg, M.H., Voskaridou, E., Kutlar, A., Loukopoulos, D., Koshy, M., Ballas, S.K., Castro, O., Barton, F. "Concordant Fetal Hemoglobin Response to Hydroxyurea in Siblings with Sickle Cell Disease." *American journal of hematology* 2003;**72**: 121-6.

48. Lanzkron, S., Strouse, J.J., Wilson, R., Beach, M.C., Haywood, C., Park, H., Witkop, C., Bass, E.B., Segal, J.B. "Systematic Review: Hydroxyurea for the Treatment of Adults with Sickle Cell Disease." *Ann Intern Med* 2008;**148**: 939-55.

49. Strouse, J.J., Lanzkron, S., Beach, M.C., Haywood, C., Park, H., Witkop, C., Wilson, R.F., Bass, E.B., Segal, J.B. "Hydroxyurea for Sickle Cell Disease: A Systematic Review for Efficacy and Toxicity in Children." *Pediatrics* 2008;**122**: 1332-42.

50. Singh, H., Dulhani, N., Kumar, B.N., Singh, P., Tiwari, P. "Effective Control of Sickle Cell Disease with Hydroxyurea Therapy." *Indian J Pharmacol* 2010;**42**: 32-5.

51. Ferster, A., Tahriri, P., Vermylen, C., Sturbois, G., Corazza, F., Fondu, P., Devalck, C., Dresse, M.F., Feremans, W., Hunninck, K., Toppet, M., Philippet, P., Van Geet, C., Sariban, E. "Five Years of Experience with Hydroxyurea in Children and Young Adults with Sickle Cell Disease." *Blood* 2001;**97**: 3628-32.

52. Steinberg, M.H., Barton, F., Castro, O., Pegelow, C.H., Ballas, S.K., Kutlar, A., Orringer, E., Bellevue, R., Olivieri, N., Eckman, J., Varma, M., Ramirez, G., Adler, B., Smith, W., Carlos, T., Ataga, K., DeCastro, L., Bigelow, C., Saunthararajah, Y., Telfer, M., Vichinsky, E., Claster, S., Shurin, S., Bridges, K., Waclawiw, M., Bonds, D., Terrin, M. "Effect of Hydroxyurea on Mortality and Morbidity in Adult Sickle Cell Anemia: Risks and Benefits up to 9 Years of Treatment." *JAMA* 2003;**289**: 1645-51.

53. Davies, S.C., Olatunji, P.O. "Blood Transfusion in Sickle Cell Disease." *Vox Sang* 1995;**68**: 145-51.

54. Davies, S.C. "Blood Transfusion in Sickle Cell Disease." *Curr Opin Hematol* 1996;**3**: 485-91.

55. Danielson, C.F. "The Role of Red Blood Cell Exchange Transfusion in the Treatment and Prevention of Complications of Sickle Cell Disease." *Ther Apher* 2002;**6**: 24-31.

56. Saylors, R.L., Watkins, B., Saccente, S., Tang, X. "Comparison of Automated Red Cell Exchange Transfusion and Simple Transfusion for the Treatment of Children with Sickle Cell Disease Acute Chest Syndrome." *Pediatr Blood Cancer* 2013;**60**: 1952-6.

57. Davies, S.C., Roberts-Harewood, M. "Blood Transfusion in Sickle Cell Disease." *Blood Rev* 1997;**11**: 57-71.

58. Campbell, L.C., Von Burton, G., Holcombe, R.F. "Transfusion Therapy in Sickle Cell Disease Patients: Methods and Acute Indications." *J La State Med Soc* 1993;**145**: 515-21.

59. Vichinsky, E.P. "The Prevention and Management of Alloimmunization in Sickle Cell Disease: The Benefit of Extended Phenotypic Matching of Red Blood Cells." *Immunohematology* 2012;**28**: 20-3.

60. Vichinsky, E.P., Earles, A., Johnson, R.A., Hoag, M.S., Williams, A., Lubin, B. "Alloimmunization in Sickle Cell Anemia and Transfusion of Racially Unmatched Blood." *N Engl J Med* 1990;**322**: 1617-21.

61. Hess, J.R. "Red Cell Changes During Storage." *Transfus Apher Sci* 2010;**43**: 51-9.

62. Zimrin, A.B., Hess, J.R. "Current Issues Relating to the Transfusion of Stored Red Blood Cells." *Vox Sang* 2009;**96**: 93-103.

63. Hogman, C.F., Meryman, H.T. "Storage Parameters Affecting Red Blood Cell Survival and Function after Transfusion." *Transfus Med Rev* 1999;**13**: 275-96.

64. Koch, C.G., Li, L., Sessler, D.I., Figueroa, P., Hoeltge, G.A., Mihaljevic, T., Blackstone, E.H. "Duration of Red-Cell Storage and Complications after Cardiac Surgery." *N Engl J Med* 2008;**358**: 1229-39.

65. Dunn, L.K., Thiele, R.H., Ma, J.Z., Sawyer, R.G., Nemergut, E.C. "Duration of Red Blood Cell Storage and Outcomes Following Orthotopic Liver Transplantation." *Liver Transpl* 2012;**18**: 475-81.

66. Fields, M.E., Hulbert, M.L., Chen, L., Berlin, A.N., Jackups, R., Spinella, P.C. "Red Blood Cell Storage Duration Is Not Associated with Clinical Outcomes for Acute Chest Syndrome in Children with Sickle Cell Disease." *Transfusion* 2015;**55**: 2714-21.

67. Ng, M.S., Ng, A.S., Chan, J., Tung, J.P., Fraser, J.F. "Effects of Packed Red Blood Cell Storage Duration on Post-Transfusion Clinical Outcomes: A Meta-Analysis and Systematic Review." *Intensive Care Med* 2015;**41**: 2087-97.

68. Redlin, M., Habazettl, H., Schoenfeld, H., Kukucka, M., Boettcher, W., Kuppe, H., Salama, A. "Red Blood Cell Storage Duration Is Associated with Various Clinical Outcomes in Pediatric Cardiac Surgery." *Transfus Med Hemother* 2014;**41**: 146-51.

69. Steiner, M.E., Ness, P.M., Assmann, S.F., Triulzi, D.J., Sloan, S.R., Delaney, M., Granger, S., Bennett-Guerrero, E., Blajchman, M.A., Scavo, V., Carson, J.L., Levy, J.H., Whitman, G., D'Andrea, P., Pulkrabek, S., Ortel, T.L., Bornikova, L., Raife, T., Puca, K.E., Kaufman, R.M., Nuttall, G.A., Young, P.P., Youssef, S., Engelman, R., Greilich, P.E., Miles, R., Josephson, C.D., Bracey, A., Cooke, R., McCullough, J., Hunsaker, R., Uhl, L., McFarland, J.G., Park, Y., Cushing, M.M., Klodell, C.T., Karanam, R., Roberts, P.R., Dyke, C., Hod, E.A., Stowell, C.P. "Effects of Red-Cell Storage Duration on Patients Undergoing Cardiac Surgery." *N Engl J Med* 2015;**372**: 1419-29.

70. Walters, M.C., Patience, M., Leisenring, W., Eckman, J.R., Scott, J.P., Mentzer, W.C., Davies, S.C., Ohene-Frempong, K., Bernaudin, F., Matthews, D.C., Storb, R., Sullivan, K.M. "Bone Marrow Transplantation for Sickle Cell Disease." *N Engl J Med* 1996;**335**: 369-76.

71. Walters, M.C., Storb, R., Patience, M., Leisenring, W., Taylor, T., Sanders, J.E., Buchanan, G.E., Rogers, Z.R., Dinndorf, P., Davies, S.C., Roberts, I.A., Dickerhoff, R., Yeager, A.M., Hsu, L., Kurtzberg, J., Ohene-Frempong, K., Bunin, N., Bernaudin, F., Wong, W.Y., Scott, J.P., Margolis, D., Vichinsky, E., Wall, D.A., Wayne, A.S., Pegelow, C., Redding-Lallinger, R., Wiley, J., Klemperer, M., Mentzer, W.C., Smith, F.O., Sullivan, K.M. "Impact of Bone Marrow Transplantation for Symptomatic Sickle Cell Disease: An Interim Report. Multicenter Investigation of Bone Marrow Transplantation for Sickle Cell Disease." *Blood* 2000;**95**: 1918-24.

72. Hansbury, E.N., Schultz, W.H., Ware, R.E., Aygun, B. "Bone Marrow Transplant Options and Preferences in a Sickle Cell Anemia Cohort on Chronic Transfusions." *Pediatr Blood Cancer* 2012;**58**: 611-5.

73. Walters, M.C., Patience, M., Leisenring, W., Eckman, J.R., Buchanan, G.R., Rogers, Z.R., Olivieri, N.E., Vichinsky, E., Davies, S.C., Mentzer, W.C., Powars, D., Scott, J.P., Bernaudin, F., Ohene-Frempong, K., Darbyshire, P.J., Wayne, A., Roberts, I.A., Dinndorf, P., Brandalise, S., Sanders, J.E., Matthews, D.C., Appelbaum, F.R., Storb, R., Sullivan, K.M. "Barriers to Bone Marrow Transplantation for Sickle Cell Anemia." *Biol Blood Marrow Transplant* 1996;**2**: 100-4.

74. Ribeil, J.A., Hacein-Bey-Abina, S., Payen, E., Magnani, A., Semeraro, M., Magrin, E., Caccavelli, L., Neven, B., Bourget, P., El Nemer, W., Bartolucci, P., Weber, L., Puy, H., Meritet, J.F., Grevent, D., Beuzard, Y., Chretien, S., Lefebvre, T., Ross, R.W., Negre, O., Veres, G., Sandler, L., Soni, S., de Montalembert, M., Blanche, S., Leboulch, P., Cavazzana, M. "Gene Therapy in a Patient with Sickle Cell Disease." *N Engl J Med* 2017;**376**: 848-55.

75. Platt, O.S., Brambilla, D.J., Rosse, W.F., Milner, P.F., Castro, O., Steinberg, M.H., Klug, P.P. "Mortality in Sickle Cell Disease. Life Expectancy and Risk Factors for Early Death." *N Engl J Med* 1994;**330**: 1639-44.

76. Makani, J., Cox, S.E., Soka, D., Komba, A.N., Oruo, J., Mwamtemi, H., Magesa, P., Rwezaula, S., Meda, E., Mgaya, J., Lowe, B., Muturi, D., Roberts, D.J., Williams, T.N., Pallangyo, K., Kitundu, J., Fegan, G., Kirkham, F.J., Marsh, K., Newton, C.R. "Mortality in Sickle Cell Anemia in Africa: A Prospective Cohort Study in Tanzania." *PLoS One* 2011;**6**: e14699.

77. Piel, F.B., Hay, S.I., Gupta, S., Weatherall, D.J., Williams, T.N. "Global Burden of Sickle Cell Anaemia in Children under Five, 2010-2050: Modelling Based on Demographics, Excess Mortality, and Interventions." *PLoS Med* 2013;**10**: e1001484.

78. Diallo, D., Tchernia, G. "Sickle Cell Disease in Africa." *Curr Opin Hematol* 2002;**9**: 111-6.

79. Tshilolo, L., Kafando, E., Sawadogo, M., Cotton, F., Vertongen, F., Ferster, A., Gulbis, B. "Neonatal Screening and Clinical Care Programmes for Sickle Cell Disorders in Sub-Saharan Africa: Lessons from Pilot Studies." *Public Health* 2008;**122**: 933-41.

80. Montagu, D., Yamey, G., Visconti, A., Harding, A., Yoong, J. "Where Do Poor Women in Developing Countries Give Birth? A Multi-Country Analysis of Demographic and Health Survey Data." *PLoS One* 2011;**6**.

81. Yang, X., Kanter, J., Piety, N.Z., Benton, M.S., Vignes, S.M., Shevkoplyas, S.S. "A Simple, Rapid, Low-Cost Diagnostic Test for Sickle Cell Disease." *Lab on a chip* 2013;**13**: 1464-7.

82. Piety, N.Z., Yang, X., Lezzar, D., George, A., Shevkoplyas, S.S. "A Rapid Paper-Based Test for Quantifying Sickle Hemoglobin in Blood Samples from Patients with Sickle Cell Disease." *American journal of hematology* 2015;**90**: 478-82.

83. Piety, N.Z., Yang, X., Kanter, J., Vignes, S.M., George, A., Shevkoplyas, S.S. "Validation of a Low-Cost Paper-Based Screening Test for Sickle Cell Anemia." *PLoS One* 2016;**11**: e0144901.

84. Brown, L.D., Cai, T.T., DasGupta, A. "Confidence Intervals for a Binomial Proportion and Asymptotic Expansions." *The Annals of Statistics* 2002;**30**: 160-201.

85. Fleiss, J.L., Gurland, B.J., Cooper, J.E. "Some Contributions to the Measurement of Psychopathology." *Br J Psychiatry* 1971;**119**: 647-56.

86. Odame, I. "Perspective: We Need a Global Solution." *Nature* 2014;**515**: S10.

87. Pass, K.A., Lane, P.A., Fernhoff, P.M., Hinton, C.F., Panny, S.R., Parks, J.S., Pelias, M.Z., Rhead, W.J., Ross, S.I., Wethers, D.L., Elsas, L.J., 2nd. "Us Newborn Screening System Guidelines Ii: Follow-up of Children, Diagnosis, Management, and Evaluation. Statement of the Council of Regional Networks for Genetic Services (Corn)." *J Pediatr* 2000;**137**: S1-46.

88. Okwi, A., Byarugaba, W., Parkes, A., M, O. "The Reliability of Sickling and Solubility Tests and Peripheral Blood Film Method for Sickle Cell Disease Screening at District Health Centers in Uganda." *Clin Mother Child Heal* 2010;**7**: 1205 - 10.

89. Ung, R., Alapan, Y., Hasan, M.N., Romelfanger, M., He, P., Tam, A., Rosanwo, T., Akkus, A., Cakar, M.A., Icoz, K., Piccone, C.M., Little, J.A., Gurkan, U.A. "Point-of-Care Screening for Sickle Cell Disease by a Mobile Micro-Electrophoresis Platform." *Blood* 2015;**126**: 3379-.

90. Kanter, J., Telen, M.J., Hoppe, C., Roberts, C.L., Kim, J.S., Yang, X. "Validation of a Novel Point of Care Testing Device for Sickle Cell Disease." *BMC Med* 2015;**13**: 225.

91. Quinn, C.T., Paniagua, M.C., DiNello, R.K., Panchal, A., Geisberg, M. "A Rapid, Inexpensive and Disposable Point-of-Care Blood Test for Sickle Cell Disease Using Novel, Highly Specific Monoclonal Antibodies." *Br J Haematol* 2016.

92. Posthuma-Trumpie, G.A., Korf, J., van Amerongen, A. "Lateral Flow (Immuno)Assay: Its Strengths, Weaknesses, Opportunities and Threats. A Literature Survey." *Anal Bioanal Chem* 2009;**393**: 569-82.

93. Simon, T.L., Snyder, E.L., Stowell, C.P., Strauss, R.G., Solheim, B.G., Petrides, M. Rossi's Principles of Transfusion Medicine: Wiley, 2011.

94. Josephson, C.D., Su, L.L., Hillyer, K.L., Hillyer, C.D. "Transfusion in the Patient with Sickle Cell Disease: A Critical Review of the Literature and Transfusion Guidelines." *Transfus Med Rev* 2007;**21**: 118-33.

95. Roback, J.D., Banks, A.A.o.B. Technical Manual: American Association of Blood Banks, 2008.

96. Hillery, C.A., Panepinto, J.A. "Pathophysiology of Stroke in Sickle Cell Disease." *Microcirculation* 2004;**11**: 195-208.

97. Wanko, S.O., Telen, M.J. "Transfusion Management in Sickle Cell Disease." *Hematol Oncol Clin North Am* 2005;**19**: 803-26, v-vi.

98. Yang, X., Kanter, J., Piety, N.Z., Benton, M.S., Vignes, S.M., Shevkoplyas, S.S. "A Simple, Rapid, Low-Cost Diagnostic Test for Sickle Cell Disease." *Lab Chip* 2013;**13**: 1464-7.

99. Itano, H.A. "Solubilities of Naturally Occurring Mixtures of Human Hemoglobin." *Arch Biochem Biophys* 1953;**47**: 148-59.

100. Nalbandian, R.M., Camp, F.R., Jr., Conte, N.F., Prothro, W.B. "Automated Mass Screening for Hemoglobin S: A Rational Method." *Health Serv Rep* 1973;**88**: 165-73.

101. Yang, X., Piety, N.Z., Vignes, S.M., Benton, M.S., Kanter, J., Shevkoplyas, S.S. "Simple Paper-Based Test for Measuring Blood Hemoglobin Concentration in Resource-Limited Settings." *Clin Chem* 2013;**59**: 1506-13.

102. Neal, F.B., Russ, J.C. Measuring Shape: Taylor & Francis, 2012.

103. Bland, J.M., Altman, D.G. "Statistical Methods for Assessing Agreement between Two Methods of Clinical Measurement." *Lancet* 1986;**1**: 307-10.

104. Serjeant, G.R. "The Natural History of Sickle Cell Disease." *Cold Spring Harb Perspect Med* 2013;**3**: a011783.

105. Evans, E.A. "New Membrane Concept Applied to the Analysis of Fluid Shear- and Micropipette-Deformed Red Blood Cells." *Biophys J* 1973;**13**: 941-54.

106. Fischer, T.M., Haest, C.W., Stohr-Liesen, M., Schmid-Schonbein, H., Skalak, R. "The Stress-Free Shape of the Red Blood Cell Membrane." *Biophys J* 1981;**34**: 409-22.

107. Gifford, S.C., Derganc, J., Shevkoplyas, S.S., Yoshida, T., Bitensky, M.W. "A Detailed Study of Time-Dependent Changes in Human Red Blood Cells: From Reticulocyte Maturation to Erythrocyte Senescence." *Br J Haematol* 2006;**135**: 395-404.

108. Greenwalt, T.J. "The How and Why of Exocytic Vesicles." *Transfusion* 2006;**46**: 143-52.

109. Berezina, T.L., Zaets, S.B., Morgan, C., Spillert, C.R., Kamiyama, M., Spolarics, Z., Deitch, E.A., Machiedo, G.W. "Influence of Storage on Red Blood Cell Rheological Properties." *J Surg Res* 2002;**102**: 6-12.

110. Park, Y., Best, C.A., Badizadegan, K., Dasari, R.R., Feld, M.S., Kuriabova, T., Henle, M.L., Levine, A.J., Popescu, G. "Measurement of Red Blood Cell Mechanics During Morphological Changes." *Proc Natl Acad Sci U S A* 2010;**107**: 6731-6.

111. Yoshida, T., Shevkoplyas, S.S. "Anaerobic Storage of Red Blood Cells." *Blood Transfusion* 2010;**8**: 220-36.

112. Nagaprasad, V., Singh, M. "Sequential Analysis of the Influence of Blood Storage on Aggregation, Deformability and Shape Parameters of Erythrocytes." *Clin Hemorheol Microcirc* 1998;**18**: 273-84.

113. Chin-Yee, I., Arya, N., d'Almeida, M.S. "The Red Cell Storage Lesion and Its Implication for Transfusion." *Transfus Sci* 1997;**18**: 447-58.

114. Cooper, R.A., Jandl, J.H. "The Role of Membrane Lipids in the Survival of Red Cells in Hereditary Spherocytosis." *The Journal of clinical investigation* 1969;**48**: 736-44.

115. Bosman, G.J., Werre, J.M., Willekens, F.L., Novotny, V.M. "Erythrocyte Ageing in Vivo and in Vitro: Structural Aspects and Implications for Transfusion." *Transfus Med* 2008;**18**: 335-47.

116. Hod, E.A., Spitalnik, S.L. "Harmful Effects of Transfusion of Older Stored Red Blood Cells: Iron and Inflammation." *Transfusion* 2011;**51**: 881-5.

117. Hod, E.A., Brittenham, G.M., Billote, G.B., Francis, R.O., Ginzburg, Y.Z., Hendrickson, J.E., Jhang, J., Schwartz, J., Sharma, S., Sheth, S., Sireci, A.N., Stephens, H.L., Stotler, B.A., Wojczyk, B.S., Zimring, J.C., Spitalnik, S.L. "Transfusion of Human Volunteers with Older, Stored Red Blood Cells Produces Extravascular Hemolysis and Circulating Non-Transferrin-Bound Iron." *Blood* 2011;**118**: 6675-82.

118. Albertini, M.C., Teodori, L., Piatti, E., Piacentini, M.P., Accorsi, A., Rocchi, M.B. "Automated Analysis of Morphometric Parameters for Accurate Definition of Erythrocyte Cell Shape." *Cytometry A* 2003;**52**: 12-8.

119. Berezina, T.L., Zaets, S.B., Machiedo, G.W. "Alterations of Red Blood Cell Shape in Patients with Severe Trauma." *J Trauma* 2004;**57**: 82-7.

120. Hogman, C.F., Lof, H., Meryman, H.T. "Storage of Red Blood Cells with Improved Maintenance of 2,3-Bisphosphoglycerate." *Transfusion* 2006;**46**: 1543-52.

121. de Korte, D., Kleine, M., Korsten, H.G., Verhoeven, A.J. "Prolonged Maintenance of 2,3-Diphosphoglycerate Acid and Adenosine Triphosphate in Red Blood Cells During Storage." *Transfusion* 2008;**48**: 1081-9.

122. Blasi, B., D'Alessandro, A., Ramundo, N., Zolla, L. "Red Blood Cell Storage and Cell Morphology." *Transfus Med* 2012;**22**: 90-6.

123. Pierre, R.V. "Red Cell Morphology and the Peripheral Blood Film." *Clin Lab Med* 2002;**22**: 25-61, v-vi.

124. Xiong, W., Ong, S.H., Lim, J.H., Foong, K.W., Liu, J., Racoceanu, D., Chong, A.G., Tan, K.S. "Automatic Area Classification in Peripheral Blood Smears." *IEEE Trans Biomed Eng* 2010;**57**: 1982-90.

125. Anggraini, D., Nugroho, A.S., Pratama, C., Rozi, I.E., Iskandar, A.A., Hartono, R.N. Automated Status Identification of Microscopic Images Obtained from Malaria Thin Blood Smears Electrical Engineering and Informatics (ICEEI), 2011 International Conference on, 2011:1-6.

126. Whitesides, G.M., Ostuni, E., Takayama, S., Jiang, X., Ingber, D.E. "Soft Lithography in Biology and Biochemistry." *Annu Rev Biomed Eng* 2001;**3**: 335-73.

127. Forouzan, O., Burns, J.M., Robichaux, J.L., Murfee, W.L., Shevkoplyas, S.S. "Passive Recruitment of Circulating Leukocytes into Capillary Sprouts from Existing Capillaries in a Microfluidic System." *Lab on a chip* 2011;**11**: 1924-32.

128. Burns, J.M., Yang, X., Forouzan, O., Sosa, J.M., Shevkoplyas, S.S. "Artificial Microvascular Network: A New Tool for Measuring Rheologic Properties of Stored Red Blood Cells." *Transfusion* 2012;**52**: 1010-23.

129. Shevkoplyas, S.S., Gifford, S.C., Yoshida, T., Bitensky, M.W. "Prototype of an in Vitro Model of the Microcirculation." *Microvasc Res* 2003;**65**: 132-6.

130. Shevkoplyas, S.S., Yoshida, T., Munn, L.L., Bitensky, M.W. "Biomimetic Autoseparation of Leukocytes from Whole Blood in a Microfluidic Device." *Anal Chem* 2005;**77**: 933-7.

131. Shevkoplyas, S.S., Yoshida, T., Gifford, S.C., Bitensky, M.W. "Direct Measurement of the Impact of Impaired Erythrocyte Deformability on Microvascular Network Perfusion in a Microfluidic Device." *Lab on a chip* 2006;**6**: 914-20.

132. Gifford, S. Methods of Multivariate Data Cluster Separation and Visualization. In: Office USPaT, ed. United States, 2013.

133. Decre, M.M., Timmermans, P.H., van der Sluis, O., Schroeders, R. "Numerical and Experimental Study of Critical Roof Collapse Conditions in Soft Lithography." *Langmuir* 2005;**21**: 7971-8.

134. Hu, Y., Osuna-Highley, E., Hua, J., Nowicki, T.S., Stolz, R., McKayle, C., Murphy, R.F. "Automated Analysis of Protein Subcellular Location in Time Series Images." *Bioinformatics* 2010;**26**: 1630-6.

135. Sammut, C., Webb, G.I. Encyclopedia of Machine Learning. New York: Springer, 2011.

136. Hess, J.R. "Measures of Stored Red Blood Cell Quality." *Vox Sang* 2014;**107**: 1-9.

137. Gifford, S.C., Spillane, A.M., Vignes, S.M., Shevkoplyas, S.S. "Controlled Incremental Filtration: A Simplified Approach to Design and Fabrication of High-Throughput Microfluidic Devices for Selective Enrichment of Particles." *Lab on a chip* 2014;**14**: 4496-505.

138. Davis, J.A., Inglis, D.W., Morton, K.J., Lawrence, D.A., Huang, L.R., Chou, S.Y., Sturm, J.C., Austin, R.H. "Deterministic Hydrodynamics: Taking Blood Apart." *Proc Natl Acad Sci U S A* 2006;**103**: 14779-84.

139. Huang, S., Hou, H.W., Kanias, T., Sertorio, J.T., Chen, H., Sinchar, D., Gladwin, M.T., Han, J. "Towards Microfluidic-Based Depletion of Stiff and Fragile Human Red Cells That Accumulate During Blood Storage." *Lab on a chip* 2015;**15**: 448-58.

140. Di Ruberto, C., Dempster, A., Khan, S., Jarra, B. "Analysis of Infected Blood Cell Images Using Morphological Operators." *Image and Vision Computing* 2002;**20**: 133-46.

141. Angulo, J., Klossa, J., Flandrin, G. "Ontology-Based Lymphocyte Population Description Using Mathematical Morphology on Colour Blood Images." *Cell Mol Biol (Noisy-le-grand)* 2006;**52**: 2-15.

142. Huh, S., Lee, D., Murphy, R.F. "Efficient Framework for Automated Classification of Subcellular Patterns in Budding Yeast." *Cytometry A* 2009;**75**: 934-40.

143. Roback, J.D. "Evidence-Based Guidelines for Blood Transfusion." *J Infus Nurs* 2012;**35**: 187-90.

144. Kim-Shapiro, D.B., Lee, J., Gladwin, M.T. "Storage Lesion: Role of Red Blood Cell Breakdown." *Transfusion* 2011;**51**: 844-51.

145. Piety, N.Z., Reinhart, W.H., Pourreau, P.H., Abidi, R., Shevkoplyas, S.S. "Shape Matters: The Effect of Red Blood Cell Shape on Perfusion of an Artificial Microvascular Network." *Transfusion* 2016;**56**: 844-51.

146. Reinhart, W.H., Piety, N.Z., Deuel, J.W., Makhro, A., Schulzki, T., Bogdanov, N., Goede, J.S., Bogdanova, A., Abidi, R., Shevkoplyas, S.S. "Washing Stored Red Blood Cells in an Albumin Solution Improves Their Morphologic and Hemorheologic Properties." *Transfusion* 2015;**55**: 1872-81.

147. Burns, J.M., Yoshida, T., Dumont, L.J., Yang, X., Piety, N.Z., Shevkoplyas, S.S. "Deterioration of Red Blood Cell Mechanical Properties Is Reduced in Anaerobic Storage." *Blood Transfus* 2016;**14**: 80-8.

148. Safeukui, I., Buffet, P.A., Deplaine, G., Perrot, S., Brousse, V., Ndour, A., Nguyen, M., Mercereau-Puijalon, O., David, P.H., Milon, G., Mohandas, N. "Quantitative Assessment of Sensing and Sequestration of Spherocytic Erythrocytes by the Human Spleen." *Blood* 2012;**120**: 424-30.

149. Simchon, S., Jan, K.M., Chien, S. "Influence of Reduced Red Cell Deformability on Regional Blood Flow." *Am J Physiol* 1987;**253**: H898-903.

150. Tsai, A.G., Cabrales, P., Intaglietta, M. "Microvascular Perfusion Upon Exchange Transfusion with Stored Red Blood Cells in Normovolemic Anemic Conditions." *Transfusion* 2004;**44**: 1626-34.

151. Chaudhary, R., Katharia, R. "Oxidative Injury as Contributory Factor for Red Cells Storage Lesion During Twenty Eight Days of Storage." *Blood Transfus* 2012;**10**: 59-62.

152. Yoshida, T., Shevkoplyas, S.S. "Anaerobic Storage of Red Blood Cells." *Blood Transfus* 2010;**8**: 220-36.

153. Yoshida, T., AuBuchon, J.P., Tryzelaar, L., Foster, K.Y., Bitensky, M.W. "Extended Storage of Red Blood Cells under Anaerobic Conditions." *Vox Sang* 2007;**92**: 22-31.

154. Yoshida, T., AuBuchon, J.P., Dumont, L.J., Gorham, J.D., Gifford, S.C., Foster, K.Y., Bitensky, M.W. "The Effects of Additive Solution Ph and Metabolic Rejuvenation on Anaerobic Storage of Red Cells." *Transfusion* 2008;**48**: 2096-105.

155. Dumont, L.J., Yoshida, T., AuBuchon, J.P. "Anaerobic Storage of Red Blood Cells in a Novel Additive Solution Improves in Vivo Recovery." *Transfusion* 2009;**49**: 458-64.

156. Hardeman, M.R., Dobbe, J.G., Ince, C. "The Laser-Assisted Optical Rotational Cell Analyzer (Lorca) as Red Blood Cell Aggregometer." *Clin Hemorheol Microcirc* 2001;**25**: 1-11.

157. Shin, S., Hou, J.X., Suh, J.S., Singh, M. "Validation and Application of a Microfluidic Ektacytometer (Rheoscan-D) in Measuring Erythrocyte Deformability." *Clin Hemorheol Microcirc* 2007;**37**: 319-28.

158. Piety, N.Z., Gifford, S.C., Yang, X., Shevkoplyas, S.S. "Quantifying Morphological Heterogeneity: A Study of More Than 1 000 000 Individual Stored Red Blood Cells." *Vox Sang* 2015;**109**: 221-30.

159. Reinhart, W.H., Piety, N.Z., Goede, J.S., Shevkoplyas, S.S. "Effect of Osmolality on Erythrocyte Rheology and Perfusion of an Artificial Microvascular Network." *Microvasc Res* 2015;**98**: 102-7.

160. Shin, S., Ku, Y., Park, M.S., Suh, J.S. "Slit-Flow Ektacytometry: Laser Diffraction in a Slit Rheometer." *Cytometry B Clin Cytom* 2005;**65**: 6-13.

161. Baskurt, O.K., Uyuklu, M., Ulker, P., Cengiz, M., Nemeth, N., Alexy, T., Shin, S., Hardeman, M.R., Meiselman, H.J. "Comparison of Three Instruments for Measuring Red Blood Cell Aggregation." *Clin Hemorheol Microcirc* 2009;**43**: 283-98.

162. Dobbe, J.G., Streekstra, G.J., Hardeman, M.R., Ince, C., Grimbergen, C.A. "Measurement of the Distribution of Red Blood Cell Deformability Using an Automated Rheoscope." *Cytometry* 2002;**50**: 313-25.

163. Dobbe, J.G., Hardeman, M.R. "Red Blood Cell Aggregation as Measured with the Lorca." *Int J Artif Organs* 2006;**29**: 641-2; author reply 3.

164. Immerman, K.L., Melaragno, A.J., Ouellet, R.P., Weinstein, R., Valeri, C.R. "Morphology of Glutaraldehyde-Fixed Preserved Red Blood Cells and 24-Hr Post-Transfusion Survival." *Cryobiology* 1983;**20**: 30-5.

165. Yang, X., Forouzan, O., Burns, J.M., Shevkoplyas, S.S. "Traffic of Leukocytes in Microfluidic Channels with Rectangular and Rounded Cross-Sections." *Lab on a chip* 2011;**11**: 3231-40.

166. Zehnder, L., Schulzki, T., Goede, J.S., Hayes, J., Reinhart, W.H. "Erythrocyte Storage in Hypertonic (Sagm) or Isotonic (Paggsm) Conservation Medium: Influence on Cell Properties." *Vox Sang* 2008;**95**: 280-7.

167. Dumont, L.J., AuBuchon, J.P. "Evaluation of Proposed Fda Criteria for the Evaluation of Radiolabeled Red Cell Recovery Trials." *Transfusion* 2008;**48**: 1053-60.

168. Aubron, C., Syres, G., Nichol, A., Bailey, M., Board, J., Magrin, G., Murray, L., Presneill, J., Sutton, J., Vallance, S., Morrison, S., Bellomo, R., Cooper, D.J. "A Pilot Feasibility Trial of Allocation of Freshest Available Red Blood Cells Versus Standard Care in Critically Ill Patients." *Transfusion* 2012;**52**: 1196-202.

169. Wang, D., Sun, J., Solomon, S.B., Klein, H.G., Natanson, C. "Transfusion of Older Stored Blood and Risk of Death: A Meta-Analysis." *Transfusion* 2012;**52**: 1184-95.

170. Lelubre, C., Vincent, J.L. "Relationship between Red Cell Storage Duration and Outcomes in Adults Receiving Red Cell Transfusions: A Systematic Review." *Crit Care* 2013;**17**: R66.

171. Solomon, S.B., Wang, D., Sun, J., Kanias, T., Feng, J., Helms, C.C., Solomon, M.A., Alimchandani, M., Quezado, M., Gladwin, M.T., Kim-Shapiro, D.B., Klein, H.G., Natanson, C. "Mortality Increases after Massive Exchange Transfusion with Older Stored Blood in Canines with Experimental Pneumonia." *Blood* 2013;**121**: 1663-72.

172. Flegel, W.A., Natanson, C., Klein, H.G. "Does Prolonged Storage of Red Blood Cells Cause Harm?" *Br J Haematol* 2014;**165**: 3-16.

173. van de Watering, L. "Red Cell Storage and Prognosis." *Vox Sang* 2011;**100**: 36-45.

174. Karon, B.S., van Buskirk, C.M., Jaben, E.A., Hoyer, J.D., Thomas, D.D. "Temporal Sequence of Major Biochemical Events During Blood Bank Storage of Packed Red Blood Cells." *Blood Transfus* 2012;**10**: 453-61.

175. Relevy, H., Koshkaryev, A., Manny, N., Yedgar, S., Barshtein, G. "Blood Banking-Induced Alteration of Red Blood Cell Flow Properties." *Transfusion* 2008;**48**: 136-46.

176. Rinalducci, S., Ferru, E., Blasi, B., Turrini, F., Zolla, L. "Oxidative Stress and Caspase-Mediated Fragmentation of Cytoplasmic Domain of Erythrocyte Band 3 During Blood Storage." *Blood Transfus* 2012;**10 Suppl 2**: s55-62.

177. Meryman, H.T., Hornblower, M.L., Syring, R.L. "Prolonged Storage of Red Cells at 4 Degrees C." *Transfusion* 1986;**26**: 500-5.

178. Mazor, D., Dvilansky, A., Meyerstein, N. "Prolonged Storage of Red Cells: The Effect of Ph, Adenine and Phosphate." *Vox Sang* 1994;**66**: 264-9.

179. Hovav, T., Yedgar, S., Manny, N., Barshtein, G. "Alteration of Red Cell Aggregability and Shape During Blood Storage." *Transfusion* 1999;**39**: 277-81.

180. Sollberger, T., Walter, R., Brand, B., Contesse, J., Meredith, D.O., Reinhart, W.H. "Influence of Prestorage Leucocyte Depletion and Storage Time on Rheologic Properties of Erythrocyte Concentrates." *Vox Sang* 2002;**82**: 191-7.

181. Chabanel, A., Reinhart, W., Chien, S. "Increased Resistance to Membrane Deformation of Shape-Transformed Human Red Blood Cells." *Blood* 1987;**69**: 739-43.

182. Reinhart, W.H., Chien, S. "Red Cell Rheology in Stomatocyte-Echinocyte Transformation: Roles of Cell Geometry and Cell Shape." *Blood* 1986;**67**: 1110-8.

183. Reinhart, S.A., Schulzki, T., Bonetti, P.O., Reinhart, W.H. "Studies on Metabolically Depleted Erythrocytes." *Clin Hemorheol Microcirc* 2014;**56**: 161-73.

184. Reinhart, S.A., Schulzki, T., Reinhart, W.H. "Albumin Reverses the Echinocytic Shape Transformation of Stored Erythrocytes." *Clin Hemorheol Microcirc* 2015;**60**: 437-49.

185. Ferrell, J.E., Jr., Huestis, W.H. "Phosphoinositide Metabolism and the Morphology of Human Erythrocytes." *J Cell Biol* 1984;**98**: 1992-8.

186. Bogdanova, A.Y., Ogunshola, O.O., Bauer, C., Gassmann, M. "Pivotal Role of Reduced Glutathione in Oxygen-Induced Regulation of the Na(+)/K(+) Pump in Mouse Erythrocyte Membranes." *J Membr Biol* 2003;**195**: 33-42.

187. Deuel, J.W., Lutz, H.U., Misselwitz, B., Goede, J.S. "Asymptomatic Elevation of the Hyperchromic Red Blood Cell Subpopulation Is Associated with Decreased Red Cell Deformability." *Ann Hematol* 2012;**91**: 1427-34.

188. Sosa, J.M., Nielsen, N.D., Vignes, S.M., Chen, T.G., Shevkoplyas, S.S. "The Relationship between Red Blood Cell Deformability Metrics and Perfusion of an Artificial Microvascular Network." *Clin Hemorheol Microcirc* 2014;**57**: 275-89.

189. Forouzan, O., Yang, X., Sosa, J.M., Burns, J.M., Shevkoplyas, S.S. "Spontaneous Oscillations of Capillary Blood Flow in Artificial Microvascular Networks." *Microvasc Res* 2012;**84**: 123-32.

190. Luten, M., Roerdinkholder-Stoelwinder, B., Schaap, N.P., de Grip, W.J., Bos, H.J., Bosman, G.J. "Survival of Red Blood Cells after Transfusion: A Comparison between Red Cells Concentrates of Different Storage Periods." *Transfusion* 2008;**48**: 1478-85.

191. Fasano, M., Curry, S., Terreno, E., Galliano, M., Fanali, G., Narciso, P., Notari, S., Ascenzi, P. "The Extraordinary Ligand Binding Properties of Human Serum Albumin." *IUBMB Life* 2005;**57**: 787-96.

192. Pirofsky, B., Cordova, M.S., Imel, T.L. "The Nonimmunologic Reaction of Globulin Molecules with the Erythrocyte Surface." *Vox Sang* 1962;**7**: 334-47.

193. Reinhart, W.H., Chien, S. "Echinocyte-Stomatocyte Transformation and Shape Control of Human Red Blood Cells: Morphological Aspects." *American journal of hematology* 1987;**24**: 1-14.

194. Sheetz, M.P., Singer, S.J. "Biological Membranes as Bilayer Couples. A Molecular Mechanism of Drug-Erythrocyte Interactions." *Proc Natl Acad Sci U S A* 1974;**71**: 4457-61.

195. Silliman, C.C., Clay, K.L., Thurman, G.W., Johnson, C.A., Ambruso, D.R. "Partial Characterization of Lipids That Develop During the Routine Storage of Blood and Prime the Neutrophil Nadph Oxidase." *J Lab Clin Med* 1994;**124**: 684-94.

196. Silliman, C.C., Moore, E.E., Kelher, M.R., Khan, S.Y., Gellar, L., Elzi, D.J. "Identification of Lipids That Accumulate During the Routine Storage of Prestorage Leukoreduced Red Blood Cells and Cause Acute Lung Injury." *Transfusion* 2011;**51**: 2549-54.

197. Maslanka, K., Uhrynowska, M., Lopacz, P., Wrobel, A., Smolenska-Sym, G., Guz, K., Lachert, E., Ostas, A., Brojer, E. "Analysis of Leucocyte Antibodies, Cytokines, Lysophospholipids and Cell Microparticles in Blood Components Implicated in Post-Transfusion Reactions with Dyspnoea." *Vox Sang* 2015;**108**: 27-36.

198. Mohandas, N., Greenquist, A.C., Shohet, S.B. "Bilayer Balance and Regulation of Red Cell Shape Changes." *J Supramol Struct* 1978;**9**: 453-8.

199. Rogausch, H. "The Flow Behavior of Lysolecithin-Induced Echinocytes." *Biorheology* 1984;**21**: 757-65.

200. Chasis, J.A., Schrier, S.L. "Membrane Deformability and the Capacity for Shape Change in the Erythrocyte." *Blood* 1989;**74**: 2562-8.

201. Duranton, C., Tanneur, V., Lang, C., Brand, V.B., Koka, S., Kasinathan, R.S., Dorsch, M., Hedrich, H.J., Baumeister, S., Lingelbach, K., Lang, F., Huber, S.M. "A High Specificity and Affinity Interaction with Serum Albumin Stimulates an Anion Conductance in Malaria-Infected Erythrocytes." *Cell Physiol Biochem* 2008;**22**: 395-404.

202. Ojala, P.J., Hirvonen, T.E., Hermansson, M., Somerharju, P., Parkkinen, J. "Acyl Chain-Dependent Effect of Lysophosphatidylcholine on Human Neutrophils." *J Leukoc Biol* 2007;**82**: 1501-9.

203. Paterakis, G.S., Laoutaris, N.P., Alexia, S.V., Siourounis, P.V., Stamulakatou, A.K., Premetis, E.E., Sakellariou, C., Terzoglou, G.N., Papassotiriou, I.G., Loukopoulos, D. "The Effect of Red Cell Shape on the Measurement of Red Cell Volume. A Proposed Method for the Comparative Assessment of This Effect among Various Haematology Analysers." *Clin Lab Haematol* 1994;**16**: 235-45.

204. Lutz, H.U., Bogdanova, A. "Mechanisms Tagging Senescent Red Blood Cells for Clearance in Healthy Humans." *Front Physiol* 2013;**4**: 387.

205. Mohanty, J.G., Nagababu, E., Rifkind, J.M. "Red Blood Cell Oxidative Stress Impairs Oxygen Delivery and Induces Red Blood Cell Aging." *Front Physiol* 2014;**5**: 84.

206. Bennett-Guerrero, E., Veldman, T.H., Doctor, A., Telen, M.J., Ortel, T.L., Reid, T.S., Mulherin, M.A., Zhu, H., Buck, R.D., Califf, R.M., McMahon, T.J. "Evolution of Adverse Changes in Stored Rbcs." *Proc Natl Acad Sci U S A* 2007;**104**: 17063-8.

207. Frank, S.M., Abazyan, B., Ono, M., Hogue, C.W., Cohen, D.B., Berkowitz, D.E., Ness, P.M., Barodka, V.M. "Decreased Erythrocyte Deformability after Transfusion and the Effects of Erythrocyte Storage Duration." *Anesth Analg* 2013;**116**: 975-81.

208. Salaria, O.N., Barodka, V.M., Hogue, C.W., Berkowitz, D.E., Ness, P.M., Wasey, J.O., Frank, S.M. "Impaired Red Blood Cell Deformability after Transfusion of Stored Allogeneic Blood but Not Autologous Salvaged Blood in Cardiac Surgery Patients." *Anesth Analg* 2014;**118**: 1179-87.

209. Reinhart, W.H., Singh, A., Straub, P.W. "Red Blood Cell Aggregation and Sedimentation: The Role of the Cell Shape." *Br J Haematol* 1989;**73**: 551-6.

210. Singh, A., Reinhart, W.H. "The Influence of Fractions of Abnormal Erythrocytes on Aggregation." *Eur J Clin Invest* 1991;**21**: 597-600.

211. Reinhart, W.H., Singh-Marchetti, M., Straub, P.W. "The Influence of Erythrocyte Shape on Suspension Viscosities." *Eur J Clin Invest* 1992;**22**: 38-44.

212. Hess, J.R., Biomedical Excellence for Safer Transfusion, C. "Scientific Problems in the Regulation of Red Blood Cell Products." *Transfusion* 2012;**52**: 1827-35.

213. Canham, P.B. "The Minimum Energy of Bending as a Possible Explanation of the Biconcave Shape of the Human Red Blood Cell." *J Theor Biol* 1970;**26**: 61-81.

214. Reinhart, W.H. "Peculiar Red Cell Shapes: Fahraeus Lecture 2011." *Clin Hemorheol Microcirc* 2011;**49**: 11-27.

215. de Oliveira, S., Saldanha, C. "An Overview About Erythrocyte Membrane." *Clin Hemorheol Microcirc* 2010;**44**: 63-74.

216. Reinhart, W.H., Pleisch, B., Harris, L.G., Lutolf, M. "Influence of Contrast Media (Iopromide, Ioxaglate, Gadolinium-Dota) on Blood Viscosity, Erythrocyte Morphology and Platelet Function." *Clin Hemorheol Microcirc* 2005;**32**: 227-39.

217. Mrowietz, C., Franke, R.P., Jung, F. "Influence of Different Radiographic Contrast Media on the Echinocyte Formation of Human Erythrocytes." *Clin Hemorheol Microcirc* 2012;**50**: 35-47.

218. Reinhart, W.H., Felix, C. "Influence of Propofol on Erythrocyte Morphology, Blood Viscosity and Platelet Function." *Clin Hemorheol Microcirc* 2003;**29**: 33-40.

219. Fischler, L., Meredith, D.O., Reinhart, W.H. "Influence of a Parenteral Fish-Oil Preparation (Omegaven) on Erythrocyte Morphology and Blood Viscosity in Vitro." *Clin Hemorheol Microcirc* 2003;**28**: 79-88.

220. Baerlocher, G.M., Beer, J.H., Owen, G.R., Meiselman, H.J., Reinhart, W.H. "The Anti-Neoplastic Drug 5-Fluorouracil Produces Echinocytosis and Affects Blood Rheology." *Br J Haematol* 1997;**99**: 426-32.

221. Suwalsky, M., Mennickent, S., Norris, B., Villena, F., Sotomayor, C.P. "Effects of the Antiepileptic Drug Carbamazepine on Human Erythrocytes." *Toxicol In Vitro* 2006;**20**: 1363-9.

222. Reinhart, W.H., Lubszky, S., Thony, S., Schulzki, T. "Interaction of Injectable Neurotropic Drugs with the Red Cell Membrane." *Toxicol In Vitro* 2014;**28**: 1274-9.

223. Manrique-Moreno, M., Suwalsky, M., Villena, F., Garidel, P. "Effects of the Nonsteroidal Anti-Inflammatory Drug Naproxen on Human Erythrocytes and on Cell Membrane Molecular Models." *Biophys Chem* 2010;**147**: 53-8.

224. Meiselman, H.J. "Rheology of Shape-Transformed Human Red Cells." *Biorheology* 1978;**15**: 225-37.

225. Li, A., Seipelt, H., Muller, C., Shi, Y., Artmann, M. "Effects of Salicylic Acid Derivatives on Red Blood Cell Membranes." *Pharmacol Toxicol* 1999;**85**: 206-11.

226. Hasler, C.R., Owen, G.R., Brunner, W., Reinhart, W.H. "Echinocytosis Induced by Haemodialysis." *Nephrol Dial Transplant* 1998;**13**: 3132-7.

227. Reinhart, W.H., Ballmer, P.E., Rohner, F., Ott, P., Straub, P.W. "The Influence of Extracorporeal Circulation on Erythrocytes and Flow Properties of Blood." *J Thorac Cardiovasc Surg* 1990;**100**: 538-45.

228. Reinhart, W.H., Piety, N.Z., Deuel, J.W., Makhro, A., Schulzki, T., Bogdanov, N., Goede, J.S., Bogdanova, A., Abidi, R., Shevkoplyas, S.S. "Washing Stored Red Blood Cells in an Albumin Solution Improves Their Morphologic and Hemorheologic Properties." *Transfusion* 2015.

229. Almizraq, R., Tchir, J.D., Holovati, J.L., Acker, J.P. "Storage of Red Blood Cells Affects Membrane Composition, Microvesiculation, and in Vitro Quality." *Transfusion* 2013;**53**: 2258-67.

230. Piety, N.Z., Gifford, S.C., Yang, X., Shevkoplyas, S.S. "Quantifying Morphological Heterogeneity: A Study of More Than 1 000 000 Individual Stored Red Blood Cells." *Vox Sang* 2015.

231. Rumsby, M.G., Trotter, J., Allan, D., Michell, R.H. "Recovery of Membrane Micro-Vesicles from Human Erythrocytes Stored for Transfusion: A Mechanism for the Erythrocyte Discocyte-to-Spherocyte Shape Transformation." *Biochem Soc Trans* 1977;**5**: 126-8.

232. Kowluru, R., Bitensky, M.W., Kowluru, A., Dembo, M., Keaton, P.A., Buican, T. "Reversible Sodium Pump Defect and Swelling in the Diabetic Rat Erythrocyte: Effects on Filterability and Implications for Microangiopathy." *Proc Natl Acad Sci U S A* 1989;**86**: 3327-31.

233. Somani, A., Steiner, M.E., Hebbel, R.P. "The Dynamic Regulation of Microcirculatory Conduit Function: Features Relevant to Transfusion Medicine." *Transfus Apher Sci* 2010;**43**: 61-8.

234. Franke, R.P., Kruger, A., Scharnweber, T., Wenzel, F., Jung, F. "Effects of Radiographic Contrast Media on the Micromorphology of the Junctional Complex of Erythrocytes Visualized by Immunocytology." *Int J Mol Sci* 2014;**15**: 16134-52.

235. Lange, Y., Steck, T.L. "Mechanism of Red Blood Cell Acanthocytosis and Echinocytosis in Vivo." *J Membr Biol* 1984;**77**: 153-9.

236. De Franceschi, L., Bosman, G.J., Mohandas, N. "Abnormal Red Cell Features Associated with Hereditary Neurodegenerative Disorders: The Neuroacanthocytosis Syndromes." *Curr Opin Hematol* 2014;**21**: 201-9.

237. Reynolds, R.M., Padfield, P.L., Seckl, J.R. "Disorders of Sodium Balance." *BMJ* 2006;**332**: 702-5.

238. Danziger, J., Zeidel, M.L. "Osmotic Homeostasis." *Clin J Am Soc Nephrol* 2014.

239. Arieff, A.I. "Hyponatremia, Convulsions, Respiratory Arrest, and Permanent Brain Damage after Elective Surgery in Healthy Women." *N Engl J Med* 1986;**314**: 1529-35.

240. Kumar, S., Berl, T. "Sodium." *Lancet* 1998;**352**: 220-8.

241. Klein, L., O'Connor, C.M., Leimberger, J.D., Gattis-Stough, W., Pina, I.L., Felker, G.M., Adams, K.F., Jr., Califf, R.M., Gheorghiade, M., Investigators, O.-C. "Lower Serum Sodium Is Associated with Increased Short-Term Mortality in Hospitalized Patients with Worsening Heart Failure: Results

from the Outcomes of a Prospective Trial of Intravenous Milrinone for Exacerbations of Chronic Heart Failure (Optime-Chf) Study." *Circulation* 2005;**111**: 2454-60.

242. Ellis, S.J. "Severe Hyponatraemia: Complications and Treatment." *QJM* 1995;**88**: 905-9.

243. Shah, M.K., Workeneh, B., Taffet, G.E. "Hypernatremia in the Geriatric Population." *Clin Interv Aging* 2014;**9**: 1987-92.

244. McManus, M.L., Churchwell, K.B., Strange, K. "Regulation of Cell Volume in Health and Disease." *N Engl J Med* 1995;**333**: 1260-6.

245. Manley, G.T., Fujimura, M., Ma, T., Noshita, N., Filiz, F., Bollen, A.W., Chan, P., Verkman, A.S. "Aquaporin-4 Deletion in Mice Reduces Brain Edema after Acute Water Intoxication and Ischemic Stroke." *Nat Med* 2000;**6**: 159-63.

246. Gallagher, P.G. "Disorders of Red Cell Volume Regulation." *Curr Opin Hematol* 2013;**20**: 201-7.

247. Reinhart, W.H., Chien, S. "Roles of Cell Geometry and Cellular Viscosity in Red Cell Passage through Narrow Pores." *Am J Physiol* 1985;**248**: C473-9.

248. Evans, E., Fung, Y.C. "Improved Measurements of the Erythrocyte Geometry." *Microvasc Res* 1972;**4**: 335-47.

249. Eskelinen, S., Saukko, P. "Effects of Glutaraldehyde and Critical Point Drying on the Shape and Size of Erythrocytes in Isotonic and Hypotonic Media." *J Microsc* 1983;**130**: 63-71.

250. Tran-Son-Tay, R., Sutera, S.P., Rao, P.R. "Determination of Red Blood Cell Membrane Viscosity from Rheoscopic Observations of Tank-Treading Motion." *Biophys J* 1984;**46**: 65-72.

251. Dodson, W.R., 3rd, Dimitrakopoulos, P. "Tank-Treading of Swollen Erythrocytes in Shear Flows." *Phys Rev E Stat Nonlin Soft Matter Phys* 2012;**85**: 021922.

252. Schmid-Schonbein, H., Wells, R. "Rheological Consequences of Osmotic Red Cell Crenation." *Pflugers Arch* 1969;**307**: 59-69.

253. Watson, P., Maughan, R.J. "Artifacts in Plasma Volume Changes Due to Hematology Analyzer-Derived Hematocrit." *Med Sci Sports Exerc* 2014;**46**: 52-9.

254. Mlekoday, H.J., Moore, R., Levitt, D.G. "Osmotic Water Permeability of the Human Red Cell. Dependence on Direction of Water Flow and Cell Volume." *J Gen Physiol* 1983;**81**: 213-20.

255. Staubli, M., Roessler, B., Straub, P.W. "Fluid Trapping of Erythrocytes under Hypoosmolar Conditions." *Blut* 1987;**54**: 239-45.

256. Clark, M.R., Mohandas, N., Shohet, S.B. "Osmotic Gradient Ektacytometry: Comprehensive Characterization of Red Cell Volume and Surface Maintenance." *Blood* 1983;**61**: 899-910.

257. Nemeth, N., Kiss, F., Klarik, Z., Miko, I. "Comparative Osmotic Gradient Ektacytometry Data on Inter-Species Differences of Experimental Animals." *Clin Hemorheol Microcirc* 2014;**57**: 1-8.

258. Overbeck, H.W., Pamnani, M.B. "Vascular Responses to Plasma Hypoosmolality in Man." *Proc Soc Exp Biol Med* 1975;**150**: 331-6.

259. Schroth, M., Plank, C., Meissner, U., Eberle, K.P., Weyand, M., Cesnjevar, R., Dotsch, J., Rascher, W. "Hypertonic-Hyperoncotic Solutions Improve Cardiac Function in Children after Open-Heart Surgery." *Pediatrics* 2006;**118**: e76-84.

260. Zakaria el, R., Tsakadze, N.L., Garrison, R.N. "Hypertonic Saline Resuscitation Improves Intestinal Microcirculation in a Rat Model of Hemorrhagic Shock." *Surgery* 2006;**140**: 579-87; discussion 87-8.

261. Coimbra, R., Hoyt, D.B., Junger, W.G., Angle, N., Wolf, P., Loomis, W., Evers, M.F. "Hypertonic Saline Resuscitation Decreases Susceptibility to Sepsis after Hemorrhagic Shock." *J Trauma* 1997;**42**: 602-6; discussion 6-7.

262. Angle, N., Hoyt, D.B., Coimbra, R., Liu, F., Herdon-Remelius, C., Loomis, W., Junger, W.G. "Hypertonic Saline Resuscitation Diminishes Lung Injury by Suppressing Neutrophil Activation after Hemorrhagic Shock." *Shock* 1998;**9**: 164-70.

263. Gonzalez, E.A., Kozar, R.A., Suliburk, J.W., Weisbrodt, N.W., Mercer, D.W., Moore, F.A. "Hypertonic Saline Resuscitation after Mesenteric Ischemia/Reperfusion Induces Ileal Apoptosis." *J Trauma* 2005;**59**: 1092-8.

264. Baskurt, O.K. Handbook of Hemorheology and Hemodynamics: IOS Press, 2007.

265. Ami, R.B., Barshtein, G., Zeltser, D., Goldberg, Y., Shapira, I., Roth, A., Keren, G., Miller, H., Prochorov, V., Eldor, A., Berliner, S., Yedgar, S. "Parameters of Red Blood Cell Aggregation as Correlates of the Inflammatory State." *Am J Physiol Heart Circ Physiol* 2001;**280**: H1982-8.

266. Goldin, Y., Tulshinski, T., Arbel, Y., Rogowski, O., Ami, R.B., Serov, J., Halperin, P., Shapira, I., Berliner, S. "Rheological Consequences of Acute Infections: The Rheodifference between Viral and Bacterial Infections." *Clin Hemorheol Microcirc* 2007;**36**: 111-9.

267. Alt, E., Amann-Vesti, B.R., Madl, C., Funk, G., Koppensteiner, R. "Platelet Aggregation and Blood Rheology in Severe Sepsis/Septic Shock: Relation to the Sepsis-Related Organ Failure Assessment (Sofa) Score." *Clin Hemorheol Microcirc* 2004;**30**: 107-15.

268. Zorio, E., Murado, J., Arizo, D., Rueda, J., Corella, D., Simo, M., Vaya, A. "Haemorheological Parameters in Young Patients with Acute Myocardial Infarction." *Clin Hemorheol Microcirc* 2008;**39**: 33-41.

269. Lee, B.K., Durairaj, A., Mehra, A., Wenby, R.B., Meiselman, H.J., Alexy, T. "Hemorheological Abnormalities in Stable Angina and Acute Coronary Syndromes." *Clin Hemorheol Microcirc* 2008;**39**: 43-51.

270. Tikhomirova, I.A., Oslyakova, A.O., Mikhailova, S.G. "Microcirculation and Blood Rheology in Patients with Cerebrovascular Disorders." *Clin Hemorheol Microcirc* 2011;**49**: 295-305.

271. Koscielny, J., Jung, E.M., Mrowietz, C., Kiesewetter, H., Latza, R. "Blood Fluidity, Fibrinogen, and Cardiovascular Risk Factors of Occlusive Arterial Disease: Results of the Aachen Study." *Clin Hemorheol Microcirc* 2004;**31**: 185-95.

272. Cicco, G., Pirrelli, A. "Red Blood Cell (Rbc) Deformability, Rbc Aggregability and Tissue Oxygenation in Hypertension." *Clin Hemorheol Microcirc* 1999;**21**: 169-77.

273. Zilberman-Kravits, D., Harman-Boehm, I., Shuster, T., Meyerstein, N. "Increased Red Cell Aggregation Is Correlated with Hba1c and Lipid Levels in Type 1 but Not Type 2 Diabetes." *Clin Hemorheol Microcirc* 2006;**35**: 463-71.

274. Toker, S., Rogowski, O., Melamed, S., Shirom, A., Shapira, I., Berliner, S., Zeltser, D. "Association of Components of the Metabolic Syndrome with the Appearance of Aggregated Red Blood Cells in the Peripheral Blood. An Unfavorable Hemorheological Finding." *Diabetes Metab Res Rev* 2005;**21**: 197-202.

275. Kwaan, H.C. "Role of Plasma Proteins in Whole Blood Viscosity: A Brief Clinical Review." *Clin Hemorheol Microcirc* 2010;**44**: 167-76.

276. Spengler, M.I., Svetaz, M.J., Leroux, M.B., Bertoluzzo, S.M., Carrara, P., Van Isseldyk, F., Petrelli, D., Parente, F.M., Bosch, P. "Erythrocyte Aggregation in Patients with Systemic Lupus Erythematosus." *Clin Hemorheol Microcirc* 2011;**47**: 279-85.

277. Vaya, A., Calvo, J., Alcala, C., Mico, L., Todoli, J., Ricart, J.M. "Rheological Alterations and Thrombotic Events in Patients with Systemic Lupus Erythematosus." *Clin Hemorheol Microcirc* 2012;**51**: 51-8.

278. Flormann, D., Kuder, E., Lipp, P., Wagner, C., Kaestner, L. "Is There a Role of C-Reactive Protein in Red Blood Cell Aggregation?" *Int J Lab Hematol* 2015;**37**: 474-82.

279. Gabay, C., Kushner, I. "Acute-Phase Proteins and Other Systemic Responses to Inflammation." *N Engl J Med* 1999;**340**: 448-54.

280. Koenig, W. "Fibrin(Ogen) in Cardiovascular Disease: An Update." *Thromb Haemost* 2003;**89**: 601-9.

281. Baskurt, O.K., Temiz, A., Meiselman, H.J. "Red Blood Cell Aggregation in Experimental Sepsis." *J Lab Clin Med* 1997;**130**: 183-90.

282. Fabry, T.L. "Mechanism of Erythrocyte Aggregation and Sedimentation." *Blood* 1987;**70**: 1572-6.

283. Katanov, D., Gompper, G., Fedosov, D.A. "Microvascular Blood Flow Resistance: Role of Red Blood Cell Migration and Dispersion." *Microvasc Res* 2015;**99**: 57-66.

284. Yaylali, Y.T., Susam, I., Demir, E., Bor-Kucukatay, M., Uludag, B., Kilic-Toprak, E., Erken, G., Dursunoglu, D. "Increased Red Blood Cell Deformability and Decreased Aggregation as Potential Adaptive Mechanisms in the Slow Coronary Flow Phenomenon." *Coron Artery Dis* 2013;**24**: 11-5.

285. Arbel, Y., Banai, S., Benhorin, J., Finkelstein, A., Herz, I., Halkin, A., Keren, G., Yedgar, S., Barashtein, G., Berliner, S. "Erythrocyte Aggregation as a Cause of Slow Flow in Patients of Acute Coronary Syndromes." *Int J Cardiol* 2012;**154**: 322-7.

286. Tripette, J., Alexy, T., Hardy-Dessources, M.D., Mougenel, D., Beltan, E., Chalabi, T., Chout, R., Etienne-Julan, M., Hue, O., Meiselman, H.J., Connes, P. "Red Blood Cell Aggregation, Aggregate Strength and Oxygen Transport Potential of Blood Are Abnormal in Both Homozygous Sickle Cell Anemia and Sickle-Hemoglobin C Disease." *Haematologica* 2009;**94**: 1060-5.

287. Vicaut, E. "Opposite Effects of Red Blood Cell Aggregation on Resistance to Blood Flow." *J Cardiovasc Surg (Torino)* 1995;**36**: 361-8.

288. Charansonney, O., Mouren, S., Dufaux, J., Duvelleroy, M., Vicaut, E. "Red Blood Cell Aggregation and Blood Viscosity in an Isolated Heart Preparation." *Biorheology* 1993;**30**: 75-84.

289. Jung, F., Mrowietz, C., Hiebl, B., Franke, R.P., Pindur, G., Sternitzky, R. "Influence of Rheological Parameters on the Velocity of Erythrocytes Passing Nailfold Capillaries in Humans." *Clin Hemorheol Microcirc* 2011;**48**: 129-39.

290. Chien, S., Usami, S., Dellenback, R.J., Gregersen, M.I., Nanninga, L.B., Guest, M.M. "Blood Viscosity: Influence of Erythrocyte Aggregation." *Science* 1967;**157**: 829-31.

291. Ong, P.K., Jain, S., Namgung, B., Woo, Y.I., Kim, S. "Cell-Free Layer Formation in Small Arterioles at Pathological Levels of Erythrocyte Aggregation." *Microcirculation* 2011;**18**: 541-51.

292. Suzuki, Y., Tateishi, N., Soutani, M., Maeda, N. "Flow Behavior of Erythrocytes in Microvessels and Glass Capillaries: Effects of Erythrocyte Deformation and Erythrocyte Aggregation." *Int J Microcirc Clin Exp* 1996;**16**: 187-94.

293. Barras, J.P. "Blood Rheology - General Review." *Bibl Haematol* 1969;**33**: 277-97.

294. Nash, G., Wenby, R., SOWEMIMOCOKER, S., Meiselman, H. "Influence of Cellular Properties on Red-Cell Aggregation." *Clinical Hemorheology* 1987;**7**: 93-108.

295. Surgenor, D.M.N. The Red Blood Cell: Elsevier Science, 2013.

296. Chong-Martinez, B., Buchanan, T.A., Wenby, R.B., Meiselman, H.J. "Decreased Red Blood Cell Aggregation Subsequent to Improved Glycaemic Control in Type 2 Diabetes Mellitus." *Diabet Med* 2003;**20**: 301-6.

297. Rampling, M.W., Whittingstall, P., Martin, G., Bignall, S., Rivers, R.P., Lissauer, T.J., Bailey, P.C. "A Comparison of the Rheologic Properties of Neonatal and Adult Blood." *Pediatr Res* 1989;**25**: 457-60.

298. Razavian, S.M., Guillemin, M.T., Guillet, R., Beuzard, Y., Boynard, M. "Assessment of Red Blood Cell Aggregation with Dextran by Ultrasonic Interferometry." *Biorheology* 1991;**28**: 89-97.

299. Sowemimo-Coker, S.O., Whittingstall, P., Pietsch, L., Bauersachs, R.M., Wenby, R.B., Meiselman, H.J. "Effects of Cellular Factors on the Aggregation Behavior of Human, Rat and Bovine Erythrocytes." *Clinical Hemorheology* 1989;**9**: 723-37.

300. Vicaut, E., Hou, X., Decuypere, L., Taccoen, A., Duvelleroy, M. "Red Blood Cell Aggregation and Microcirculation in Rat Cremaster Muscle." *Int J Microcirc Clin Exp* 1994;**14**: 14-21.

301. Brust, M., Aouane, O., Thiebaud, M., Flormann, D., Verdier, C., Kaestner, L., Laschke, M.W., Selmi, H., Benyoussef, A., Podgorski, T., Coupier, G., Misbah, C., Wagner, C. "The Plasma Protein Fibrinogen Stabilizes Clusters of Red Blood Cells in Microcapillary Flows." *Sci Rep* 2014;**4**: 4348.

302. Kim, S., Popel, A.S., Intaglietta, M., Johnson, P.C. "Aggregate Formation of Erythrocytes in Postcapillary Venules." *Am J Physiol Heart Circ Physiol* 2005;**288**: H584-90.

303. McHedlishvili, G., Gobejishvili, L., Beritashvili, N. "Effect of Intensified Red Blood Cell Aggregability on Arterial Pressure and Mesenteric Microcirculation." *Microvasc Res* 1993;**45**: 233-42.

304. Baskurt, O.K., Bor-Kucukatay, M., Yalcin, O. "The Effect of Red Blood Cell Aggregation on Blood Flow Resistance." *Biorheology* 1999;**36**: 447-52.

305. Braasch, D. "The Missing Negative Effect of Red Cell Aggregation Upon Blood Flow in Small Capillaries at Low Shear Forces." *Biorheology Suppl* 1984;**1**: 227-30.

306. Cho, S., Namgung, B., Kim, H.S., Leo, H.L., Kim, S. "Effect of Erythrocyte Aggregation at Pathological Levels on No/O2 Transport in Small Arterioles." *Clin Hemorheol Microcirc* 2015;**59**: 163-75.

307. Verkeste, C.M., Boekkooi, P.F., Saxena, P.R., Peeters, L.L. "Increased Red Cell Aggregation Does Not Reduce Uteroplacental Blood Flow in the Awake, Hemoconcentrated, Late-Pregnant Guinea Pig." *Pediatr Res* 1992;**31**: 91-3.

308. Yalcin, O., Uyuklu, M., Armstrong, J.K., Meiselman, H.J., Baskurt, O.K. "Graded Alterations of Rbc Aggregation Influence in Vivo Blood Flow Resistance." *Am J Physiol Heart Circ Physiol* 2004;**287**: H2644-50.

309. Baskurt, O.K., Meiselman, H.J. "Rbc Aggregation: More Important Than Rbc Adhesion to Endothelial Cells as a Determinant of in Vivo Blood Flow in Health and Disease." *Microcirculation* 2008;**15**: 585-90.

310. Bishop, J.J., Nance, P.R., Popel, A.S., Intaglietta, M., Johnson, P.C. "Effect of Erythrocyte Aggregation on Velocity Profiles in Venules." *Am J Physiol Heart Circ Physiol* 2001;**280**: H222-36.

311. Tripette, J., Nguyen, L.C., Allard, L., Robillard, P., Soulez, G., Cloutier, G. "In Vivo Venous Assessment of Red Blood Cell Aggregate Sizes in Diabetic Patients with a Quantitative Cellular Ultrasound Imaging Method: Proof of Concept." *PLoS One* 2015;**10**: e0124712.

312. Reinhart, W.H., Lutolf, O., Nydegger, U.R., Mahler, F., Straub, P.W. "Plasmapheresis for Hyperviscosity Syndrome in Macroglobulinemia Waldenstrom and Multiple Myeloma: Influence on Blood Rheology and the Microcirculation." *J Lab Clin Med* 1992;**119**: 69-76.

313. Fahraeus, R., Lindqvist, T. "The Viscosity of Blood in Narrow Capillary Tubes." *American Journal of Physiology* 1931;**96**: 562-8.

314. Secomb, T.W., Pries, A.R., Gaehtgens, P. "Hematocrit Fluctuations within Capillary Tubes and Estimation of Fahraeus Effect." *Int J Microcirc Clin Exp* 1987;**5**: 335-45.

315. Baskurt, O.K., Meiselman, H.J. "Erythrocyte Aggregation: Basic Aspects and Clinical Importance." *Clin Hemorheol Microcirc* 2013;**53**: 23-37.

316. Hennerici, M.G., Kay, R., Bogousslavsky, J., Lenzi, G.L., Verstraete, M., Orgogozo, J.M., investigators, E. "Intravenous Ancrod for Acute Ischaemic Stroke in the European Stroke Treatment with Ancrod Trial: A Randomised Controlled Trial." *Lancet* 2006;**368**: 1871-8.

317. Levy, D.E., del Zoppo, G.J., Demaerschalk, B.M., Demchuk, A.M., Diener, H.C., Howard, G., Kaste, M., Pancioli, A.M., Ringelstein, E.B., Spatareanu, C., Wasiewski, W.W. "Ancrod in Acute Ischemic Stroke: Results of 500 Subjects Beginning Treatment within 6 Hours of Stroke Onset in the Ancrod Stroke Program." *Stroke* 2009;**40**: 3796-803.

318. Matsuda, H., Shoemaker, W.C. "Survivor's and Nonsurvivors' Responses to Dextran 40. Hemodynamic and Oxygen Transport Changes in Critically Ill Patients." *Arch Surg* 1975;**110**: 301-5.

319. Dubin, A., Pozo, M.O., Casabella, C.A., Murias, G., Palizas, F., Jr., Moseinco, M.C., Kanoore Edul, V.S., Palizas, F., Estenssoro, E., Ince, C. "Comparison of 6% Hydroxyethyl Starch 130/0.4 and Saline Solution for Resuscitation of the Microcirculation During the Early Goal-Directed Therapy of Septic Patients." *J Crit Care* 2010;**25**: 659 e1-8.

320. Perner, A., Haase, N., Winkel, P., Guttormsen, A.B., Tenhunen, J., Klemenzson, G., Muller, R.G., Aneman, A., Wetterslev, J. "Long-Term Outcomes in Patients with Severe Sepsis Randomised to Resuscitation with Hydroxyethyl Starch 130/0.42 or Ringer's Acetate." *Intensive Care Med* 2014;**40**: 927-34.

321. Morariu, A.M., Gu, Y.J., Huet, R.C., Siemons, W.A., Rakhorst, G., Oeveren, W.V. "Red Blood Cell Aggregation During Cardiopulmonary Bypass: A Pathogenic Cofactor in Endothelial Cell Activation?" *Eur J Cardiothorac Surg* 2004;**26**: 939-46.

322. Karakala, N., Raghunathan, K., Shaw, A.D. "Intravenous Fluids in Sepsis: What to Use and What to Avoid." *Curr Opin Crit Care* 2013;**19**: 537-43.

323. Mutter, T.C., Ruth, C.A., Dart, A.B. "Hydroxyethyl Starch (Hes) Versus Other Fluid Therapies: Effects on Kidney Function." *Cochrane Database Syst Rev* 2013;**7**: CD007594.

324. Qureshi, S.H., Rizvi, S.I., Patel, N.N., Murphy, G.J. "Meta-Analysis of Colloids Versus Crystalloids in Critically Ill, Trauma and Surgical Patients." *Br J Surg* 2015.

325. Rochwerg, B., Alhazzani, W., Sindi, A., Heels-Ansdell, D., Thabane, L., Fox-Robichaud, A., Mbuagbaw, L., Szczeklik, W., Alshamsi, F., Altayyar, S., Ip, W.C., Li, G., Wang, M., Wludarczyk, A., Zhou, Q., Guyatt, G.H., Cook, D.J., Jaeschke, R., Annane, D., Fluids in, S., Septic Shock, G. "Fluid Resuscitation in Sepsis: A Systematic Review and Network Meta-Analysis." *Ann Intern Med* 2014;**161**: 347-55.

326. Tseng, M.Y., Hutchinson, P.J., Kirkpatrick, P.J. "Effects of Fluid Therapy Following Aneurysmal Subarachnoid Haemorrhage: A Prospective Clinical Study." *Br J Neurosurg* 2008;**22**: 257-68.

327. Zhong, J.Z., Wei, D., Pan, H.F., Chen, Y.J., Liang, X.A., Yang, Z.Y., Tang, H.B. "Colloid Solutions for Fluid Resuscitation in Patients with Sepsis: Systematic Review of Randomized Controlled Trials." *J Emerg Med* 2013;**45**: 485-95.

328. Pries, A.R., Neuhaus, D., Gaehtgens, P. "Blood Viscosity in Tube Flow: Dependence on Diameter and Hematocrit." *Am J Physiol* 1992;**263**: H1770-8.

329. Crowell, J.W., Smith, E.E. "Determinant of the Optimal Hematocrit." *J Appl Physiol* 1967;**22**: 501-4.

330. Stark, H., Schuster, S. "Comparison of Various Approaches to Calculating the Optimal Hematocrit in Vertebrates." *J Appl Physiol (1985)* 2012;**113**: 355-67.

331. Reinhart, W.H. "The Optimum Hematocrit." *Clin Hemorheol Microcirc* 2016.

332. Van Tiel, E., Peeters, P.H., Smit, H.A., Nagelkerke, N.J., Van Loon, A.J., Grobbee, D.E., Bueno-de-Mesquita, H.B. "Quitting Smoking May Restore Hematological Characteristics within Five Years." *Ann Epidemiol* 2002;**12**: 378-88.

333. Jelkmann, W., Lundby, C. "Blood Doping and Its Detection." *Blood* 2011;**118**: 2395-404.

334. Annaheim, S., Jacob, M., Krafft, A., Breymann, C., Rehm, M., Boutellier, U. "Rhepo Improves Time to Exhaustion by Non-Hematopoietic Factors in Humans." *Eur J Appl Physiol* 2016;**116**: 623-33.

335. Besarab, A., Bolton, W.K., Browne, J.K., Egrie, J.C., Nissenson, A.R., Okamoto, D.M., Schwab, S.J., Goodkin, D.A. "The Effects of Normal as Compared with Low Hematocrit Values in Patients with Cardiac Disease Who Are Receiving Hemodialysis and Epoetin." *N Engl J Med* 1998;**339**: 584-90.

336. Singh, A.K., Szczech, L., Tang, K.L., Barnhart, H., Sapp, S., Wolfson, M., Reddan, D., Investigators, C. "Correction of Anemia with Epoetin Alfa in Chronic Kidney Disease." *N Engl J Med* 2006;**355**: 2085-98.

337. Bohlius, J., Schmidlin, K., Brillant, C., Schwarzer, G., Trelle, S., Seidenfeld, J., Zwahlen, M., Clarke, M., Weingart, O., Kluge, S., Piper, M., Rades, D., Steensma, D.P., Djulbegovic, B., Fey, M.F., Ray-Coquard, I., Machtay, M., Moebus, V., Thomas, G., Untch, M., Schumacher, M., Egger, M., Engert, A. "Recombinant Human Erythropoiesis-Stimulating Agents and Mortality in Patients with Cancer: A Meta-Analysis of Randomised Trials." *Lancet* 2009;**373**: 1532-42.

338. Pfeffer, M.A., Burdmann, E.A., Chen, C.Y., Cooper, M.E., de Zeeuw, D., Eckardt, K.U., Feyzi, J.M., Ivanovich, P., Kewalramani, R., Levey, A.S., Lewis, E.F., McGill, J.B., McMurray, J.J.,

Parfrey, P., Parving, H.H., Remuzzi, G., Singh, A.K., Solomon, S.D., Toto, R., Investigators, T. "A Trial of Darbepoetin Alfa in Type 2 Diabetes and Chronic Kidney Disease." *N Engl J Med* 2009;**361**: 2019-32.

339. Palmer, S.C., Navaneethan, S.D., Craig, J.C., Johnson, D.W., Tonelli, M., Garg, A.X., Pellegrini, F., Ravani, P., Jardine, M., Perkovic, V., Graziano, G., McGee, R., Nicolucci, A., Tognoni, G., Strippoli, G.F. "Meta-Analysis: Erythropoiesis-Stimulating Agents in Patients with Chronic Kidney Disease." *Ann Intern Med* 2010;**153**: 23-33.

340. Swedberg, K., Young, J.B., Anand, I.S., Cheng, S., Desai, A.S., Diaz, R., Maggioni, A.P., McMurray, J.J., O'Connor, C., Pfeffer, M.A., Solomon, S.D., Sun, Y., Tendera, M., van Veldhuisen, D.J., Committees, R.-H., Investigators, R.-H. "Treatment of Anemia with Darbepoetin Alfa in Systolic Heart Failure." *N Engl J Med* 2013;**368**: 1210-9.

341. Carson, J.L., Grossman, B.J., Kleinman, S., Tinmouth, A.T., Marques, M.B., Fung, M.K., Holcomb, J.B., Illoh, O., Kaplan, L.J., Katz, L.M., Rao, S.V., Roback, J.D., Shander, A., Tobian, A.A., Weinstein, R., Swinton McLaughlin, L.G., Djulbegovic, B., Clinical Transfusion Medicine Committee of the, A. "Red Blood Cell Transfusion: A Clinical Practice Guideline from the Aabb*." *Ann Intern Med* 2012;**157**: 49-58.

342. Lacroix, J., Tucci, M., Du Pont-Thibodeau, G. "Red Blood Cell Transfusion Decision Making in Critically Ill Children." *Curr Opin Pediatr* 2015;**27**: 286-91.

343. Pirofsky, B. "The Determination of Blood Viscosity in Man by a Method Based on Poiseuille's Law." *The Journal of clinical investigation* 1953;**32**: 292-8.

344. Stone, H.O., Thompson, H.K., Jr., Schmidt-Nielsen, K. "Influence of Erythrocytes on Blood Viscosity." *Am J Physiol* 1968;**214**: 913-8.

345. Stadler, A.A., Zilow, E.P., Linderkamp, O. "Blood Viscosity and Optimal Hematocrit in Narrow Tubes." *Biorheology* 1990;**27**: 779-88.

346. Linderkamp, O., Stadler, A.A., Zilow, E.P. "Blood Viscosity and Optimal Hematocrit in Preterm and Full-Term Neonates in 50- to 500-Micrometer Tubes." *Pediatr Res* 1992;**32**: 97-102.

347. McKay, C.B., Meiselman, H.J. "Osmolality- and Hematocrit-Mediated Flow Behavior of Rbc Suspensions in 33 Micrometer Id Tubes." *Biorheology* 1989;**26**: 863-74.

348. Bogar, L., Juricskay, I., Kesmarky, G., Kenyeres, P., Toth, K. "Erythrocyte Transport Efficacy of Human Blood: A Rheological Point of View." *Eur J Clin Invest* 2005;**35**: 687-90.

349. Withers, P.C., Hillman, S.S., Hedrick, M.S., Kimmel, P.B. "Optimal Hematocrit Theory During Activity in the Bullfrog (Rana Catesbeiana)." *Comp Biochem Physiol A Comp Physiol* 1991;**99**: 55-60.

350. Kiel, J.W., Shepherd, A.P. "Optimal Hematocrit for Canine Gastric Oxygenation." *Am J Physiol* 1989;**256**: H472-7.

351. Pries, A.R., Secomb, T.W., Gaehtgens, P., Gross, J.F. "Blood Flow in Microvascular Networks. Experiments and Simulation." *Circ Res* 1990;**67**: 826-34.

352. Kiani, M.F., Pries, A.R., Hsu, L.L., Sarelius, I.H., Cokelet, G.R. "Fluctuations in Microvascular Blood Flow Parameters Caused by Hemodynamic Mechanisms." *Am J Physiol* 1994;**266**: H1822-8.

353. Pries, A.R., Secomb, T.W. "Rheology of the Microcirculation." *Clin Hemorheol Microcirc* 2003;**29**: 143-8.

354. Pries, A.R., Kuebler, W.M. "Normal Endothelium." *Handb Exp Pharmacol* 2006: 1-40.

355. Reinhart, W.H., Piety, N.Z., Shevkoplyas, S.S. "Influence of Red Blood Cell Aggregation on Perfusion of an Artificial Microvascular Network." *Microcirculation* 2016.

356. Detterich, J., Alexy, T., Rabai, M., Wenby, R., Dongelyan, A., Coates, T., Wood, J., Meiselman, H. "Low-Shear Red Blood Cell Oxygen Transport Effectiveness Is Adversely Affected by Transfusion and Further Worsened by Deoxygenation in Sickle Cell Disease Patients on Chronic Transfusion Therapy." *Transfusion* 2013;**53**: 297-305.

357. Nemeth, N., Alexy, T., Furka, A., Baskurt, O.K., Meiselman, H.J., Furka, I., Miko, I. "Inter-Species Differences in Hematocrit to Blood Viscosity Ratio." *Biorheology* 2009;**46**: 155-65.

358. Schmalzer, E.A., Lee, J.O., Brown, A.K., Usami, S., Chien, S. "Viscosity of Mixtures of Sickle and Normal Red Cells at Varying Hematocrit Levels. Implications for Transfusion." *Transfusion* 1987;**27**: 228-33.

359. Marchioli, R., Finazzi, G., Specchia, G., Cacciola, R., Cavazzina, R., Cilloni, D., De Stefano, V., Elli, E., Iurlo, A., Latagliata, R., Lunghi, F., Lunghi, M., Marfisi, R.M., Musto, P., Masciulli, A.,

Musolino, C., Cascavilla, N., Quarta, G., Randi, M.L., Rapezzi, D., Ruggeri, M., Rumi, E., Scortechini, A.R., Santini, S., Scarano, M., Siragusa, S., Spadea, A., Tieghi, A., Angelucci, E., Visani, G., Vannucchi, A.M., Barbui, T., Group, C.-P.C. "Cardiovascular Events and Intensity of Treatment in Polycythemia Vera." *N Engl J Med* 2013;**368**: 22-33.

360. Drueke, T.B., Locatelli, F., Clyne, N., Eckardt, K.U., Macdougall, I.C., Tsakiris, D., Burger, H.U., Scherhag, A., Investigators, C. "Normalization of Hemoglobin Level in Patients with Chronic Kidney Disease and Anemia." *N Engl J Med* 2006;**355**: 2071-84.

361. Phrommintikul, A., Haas, S.J., Elsik, M., Krum, H. "Mortality and Target Haemoglobin Concentrations in Anaemic Patients with Chronic Kidney Disease Treated with Erythropoietin: A Meta-Analysis." *Lancet* 2007;**369**: 381-8.

362. Sadaka, F., Trottier, S., Tannehill, D., Donnelly, P.L., Griffin, M.T., Bunaye, Z., O'Brien, J., Korobey, M., Lakshmanan, R. "Transfusion of Red Blood Cells Is Associated with Improved Central Venous Oxygen Saturation but Not Mortality in Septic Shock Patients." *J Clin Med Res* 2014;**6**: 422-8.

363. Holst, L.B., Haase, N., Wetterslev, J., Wernerman, J., Guttormsen, A.B., Karlsson, S., Johansson, P.I., Aneman, A., Vang, M.L., Winding, R., Nebrich, L., Nibro, H.L., Rasmussen, B.S., Lauridsen, J.R., Nielsen, J.S., Oldner, A., Pettila, V., Cronhjort, M.B., Andersen, L.H., Pedersen, U.G., Reiter, N., Wiis, J., White, J.O., Russell, L., Thornberg, K.J., Hjortrup, P.B., Muller, R.G., Moller, M.H., Steensen, M., Tjader, I., Kilsand, K., Odeberg-Wernerman, S., Sjobo, B., Bundgaard, H., Thyo, M.A., Lodahl, D., Maerkedahl, R., Albeck, C., Illum, D., Kruse, M., Winkel, P., Perner, A., Group, T.T., Scandinavian Critical Care Trials, G. "Lower Versus Higher Hemoglobin Threshold for Transfusion in Septic Shock." *N Engl J Med* 2014;**371**: 1381-91.

364. Hebert, P.C., Wells, G., Martin, C., Tweeddale, M., Marshall, J., Blajchman, M., Pagliarello, G., Sandham, D., Schweitzer, I.I., Boisvert, D., Calder, L. "Variation in Red Cell Transfusion Practice in the Intensive Care Unit: A Multicentre Cohort Study." *Crit Care* 1999;**3**: 57-63.

365. Lacroix, J., Hebert, P.C., Hutchison, J.S., Hume, H.A., Tucci, M., Ducruet, T., Gauvin, F., Collet, J.P., Toledano, B.J., Robillard, P., Joffe, A., Biarent, D., Meert, K., Peters, M.J., Investigators, T.,

Canadian Critical Care Trials, G., Pediatric Acute Lung, I., Sepsis Investigators, N. "Transfusion Strategies for Patients in Pediatric Intensive Care Units." *N Engl J Med* 2007;**356**: 1609-19.

366. Villanueva, C., Colomo, A., Bosch, A., Concepcion, M., Hernandez-Gea, V., Aracil, C., Graupera, I., Poca, M., Alvarez-Urturi, C., Gordillo, J., Guarner-Argente, C., Santalo, M., Muniz, E., Guarner, C. "Transfusion Strategies for Acute Upper Gastrointestinal Bleeding." *N Engl J Med* 2013;**368**: 11-21.

367. Ghali, J.K., Anand, I.S., Abraham, W.T., Fonarow, G.C., Greenberg, B., Krum, H., Massie, B.M., Wasserman, S.M., Trotman, M.L., Sun, Y., Knusel, B., Armstrong, P., Study of Anemia in Heart Failure Trial, G. "Randomized Double-Blind Trial of Darbepoetin Alfa in Patients with Symptomatic Heart Failure and Anemia." *Circulation* 2008;**117**: 526-35.

368. Kulier, A., Levin, J., Moser, R., Rumpold-Seitlinger, G., Tudor, I.C., Snyder-Ramos, S.A., Moehnle, P., Mangano, D.T., Investigators of the Multicenter Study of Perioperative Ischemia Research, G., Ischemia, R., Education, F. "Impact of Preoperative Anemia on Outcome in Patients Undergoing Coronary Artery Bypass Graft Surgery." *Circulation* 2007;**116**: 471-9.

369. Musallam, K.M., Tamim, H.M., Richards, T., Spahn, D.R., Rosendaal, F.R., Habbal, A., Khreiss, M., Dahdaleh, F.S., Khavandi, K., Sfeir, P.M., Soweid, A., Hoballah, J.J., Taher, A.T., Jamali, F.R. "Preoperative Anaemia and Postoperative Outcomes in Non-Cardiac Surgery: A Retrospective Cohort Study." *Lancet* 2011;**378**: 1396-407.

370. Carson, J.L., Terrin, M.L., Noveck, H., Sanders, D.W., Chaitman, B.R., Rhoads, G.G., Nemo, G., Dragert, K., Beaupre, L., Hildebrand, K., Macaulay, W., Lewis, C., Cook, D.R., Dobbin, G., Zakriya, K.J., Apple, F.S., Horney, R.A., Magaziner, J., Investigators, F. "Liberal or Restrictive Transfusion in High-Risk Patients after Hip Surgery." *N Engl J Med* 2011;**365**: 2453-62.

371. Murphy, G.J., Reeves, B.C., Rogers, C.A., Rizvi, S.I., Culliford, L., Angelini, G.D. "Increased Mortality, Postoperative Morbidity, and Cost after Red Blood Cell Transfusion in Patients Having Cardiac Surgery." *Circulation* 2007;**116**: 2544-52.

372. Murphy, G.J., Pike, K., Rogers, C.A., Wordsworth, S., Stokes, E.A., Angelini, G.D., Reeves, B.C., Investigators, T.I. "Liberal or Restrictive Transfusion after Cardiac Surgery." *N Engl J Med* 2015;**372**: 997-1008.

373. Aapro, M., Moebus, V., Nitz, U., O'Shaughnessy, J., Pronzato, P., Untch, M., Tomita, D., Bohac, C., Leyland-Jones, B. "Safety and Efficacy Outcomes with Erythropoiesis-Stimulating Agents in Patients with Breast Cancer: A Meta-Analysis." *Ann Oncol* 2015;**26**: 688-95.

374. Ernst, E., Matrai, A., Kollar, L. "Placebo-Controlled, Double-Blind Study of Haemodilution in Peripheral Arterial Disease." *Lancet* 1987;**1**: 1449-51.

375. Rudofsky, G., Strubel, G., Michler, E., Kuegler, C., Biro, F. "Influence of Fibrinogen and Hematocrit on the Early Outcome of Angioplasty in Patients with Paod." *J Endovasc Ther* 2004;**11**: 125-31.

376. Bag, S., Behera, A., Khandelwal, N., Bapuraj, J.R., Vasishta, R.K. "Improvement in Blood Supply after "Heparin-Dextran" Therapy in Patients of Buerger's Disease with Critical Limb Ischemia." *Indian J Surg* 2013;**75**: 462-8.

APPENDIX I Curriculum Vitae

NATHANIEL Z. PIETY

Department of Biomedical Engineering
Cullen College of Engineering, University of Houston
3605 Cullen Blvd, Room 2009, Houston, TX 77204-5060
phone: +1 (847) 757-0237, email: nzpiety@uh.edu

EMPLOYMENT

2013 – present **University of Houston** Houston, TX

- Graduate Research Assistant, Cullen College of Engineering, Department of Biomedical Engineering

2011 – 2013 **Tulane University** New Orleans, LA

- Undergraduate Research Assistant, Department of Biomedical Engineering

EDUCATION

2013 – present **University of Houston** Houston, TX

- PhD in Biomedical Engineering (In Progress)
  Advisor: Sergey S. Shevkoplyas, PhD

2009 – 2013 **Tulane University** New Orleans, LA

- BSE in Biomedical Engineering, Cum Laude, Departmental Honors
  Advisor: Sergey S. Shevkoplyas, PhD
- BS in Mathematics, Cum Laude
  Advisor: Tewodros Amdeberhan, PhD
- BA in Anthropology, Cum Laude
  Advisor: Trenton W. Holliday, PhD

PROFESSIONAL MEMBERSHIPS

2015 – present	Member, American Heart Association (AHA)
2013 – present	Member, Biomedical Engineering Society (BMES)
2013 – present	Member, Order of the Engineer
2012 – present	Presidential Member, National Society of Leadership and Success (NSLS)

AWARDS AND HONORS

2016	Runner-Up Poster Award, 2016 BSGS Annual Graduate Student Symposium
2016	Biomedical Engineering Department Travel Award, University of Houston
2016	Cullen Graduate Fellowship Travel Grant, University of Houston
2016	Outstanding Abstract Award, 2016 AABB Annual Meeting

2016	NSF/IEEE/Akay Fellowship, 15th International BIO-X Summer School
2014	Top Poster Award, 2014 AABB Annual Meeting
2014	Runner-Up Award, GRaSP Demonstration, University of Houston
2013 – 2017	Presidential Matching Scholarship, University of Houston
2013	Departmental Honors, Tulane University
2010 – 2013	Dean's List, Tulane University
2009 – 2013	Distinguished Scholar Award, Tulane University

RESEARCH SUPPORT

ACTIVE

Predoctoral Fellowship, American Heart Association
01/01/2015 - 12/31/2017 $52,000
Role: principal-investigator
"Paper-based monitoring of sickle hemoglobin for stroke prevention"
The objective of this project is to further optimize the previously developed paper-based sickle hemoglobin assay to measure HbS during transfusion, and to determine if current transfusion practice is optimized to prevent stroke and negative transfusion side effects.

COMPLETED

2014 Summer Grant, Whitaker International Program
06/01/2014 - 07/27/2014 $10,500
Role: co-investigator
"An Ultra-Low-Cost, Paper-Based Test for Sickle Cell Disease"
The objective of this project is to determine the impact of ambient temperature and relative humidity on the formation of blood stains in paper substrates, and to develop integrated paper-based temperature and humidity sensors.

2013 Intramural Research Training Award, National Institutes of Health
06/17/2013 - 08/09/2013 $3,887
Role: co-investigator
"Antigen-Antibody Mediated Rheological Changes in Artificial Microvascular Networks"
The objective of this project is to model adverse transfusion reactions by quantifying the perfusion rate of red blood cells (RBCs) exposed to ABO/Rh antibodies in an artificial microvascular network (AMVN).

PEER-REVIEWED PUBLICATIONS

(12) Piety NZ, George A, Serrano S, Lanzi MR, Patel PR, Noli MP, Kahan S, Nirenberg JF, Airewele G, Shevkoplyas SS (**2017**) "A paper-based test for screening newborns for sickle cell disease," ***Scientific Reports***, DOI:10.1038/srep45488

(11) Xia H, Khanal G, Strachan BC, Vörös E, Piety NZ, Gifford SC, Shevkoplyas SS (**2017**) "Washing in hypotonic saline reduces the fraction of irreversibly-damaged cells in stored blood: a proof-of-concept study," ***Blood Transfusion***, *in press*

(10) Reinhart WH, Piety NZ, Shevkoplyas SS (**2016**) "Influence of red blood cell aggregation on perfusion of an artificial microvascular network," ***Microcirculation***, DOI:10.1111/micc.12317 (Times Cited: 1)

(9) Piety NZ, Yang X, Kanter J, Vignes SM, George A, Shevkoplyas SS (**2016**) "Validation of a low-cost paper-based screening test for sickle cell anemia," ***PLoS ONE***, 11(1): e0144901 (Times Cited: 3)

(8) Piety NZ, Reinhart WH, Pourreau PH, Abidi R, Shevkoplyas SS (**2015**) "Shape matters: the effect of red blood cell shape on perfusion of an artificial microvascular network," ***Transfusion***, 56(4): 844-851 (Times Cited: 4)

(7) Burns JM, Yoshida T, Dumont LJ, Yang X, Piety NZ, Shevkoplyas SS (**2015**) "Deterioration of red blood cell mechanical properties is reduced in anaerobic storage," ***Blood Transfusion***, 14(1): 80 – 88 (Times Cited: 2) (front cover)

(6) Piety NZ, Gifford SC, Yang X, Shevkoplyas SS (**2015**) "Quantifying morphological heterogeneity: a study of more than 1 000 000 individual stored red blood cells," ***Vox Sanguinis***, 109(3): 221 – 230 (Times Cited: 3)

(5) Piety NZ, Yang X, Lezzar D, George A, Shevkoplyas SS (**2015**) "A rapid paper-based test for quantifying sickle hemoglobin in blood samples from patients with sickle cell disease," ***American Journal of Hematology***, 90(6): 478 – 482 (Times Cited: 7)

(4) Reinhart WH, Piety NZ, Deuel JW, Makhro A, Schulzki T, Bogdanov N, Goede JS, Bogdanova A, Abidi R, Shevkoplyas SS (**2015**) "Washing stored red blood cells in an albumin solution improves their morphologic and hemorheologic properties," ***Transfusion***, 55(8): 1872 – 1881 (Times Cited: 11) (front cover)

(3) Reinhart WH, Piety NZ, Goede JS, Shevkoplyas SS (**2015**) "Effect of osmolality on erythrocyte rheology and perfusion of an artificial microvascular network," ***Microvascular Research***, 98: 102 – 107 (Times Cited: 7)

(2) Yang X, Piety NZ, Vignes SM, Benton MS, Kanter J, Shevkoplyas SS (**2013**) "Simple paper-based test for measuring blood hemoglobin concentration in resource-limited settings," ***Clinical Chemistry***, 59(10): 1506 – 1513 (Times Cited: 31)

(1) Yang X, Kanter J, Piety NZ, Benton MS, Vignes SM, Shevkoplyas SS (**2013**) "A simple, rapid, low-cost diagnostic test for sickle cell disease," ***Lab on a Chip***, 13(8): 1464 – 1467 (Times Cited: 37) (back cover)

PATENTS AND PATENT APPLICATIONS

2. Piety NZ, Bigazzi MO, Peucker KF, Relle ES, Algu NW, Ellis EN (2013) "Visco-Elastic Protection Device," US Provisional App. No. 61/813,341
1. Shevkoplyas SS, Yang X, Washko JK, Piety NZ (2012) "Paper Based Diagnostic Test," US Provisional App. No. 61/692,994 (Times Cited: 1)

PRESENTATIONS

- *Anaerobic Conditions Reduce Deterioration of Rheological Properties of Stored Red Blood Cells*. Piety NZ, Stutz J, Yilmaz N, Xia H, Yoshida T, Shevkoplyas SS. Oral Presentation at 2016 AABB Annual Meeting, Orlando, FL, October 22-25, 2016 (outstanding abstract award).
- *A Simple Disposable Device for Bedside Washing of Stored Red Blood Cells*. Vörös E, Piety NZ, Shevkoplyas SS. Poster at 2016 AABB Annual Meeting, Orlando, FL, October 22-25, 2016.
- *Removal of Irreparably Damaged Cells from Stored Blood by Washing in Hypotonic Saline*. Xia H, Khanal G, Strachan B, Piety NZ, Gifford SC, Shevkoplyas SS. Poster at 2016 AABB Annual Meeting, Orlando, FL, October 22-25, 2016.
- *Anaerobic Conditions Reduce Damage to Red Blood Cells during Hypothermic Storage*. Piety NZ, Stutz J, Yilmaz N, Xia H, Yoshida T, Shevkoplyas SS. Oral Presentation at 2016 BMES Annual Meeting, Minneapolis, MN, October 5-8, 2016.
- *A Distributable Paper-based Diagnostic Kit for Point-of-Care Screening for Sickle Cell Disease*. Torabian K, Lezzar D, Piety NZ, George A, Shevkoplyas SS. Oral Presentation at 2016 BMES Annual Meeting, Minneapolis, MN, October 5-8, 2016.

- *A Simple Device for Bedside Washing of Stored Red Blood Cells*. Vörös E, Piety NZ, Shevkoplyas SS. Oral Presentation at 2016 BMES Annual Meeting, Minneapolis, MN, October 5-8, 2016.
- *Comparative Deformability and Microfluidic Perfusion of Human and Nonhuman Red Blood Cells*. Murugan P, Torabian K, Piety NZ, Shevkoplyas SS. Oral Presentation at 2016 BMES Annual Meeting, Minneapolis, MN, October 5-8, 2016.
- *Influence of Red Blood Cell Aggregation on Perfusion of an Artificial Microvascular Network*. Piety NZ, Reinhart WH, Shevkoplyas SS. Poster at 2016 BMES Annual Meeting, Minneapolis, MN, October 5-8, 2016.
- *Paper-Based Test for Indirect Screening of Newborns for Sickle Cell Disease*. Piety NZ, George A, Serrano S, Lanzi MR, Patel PR, Noli MP, Kahan S, Nirenberg D, Camanda J, Airewell GE, Shevkoplyas SS. Poster at 2016 BMES Annual Meeting, Minneapolis, MN, October 5-8, 2016.
- *Towards Universal Sickle Cell Disease Screening in Resource-Limited Settings: Clinical Feasibility of a Paper-Based test for Newborns and Mothers*. Piety NZ, George A, Serrano S, Lanzi MR, Patel PR, Noli MP, Kahan S, Nirenberg D, Camanda J, Airewell GE, Shevkoplyas SS. Poster at 2016 Annual Sickle Cell Disease Research Meeting, Ft. Lauderdale, FL, April 15-18, 2016.
- *Initial Clinical Validation of a Rapid, Low-Cost, Paper-Based Diagnostic Test for Sickle Cell Anemia as a Tool to Facilitate Newborn Screening in Resource-Limited Settings*. Piety NZ, George A, Serrano S, Lanzi MR, Patel PR, Noli MP, Nirenberg D, Camanda J, Airewell GE, Shevkoplyas SS. Poster at 2015 ASH Annual Meeting, San Diego, CA, December 3-6, 2015.
- *Clinical Validation of a Paper-Based Screening and Diagnostic Test for Sickle Cell Anemia in Angola*. Piety NZ, George A, Patel PR, Nirenberg D, Airewell GE, Shevkoplyas SS. Oral Presentation at 2015 BMES Annual Meeting, Tampa, FL, October 7-10, 2015.
- *Paper-Based Test for Screening Newborns for Sickle Cell Anemia in Resource-Limited Settings*. Piety NZ, George A, Patel PR, Nirenberg D, Airewell GE, Shevkoplyas SS. Oral Presentation at 2015 BMES Annual Meeting, Tampa, FL, October 7-10, 2015.
- *Shape Matters: Effect of Red Blood Cell Shape on Perfusion of an Artificial Microvascular Network*. Piety NZ, Reinhart WH, Pourreau PH, Abidi R, Shevkoplyas SS. Oral Presentation at 2015 BMES Annual Meeting, Tampa, FL, October 7-10, 2015.
- *A Simple Approach for Removal of Irreparably Damaged Cells from Stored Blood*. Xia H, Strachan BC, Piety NZ, Gifford SC, Shevkoplyas SS. Poster at 2015 BMES Annual Meeting, Tampa, FL, October 7-10, 2015.
- *Initial Clinical Validation of a Rapid, Low-Cost, Paper-Based Diagnostic Test for Sickle Cell Anemia as a Tool to Facilitate Newborn Screening in Resource-Limited Settings*. Piety NZ, George A, Serrano S, Lanzi MR, Patel PR, Noli MP, Nirenberg D, Camanda J, Airewele G, Shevkoplyas SS. Poster at 2015 ASPHO Annual Meeting, Phoenix, AZ, May 6-9, 2015.
- *Clinical feasibility of screening newborns for sickle cell disease using a novel paper-based test*. Piety NZ, George A, Patel PR, Nirenberg D, Airewele GE, Shevkoplyas SS. Oral Presentation at 2015 Annual Sickle Cell Disease Research Meeting, Hollywood, FL, April 10-13, 2015.
- *Paper-Based Assay for Quantification of HbS in Blood of Sickle Cell Disease Patients*. Piety NZ, Yang X, Dinu BR, George A, Shevkoplyas SS. Poster at 2014 ASH Annual Meeting, San Francisco, CA, December 6-9, 2014.
- *Ultra-low-cost, paper-based test for sickle cell disease in resource-limited settings*. Piety NZ, Lezzar D, Gifford SC, Shevkoplyas SS. Demonstration/Performance at Graduate Research and Scholarship Projects (GRaSP) Day at University of Houston, Houston, TX, October 31, 2014 (runner-up award).
- *Microfluidic System for High-Throughput Morphology Classification: Analysis of More Than One Million Red Blood Cells*. Piety NZ, Gifford SC, Yang X, Shevkoplyas SS. Poster at 2014 AABB Annual Meeting, Philadelphia, PA, October 25-28, 2014.
- *Paper-Based Assay for Quantification of HbS and Diagnosis of Sickle Cell Disease*. Piety NZ, Yang X, Dinu BR, George A, Shevkoplyas SS. Poster at 2014 AABB Annual Meeting, Philadelphia, PA, October 25-28, 2014 (top poster award).
- *Paper-based assay for point-of-care quantification of HbS content in blood of sickle cell disease patients*. Piety NZ, Yang X, Dinu BR, George A, Shevkoplyas SS. Oral Presentation at 2014 BMES Annual Meeting, San Antonio, TX, October 22-25, 2014.

- *Simple microfluidic device for automated, high-throughput morphological analysis of stored red blood cells*. Piety NZ, Gifford SC, Yang X, Shevkoplyas SS. Oral Presentation at 2014 BMES Annual Meeting, San Antonio, TX, October 22-25, 2014.
- *A low-cost, paper-based assay for diagnosis of sickle cell disease in resource-limited settings*. Piety NZ, Yang X, Dinu BR, George A, Shevkoplyas SS. Oral Presentation at 2014 BMES Annual Meeting, San Antonio, TX, October 22-25, 2014.
- *Low-cost, Paper-based Sickle Hemoglobin Assay*. Piety NZ, Yang X, Dinu BR, George A, Shevkoplyas SS. Oral Presentation at Åbo Akademi, Turku, Finland, June 25, 2014.
- *Quantification of Hb S content in blood of sickle cell disease patients using a paper-based assay*. Yang X, Piety NZ, Dinu BR, George A, Shevkoplyas SS. Poster at 2014 Annual Sickle Cell Disease Research Meeting, Miami, FL, April 11-14, 2014.
- *Automated quantification of morphological deterioration of red blood cells during hypothermic storage using a simple microfluidic device*. Piety NZ, Yang X, Gifford SC, Huynh RA, Shevkoplyas SS. Poster at 2013 BMES Annual Meeting, Seattle, WA, September 25-28, 2013.
- *Antigen-Antibody Mediated Rheological Changes in Artificial Microvascular Networks*. Piety NZ, Yuan Y, Shevkoplyas SS, Flegel WA. Poster at 2013 NIH Summer Research Program Poster Day, Bethesda, MD, August 8, 2013.
- *A Simple, Rapid, Low-Cost Paper-Based Microfluidic Device for the Diagnosis of Sickle Cell Disease*. Piety NZ, Yang X, Kanter J, Benton M, Vignes SM, Shevkoplyas SS. Oral Presentation at 2013 Biomedical Engineering Undergraduate Research and Design Conference, New Orleans, LA, January 28, 2013.
- *A Simple, Rapid, Low-Cost Test for the Diagnosis of Sickle Cell Disease Using a Paper-Based Hemoglobin Solubility Assay.* Yang X, Kanter J, Piety NZ, Benton M, Vignes SM, Shevkoplyas SS. Oral presentation at 2012 ASH (American Society of Hematology) Annual Meeting and Exposition, Atlanta, GA, December 8-11, 2012.
- *A Simple Microfluidic Device for Automated, High-Throughput Evaluation of Morphology of Stored Red Blood Cells*. Yang X, Piety NZ, Triscott MI, Shevkoplyas SS. Poster at 2012 BMES Annual Meeting, Atlanta, GA, October 24-27, 2012.
- *A Simple Microfluidic Device for Automated, High-Throughput Evaluation of Morphology of Stored Red Blood Cells.* Yang X, Piety NZ, Triscott MI, Shevkoplyas SS. Poster at 2012 AABB Annual Meeting, Boston, MA, October 6-9, 2012.

REFERENCES

Sergey S. Shevkoplyas, PhD (Research Advisor)
Associate Professor
University of Houston, Cullen College of Engineering, Department of Biomedical Engineering
3605 Cullen Blvd, Room 2009, Houston, TX 77204-5060
Phone: (713) 743-5696
sshevkop@central.uh.edu

Metin Akay, PhD (Department Chair)
Founding Chair
John S. Dunn Endowed Chair Professor
University of Houston, Cullen College of Engineering, Department of Biomedical Engineering
3605 Cullen Blvd, Room 2027, Houston, TX 77204-5060
Phone: (713) 743-2501
makay@uh.edu